Signal Processing Techniques for Enhancement of Defect Detection in Ultrasonic Guided Waves Inspection of Pipelines

A thesis submitted for the degree of Doctor of Philosophy

by

Houman Nakhli Mahal

Department of Electronics & Computer Engineering,
College of Engineering, Design and Physical Sciences,
Brunel University London

Declaration of Authorship

I hereby certify that the work presented in this thesis is entirely my own original work, except where due reference is made. This work has not been previously submitted for an award at any higher educational institute.

Signal Processing Techniques for Enhancement of Defect Detection in Ultrasonic Guided Waves Inspection of Pipelines

Department of Electronics & Computer Engineering,
College of Engineering, Design and Physical Sciences,
Brunel University London

By Houman Nakhli Mahal

Abstract

Pipelines are the main means of transferring oil and gas. In order to avoid failure, they require regular inspection to locate defects and repair them accordingly. Ultrasonic guided waves (UGW) allows long-range inspection of pipelines from one test point. Determining the location of defects is a challenging and manual process. The main aim of this thesis is to develop novel signal processing algorithms for enhancement of data interpretation of UGW tests.

The first step of this thesis was to investigate the operation of the device and the existing sources of noise from the literature. Afterward, based on the literature, three different methods were investigated for approaching the inspection problem of UGW. The first one was to utilize the individual signals from the transducer array to develop a defect identification algorithm. Detection of defects was done based on the spatial differences in the received signals from each time sample. The second was to change the current processing algorithm of the device, in order to enhance the SNR of the results; therefore, an adaptive filtering algorithm was implemented in order to remove significant amount of coherent noise from the tests. The third method was to use the power spectrum to develop a defect identification algorithm; Hence, an algorithm was developed that allowed detection of defects based on a comparison between the power spectrum of the reference signal with the one gathered from each time sample of the results.

All of the aforementioned algorithms were validated using simulated data generated by a finite element model as well as experimental trials on real pipes. It was demonstrated that not only the algorithms are capable of enhancing the defect detection, but also the current signal processing routine of the device can be modified to produce better results.

Keywords – Non-Destructive Testing (NDT), Ultrasonic Guided Wave (UGW), Multi-Modal Processing, Signal to Noise Ratio (SNR) Enhancement, Defect Identification, Pipeline Inspection

This thesis is dedicated to my parents,

Mrs. Zahra AbbassiFard & Mr. Hasan Nakhli Mahal

For their endless love and support.

Table of Contents

List of Figures

List of Tables

Abbreviations

ALE	**A**daptive **L**inear **E**nhancer
ANC	**A**daptive **N**oise **C**anceller
BW	**B**and**w**idth
C0	**C**ondition **0** - Refers to the first condition required for the algorithm developed in Chapter 6
C1	**C**ondition **1** - Refers to the second condition required for the algorithm developed in Chapter 6
C2	**C**ondition **2** - Refers to the third condition required for the algorithm developed in Chapter 6
C3	**C**ondition **3** - Refers to the fourth condition required for the algorithm developed in Chapter 6
C4	**C**ondition **4** - Refers to the fifth condition required for the algorithm developed in Chapter 6
CSA	**C**ross-**S**ectional **A**rea
DAC	**D**istance **A**mplitude **C**orrection
F(n, m)	**F**lexural Wave Mode with circumferential variations of **n** and wavenumber of **m**
FEM	**F**inite **E**lement **M**odel
FIR	**F**inite **I**mpulse **R**esponse
L(0, m)	Axisymmetric **L**ongitudinal Wave mode with wave number of **m**
LMS	**L**east **M**ean **S**quare
NDT	**N**on-**D**estructive **T**esting
NLMS	**N**ormalized **L**east **M**ean **S**quare
RLS	**R**ecursive **L**east **Square**
SNR	**S**ignal to **N**oise **R**atio
SSP	**S**plit **S**pectrum **P**rocessing
T(0, m)	Axisymmetric **T**orsional Wave mode with wave number of **m**
TF	**T**ransfer **F**unction
UGW	**U**ltrasonic **G**uided **W**aves

Chapter One

Introduction

1.1 Chapter Overview

This chapter presents the motivations behind the need for the development of non-destructive testing technologies for inspection of pipelines. Furthermore, it provides information regarding the aim and objectives of the thesis, followed by the used methodology in achieving them. The overview of the thesis and contributions to knowledge is given in the later parts of this chapter.

1.2 Motivation

Pipelines are a safe method of energy transportation in the industry. The main means of transporting oil and gas, which are still one of the world's primary fuel source, are pipelines [1], [2]. Hence, they are designed with high established standards [3]. Nonetheless, they are not prone to failure. The safety of pipelines is dependent on its design, operation, maintenance, and management. These factors can make the operation of in-service pipelines unsafe. One of the main causes is the aging of the current pipelines in the industry. This increases the chance of pipeline failures due to in-service defects (E.g. damage, corrosion) [4]. Any form of elementary damage in pipes that could cause a system failure is known as a defect [5].

In 2015, Chio Lam conducted an statistical analyses of historical pipeline incident data collected between 2002 and 2013 by the Pipeline and Hazardous Material Safety Administration (PHMSA) of the United States Department of Transportation [6]. In his research, he investigated the relevant failure factors and mileage data of the onshore gas transmission pipelines in order to develop a probability of ignition model for ruptures of these pipelines. The distribution of the underlying causes of incidents during those years is illustrated in Figure 1.1. As can be seen, corrosion incidents were one of the leading causes of failure with total percentage of 32%.

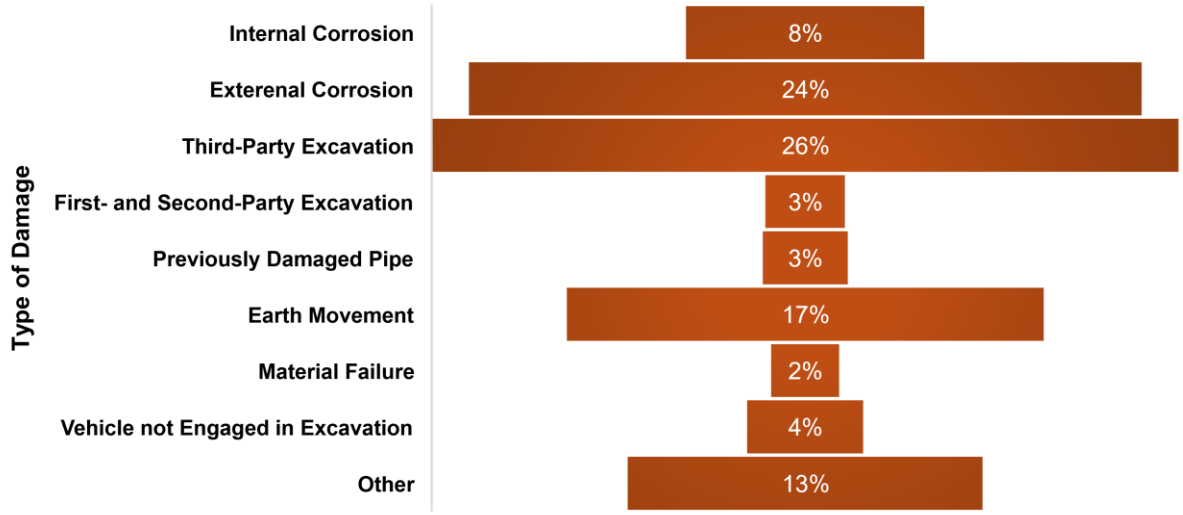

Figure 1.1. Distribution of all pipe-related incidents between 2002 and 2013 by failure cause [6].

These incidents can lead to failures that are both harmful to the environment and expensive for the industries. In the case of failure of pipelines, not only the raw material is lost, but also significant amount of expenditure must be spent in covering the costs associated with the aftermath of the incident. With regards to the latest data released by PHMSA [7] for pipeline

incidents recorded in the United States, from 2002 onward, each year approximately 600 incidents are recorded. Figure 1.2 illustrates the pipeline incident reports between years 1999 – 2008 [7]. This figure, (a) shows the statistics regarding the number of casualties and the total costs for all incidents occurred in each calendar year and (b) shows the average distribution of the underlying causes of the incidents. These figures demonstrate that, even with the progressive advancements of inspection technologies during these past years, the number of reported incidents did not decrease. Furthermore, Corrosion still remains one of the leading underlying causes of recorded incidents. Many of these incidents can be prevented by regular inspection and maintenance of pipelines. E.g. Corrosion generally takes place over a long duration of time. By inspecting the pipes regularly, the growth rate of the corrosion patches within pipes can be monitored and the required maintenance can be scheduled long before the expected failure of the pipelines. Doing so, not only reduces the number of incidents but the costs associated with dealing with the aftermath of the failures.

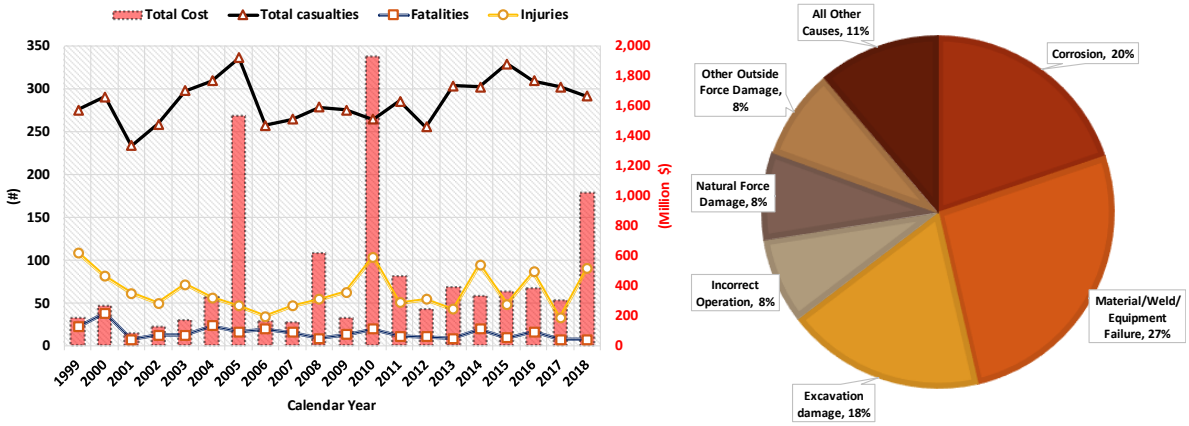

(a) (b)

Figure 1.2. Pipeline incident reports for the years 1999 – 2018 in the United States. (a) Shows the total number of casualties and total cost (in US Dollars) of all incidents that occurred in each calendar year and (b) shows the average distribution of underlying causes of incidents within these years.

An example of one of the tragic failures of pipelines is the Trans-Alaskan pipeline in the United States. In 2007, the British Petroleum's Trans-Alaskan pipeline was failed due to internal Corrosion resulted in leakage of over 200,000 gallons of crude oil into the clean water. Not only the company was obligated to pay a fine of $12 million, a sum of $4 million as a community service payment, a $4 million restitution payment [8]. These figures are exclusive of the company's operating business loss associated with that incident. Needless to say, it also affected the clean water in the area and the environment. Figure 1.3 shows the Trans-Alaskan site after the incident.

Figure 1.3. Clean up of the Oil Spill at BP's Trans-Alaskan pipeline [9].

1.3 Non-Destructive Testing of Pipelines

All engineered structures have an expected life span. Nonetheless, due to their location of placement, operation, and other environmental conditions, this expected life span can be shortened. Therefore, in order to prevent failure of structures, they must be inspected and maintained on a regular basis; especially in the case of structures that are close to the end of their life span.

There are two types of inspection: (1) Destructive Testing (DT), and (2) Non-Destructive Testing (NDT). As the names suggest, in the results of the test are generated by destroying the testing sample or a part of the sample. On the other hand, NDT allows inspection of structures without affecting their structural integrity. The other advantage of NDT is that in some cases, the tests can be carried out without the need for interfering with the operation of the structure. The most common NDT testing methods are [10], [11]: Eddy Current, Magnetic-Particle, Visual, Radiographic, Liquid Penetrant, and Ultrasonic Testing. Data interpretation thorough these techniques are still a manual process that is done by highly trained and experienced inspectors. Generally, three qualification levels of (I, II, III) exists for each of the categories. Parts of these training require formal education, where approximately between 40-80 hours of training needed per level by the training schools [12]. The other part is built on the field, in the format of work experience. Therefore, development of Level III inspectors requires a lot of time and expenditure [13]. This increases the total cost of inspections.

Two of the common conventional methods of inspecting pipelines are Electromagnetic and Conventional Ultrasonic Testing [14]–[16]. These methods, due to their sensitivity and accuracy of detection, are great for assessing the integrity of welds and small localized

features. However, it is sometimes infeasible in inspection of the full area of the pipe length due to their limited range [16]. This is especially true for the case of buried and insulated pipes where the cost of inspection can increase to more than $50k [17], [18]. The main reason for this infeasibility and increments of cost is the access requirements to the required inspection area of the pipes.

Ultrasonic Guided Wave (UGW) decreases this cost significantly by allowing long-range inspection of pipelines from one single inspection point. As opposed to the conventional ultrasonic, the focus of UGW testing is on the identification of defects in the length of the pipes. This is done by using low-frequency ultrasound that can propagate along the pipe wall. This reduction in access points reduces the total cost associated with pipeline inspection significantly. Hence, this technology is more attractive in comparison to its conventional counterparts, e.g. Ultrasonic testing, in long-range inspection of the pipelines.

This research is sponsored by National Structural Integrity Research Centre (NSIRC), located in TWI Ltd. TWI routinely inspect their industrial client's pipelines using this device and providing new signal processing methods in this field can greatly benefit the industry. As such, the main focus is on the development of signal processing algorithm for inspection of Steel pipes with Teletest equipment [19] (See Section 3). However, the investigated signal processing methods are designed to be generic and can be applied to other inspection devices with minor to no adjustments to the main algorithms. Although this research was this research was conducted but the reported work done in this thesis is my own.

1.3.1 Current Challenges of UGW Inspection

UGWs are inherently multimodal and dispersive. This inherit nature of UGWs, introduce a number of challenges in the practical inspection of pipelines [2], [17], [20], [21]:

- In each frequency range, multiple UGW modes exist. It is nearly impossible to have an excitation using only one single wave mode. Furthermore, the dispersion of UGWS in time and space, degrade the performance and resolution of inspection. Both of these factors result in the presence of coherent noise in the inspections.
- Characteristics of the inspection device such as the transducers' transfer functions [22], the UGW transducer array [23], placement of transducers [24], and etc, affect the generated waveform at the point of excitation and can lead to increase of the coherent noise.
- The scattering and attenuation of UGW are affected by surrounding materials of the pipe, such as coatings. This significantly reduces the transmitted energy of the wave and inspection range.

- Currently, data interpretation is a highly-skilled job which is done manually by the inspectors. Due to the presence of coherent noise, the identification of defects is a challenging task which is based on the judgment of the inspectors in many cases.

These challenges affect the overall performance of UGW inspection and reduce the pull of this technology in attracting new customers.

1.4 Aims and Objectives

The main aim and focus of this thesis are development of novel signal processing algorithms that enhance the data interpretation of inspection results in terms of accuracy and of defect detection. These signal processing techniques must be feasibly applicable to the current inspection devices; hence, they should not increase the cost of the device and inspection. It is hoped that by development of such algorithms lead, UGW testing becomes more attractive to a range of wider range of customers within the industry where pipelines can be inspected more frequently with less cost. This can eventually lead to the reduction of the number of recorded incidents and the costs associated with them.

1.4.1 Objectives

The objectives of this research were as follows:

- Investigation of the current state-of-the-art signal processing methods applied to UGW inspection of pipelines.
- Investigation of the inspection device and identification of new post-processing methods.
- Development of a Finite-Element Model to generate simulated signals that are highly contaminated by coherent noise.
- Usage of inherent characteristics of guided waves in distinguishing between the signal achieved from the defects and coherent noises.
- Enhancement of data interpretation in the UGW test through development of novel signal processing algorithms.
- The algorithms must be feasibly applicable to the current inspection approach and device.
- Development and description of new signal processing methods that can help with eventual automation of UGW inspection.
- Engagement in research society and publication of undertaken research.

1.5 Research Methodology

Ssignal interpretation is one of the challenging aspects of UGW inspection of pipelines. This is due to the background characteristics of UGWs such as the existence of multiple wave modes and wave mode conversion. Currently, this inspection is only possible through trained inspectors. The main aim of this thesis is to develop signal processing algorithms that can enhance data interpretation and make this process easier. These techniques must be in line with the current approach used for guided wave testing and be able to feasibly integrate with the current inspection devices.

With regards to the specified aim and objectives, three main topics were required to be investigated in the literature review with a focus on UGW inspection of pipelines:

1. **Background of UGW:** the purpose of this stage was to identify the characteristics of UGW waves. Doing so helped with a better understanding of wave structure and the reason behind existence of coherent noise in the inspection.
2. **UGW inspection approach and devices:** this resulted in the understanding of the current requirement for inspection and the device's current capability. Knowing this helps with specifying the current limitations and identifying the possible ways of developing algorithms that can be feasibly applied to current device. Furthermore, it helped with understanding how the coherent noise is generated in the inspections.
3. **State-of-the-art signal processing algorithms:** before developing the signal processing algorithms in this thesis, a literature review was carried on the signal processing algorithms. The focus was mostly on the techniques which are applied on UGW signals especially in the case of pipelines. This helped with the identification of the common approaches and problems faced by the research community in this field.

In the literature, it was found that the existing noise in UGW inspection varies on a case by case basis and is highly time-varying within each test case. Another objective of this thesis was to use the inherent characteristics of guided waves in order to either reduce the amount of noise or detect the defect signal location. Doing so results in development of algorithms that are not case dependent.

After this literature review, with the aforementioned objectives in mind, possible routes for the development of signal processing algorithms were identified. The focus was on selecting routes with limited conducted research in the literature, which in authors perspective, had great potential both for enhancement of data interpretation and further development.

In the second stage of this research, a finite-element model was produced that could generate simulated defect signals contaminated by a high amount of coherent noise. Without coherent noise, the defects signal could be easily detected in the tests. Therefore, the main achievement of this model was generation of simulated coherent noise with the same characteristics of real-life inspection. Furthermore, it provides a strategy for other researchers in the field with no access to practical experimental data, to generate signals with high amount of coherent noise and use them to develop signal processing algorithms. The algorithms were initially developed and validated on the simulated data. Doing so reduces the overall cost of algorithm development. Afterward, the performance evaluation of each algorithm was done experimentally in the laboratory trials. In order to achieve a better insight into the performance of the developed algorithms, various testing conditions were assessed such as multiple excitation frequencies, defect sizes, and defect locations.

The last major objective of this thesis was to engage with the research community and distribute the achieved results within the community. This was done in the format of conferences and workshops presentations, and journal publications.

Figure 1.4 illustrates the outline of the aforementioned research methodology.

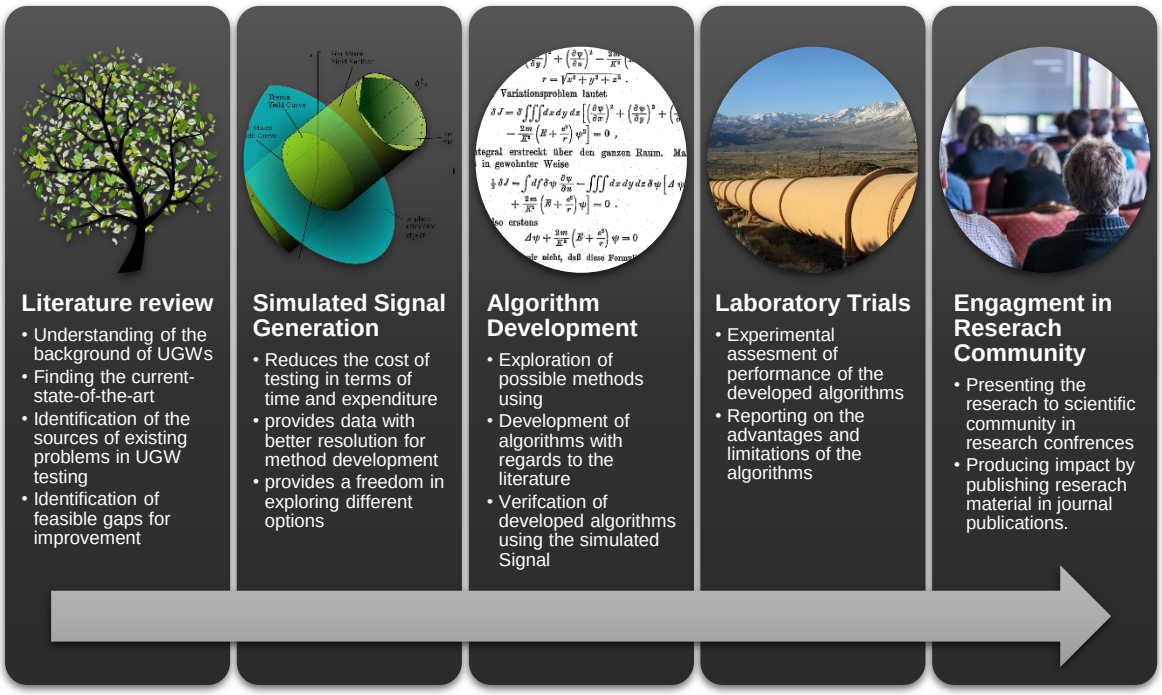

Figure 1.4. Outline of the research methodology.

1.6 Thesis Structure

This Chapter introduces the scope and motivation of the research. Chapter 2 provides the required background information regarding both the technology and the literature. Chapter 3 describes the setup of both laboratory trials and the finite element model. Furthermore, in this chapter the limitations of the excitation waveform selection are explained and examples of the coherent noises in the tests are illustrated. Chapter 4 covers the development of the first signal processing algorithm that uses the spatial differences between the wave achieved from individual signals of the device in order to identify the defect signal. Afterward, the second signal processing algorithm which enhances the signal to noise ratio of the defect by modifying the propagation routine of the device is described in Chapter 5. The development of the third signal processing which uses the spectral differences of the waves in order to identify the defects is covered in Chapter 6. In the last Chapter, the research is concluded and recommendations for further works are given.

1.7 Contribution to Knowledge

1. In the initial stage of this research, a new approach of the generation of simulated signal which is contaminated by coherent noise using finite element model is described. This model duplicates the current setup used in the UGW inspection where all of the required signal processing routines of the device must be used. Using this model, the practical behavior of coherent noises can be simulated; hence, the data generated from this model can be used for development of signal processing without the need for laboratory trials.
2. One of the possible routes to enable defect detection with higher accuracy was to use the spatial differences between the waves. This approach is developed and validated in Chapter 4. Using the developed FEM model, difference between the spatial arrival patterns of the signals received from defect and coherent noise was illustrated. This was the basis on which a novel signal processing algorithm was designed to exploit these differences using the individual signals from the transducers rather than the single time signal achieved from the post-processing propagation routine of the inspection device. This chapter demonstrated that it is possible to use the signals from individual arrays, and by doing so consider the spatial differences between the signal of interest and coherent noise, in order to detect the defect location more accurately. Furthermore, it demonstrated that such method can eventually lead to automation of the inspection.
3. Chapter 5 proposed a novel approach for the recombination of signals and generating the data required for interpretation. The idea was to re-design the summation algorithm

done for generation of unidirectional signals in the device. It was demonstrated that, by implementing an adaptive filtering algorithm, the signal to noise ratio of the defects signal can be significantly improved; especially in the case of highly variable spatial noise. Furthermore, it was demonstrated that by consider the spatial differences between wave modes, new algorithms can be developed that can reduce the total amount of noise in the inspection result. The results of this chapter suggest that the current approach used in post-processing propagation routine of the device is not the best-optimized method of achieving the inspection result.

4. The results of the aforementioned chapters illustrated that the focus of the research community, rather than developing signal processing methods for the results generated after the propagation routine of the device, can be on development of algorithms that consider the spatial characteristics of the wave modes. Doing so can increase the accuracy of inspection result significantly and provides the possibility of applying the algorithms developed in the literature to the results generated by such method.
5. In Chapter 6, the results generated by the post-processing propagation routine of the device was used in order to develop a defect identification method. The main concept in this technique was to use the spectral differences between the received signals of the defects and coherent noise. Even though the coherent noise is within the same bandwidth of the excitation sequence, it was demonstrated that distinguishable differences exist in the power spectrums achieved from the defect and coherent noise signals of the windowed sequences of the inspection result. This led to development of an algorithm that could successfully exploit these differences and detect the defect location.

1.7.1 Publications Arising from the PhD

Journal papers

H. Nakhli Mahal, K. Yang, and A. K. Nandi, “Detection of Defects Using Spatial Variances of Guided-Wave Modes in Testing of Pipes,” Appl. Sci., vol. 8, no. 12, p. 2378, 2018.

H. Nakhli Mahal, K. Yang, and A. K. Nandi, “Improved Defect Detection Using Adaptive Leaky NLMS Filter in Guided-Wave Testing of Pipelines,” Appl. Sci., vol. 9, no. 2, pp. 1–23, 2019.

H. Nakhli Mahal, K. Yang, and A. K. Nandi, “Defect Detection using Power Spectrum of Torsional Waves in Guided-Wave Inspection of Pipelines,” Appl. Sci., vol. 9, no. 7, 2019.

Conference Papers

H. Nakhli Mahal, P. Mudge, and A. K. Nandi, “Comparison of coded excitations in the presence of variable transducer transfer functions in ultrasonic guided wave testing of pipelines,” in 9th European Workshop on Structural Health Monitoring, 2018.

H. Nakhli Mahal, A. K. Nandi, and P. Mudge, “Enhancement of Signal to Noise Ratio in Ultrasonic Guided Wave Inspection of Pipelines,” in NSRIC 2018, 2018.

H. Nakhli Mahal, P. Mudge, and A. K. Nandi, “Noise removal using adaptive filtering for ultrasonic guided wave testing of pipelines,” in 57th Annual British Conference on Non-Destructive Testing, 2018, pp. 1–9.

H. Nakhli Mahal, A. K. Nandi, and K. Yang, “Detection of Defects in Guided-Wave inspection of pipelines,” in NSIRC 2019, 2019.

Chapter Two

Literature Review

2.1 Overview

This chapter covers the background required for understanding the characteristics of guided waves in pipes. Afterward, it describes the approach used to achieve practical inspection of pipelines and explains the underlying operational principles of the inspection device. This includes the description of both the devices' hardware and the signal processing algorithms used for enabling general inspection of pipelines. The later part of this chapter serves as a review with regards to the state-of-the-art signal processing algorithms and possible gaps of improvement.

2.2 Ultrasonic guided waves

Elasticity of materials enables its elementary volume to restore their original positions in response to a displacement force applied to them. By exciting the movement of elementary volume in an elastic medium, elastic waves are generated which can propagate through and interact with the features of the object. These interactions can be monitored and used for describing the characteristics of the object. Based on this property, ultrasonic testing is established where the interaction of ultrasonic waves, which are sounds waves with frequencies above 20 kHz, with the material is inspected in order to assess the integrity of it. Traditionally, ultrasonic testing includes exciting high-frequency sound waves, typically in MHz region, in order to inspect a focused region where the transmitter (transducer) is located.

However, if a three-dimensional medium is bounded by at least one surface, by using lower frequencies, the waves are able to travel into the adjacent elementary volume. Therefore, bounding the medium with two equidistance surfaces would cause the waves to be guided within the medium; the generated waves are commonly known as guided waves. This property allows the inspection of long-range ultrasonic inspection, otherwise known as ultrasonic guided wave testing. The guided wave propagating along a pipe reflects its energy when encountering discontinuities like metal-loss defects or geometric features such as welds or pipe supports. The amount of energy reflected is in direct relation with the cross-sectional area of the feature [25], [26].

2.2.1 Guided wave modes in pipes

Guided waves are multimodal [17]. Depending on the excitation frequency, multiple wave modes can be generated at the point of excitation. These modes are categorized based on their displacement patterns (mode shapes) within the structure. The main categories of guided waves in pipes are axisymmetric torsional and longitudinal waves and non-axisymmetric flexural waves.

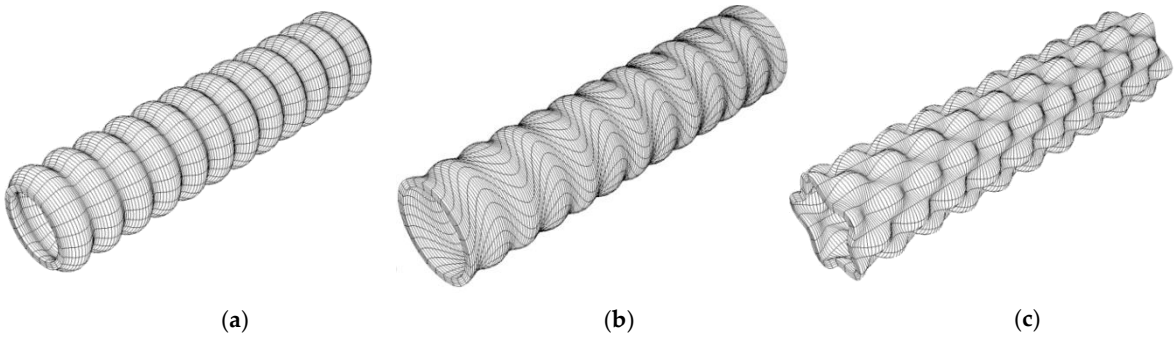

Figure 2.1. Illustration of (from right to left) longitudinal, torsional and flexural wave modes [27].

Figure 2.1 shows the three families of wave modes existing in UGW testing of pipes which are longitudinal, torsional, and flexural wave modes. Both longitudinal and torsional wave modes have rotationally symmetrical movement along the axis (axisymmetric), while flexurals are non-axisymmetric and therefore are not generally needed for the purpose of inspection.

2.2.1.1 Nomenclature

The popular nomenclature used for them is in the format of X(n,m), where X can be replaced by letters L for longitudinal, T for torsional, and F for flexural waves; n shows the harmonic variations of displacement and stress around the circumference; and m represents the order of existence of the wave mode [28]. In an ideal scenario, a single pure family of axisymmetric waves in their non-dispersive region should be excited for general inspection. Nonetheless, this is not possible due to the variations in excitation and reception transfer functions of transducers in real-life scenarios. Furthermore, the interaction of wave modes with the pipe also leads to the generation of different wave modes, which is commonly known as a wave mode conversion phenomenon [17], [29], [30].

2.2.2 Dispersion

Besides the multimodal nature of UGWs, they can have dispersive propagation. Dispersion causes the energy of a signal to spread out in space and time as it propagates [31]. It is dependent on the frequency of the wave mode and the structure under test; meaning different frequencies of wave modes can have different speeds of propagation. Two difference wave velocities exist [32]:

1. **Group Velocity - c_g:** Represents the velocity with which the overall shape of wave (envelope) propagates through space/time.
2. **Phase Velocity - c_p:** Is the rate at which the phase of the wave propagates in space/time.

Dispersion occurs in cases where the group and phase velocity of a wave mode are not matching. The T(0,1) wave mode is non-dispersive and travels with a constant speed of approximately 3260m/s over all frequencies in steel pipes. The relation between the group or phase velocity with frequency, which is called dispersion curves, can be calculated both analytically and experimentally [33].

Figure 2.2a shows an example of a dispersion curve calculated from the eight-inch schedule 40 steel pipe using RAPID software [34]. Wilcox et al. introduced a method to use dispersion curves in order to both simulate [35] and remove [31] the effect of dispersion**.** Using the developed formula, an example of a dispersive wave is shown in Figure 2.2b; the shown wave

propagation is based on the dispersion curves of F (4,2). Unlike T (0,1), which is nondispersive across its whole frequency range [33], flexural waves are dispersive. Also, in this figure, the difference between the phase and group velocities are illustrated. Dispersion is usually undesirable[1] due to the fact that it can degrade temporal/spatial resolution, sensitivity, and amplitude of the received wave packet [35]. Therefore, for ease of inspection, the torsional wave which is both axisymmetric and nondispersive is used.

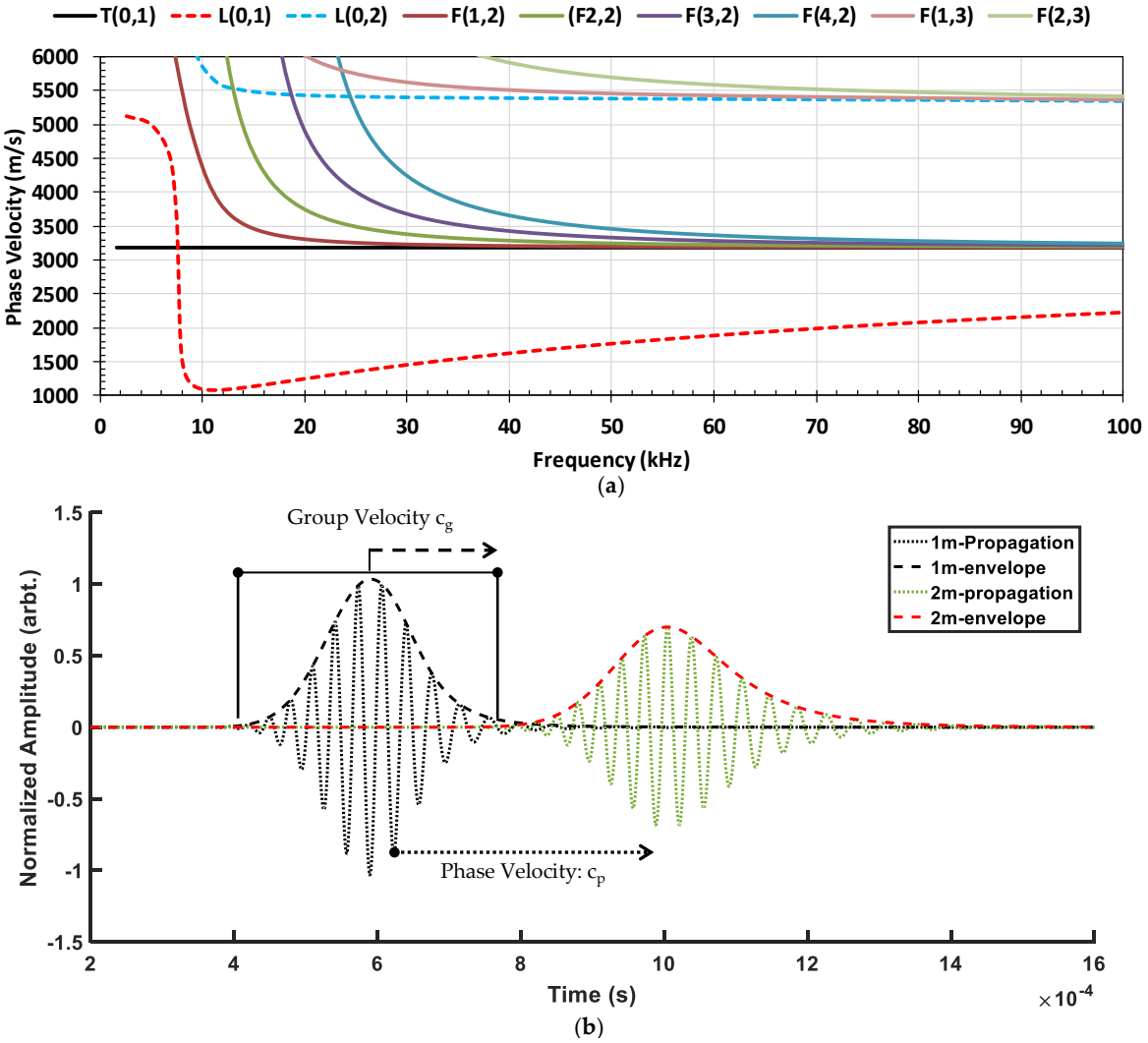

Figure 2.2. (a) Example dispersion curve of T(0,1) wave mode in an 8″ schedule 40 steel pipe. (b) The effect of dispersion on a simulated flexural wave for two propagation distances [36].

2.2.3 Attenuation

Attenuation is the gradual loss in intensity of elastic waves through a medium. It can be defined as the reduction in amplitude with regards to the propagation distance. Attenuation can be divided into two subcategories, (1) Intrinsic attenuation which is the reduction of signal

[1] Excitations of dispersive waves are used in UGW focusing methods to enhance system resolution. Flexural waves can also help sizing defects.

power during transmission by absorption and (2) Extrinsic attenuation that is the reduction of signal power through reflection and accompanied mode conversion by an impedance contrast [37]. In simple form, the system transfer function |H(x, w)| can be considered as shown in equation (2.1):

$$|H(x,w)| = E(w)\, A(x,w)\, D(w) \tag{2.1}$$

where E(w), A(x,w), D(w) are excitability, attenuation, and detectability of the guided wave mode at the transmission, propagation, and reception phases respectively. The excitability is the ability of the transducer for exciting the required frequency components and detectability is the transducer's ability in receiving them. As pulse-echo method is used for UGW testing, the same transducers are used and therefore, the excitability and detectability transfer functions will be the same. Zeng et. al. [38] developed a method to extract the transfer function of a transducer and compensate for its effect in testing plates using Lamb waves. The attenuation is also dependant on the distance and several other factors such as:

- Signal spreading due to dispersion
- Signal spreading due to beam divergence
- Material damping
- Leakage into surrounding media
- Scattering of the wave

2.2.4 Wave mode conversion

In an event where a discontinuity exists in the propagation path of guided waves, the guided waves scatter from the discontinuity with a proportion of energy traveling opposite to the original direction of propagation. However, this scattering does not always result in generation of the same wave mode, especially in the case of non-axisymmetric discontinuities. Based on the geometry of the discontinuity and the characteristics of excitation sequence, different wave modes with different reflection coefficients can be generated [37], [39], [40]. In most cases of axisymmetric wave excitation, the resultant incident wave will also include a significant proportion of axisymmetric waves. Nonetheless, the wave mode conversion to flexural waves also occurs since no feature is perfectly in practice axisymmetric.

Fundamental axisymmetric wave modes have a ‘family’ of flexural wave modes associated with them. The families are defined based on their spatial mode shape and propagation characteristics. As an example, the family of F(n,2) wave modes (where n > 0) is associated to the fundamental axisymmetric wave mode of T(0,1); this association is based on the similarities of their harmonic variation in displacement patterns about the pipe’s circumference [29], [30]. Majority of mode conversion occurs within their associated family of flexural waves.

2.3 Characteristics of the inspection device

General inspection using most of the guided waves devices follow's the same background principle. That is to generate a unidirectional axisymmetric wave. In this thesis, the Teletest Focus Device has been used [19] (illustrated in Figure 2.3). This device was initially developed in Plant Integrity (PI) Ltd, a subsidiary of The Welding Institute (TWI) of United Kingdom. In 2017, the Teletest Focus was sold to EddifyUK [41].

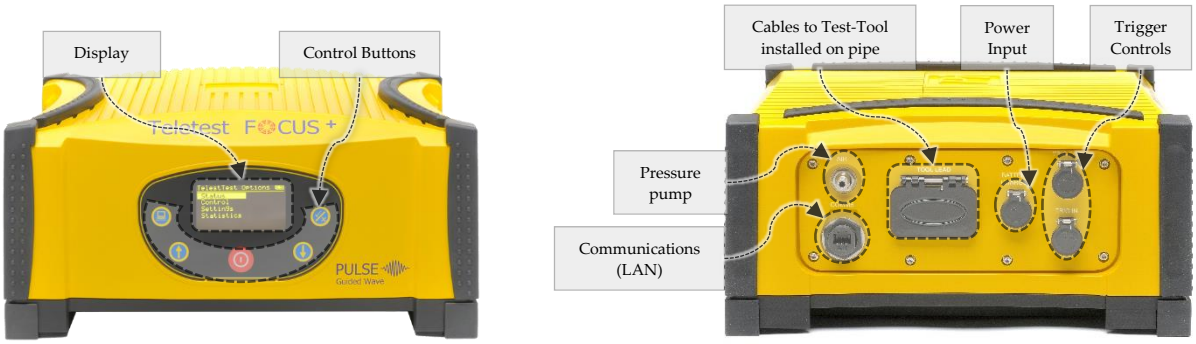

(**a**) Front Panel (**b**) Side Panel - Connectors

Figure 2.3. Teletest Mk.4 (Focus Enabled). (a) shows the front panel [42] and (b) shows the side panel of the device.

Teletest device maximum sampling rate is at 1MHz and it is capable of signal averaging by 1M times. The nominal operating frequency used for inspecting the pipelines is in the range of 20 – 300 kHz [42]. The device uses custom made broadband transducers that are designed and manufactured by the company. These transducers are made from PZT materials and require no-coupling (dry-coupled); therefore, in order to amplify the gain of these transducers, the device includes an internal electric pump which increases the coupling force of the transducer surface and the surface medium [32]. Figure 2.4a shows a transducer module that includes three longitudinal transducers and two torsional transducers.

The general excitation frequency for inspection of pipelines using UGWs is in the range of 20 – 100 kHz [23]. Teletest transducers are designed to have a flat frequency response in this range. Nonetheless, this frequency response is affected by various factors in the inspection [17], [22], [24], [43]. One of the major factors which affect this frequency response is the applied pressure on transducers [22]. This force can change the resonance frequency of transducers and introduce non-linearity in the transfer function (TF) of the transducers.

Figure 2.4b-c illustrates examples of the produced velocity under the transducers surface with regards to the frequency when the applied pressure load on the transducers are 0 and 350 Newtons (N), respectively [22]. Comparing (b) and (c), it can be seen that by varying only the applied pressure load on top of transducers, significant changes are introduced in certain regions and frequencies. On the other hand, other factors such as characteristics of the test

specimen's [17], [23], [44], [45], quality of production, and etc, also affect the frequency response of the transducers. Some of these conditions, such as the equal distribution of the pressure on top of each transducer and the condition of the surface underneath the transducer cannot be predicted and are variable in each inspection. Therefore, all these non-linearities affect the overall TF of the system and generate unwanted wave modes at the point of excitation.

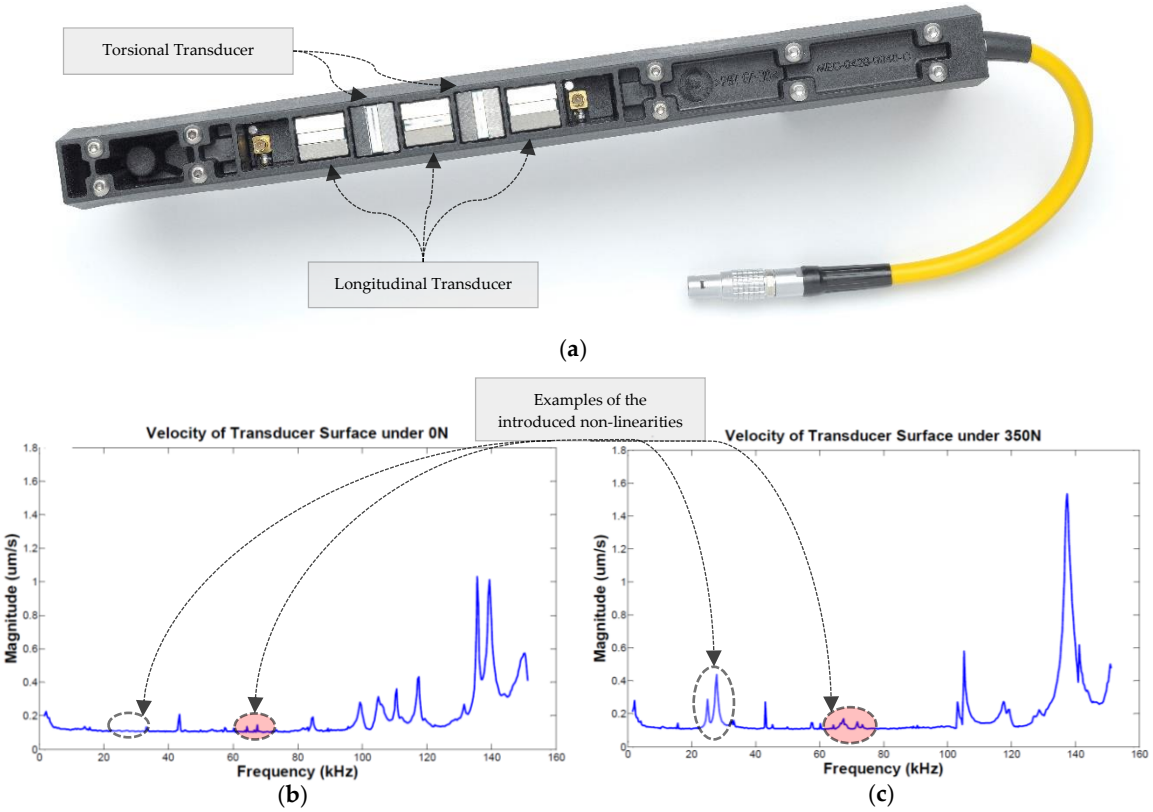

Figure 2.4. (a) Teletest transducer module with 5 transducers installed. (b) and (c) shows the TF of a single transducer on a plate under no pressure force and 350 N force, respectively [22]. Examples of non-linearities in these TFs are marked within the figure using black dotted circles.

As explained previously, for general inspection, there is a need for generating a unidirectional axisymmetric wave. In order to generate an ideal axisymmetric wave, there is a need for having a full surface coverage around the circumference of the pipe. In practice, the surface of the transducers is small and cannot cover the whole circumference of the pipe. However, as it was proved in the literature [32], it is possible to generate a quasi-axisymmetric wave by using a number of equally placed transducers around the circumference of the pipe. The number of transducers required for each segment depends on the radius of the pipe [23], [24], [32], [46]. Using this approach, non-axisymmetric waves are also generated, but they are canceled out after a short propagation distance. Teletest uses a collar (test tool) which consists of multiple rings where each ring includes a number of linearly spaced transducer

[32]. Longitudinal waves can be generated by aligning the transducers to the axial direction and torsional waves can be achieved by rotating this alignment by 90° to achieve circumferential displacement. Each ring is divided into 8 segments (A-H); the signals from each transducer are assigned to one of these segments (Figure 2.5).

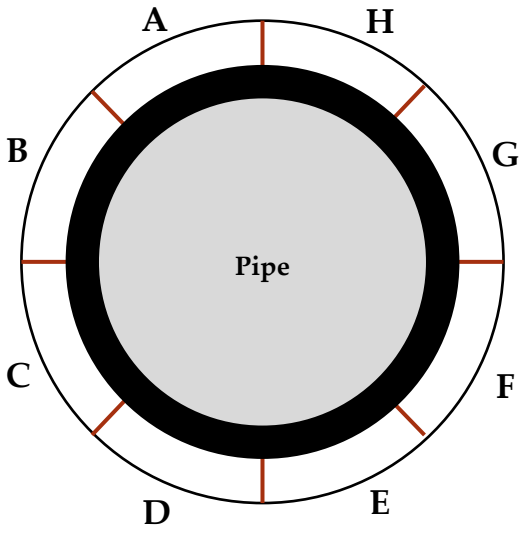

Figure 2.5. Illustration of a single ring used placed around the circumference of a pipe for exciting an axisymmetric waveform.

The second requirement for the inspection is to achieve a unidirectional wave. The main aim of general UGW inspection is to find the defects in the axial direction (length) of the pipe. As shown in Figure 2.6, there are two testing directions. In order to know which side of the test tool defects are located and allow easier interpretation of the results, the inspection is done twice in both directions. In each case, when the test direction is decided, the excited wave should travel only within that direction (forward testing direction). Therefore, there is a need for having a procedure that eliminates the excitation and reception of waves in the unwanted test direction.

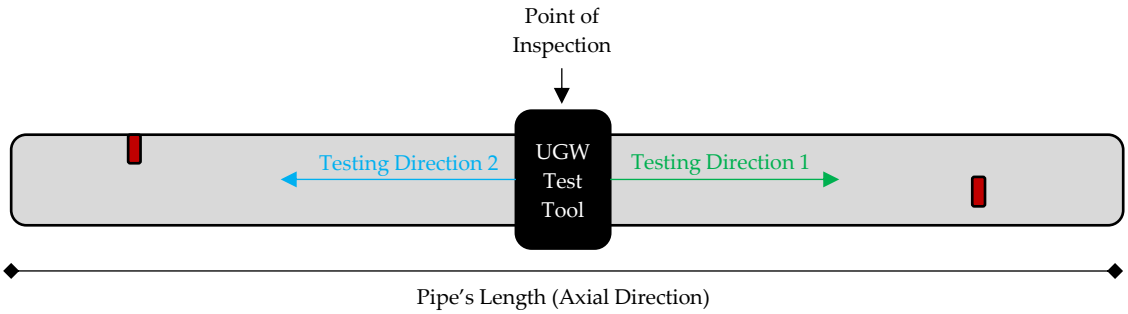

Figure 2.6. Illustration of the testing directions in UGW testing of pipes.

Teletest transducers excite waves in both axial directions. Nonetheless, it is possible to achieve a unidirectional wave using an array of transducers. This follows the same principles

of phased array inspections in ultrasonic testing where the principle of wave superposition is used to enhance the energy of the transmitted wave on a particular propagation distance by manipulating the start time of transmission. However, instead of enhancing the waves, phase delays are introduced to create a destructive superposition on the wave traveling in the opposite testing direction[2] [23], [45], [47], [48]. When a wave is received from the opposite direction, it's energy is reduce using post-processing routine (in the software side) of the device. However, these waves propagate past the test tool and interact with pipe's features in the intended testing direction. Any reflections caused by such indirect waves (or signals) have the same characteristics as those created by the wave excited in the intended direction. These are known as mirror signals which are caused by scattering of indirect travel of waves with the features.

The complete test tool of Teletest installed on pipes to enable excitation of a unidirectional axisymmetric wave is a transducer array, commonly known as Collar. This Collar comprises of multiple rings of transducers placed axially apart from each other to enable control of test direction, where each ring consists of a number of equally placed transducers to enable axisymmetric wave generation. Figure 2.7a shows an example of the Teletest collar and (b) illustrates the schematic of the three-ring collar placement on a pipe. The distance between each ring, d, is commonly known as ring spacing.

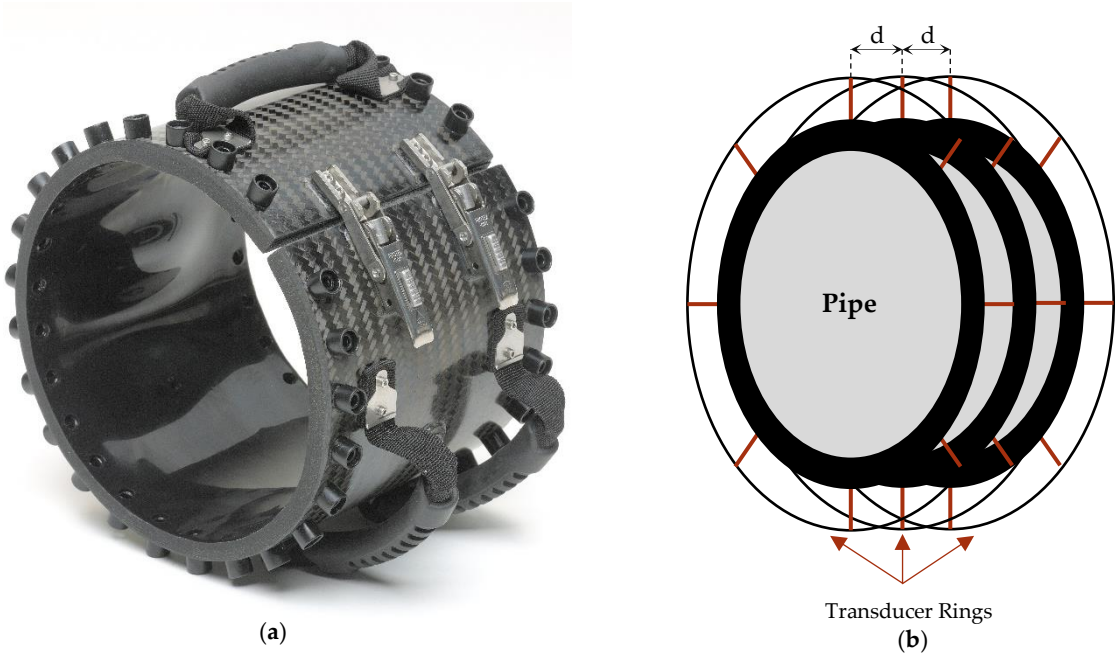

Figure 2.7. (a) shows the Teletest UGW test tool (collar) and (b) illustrates the schematic of a three-ring collar placement on a pipe with ring spacing distance of d.

[2] Refer to Section 2.4 for more information about the phase delaying operation.

Figure 2.8 shows an example of the entire setup of the UGW inspection of pipes. As can be seen, three main devices are needed. The first is the Teletest Collar equipped with the required type and number of transducer modules. The collar is installed and fitted onto pipes using two clamps. The second is the Teletest Unit which is generally located near to the Collar. The Unit is connected using two sets of cables, one for pressurizing the Collar and the other to enable signal transmission and reception to each segment of the rings. The third is a computer with the Teletest software installed. The computer acts as a control unit for controlling excitation waveform and post-processing the received signals.

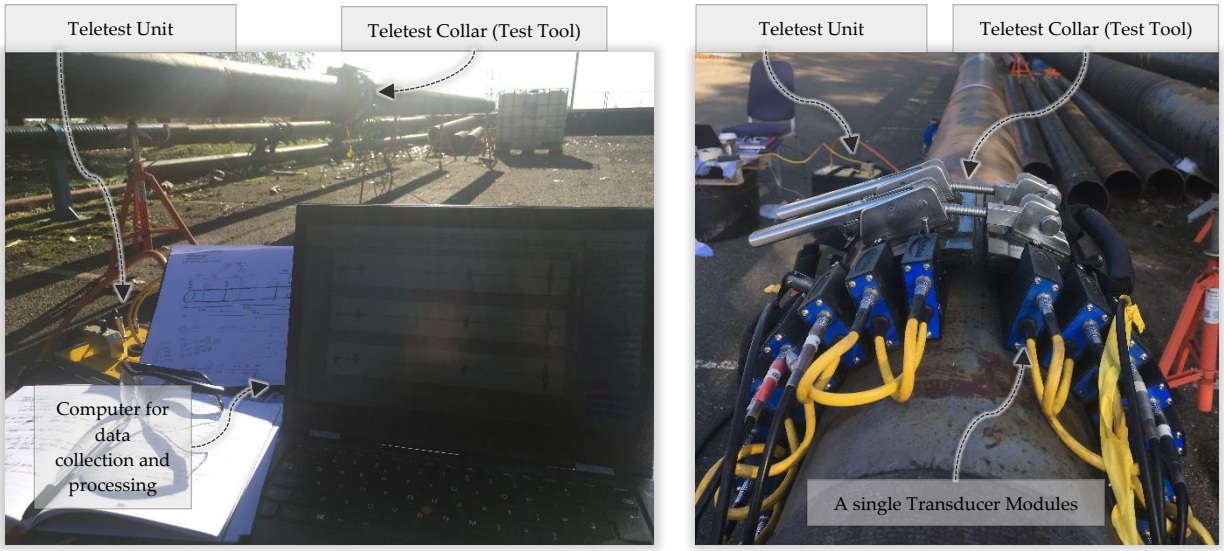

(**a**) (**b**)

Figure 2.8. Example of UGW inspection setup where (a) shows the Teletest unit and computer and (b) shows the Collar with installed transducer modules.

Figure 2.9 shows an example of a post-processed signal which is used to determine defects location in-field inspections. The most recent standard for interpretation this result is published by ASTM in 2017 [49]. The interpretation is done with the help of four distance amplitude correction (DAC) curves that are fitted to the response of the pipe welds. The pipe welds are generally done axisymmetrical and are considered as 20% reflectors. Therefore, by fitting the DAC curves to pipe welds, the non-linear attenuation of the material can be determined which aids the data interpretation. The defect detection is done with regards to the Signal to Noise Ratio (SNR). Using the DAC curves a background noise threshold level can be determined where any signals with greater SNR than this background noise are reported as a defect signal. In cases where the background noise is low in comparison to the weld signal, the detection of defects will depend on the judgment of the inspectors [23], [45]. Therefore, UGW data interpretation is a skilled job that requires training and experience.

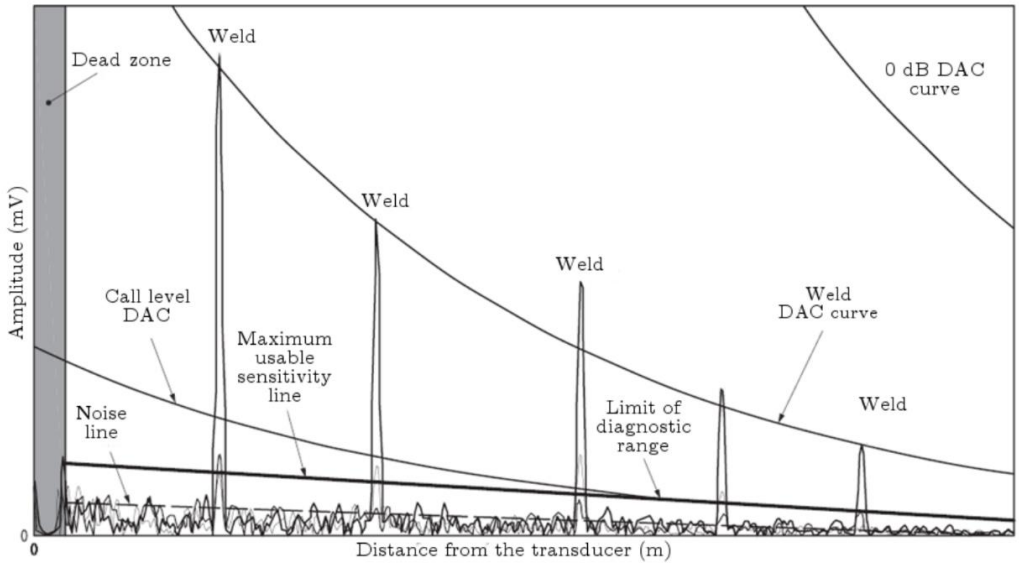

Figure 2.9. A practical example of a typical UGW inspection result [23].

Three main categories of signals are expected to be received in guided-wave tests which are shown in Figure 3. The first signal is the superposition of the axisymmetric and flexurals waves where it is located on a true defect location. The second is the created flexurals due to wave mode conversion [39]. These flexural signals exhibit the same characteristics of excitation waveform. Furthermore, they are also time-invariant and cannot be removed using averaging techniques. Hence, in this research these flexural waves are referred to as coherent noise which can lead to the detection of false alarms. The third category is the non-coherent noise, which is not correlated to the excitation sequence. This category is the main one that can be removed using generalized filtering techniques, as their characteristic is completely different from the excitation sequence.

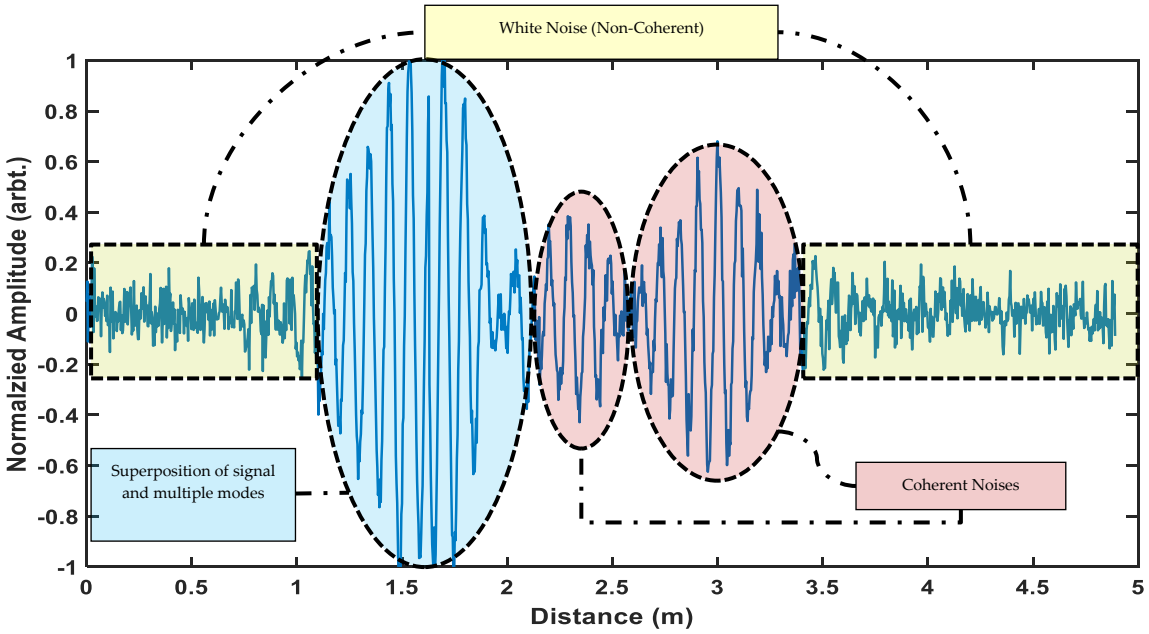

Figure 2.10. Illustration of simplified categorise of signals in the guided wave inspection [50].

2.4 Signal propagation routine for general UGW inspection

In this thesis, the general UGW inspection is referred to as the most common and first step of the inspection which results in generation of A-Scan. The A-Scans are the main source of data used by the inspectors. All other inspections, such as Focusing techniques that require advanced phase-delaying operation, are done with respect to the A-Scans. The main aim of this thesis is to enhance the data interpretation from the A-Scans; hence, in this section the main focus is on the signal processing routine used for the general inspection.

As mentioned previously, two requirements exist in excitation and acquisition of signals. The first requirement is to generate axisymmetric waves which are done by using multiple transducers placed linearly on the circumference of the pipe. In the reception side, all received signals from each ring are added together in order to reduce the effect of non-axisymmetric wave modes. The other requirement is to generate a unidirectional wave. This is done by applying a phase delay to the signals from multiple rings [44].

In Teletest, two types of Collars exist for controlling the test direction. Their difference is in a number of transducer rings; one includes 2 and the other includes 3 rings of transducers. The torsional wave can be generated using both Collars. However, in order to generate a pure longitudinal mode, there is a need for having 3 rings of transducers. This is due to that, even at low frequencies, two longitudinal modes of L(0,1) and L(0,2) are generated. The desired wave mode for testing is L(0,2) and the purpose of the 3 ring Collar is to enable excitation of the desired L(0,2) wave mode in one testing direction while canceling the undesired L(0,1) [23], [45], [48].

Nonetheless, the basis of the operation of both Collars is the same. That is to manipulate the signals of each ring in order to apply a destructive interference on the waves traveling in the opposite testing direction. This is done by applying a phase delay in the frequency domain of the excitation waveform. Introducing a phase delay in the frequency domain has the same effect as delaying the start time in the time domain. For non-dispersive regions of the waves, all frequency content will be delayed by a constant time and there is no major advantage calculating the required wave in the frequency domain. However, if there is a need for generating a dispersive wave mode, it is important to consider the variability in the phase speeds of each frequency. Therefore, the amount of delay applied to each frequency is dependent on the dispersion curves of the wave mode. In 2003, Wilcox et al. developed an algorithm to predict the wave propagation based on the dispersion curves [31], [51]:

$$u(x,t)= \int_{-\infty}^{\infty} F(w)e^{i(k(w)x-wt)}dw \qquad (2.2)$$

where x is the distance of propagation, t is a point in time, F(w) is the Fourier Transform of the time original time-domain sequence u(x,t), w is the angular frequency and k(w) is the circular wave number of the wave mode of interest. The circular wave number is defined as [32]:

$$k(w)=\frac{w}{v_{ph}(w)} \tag{2.3}$$

where v_{ph} is the phase velocity of the wave mode. Figure 2.11 shows a schematic diagram of a 2 ring (a) and 3 rings (b) transducer placement on the surface of the pipe's wall with ring spacing of d. In the two-ring system the following procedure applies [23]:

- **Ring 1:** The excitation sequence remains unchanged and is not affected by the phase delaying operation.
- **Ring 2:** The excitation sequence is delayed using equation (2.2) with the same distance as the ring spacing, d, and is inverted. Using this approach, the wave traveling in the opposite direction from Ring 1 is canceled underneath Ring 2.

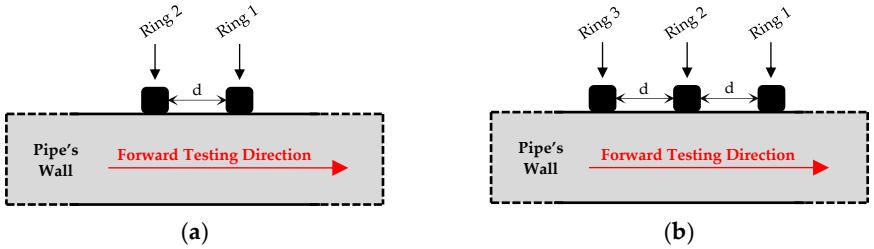

Figure 2.11. Diagram of the distribution of transducers on the surface of the pipe's wall in (a) 2 ring and (b) 3 ring. The black boxes show the centre of wave generation for each transducer.

In the three-ring system, the following procedure is used [23]:

- **Ring 1:** Is the original excitation sequence without any delays.
- **Ring 3:** Is the excitation sequence delayed to a distance, d, using equation (2.2).
- **Ring 2:** is the inverted summation of signals applied to Ring 1 and Ring 2.

In both systems, the signals are normalised, so the amplitudes fall in the range of -1 and 1. In summary, the general propagation routine for the three-ring system is illustrated in Figure 2.12.

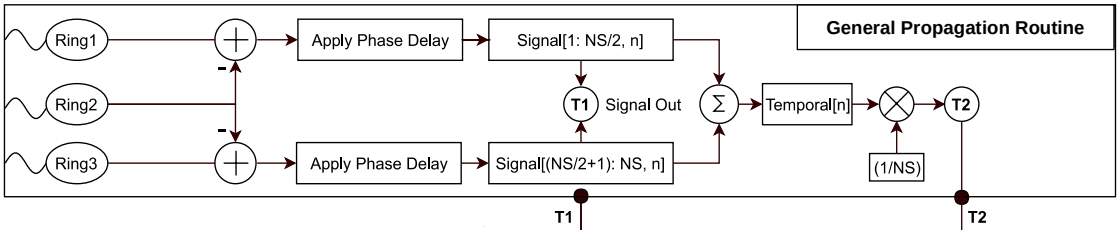

Figure 2.12. Signal propagation routine of the Teletest Device.

2.5 Signal Processing Literature

One of the initial techniques developed for signal processing of guided waves is the work of Wilcox et al. [31], which uses previously calculated dispersion curves in order to compensate for the effect of dispersion for the wave mode of interest in a certain propagation distance. In 2013, Zeng et al. [52] used the basis of the dispersion compensation technique and introduced a novel method to design waveforms in order to pre-compensate for a certain propagation distance.

Pulse compression is another approach that has been previously investigated in the literature. Instead of exciting a narrowband sine wave sequence, pulse compression uses a known coded sequence and processes the received signal by applying match-filtering in order to detect the known sequence. One of the initial attempts of testing pulse compression in the guided waves was done by Rodriguez et al. [53], [54], where chirp sequences were excited using air-coupled piezoelectric transducer in order to generate Lamb waves in aluminum plates. Higher SNR and peak values for the signals of interests were achieved in the experiments; however, the effect of dispersion was not considered, and therefore a decrease in signal amplitude was expected. In 2010, they published another paper using the same system where the phase modulation based on Golay codes were used where the enhancement of 21 dB in SNR using a 16-bit Golay code was achieved compared to the conventional pulse transmission. Mehmet et al. [55], [56], introduced an iterative dispersion compensation for removing the dispersion effect of guided waves propagation. Most recently, Malo et al. [57] developed a two-dimensional compressed pulse analysis in order to enhance the achieved SNR of each wave mode. In the pulse compression approaches, the results are always a trade-off between the spatial resolution and SNR, as having a result with higher propagation energy and δ-like correlation means that the signal duration must be increased. Furthermore, the transfer function of the excitation system can affect the accuracy of the coded waveforms. These two factors indicate that the initial waveform design and the accuracy of inspection using this method depend on the testing conditions.

Other approaches have also been reported in the literature where narrowband sine waves were used as excitation sequence. Kamran et al. investigated split-spectrum processing [58]–[60], where the time-domain signal is decomposed into multiple signals in different frequency bands, and then recombined in time-domain in order to remove the coherent noise. In their most recent work [60], it was reported that using the optimum filter parameters and polarity thresholding method for recombination, the SNR of defects with sizes as small as 2% cross-sectional area could be improved significantly. Nonetheless, the technique depends on various parameters which can depend on the pipes' characteristics. Another recently

developed method is the spectral subtraction, investigated by Duan et al. [61]. In this method, the noise signature is calculated using a small section of the retrieved signal where no real pipe feature exists. Afterward, this signal is subtracted from the total signal using a sliding window where a significant reduction of coherent noise levels could be achieved. Nonetheless, achieving noise signature in the practical inspection of pipelines is difficult as the location of defects and even pipe features might be unknown.

The common concept in all of the aforementioned signal processing methods is to use the differences between the characteristics of each wave mode in order to enhance data interpretation. This enhancement was done either by enhancing the SNR of the results or by enabling the detection of defects location using the signal processing algorithms. However, the full potential of the system has not yet been established. The UGW inspection devices are currently producing a multidimensional signal using arrays of transducers but in the mentioned works, only a single signal generated after applying the signal propagation routine of the device is post-processed. This signal propagation routine of the device creates the inspection data by summing the phase-delayed version of all transducers together. This routine was developed to reduce the received flexural signals and achieve a unidirectional inspection [4,5].

On the other hand, as it was mentioned in Section 2.4, inspection device includes an array of transducers; hence, another approach would be to use a wider number of transducers. Array processing techniques that use individual signals are generally used for imaging and focusing applications [21–27]. However, these algorithms are computationally expensive and might require the individual excitation of transducers [26], or a phased array focusing of the transducers [23], rather than synthetic focusing, where all transducers in the array are excited at the same time [21]. This adds to the complexity of data interpretation. Furthermore, the goal of these algorithms is capturing an image of a segment of the pipe to produce more information regarding the defect's characteristics rather than the detection of the defect location.

In the literature, limited research was conducted in the field of active noise cancellation using filtering approaches. In the field of signal processing, filtering is one of the most common processes [62]. When the characteristics of noise are known, static filters can be designed that remove the non-coherent unwanted noise of tests (passive noise cancellation). As an example, when the expected bandwidth of the received signal is between 30 and 60 kHz, all other frequencies can be filtered. However, in most real-life scenarios, designing an optimum static filter is not possible since: (1) the characteristic of the noise is not known beforehand and (2) the noise can be iteratively changing. On the other hand, by providing the right multidimensional signal to adaptive filters, it is possible to remove such noise from the tests.

Adaptive filters have been applied in a variety of industries such as communications radar, ultrasonic and medical. The basic concept of adaptive noise cancellers was introduced by Widrow et al. in 1975 [63]. Their work developed the already existing Wiener filter model in order to utilize the residual signal for the adaptive update of the filter weights. Many of the derived algorithms, as well as applications, were explained in his work, including the cancellation of periodic interference in electrocardiography and speech signals. Using the same principles, Rajesh et al. [64] proposed an adaptive noise-canceling method for the removal of background noise where the closest sensor to the abdomen of a pregnant patient is used as the reference signal, with the maternal signal captured by a sensor in a different position. By using this configuration, they were able to extract the wanted Fetal signal which was obscured by the signal received from the maternal heart rate. In 2003 [65], Hernandez implemented the adaptive linear enhancer (ALE) algorithm to increase the SNR by using the delayed version of the same signal as the input to the adaptive filter. Ramli et al. [66] reviewed different adaption algorithms, such as the least mean square (LMS), normalized-LMS (NLMS), leaky-LMS and recursive least square (RLS), where it was reported all of these approaches are capable of enhancing the SNR. In communications and speech analysis, one of the common uses of an adaptive noise canceller (ANC) is for echo cancellation [67], [68], which can be generated by hybrid transformers while transmitting data, or from the multipath mitigation of the signals to the microphone. In radar technology [69], [70], adaptive filters are widely used for multipath cancellation, clutter rejection, and spatial noise reduction by using adaptive beamforming. In ultrasonic testing, Zhu et al. [71] used adaptive filters in order to increase the SNR in ultrasonic NDT of highly scattered materials. In 2010, Monroe et al. [72], tested this configuration for clutter rejection and detection of small targets in ultrasonic backscattered signals. Both researchers reported that adaptive filtering is a robust method of filtering the random ultrasonic grain noise created by the structure. It was reported that if the ultrasonic beam is moved less than a beam width away from the position, the echo from a structural feature is closely related while the grain noise varies. The results were evaluated experimentally using NLMS where an improvement of 5–10 dB was observed with fixed parameters.

In guided waves testing, the noise is time-varying. While the excited wave mode is non-dispersive and axisymmetric, the flexural waves change in time. Observing the signal from different points of the pipe the axisymmetric waves will have similar characteristics, while the flexural waves will be variable. Therefore, instead of using the post-processed signal achieved from the signal processing routine, the signals from different axial locations in the array can be used to design an active noise cancellation system using adaptive filters. One of the approaches for updating the adaptive filter weights that can potentially be applied to guided

wave signals is the Leaky NLMS method. The NLMS method reduces the amplification of gradient noise and also provides a faster rate of convergence than the LMS algorithm [73], [74]; therefore, it is more suited for guided waves applications with time-varying noise. Furthermore, the introduction of a leakage factor in the update function for the filter weights limits the divergence of the filter weights. Leakage methods were initially introduced to decrease performance degradation caused by limited-precision hardware [75]. The process is equivalent to the introduction of a white noise sequence to the input signal [74]. In the context of these guided waves, the main advantage of applying a leakage factor is to allow faster adaption of the filter weights to the existing noise of each iteration. The performance of leaky NLMS algorithms was analysed by Sayed et al. [76] and the stability of the algorithm was investigated by Bismor et al. [77]. In mathematical formulation, introducing the leakage factor would only reduce the effect of past filter weights. Therefore, if the same principles of the NLMS algorithm are used, the algorithm will remain stable and bounded.

2.5.1 Summary of the processing stages in UGW inspection of pipes

Three main stages exist in testing using UGW: (1) Excitation, (2) Propagation, and (3) Acquisition. Figure 2.13 outlines the main processes within each different stage.

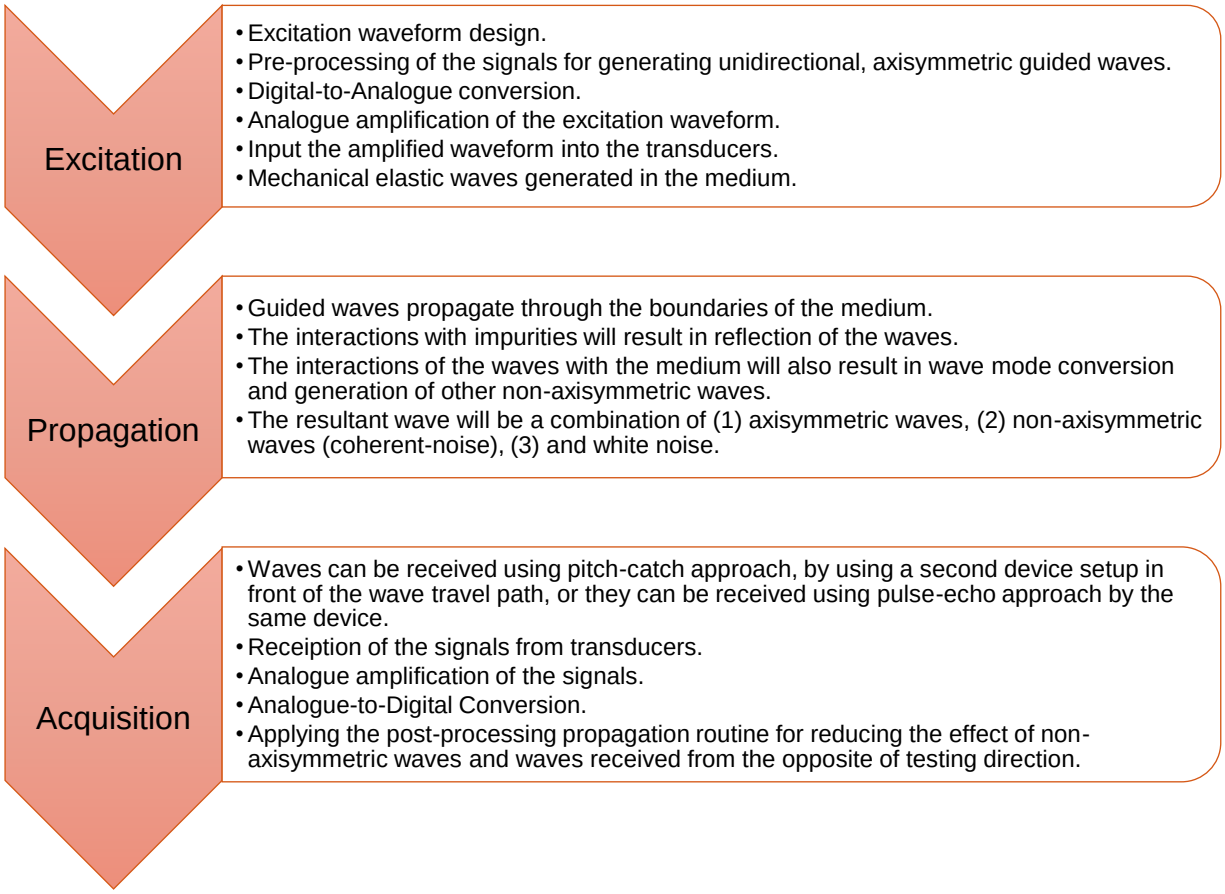

Figure 2.13. Outline of different stages in the UGW inspection of pipes.

Various signal processing methods are developed in the literature which targets an individual or multiple process within these stages in order to enhance UGW data interpretation:

1. **Excitation Stage – Pre-Processing:** Pre-processing techniques are applied to the excitation stage. These include techniques which require waveform manipulation such as coded-excitations [2], [55]–[57], [78] and active focusing [79], [80]. Also, there are techniques to pre-compensate for the effect of dispersion by changing the excitation sequence [52]. The limitation of pre-processing techniques is the TF of the system as a whole. In some cases, the designed waveform cannot be perfectly excited, which significantly affects the results achieved from this stage. On the other hand, in cases where environmental conditions and TFs of the testing are known or do not have a significant effect on the output, then pre-processing techniques can enhance the energy of the excitation sequence significantly.
2. **Propagation:** The literature on this stage is very limited. In practical inspection, the exact features geometry and the interactions of the wave with these features are unknown. Therefore, it is difficult to design signal processing techniques for general inspection that can manipulate these interactions between the wave and structure in order to enhance the inspection result. However, by knowing the location of defects, some signal processing techniques were developed in the literature that gives limited control over this stage. e.g. in active-focusing, the waves are targeted to a defect location in order to generate a stronger response from the defect. Using such techniques require manipulation of the excitation sequence in order to generate a certain waveform in a specific range. Furthermore, post-processing techniques can be implemented to further enhance the results achieved from these techniques. The information gathered from such algorithms can help to specify the defect type and size.
3. **Acquisition – Post-processing:** Most of the signal processing techniques applied to UGW inspection of pipelines target this stage. They are typically applied to the results achieved after applying the device's signal propagation routine. All techniques such as SSP [27], [59], [60], Pulse-Compression [2], [55]–[57], Focusing techniques [79], active denoising using spectral subtraction [61], and etc. are applied or have a component which needs to be applied within this stage. There are two advantages in post-processing the results: the first being that there is no need of changing any excitation sequence or the device and it can be readily applied to the previous data gathered from the same device. The second is that developing post-processing techniques improves the resolution and accuracy of the results which reduces the cost of device and inspection.

2.6 Identified gaps in the literature

The main challenge in data interpretation are the dispersive nature and existence of multiple wave modes in UGW. Data interpretation is done with the help of SNR and DAC curves. The focus of this thesis is to develop post-processing techniques that can be feasibly applied to the current device configuration and help the inspectors in interpreting the results of inspection at no additional cost. This can be achieved by either developing signal processing algorithms that enhance the defects' SNR or enabling defect detection.

Most of the aforementioned techniques in the literature post-processes a single signal resulted from the device's propagation routine in order to enhance the results achieved from the tests. However, UGW testing devices have an array of transducers. Limited research was conducted in the literature with regards to the development of methods that utilize the individual signals of the transducer array in detection of defects. The hypothesis is that by using the spatial arrangement of the transducers, additional information regarding the received waves can be gathered that helps distinguish the defects' signal from the coherent noise. This approach is investigated in Chapter 4 which leads to development of a novel statistical algorithm that is able to detect the defects' location based on the spatial difference between the wave modes.

Furthermore, it was noted that limited research was conducted in enhancing the recombination algorithm used in the signal propagation routine of the inspection device. The hypothesis is that by modifying and changing the summation processed, it is possible to enhance the SNR of the defects. This approach was successfully demonstrated in Chapter 5 by implementing a recombination algorithm based on adaptive filters that resulted in the enhancement of defects' SNR.

Moreover, techniques such as SSP are able to reduce the coherent noise based on the differences in the frequency spectrum of axisymmetric and flexural waves. However, limited research was conducted with regards to the development of defect identification algorithms using these differences in the frequency spectrum. In Chapter 6, the feasibility of defect detection using the power spectrum is investigated. A signal processing algorithm is developed which can successfully detect the defects based on the comparison of the power spectrums of the inspection data and the excitation sequence.

Chapter Three

Test Setup

3.1 Overview

In this Chapter, both the simulated (Section 3.3) and experimental setup for laboratory trials (Section 3.2) for data generation is explained. The aim of simulated data was to investigate wave propagation and develop signal processing algorithms. The model produced results with higher resolution, especially in the case of spatial reception of the waves and provided easier understanding of the wave propagation in UGW testing of pipelines. Furthermore, developing the algorithms on FEM reduced the total cost required for testing. The main difference of the developed FEM model was the generation of flexural waves at the point of excitation; which increased the amount of existing coherent noise in the results and the difficulty in data interpretation. The validation and assessment of the performance of signal processing algorithms were done using laboratory trials on real experimental pipes. This assessment was performed with regards to variable defect size, defect location, and excitation frequencies. Expected signal routes for laboratory trials and FEM model is illustrated in Figure 3.4 and Figure 3.10, respectively. These setups were used in all chapters.

3.2 Laboratory trials

The aims of these trials was to validate and assess the performance of developed algorithms. In this section, the selection of excitation waveform (Section 3.2.1), the geometry of defects and their placement location (Section 3.2.2), and the expected signal routes (Section 3.2.3) are explained.

3.2.1 Selection of excitation waveform

As explained previously, a non-dispersive axisymmetric wave is required for a general inspection[3] of pipelines using UGW. Two families of axisymmetric waves exist in cylindrical structures, Longitudinal and Torsional. The reported nominal frequency for pipeline inspection is in the range of 20 – 100 kHz [29]. This limits the feasible wave modes for excitation to L(0,1), L(0,2), and T(0,1). An example of dispersion curves of the available axisymmetric wave mods for an eight-inch schedule 40 steel pipe is generated by RAPID [34] and is shown in Figure 3.1. As can be seen, in the range of 20 – 100 kHz, two longitudinal wave modes exist; L(0,2) is generally the non-dispersive and L(0,1) is a dispersive wave mode in most pipes. Therefore, if excitation of longitudinal wave is required, the goal is to cancel the L(0,2) wave mode which can be achieved using arrays of transducers[4]; however, due to the wave mode conversion phenomenon, this wave mode is generated during inspection. On the other hand, only one existing torsional wave mode, T(0,1), can be excited in this region which is non-dispersive across using all frequencies. These are a common observation with regards to the dispersion curves of most of the pipe sizes. Furthermore, T(0,1) is generally less affected by the surrounding materials of the pipes such as coatings or the liquid inside the pipes [25], [45], [81]. Hence, with regards to the aforementioned literature, it is better to excite a T(0,1) wave mode for general inspection [48], [82], [83].

The energy of the generated wave is dependent on the excitation frequency[5]. Lower frequencies tend to produce higher displacement energy and are generally less affected by the attenuation of coatings [25], [81], [84]. On the other hand, the TF of Teletest transducers is highly variable in region of 20 kHz[3]. Hence, the selected excitation wave is T(0,1) with frequencies in range of 30 – 50 kHz. Doing so, maximize the energy output of the waves and allows easier interpreting of the results. The selected waveform for excitation is a 10 cycle Hann-Windowed sine wave which is one of the most common waveforms for general UGW inspection of pipelines [47].

[3] See Chapter 2.
[4] See Section 2.3 in Chapter 2.
[5] See Section 3.3.4.

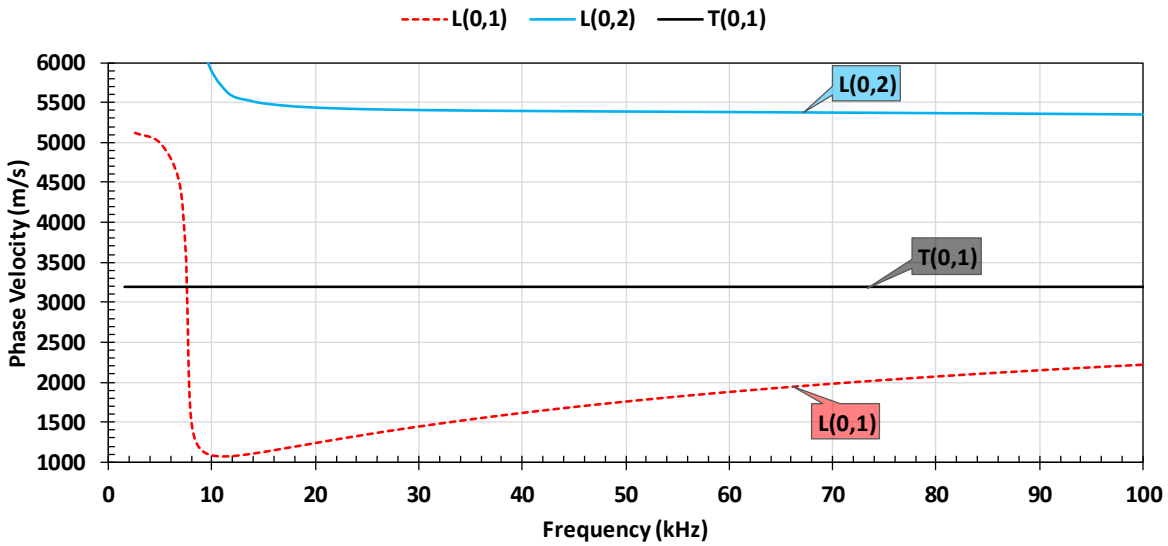

Figure 3.1. Example of dispersion curves created by RAPID software for an eight-inch schedule 40 pipes showing only the available axisymmetric wave modes.

3.2.2 Defect's schematic

The most common type of defect in pipes is corrosion. Creating corrosion patches in the pipes is a time consuming and expensive procedure. Nonetheless, the response of any type of metal-loss within the pipe is approximately the same. Therefore, a common approach in laboratory trials is to introduce a material loss. Since the main focus of this thesis is to develop signal processing algorithms, the second approach is chosen. The defects are created using a saw-cut by thinning the wall thickness of the pipes' circumference. A common practice to specify the defect size in UGW inspection is to specify the percentage of Cross-Sectional Area (CSA) loss within the circumference of the pipe. Figure 3.2 illustrates the schematic of the introduced defects in the laboratory trials with an example test case showing the 3% CSA material loss in the wall thickness of the pipe.

Figure 3.2. (a) Schematic of defects with examples of cord length (b) and depth (c) of a 3% CSA defect.

Table 3.1 specifies the defect sizes in the tests. Seven different defect sizes starting from 2% CSA to 8% CSA is used. The detectability of the defects is dependent on the SNR of the results rather than the defect type. Therefore, defect with smaller CSA sizes are harder to detect.

Table 3.1. Defects specifications

CSA (%)	Defect Depth (mm)	Cord Length (mm)	Arc Length (mm)
2	3.10	51.75	52.24
3	4.10	59.37	60.12
4	5.00	65.43	66.48
5	5.80	70.34	71.61
6	6.50	74.34	75.85
7	7.20	78.12	79.87
8	7.90	81.69	83.71

In inspections, the detection of defects is done with the help of Signal to Noise Ratio. In this thesis, the SNR is calculated using (3.1):

$$\text{SNR}=20*\log10\left(\frac{\sqrt{\frac{1}{\mathrm{N}}\sum_{1}^{\mathrm{N}} Signal[n]^2}}{\sqrt{\frac{1}{\mathrm{M}}\sum_{1}^{\mathrm{M}} Noise[m]^2}}\right) \quad (3.1)$$

where the Signal represents the samples where the defect signal is expected to be received and every other sample that does not represent a feature (e.g. pipe end, defect, etc.) is considered as the Noise. Therefore, the nominator represents the energy of the defect signal and the denominator represents the energy of the noise. The SNR of defects is demonstrated in Table 3.2 and is plotted in Figure 3.3 where results of Defect 1 and 2 are illustrated in (a) and (b), respectively.

Table 3.2. The SNR of each defect with respect to the test frequency

	CSA	Frequency (kHz)										
	(%)	**30**	**32**	**34**	**36**	**38**	**40**	**42**	**44**	**46**	**48**	**50**
Defect 1	**8**	14.6	16.8	19.6	21.0	21.7	22.2	21.8	20.4	18.3	15.7	12.6
	7	13.5	15.5	18.1	19.6	20.6	21.3	20.9	19.4	17.2	14.5	11.3
	6	11.7	13.5	15.8	17.8	18.7	19.3	18.7	17.2	15.0	12.4	9.2
	5	9.2	11.0	13.7	15.0	16.0	16.7	16.0	14.4	12.0	9.3	6.1
	4	7.1	8.8	11.1	12.1	13.1	13.7	13.2	11.7	9.5	6.8	3.5
	3	4.2	5.9	8.1	8.6	9.0	9.5	9.0	7.6	5.4	2.8	−0.5
	2	1.4	2.6	3.1	2.3	2.0	2.7	3.2	2.6	0.9	-1.4	-4.4
Defect 2	**8**	16.0	20.3	21.5	22.3	20.8	17.8	15.8	14.1	11.3	8.2	4.5
	7	14.8	19.0	20.4	21.1	19.3	16.3	14.6	12.8	10.1	7.1	3.4
	6	12.4	16.6	18.1	19.1	17.0	13.8	12.1	10.3	7.6	4.6	1.20
	5	10.1	14.1	15.7	16.6	14.2	10.8	9.4	7.6	5.0	2.2	-1.0
	4	8.2	12.1	13.5	14.2	11.6	8.2	7.0	5.2	2.5	-0.0	-3.0
	3	5.9	9.6	10.7	11.1	8.0	3.9	2.9	1.6	-0.7	-2.6	-5.2
	2	5.0	8.5	9.3	9.5	5.8	1.5	-0.0	-1.3	-2.9	-4.9	-6.7

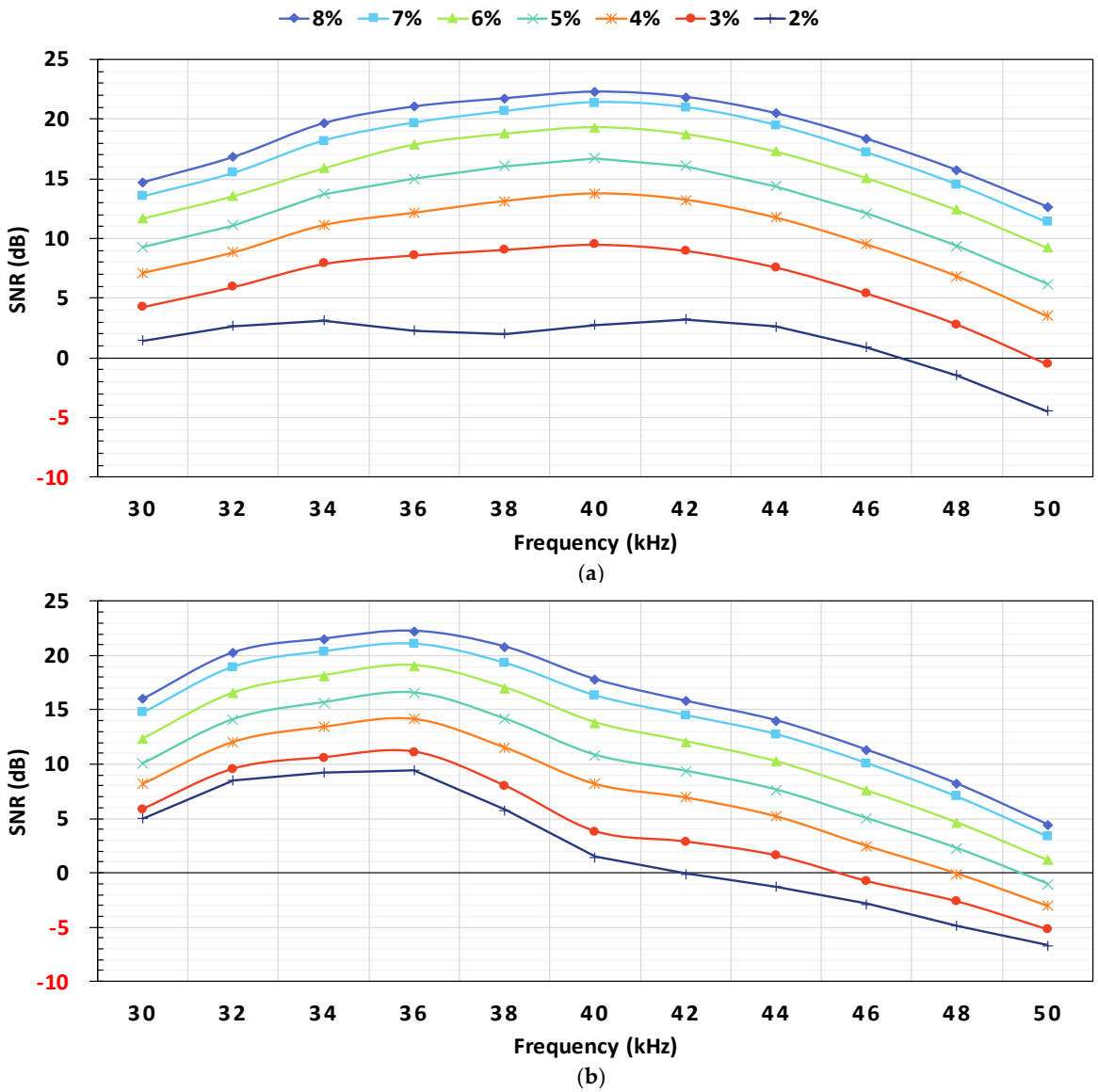

Figure 3.3. The generated SNR of (a) Defect 1 and (b) Defect 2 for each defect size with respect to the test frequencies.

3.2.3 Pipe's schematic and signal routes

The test specimen used in the laboratory trials is an eight-inch schedule 40 steel pipe which is one of the common pipes used in the oil and gas industry. The total length of the pipe is 6 meters. The test tool is installed 1.5 m apart from the back end of the pipe and the forward test direction is selected towards the front end of the pipe. The signal processing algorithms will be tested with regards to two different defect locations; Defect 1 which is located 3 m and Defect 2 which is located 4 m away from the inspection point. Figure 3.4 illustrates the schematic of this test setup with the expected signal routes for both direct and indirect signals.

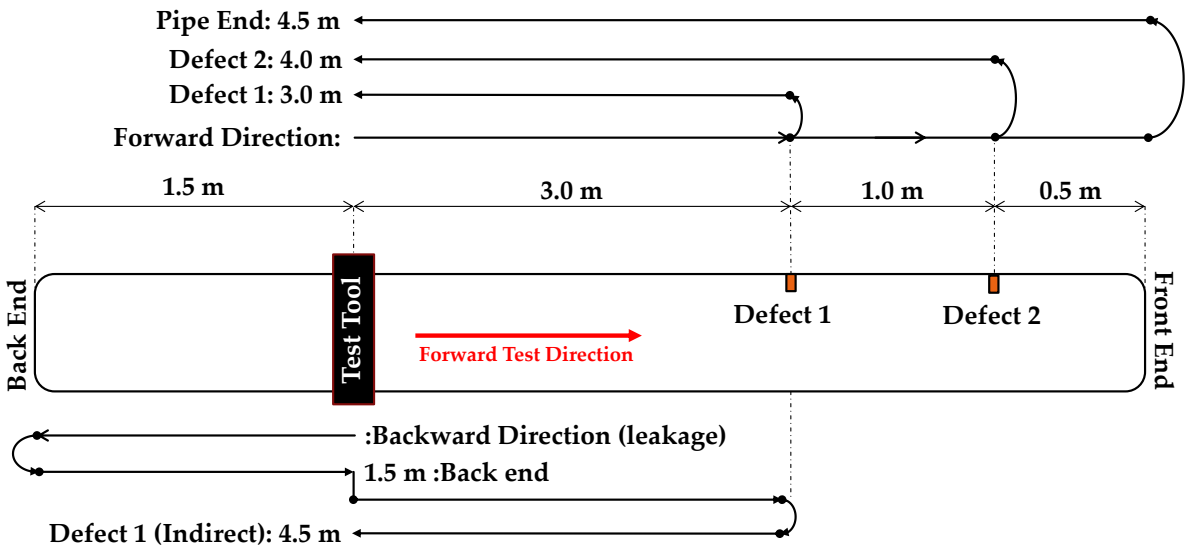

Figure 3.4. Schematic of the setup in laboratory trials and the expected signal routes.

Defect 1 was initially created, and the data of each defect size was captured with multiple frequencies. Afterward, the same procedure was repeated for Defect 2. Both defects have similar shapes and are created using the same procedure. The main difference is in their location. Although both can be considered as defects with same size and characteristics, the amount of coherent noise in the second defect location is greater than the first defect.

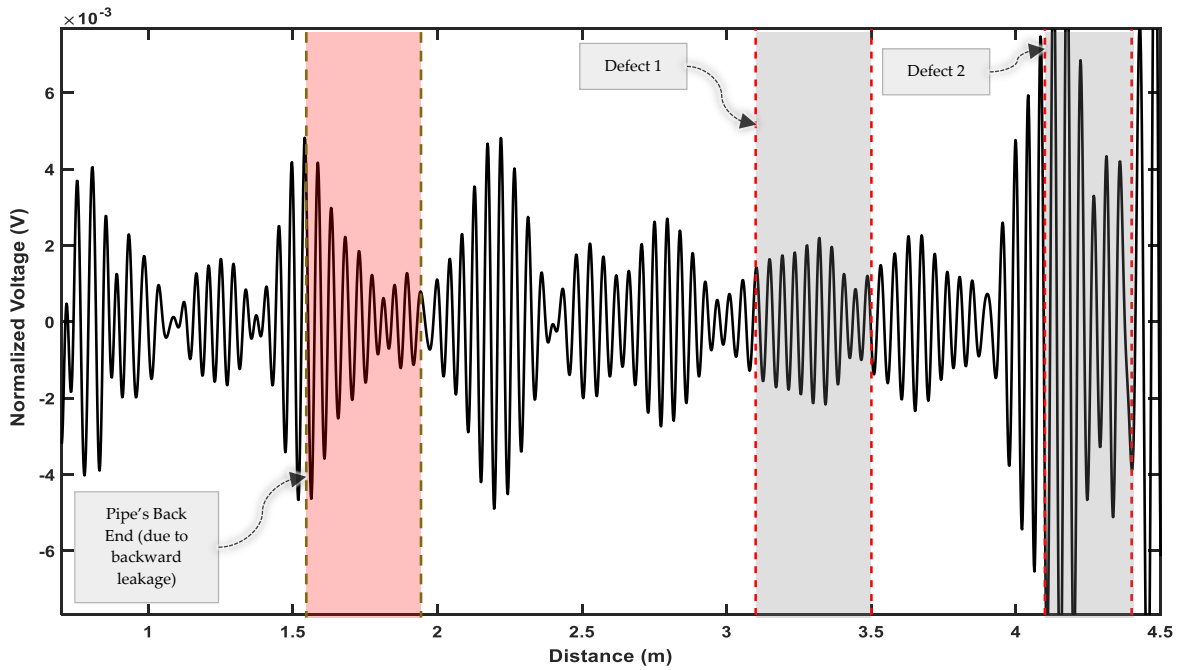

Figure 3.5. Baseline generated from 37 kHz excitation frequency (black line) where the expected location of the signal received from each feature is marked.

Figure 3.5 shows a baseline of the test specimen using 37 kHz which evidently demonstrates that the second defect location consists of stronger coherent noise. This was the main reason

for selecting this location for the placement of Defect 2. Furthermore, this location is closer to the pipe end. The goal of this setup is to assess the capability of the techniques in three main goals. The first and foremost is to verify the feasibility of applying the same signal processing algorithm to multiple defects within the same test specimen. The second is to assess the effect of regional coherent noise on the performance of the algorithm. The last is that it verifies the feasibility of applying the algorithms on defects located near strong features (pipe end).

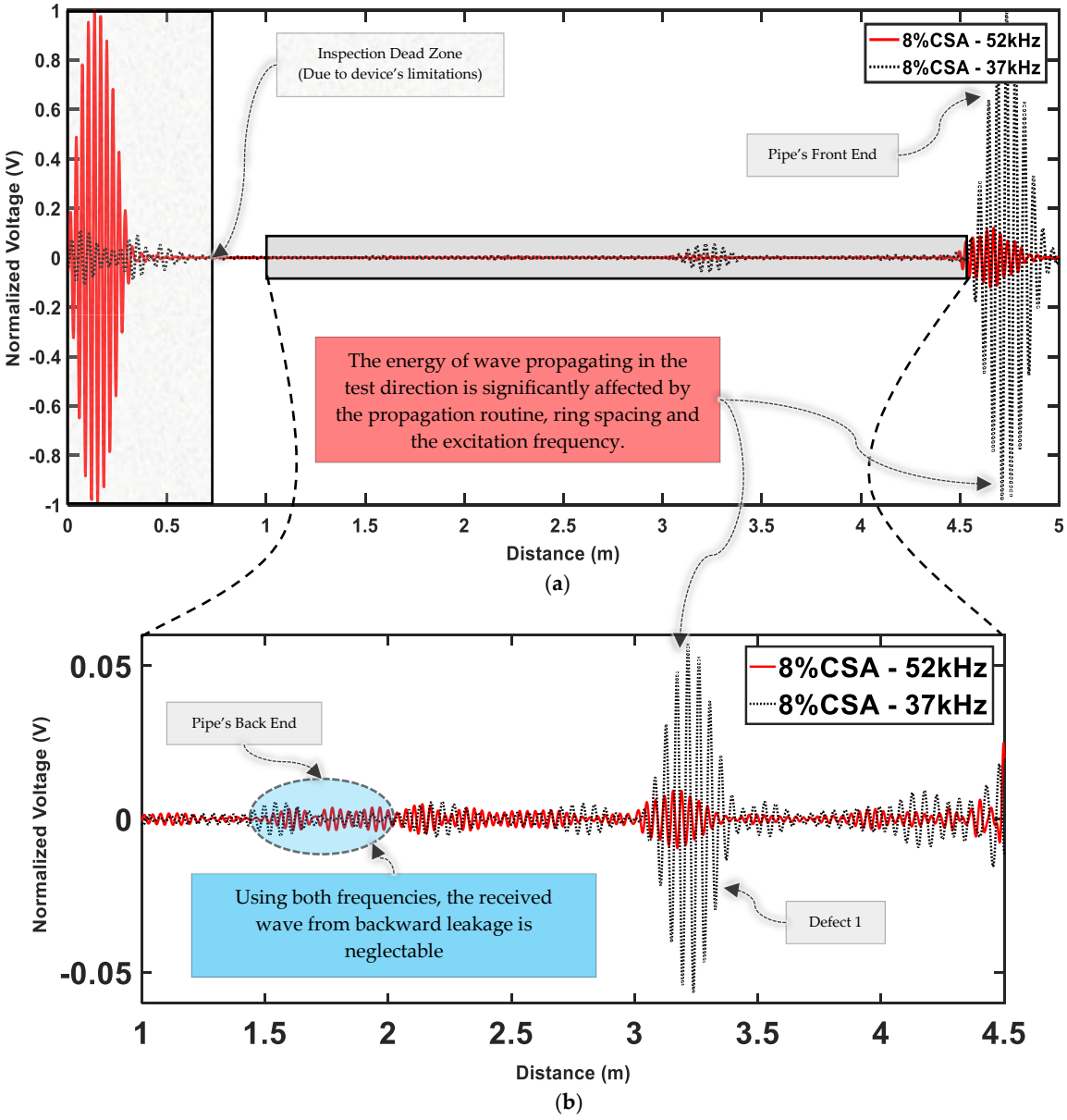

Figure 3.6. Illustration of performance of propagation routine in achieving a unidirectional signal using two frequencies of 52 (red line) and 37 kHz (black dotted line). The signal received from Defect 1 with 8% CSA is located between 3 – 3.5 m, Pipe's Back End is between 1.5 – 2 m and Pipe's Front End is between 4.5 – 5 m. (a) shows the overall result with the pipe's front-end response. For better illustration of the defect and noise regions, (b) shows the zoomed-in region in the range of 1 – 4.5 m.

Figure 3.6 compares the results using two excitation frequencies of 37 and 52 kHz on Defect-1 with 8% CSA size. The purpose of this figure is to illustrate the effect of the propagation

routine on the signals traveling in and opposite to the test direction. (a) shows the results including the pipe end and dead zone of this inspection. The dead zone is defined as a region close to the inspection point where the received signals are not representative of the actual results. The reason for this dead zone is the inherent design of the device where the amplifiers and transducers are still affected by the excitation. As an example, transducers will continue with their movement even after the excitation sequence stops which will introduce the noise in the reading of signals. Hence, the signals received from this region are not accurate and cannot be used for inspection. In (b), the region between 1.0 – 4.5 m is enlarged the defect region and backward leakage.

As explained previously, backward leakage is a wave generated at the point of excitation which is traveling opposite to the intended test direction. the main purpose of the propagation routine is to reduce or preferably eliminate, this backward leakage and any wave that is received from the opposite direction. With regards to the signal routes shown in Figure 3.4, the signal from backward leakage is expected to be received between 1.5 – 2 m. In Figure 3.6b, it is illustrated that using both excitation sequences, signal received due to this backward leakage is significantly reduced. On the other hand, it can be seen that the signal received from 37 kHz on Defect 1 region (3 – 3.5 m) is stronger than the one from 52 kHz. The same trend is observed with regards to the signal of pipe's front end (received in between 4.5 – 5 m) in Figure 3.6a. The cause of this phenomenon is, in fact, the propagation routine. While the main focus of propagation routine is to eliminate the backward leakage, it also affects the forward propagation as the waves are generated in both directions. Since fixed ring spacing is used, using some frequencies, the forward propagations of rings can be overlapping; this will cause constructive superposition of waves and enhances the energy of forwarding propagating waves. On the other hand, it also means that it can result in destructive superposition for some frequencies. Therefore, not all frequencies are recommended for inspection. The power output of each frequency with regards to the propagation routine is affected by the dispersion curves, ring spacing and number of used rings.

3.3 Finite element modeling

The main goal in this thesis is to develop signal processing algorithms that enhance data interpretation in the presence of coherent noise. In order to increase the difficulty of defect detection, unlike other developed FEM models in the literature, this model inherently generates coherent flexural noise by using variable TFs for each source point of excitation. This FEM model was developed using ABAQUS software [85]. The setup of this model is explained in Section 3.3.1, followed by the expected signal routes in Section 3.3.2. Section 3.3.3 demonstrates the difference between using ideal or variable TFs at the point of

excitation. The effect of quasi-axisymmetric wave generation and the used signal processing routine for the generation of unidirectional signals on excitation frequency is explained in 3.3.4.

3.3.1 FEM Setup

The simulated pipe is based on the characteristics of an 8-inch schedule 40 steel pipe with a length of 6 m, an outer diameter of 219.1 mm, a thickness of 8.18 mm, Young's Modulus of 210 GPa, density of 7850 kg⁄m^3 and Poisson's Ratio of 0.3. The excitation frequency in the test was 30 kHz. In order to capture the smallest wavelength in the operating frequency, at least 8 elements are required in the axial direction [32], [86], [87]. Therefore, the global seed size was set as 2.5 mm and the time increment was set as 10×10^{-7} s to provide a satisfactory accuracy in generation and reception of all the wave modes within the frequency band. The modeled test tool included 3 rings of 32 linearly spaced source points, located 1 m away from the back end of the pipe. Each source point of the rings is numbered clockwise starting from 90°. The schematic of this setup is illustrated in Figure 3.7.

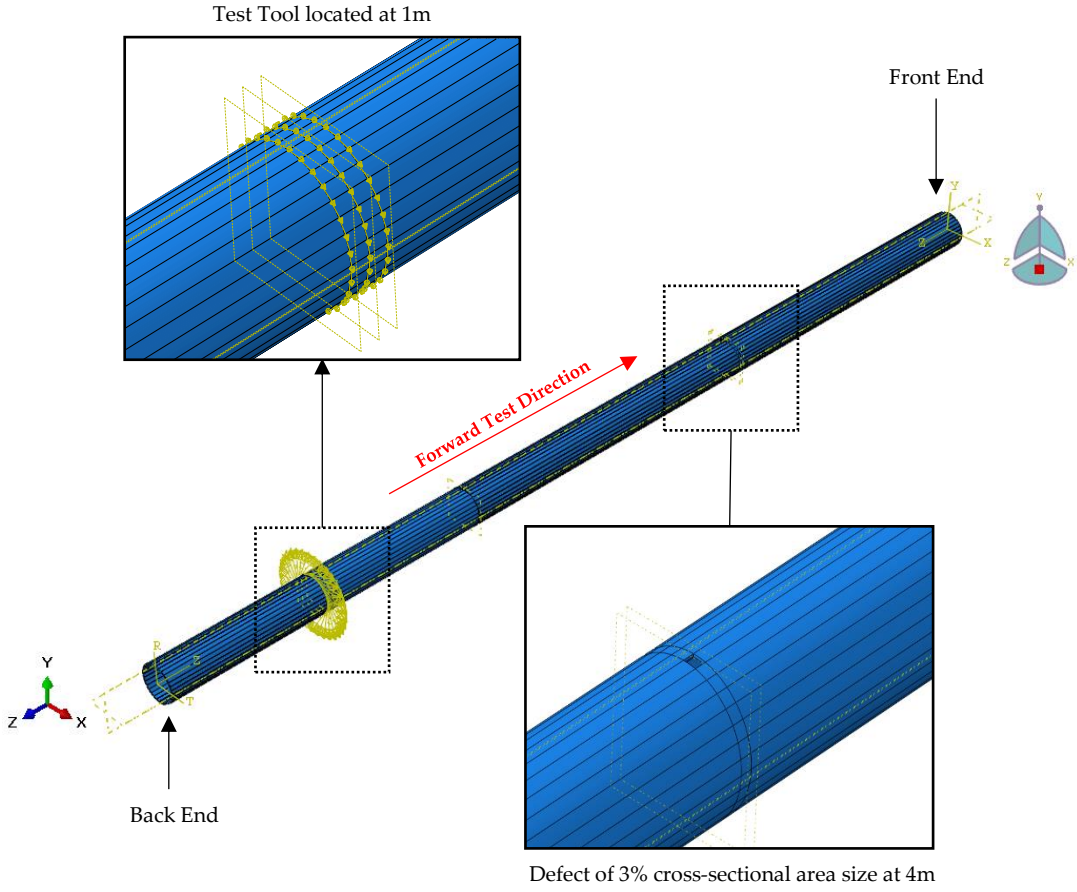

Figure 3.7. Schematic of the FEM where the Test Tool (3-rings) and defect are located at 1 and 4 m away from the back end of the pipe, respectively.

This type of FEM simulation of guided waves signals in pipes was developed in previous studies [24], [46], [87]–[90]. The generated models have also been validated by confirming the accuracy of the received signals from both the device [90] and 3D laser vibrometer [24], [87].

Nonetheless, this type of FEM generally produces a limited amount of noise due to the perfect condition of the model. The main aim of this paper and the developed model is to investigate the performance of the algorithm in the presence of coherent noise. Therefore, in order to generate flexural noise in the test, different TFs were applied to the excitation sequence of each source point. Since the minimum satisfactory number of elements is used, the TFs will not affect the integrity of the model and all the existing wave modes in the test will be captured. Apart from these TFs, all other limits and parameters were in line with the verified models in the previous studies.

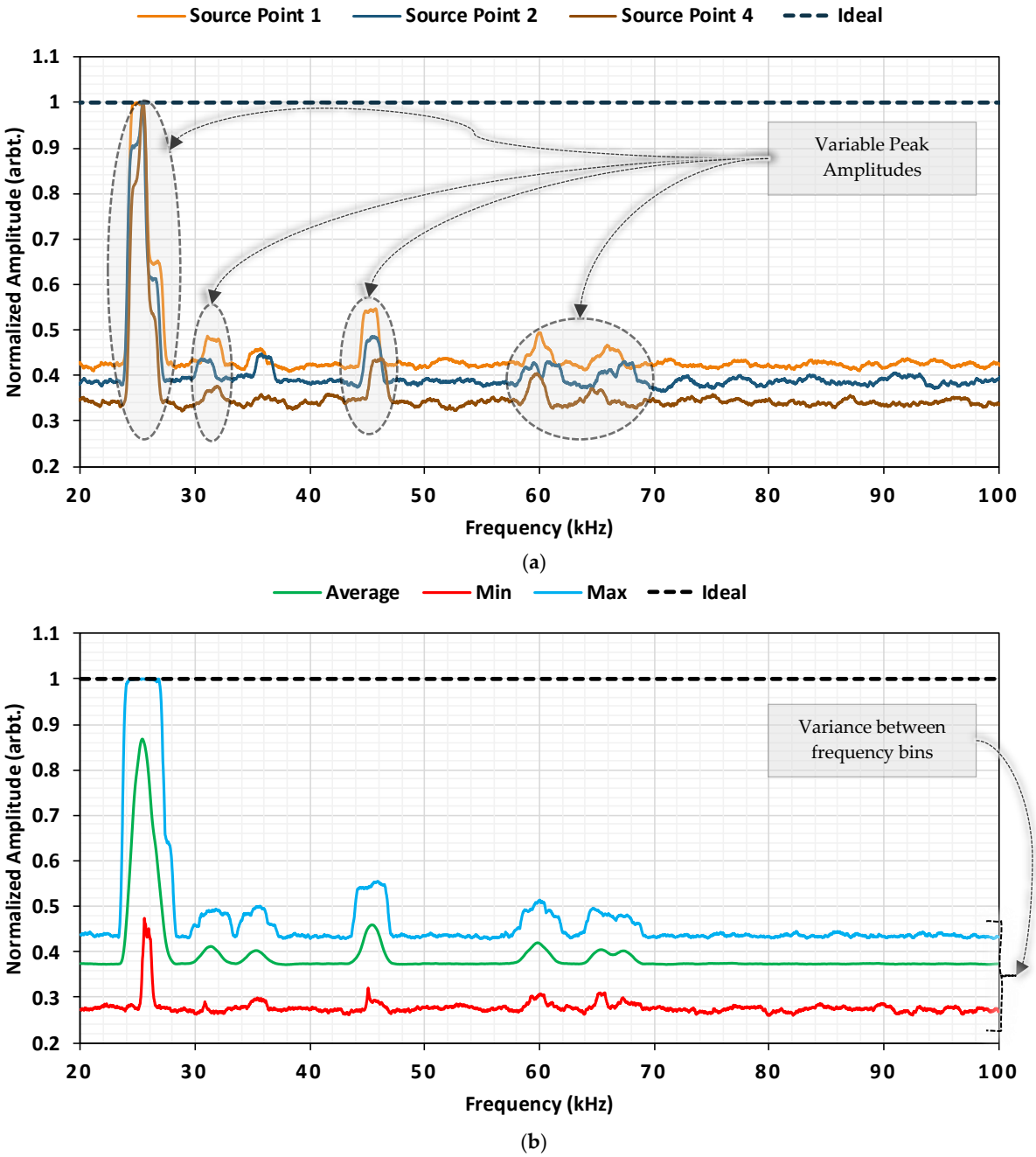

Figure 3.8. Example of designed TFs where (a) compares 3 different source points vs the ideal one and (b) shows the maximum, average, and minimum amplitudes of the frequency bins across all used TFs in one test case.

In 2013, Engineer [22] extracted the broadband frequency response of transducers with regards to various coupling forces using Teletest piezo-electric transducers. The variability of transducers' TF is explained in Section 2.3 and an example of the resultant displacement magnitude of the transducers under different pressure forces is given in Figure 2.4b-c. The reported TF was used as a reference and variability in terms of amplitude and phase was introduced to generate a variable TF for each transducer. Figure 3.8a shows examples of designed TFs used in a FEM test case where (a) illustrates the TFs used for three different source points and (b) shows the maximum, minimum, and average values across all used TFs in this test case.

Afterward, TFs are multiplied by the ideal excitation's frequency response, which is a 10 cycle 30 kHz Hann-windowed sine wave and then inverted back into the time domain. The generated time-domain signals are used as input files for each of the source points. Additionally, the signals of the second array are phase delayed and inverted with regards to the 30 mm ring spacing cancellation algorithm [23], [47]. The overall system works in the pulse-echo mode and the signals were received from the same ideal point sources. Figure 3.9 shows the flowchart of signal generation for the FEM test case. The signal generation, as well as the post-processing, were done using MATLAB-R2016a [91]. On the reception side, in order to increase the coherent noise and difficulty of defect detection, signals of fewer source points can be used for processing. Furthermore, this selection of points can be non-symmetric which further increases the amount of coherent noise generated in the results.

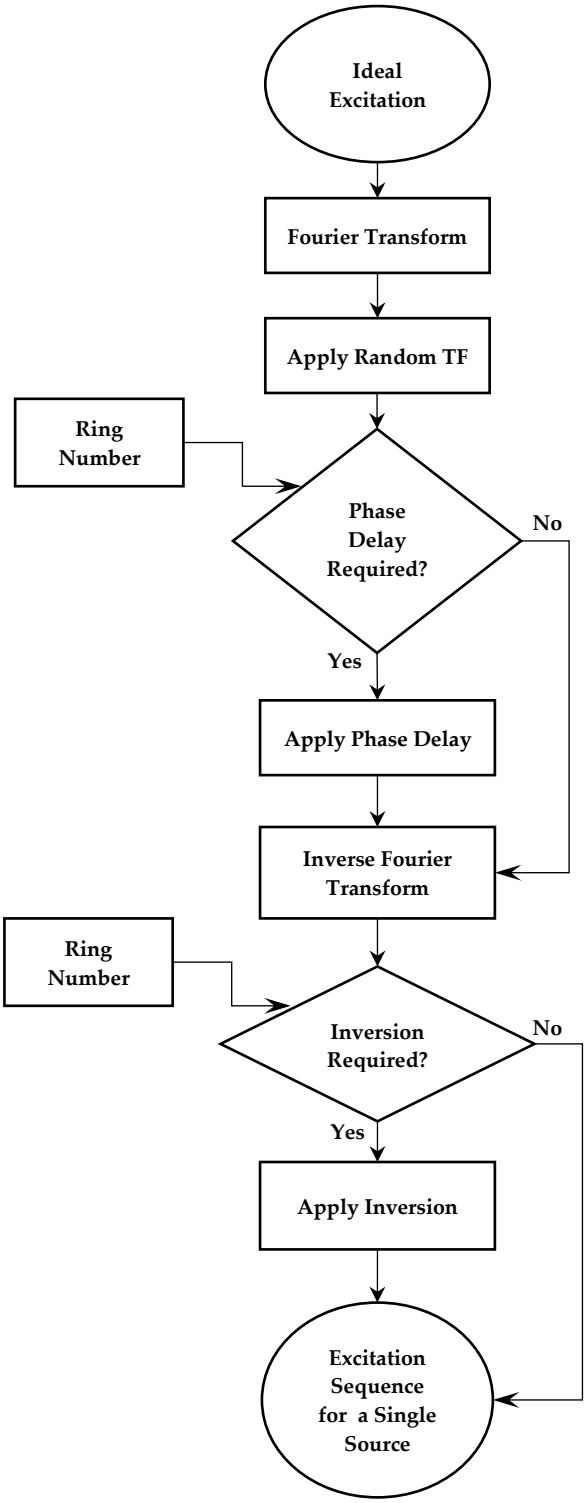

Figure 3.9. Flowchart of signal generation for FEM test case.

3.3.2 Signal Routes

The signal routes of the FEM test are shown in Figure 3.10. As can be seen, the first directly received signal from the forward test direction is the defect signal which is received at 3 m, followed by the front-end signal at 5 m. However, as the TF and linearity of reception points are not ideal, a backward leakage signal will exist, propagating in the forward direction.

This leakage would be received at 1 m but due to the backward cancellation algorithm, it will not be observable. However, the reflection of this signal with the defect signal would be received from the forward direction, leading to a false alarm at 4 m. In these tests, since both signals at 3 and 4 m have the same characteristics, they are both considered defect signals even though the second signal is a false detection.

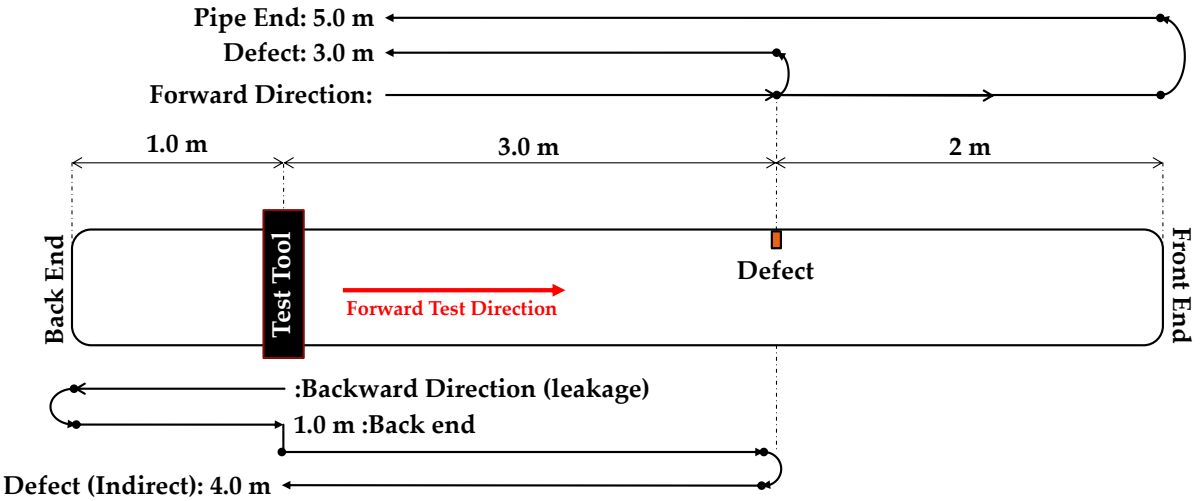

Figure 3.10. Schematic of the pipe set up in the FEM model and the expected signal routes.

3.3.3 Comparison between Ideal and Non-Ideal Excitation

Figure 3.11 to Figure 3.13 illustrates the 3D representation of wave propagation (in terms of displacement) on the surface of the pipe. In these figures, the excitation sequences are a 10-cycle Hann-windowed sine wave and the backward cancellation algorithm is applied. The focus of these features is the non-linearities in the circumferential distribution of each cycle within different wave packages. Circumferential displacement for a perfect torsional wave is expected to be perfectly axisymmetric. In the axial direction, differences between wave cycles can exist due to other propagation effects such as attenuation and backward cancellation. The ideal test case where no TFs are applied to the excitation sequences is shown in Figure 3.11. On the other hand, variable TFs are applied to the excitation sequences used in Figure 3.13 and Figure 3.14.

Figure 3.11a shows the generated wave in the ideal test case. As can be seen, only a single wave is propagating align with the forward test direction (towards the right end of the pipe). Also, approximately no coherent noise (flexural waves) is observable within this wave. This validates the effectiveness of the signal processing routine used for the generation of waves since no backward leakage is generated and the wave is perfectly axisymmetric.

Figure 3.11(b-c). shows the scattering results of the ideal wave (illustrated in Figure 3.11a) with the defect. (b) is the rebound wave generated which is traveling towards the test point and (c) is the remaining energy of the ideal wave traveling towards the pipe's front end. With regards to these figures, the following hypothesis are drawn:

- The energy of the rebound wave is significantly less than the remaining energy of the wave traveling in the forward test direction. This wave is the main required for determining the defect location.
- A significant amount of low order flexurals are observed in the rebound wave. On the other hand, the remaining wave traveling in the forward direction is less affected by the flexural waves as it contains most of the energy from the ideal excitation.
- Although ideal axisymmetric wave was generated at the point of excitation, flexural waves were introduced by the wave mode conversion of the defects. Hence, the removal of flexural waves completely from the tests is a challenging task.

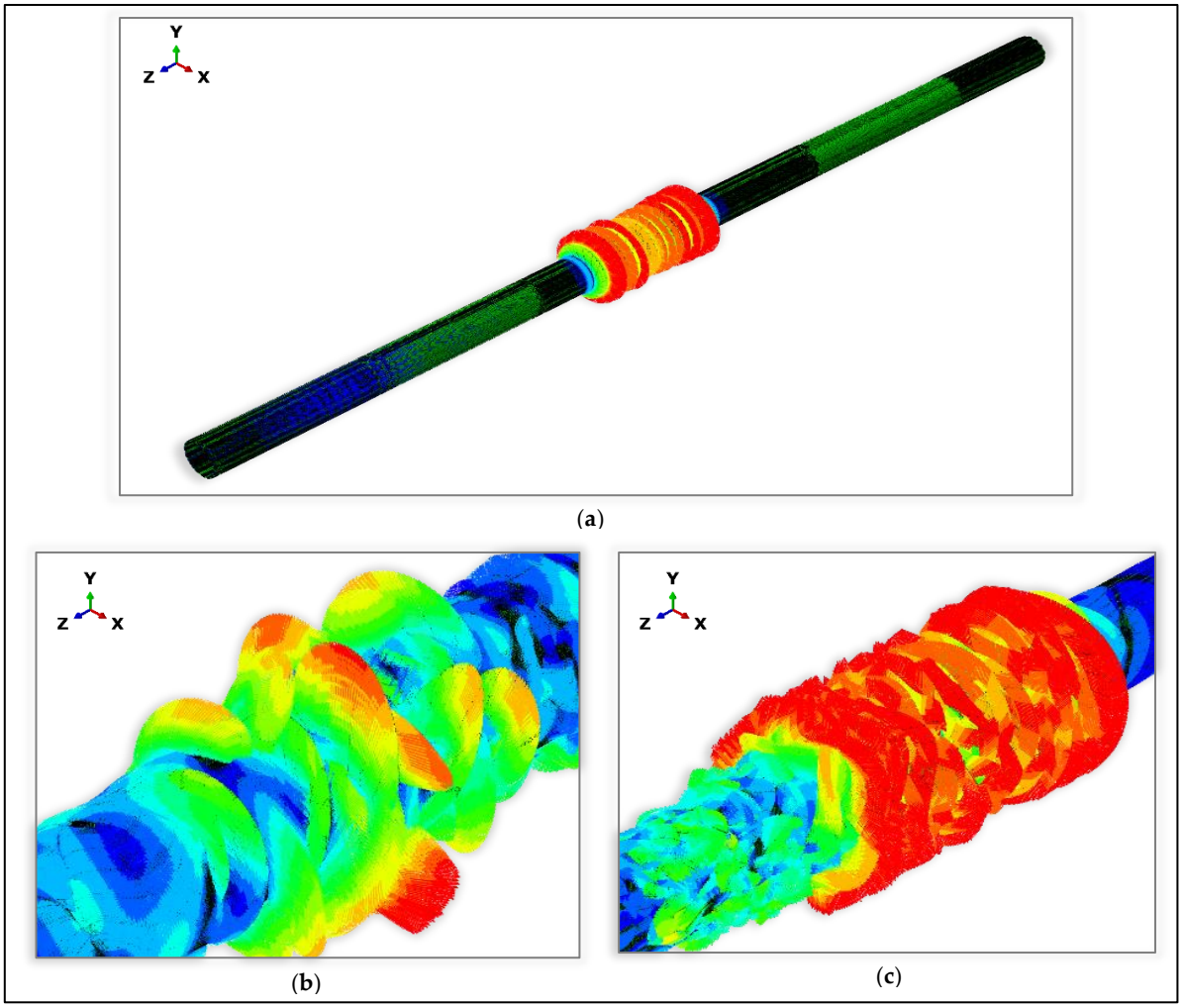

Figure 3.11. 3D representations of wave propagation in a FEM test case where ideal TFs are assumed. (a) shows the excitation waveform test direction, (b) shows the scattered waveform generated from

defect traveling backward and (c) shows the resultant forward propagation of the excitation wave traveling towards the pipe's front end.

Figure 3.12 illustrates the effect of applying variable TFs to the excitation sequences of each source point at the excitation point. As opposed to the ideal scenario, the backward cancellation algorithm is no longer capable of removing the wave traveling in the opposite test direction. This results in backward leakage, which propagates towards the pipe's back end (left side). Furthermore, the array is able to cancel the flexural waves only if the source points are placed linearly across the circumference of the pipe and all the source points are exciting the same excitation sequences. Hence, due to the variability of the TFs, the array system is no longer capable of canceling all flexural waves. This affects the forward propagating wave, the backward leakage, and the overall coherent noise level within the structure. Hence, the excited wave for testing is no longer ideal at the point of excitation and is contaminated by the flexural waves.

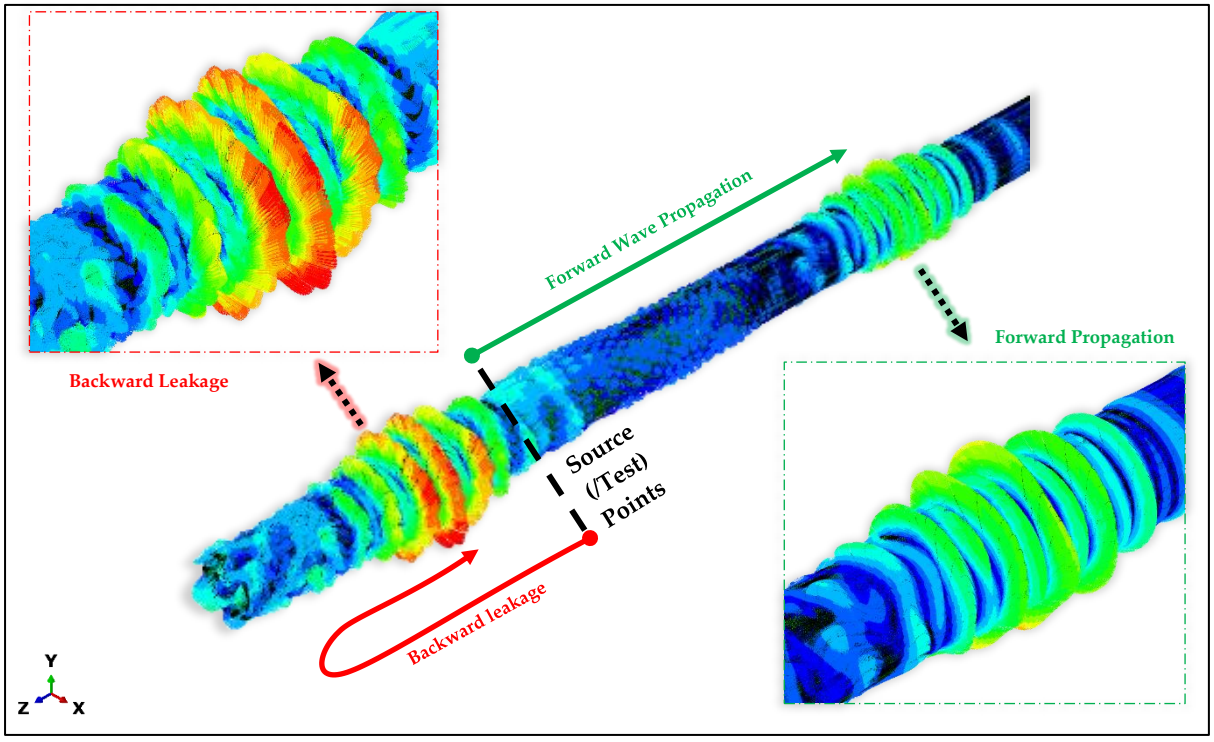

Figure 3.12. 3D representation of generated waves at the point of excitation in a FEM test case where random TFs are applied to each the excitation sequence of each source point. The backward leakage and non-linearities are introduced due to variability in TFs of each source point.

Figure 3.14 shows the signal of an individual point without TF (black line) and with TF (red line). As can be seen, by using TFs at the point of excitation, the forward amplitude of the pipe end (located between 5 – 6 m) is reduced and the result is significantly affected by the flexural waves (e.g. 2 – 3 m).

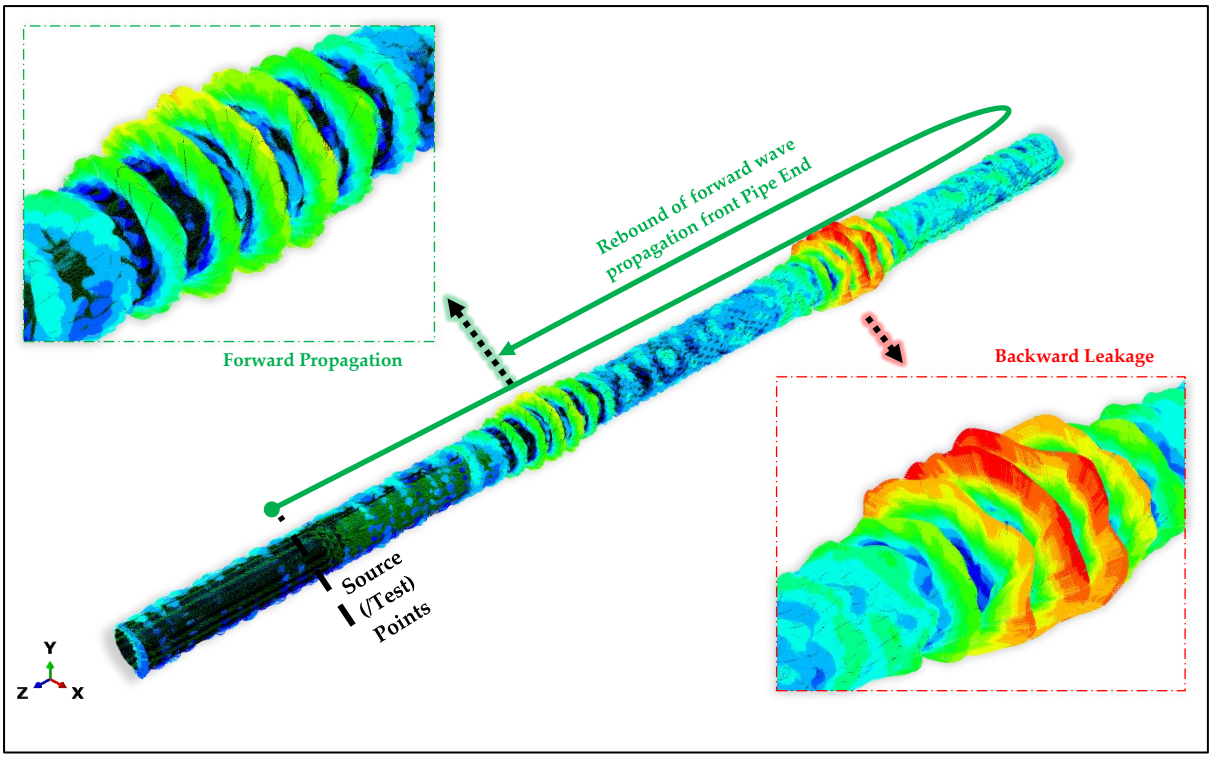

Figure 3.13. 3D representation of the return of non-ideal excitation from pipe end in a FEM test case. Both forward propagation and backward leakage are affected by the coherent noise generated from the defect.

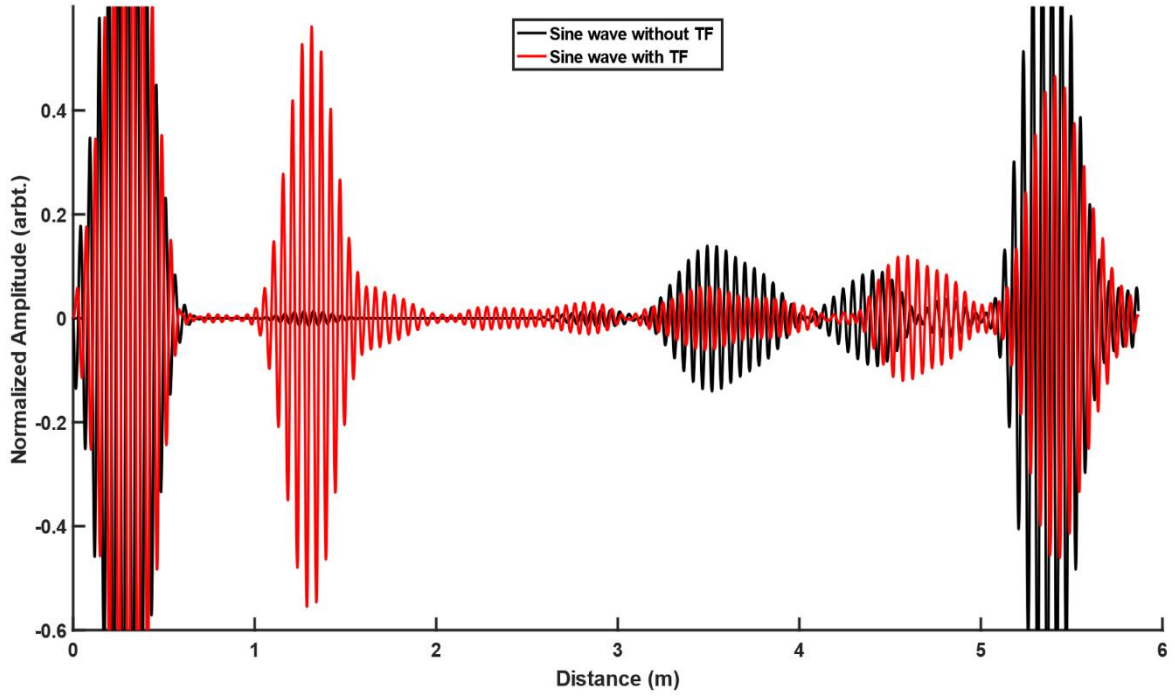

Figure 3.14. Comparison of signals received from a single source point reception with (red) and without (black) the TFs. In this figure, no TF or backward cancellation is applied at the reception side.

3.3.4 Effect of using arrays for wave generation

As explained previously, arrays are used for generating an axisymmetric unidirectional wave. With regard to the backward cancellation algorithm, certain frequencies are expected to have higher excitation energies[6]. In order to illustrate the effect of frequency on the outcome of the resultant wave propagating in forwarding direction, a chirp signal is used as excitation sequence to a FEM test case. A chirp signal is a type of signal where its' frequency content changes with time. In this test case, a linear chirp signal is used with starting frequency of 20 kHz and ending frequency of 100 kHz. This signal is windowed using a Tukey function with value of 0.15 [78].

Figure 3.15 shows the comparison between the excited and received waveforms without using variable TFs. (a) shows excitation of a single ring without any backward cancellation applied and (b) shows a 2-ring excitation with backward cancellation algorithm applied. The resultant propagating wave (after a short distance of 0.003 m) is shown in the second axis by red lines. in both cases, no variable TFs were introduced to the excitation sequence. As can be seen in (a), even without using a backward cancellation algorithm, the resultant displacement in the received wave is significantly less than the transmitted wave. Furthermore, as the frequency increases with time, it is evident that higher frequencies are resulting in less displacement in the structure. One of the main reasons behind these reductions is that rather than pure axisymmetric waves, quasi-axisymmetric waves are generated. If a uniform excitation is loaded around all of the circumferences, a pure axisymmetric wave is generated where these variations are not observed [78]. On the other hand, by placing linear excitation points around the circumference, both axisymmetric and flexural waves are generated at the point of excitation. However, due to the linear placement of excitation points and the excitation of similar waveforms, the flexural waves are canceled after a short propagation distance and only the axisymmetric wave remains [32]. Since higher frequencies result in generation of more flexural waves, it is expected that lower frequencies result in generation of axisymmetric waves with higher displacements (in comparison to the higher frequencies). On the other hand, applying the backward cancellation algorithm also affects the resultant displacement outcome using each frequency. This is shown in Figure 3.15 where the received signal of forwarding propagation (red line) is significantly reduced in the region of 50 kHz (230 – 260 μs). Such differences are also noted in experimental results using both sine waves [24] and chirp signals as excitation sequences [23].

[6] See Section 2.4 for further information about the signal processing routine.

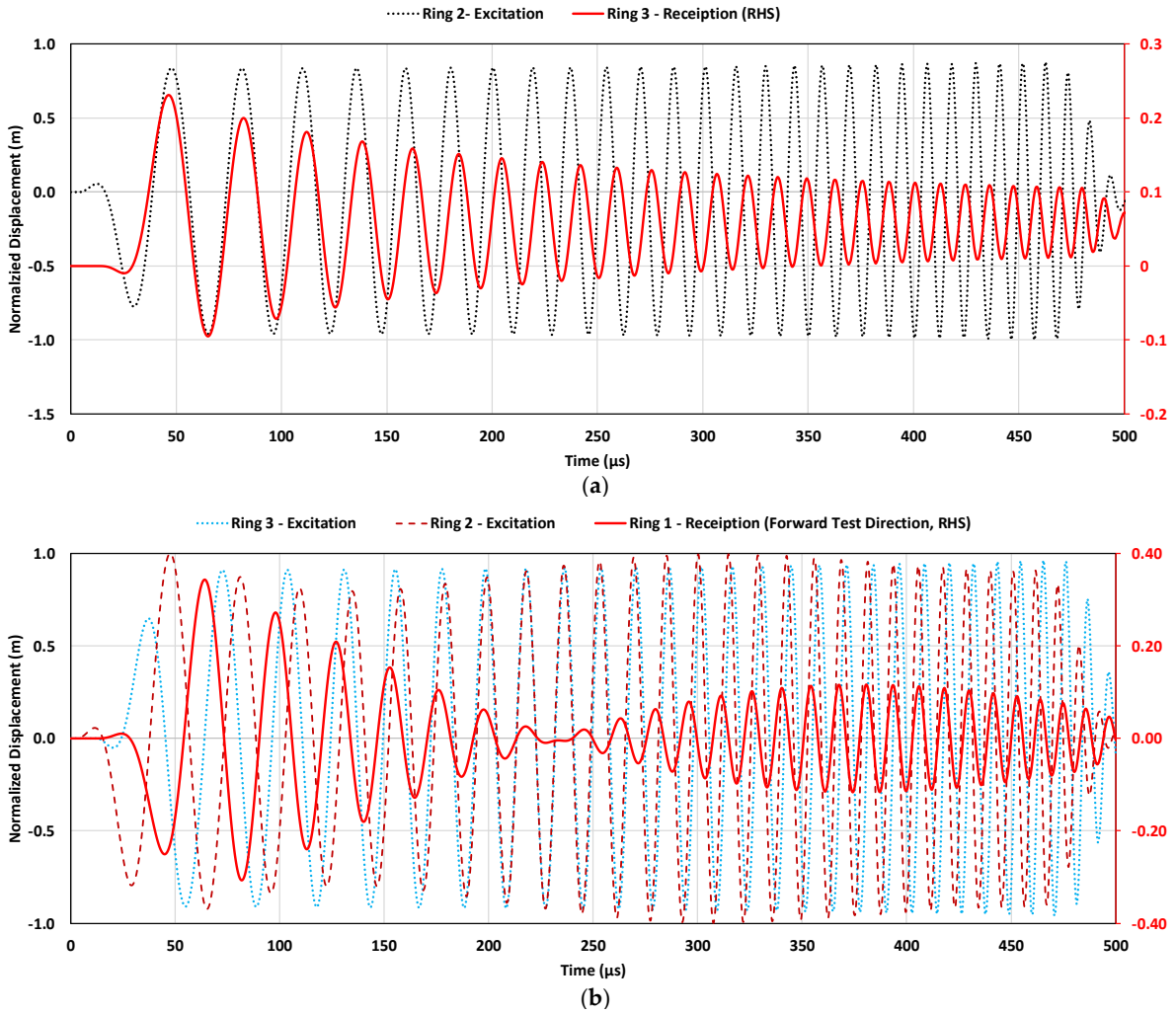

Figure 3.15. Effect of unidirectional torsional wave excitation using the FEM model. (a) shows the comparison between excitation sequence and the reception after a short propagation distance and (b) shows the additional effect of backward cancellation on forwarding propagation.

3.4 Chapter Summary

In this chapter, the setup of laboratory trials and the FEM model are described in Sections 3.2 and 3.3, respectively. T(0,1) was selected as the main wave mode of operation. In terms of excitation frequency, it was decided to use frequencies in the range of 30 – 50 kHz. The main waveform signal is a 10 cycle Hann-windowed sine wave. Two defect location exists in laboratory trials where the second location (Defect 2) observes higher amount of coherent noise. Both defect locations are assessed with different defect sizes, starting from 2% CSA to 8% CSA with incremental steps of 1%CSA. The FEM model is mainly designed for development of signal processing algorithm. Hence, random TFs were introduced to the excitation source points in order to increase the amount of coherent noise in the tests. The effect of the variability of TFs is explained in Section 3.3.3. Furthermore, the overall effect of

using arrays is described with both simulated (See Sections 3.3.3 & 3.3.4) and experimental data (see Section 3.2.3).

Chapter Four

Defect Detection Using Spatial Differences between UGW modes

4.1 Overview

In this chapter, a novel algorithm is designed which uses spatial and temporal differences of the wave modes in order to identify the defect signals. Most of the signal processing algorithms in the literature review, use a single time-domain signal achieved from the device's general propagation routine and further process it in order to increase the SNR or detect the defect. Nonetheless, the device consists of rings of at least 24 transducers. Unlike other algorithms for defect detection, the proposed algorithm considers the spatial differences between the wave modes by utilizing the information gained from individual sensors. The performance assessment was done using both simulated and experimental data where the algorithm could successfully detect defects with sizes as small as 2% CSA. On the other hand, the other aim of the proposed algorithm is to illustrate the possibility of using all of the individual transducers for defect detection rather than using the single signal achieved after the general propagation routine of the device; by using this approach and considering the spatial differences between wave modes, more accurate processing algorithms can be designed which leads to easier interpretation of the results during inspection. The reported results confirm the feasibility as well as the capability of the developed algorithm and mentioned approach.

A part of the research conducted in this chapter has been presented in the National Structural Integrity Research Centre (NSIRC) Conference, Cambridge, United Kingdom in July 2019 [92]. Furthermore, this chapter resulted in a journal publication in MDPI Applied Sciences [93].

This chapter starts with an introduction to the spatial arrival of different guided wave modes from features (in Section 4.2). After illustrating the main differences between the required wave mode and unwanted spatial noise, the methodology used for identification of the defect is explained in Section 4.3. In order to provide a better description of different processing stages of this algorithm, in Section 4.4, the algorithm is applied to a simulated signal where each step is illustrated. The experimental validation was done on two defect locations; where, in

comparison to the first defect, the second defect is located in a region more affected by the local coherent spatial noise. In Sections 4.5 and 4.6, the results of the first defect and second defect are reported, respectively. The overall comparison of the results is undertaken in Section 4.7 followed by conclusions of this chapter in Section 4.8.

4.2 Spatial variances of the wave modes

UGWs are multimodal and dispersive. When an excited axisymmetric wave hits a feature, the resultant scattered wave would consist of the excited axisymmetric and its associated flexural waves. Depending on the feature shapes, the energy distribution of each of the created wave modes would be different. As an example, a perfectly axisymmetric feature in the ideal scenario would result in the generation of a perfect axisymmetric response with no other flexural waves. In these scenarios, if the axisymmetric wave is stronger than the coherent regional noises in the area, an anomaly is reported by the inspectors. However, since it is a visual interpretation, in some scenarios, the resultant mixture of flexurals can easily lead to false alarms due to their coherence to the expected received signal. Furthermore, the axisymmetric wave can be smaller than the local noise level, and therefore would not be detected. These are some of the main challenges faced when inspecting the temporal domain.

Figure 4.1 shows the spatial arrival of the signals received from two rings of 32 source points. These signals are generated by the finite element model (FEM) [78]. In this setup, ideal source points are assumed, which leads to the generation of a perfect T(0,1) wave mode in all of the figures except (b) and (i), where the frequency response of each transducer is variable. The red and blue signals are showing the first and second ring, respectively, and the reference is illustrated by the black dotted line. Thus, the values inside the reference would mean a negative phase, and values higher than the circle would mean a positive amplitude of the individual transducer.

4.2.1 Pipe End

The received signals from the pipe end are shown in Figure 4.1a–c. As can be seen in (a), a pure T(0,1) wave is generated, since both the excitation sequence and the feature are perfectly axisymmetric. However, in the cases of (b) and (c), where the flexurals are created by imperfect excitation and from wave mode conversion, respectively, the received response is the superposition of T(0,1) and flexural waves. The scattering from the pipe end would result in all of the energy of the wave to be reflected. Thus, a strong proportion of the received signal energy corresponds to the T(0,1) wave, and small variations are caused by flexural waves.

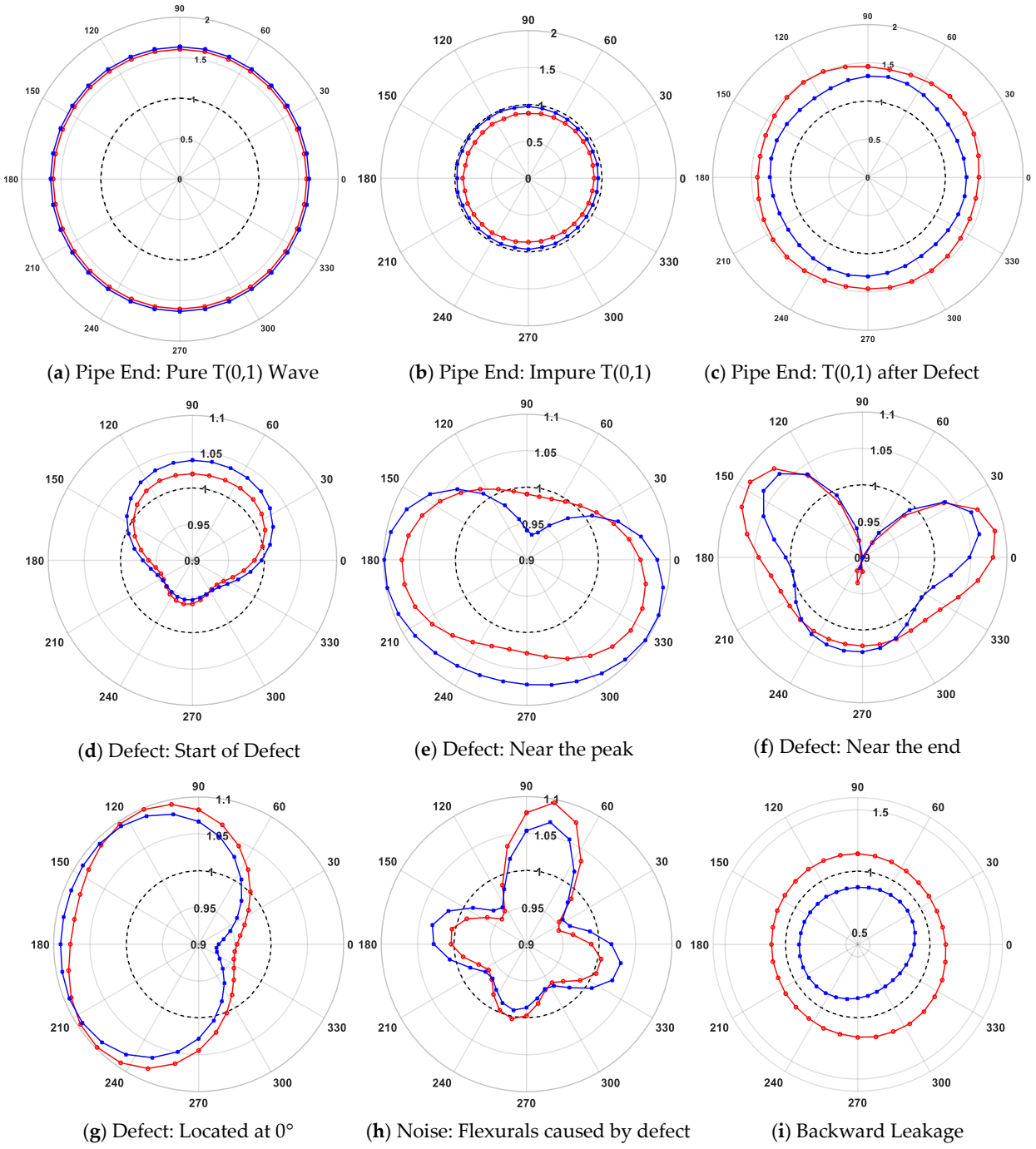

(**a**) Pipe End: Pure T(0,1) Wave (**b**) Pipe End: Impure T(0,1) (**c**) Pipe End: T(0,1) after Defect

(**d**) Defect: Start of Defect (**e**) Defect: Near the peak (**f**) Defect: Near the end

(**g**) Defect: Located at 0° (**h**) Noise: Flexurals caused by defect (**i**) Backward Leakage

Figure 4.1: Spatial signal reception from two rings of 32 sour points from various features where the red, blue, and black dotted lines are showing the first ring, second ring, and reference offset.

4.2.2 Defect

In cases (d)–(g) of Figure 4.1, the received waves are generated from a non-axisymmetric defect with a cross-sectional area size of 3%. The shown signals are different sequences from various times with respect to the temporal domain signal. The capture times are shown in Figure 4.2b where the red line is representing case (d), the blue line is representing case (e), and the green line is representing case (f). Case (g) is captured at the same time as case (e), but the generated wave is from a defect located at 0° (the right side of

the pipe), while the other cases were from a defect angled at 90° (top side). Four important hypohesis are illustrated from the figures:

1. Unlike the pipe end, defects that are non-axisymmetric features will inherently generate flexural waves. Nonetheless, the strongest energy will be associated with the T(0,1) wave.
2. The end of the signal envelope will contain more flexural waves compared to the start of the envelope. At the start of the envelope, at most one cyclic variation will exist in the spatial domain, which would represent a low-order flexural wave mode. Nonetheless, near the end of the envelope, higher-order variations (three or more) are starting to increase. This is because after the centre of the envelope, the power of the T(0,1) wave is starting to decrease, and the higher-order flexural with a lower travel speed is beginning to arrive.
3. The strongest energy of the T(0,1) wave is associated with the peak of each cycle in the temporal domain, where most of the transducers will have the same phase.
4. When the angle of the defect is changed, the direction of the arrival changes, but the phases and the overall formation of the wave remain the same.

4.2.3 Coherent Noise

The spatial arrival of the flexural noises created by the wave mode conversion and the backward leakage due to the imperfect excitation is shown in Figure 4.1h-i, respectively. Their corresponding time-domain signals are shown in Figure 4.2b,c. As can be seen, for the flexural signal, the reception point phases are highly non-symmetric, which is completely different from the case of the defect signal.

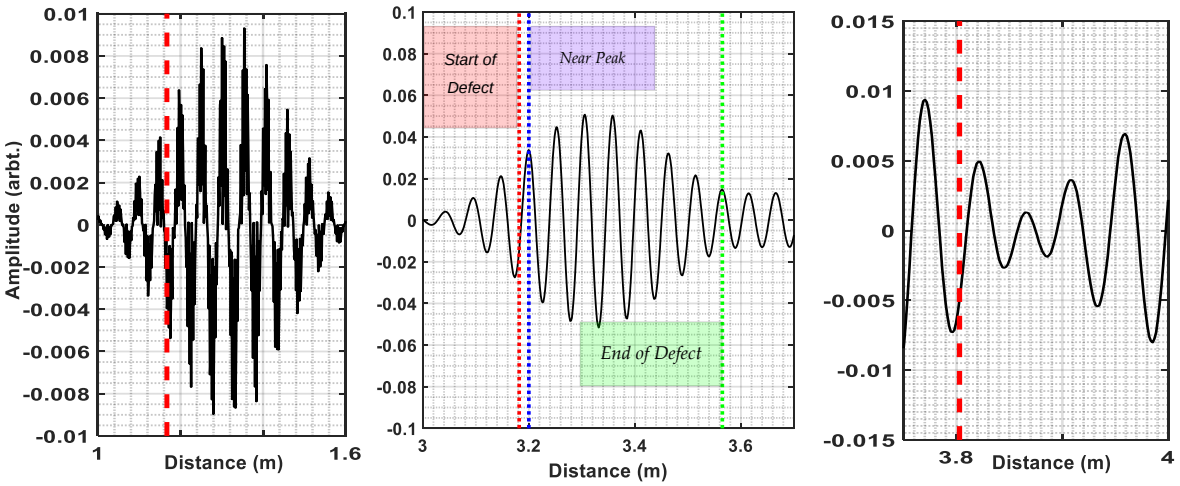

(**a**) Backward Leakage (**b**) Defect (**c**) Flexurals

Figure 4.2: Temporal domain of cases (d)-(i) from Figure 4.1.

Backward cancellation is not always perfect, due to the fixed ring spacing and the variance along the received waves from each transducer. In the temporal domain, these waves might still be detected, but when one looks at the phases between the two rings, it is observable that the two rings would have the exact opposite phases. Thus, it would be easier to detect signals received from the opposite direction in the spatial domain.

4.3 Methodology

In the previous section, it was demonstrated that in the case of flexural waves, high-order sinusoidal variation along the pipe's circumference would be created. In ideal scenarios, where a perfect axisymmetric wave hits a perfect axisymmetric feature, the received amplitude in each transducer must be the same. However, due to the imperfections of the transducers and the testing conditions, there will be variance along each of the received amplitudes from the transducers; nonetheless, they all will have the same phase. Similar to the pipe end, defects would generate a significant amount of torsional mode. However, they also do create flexurals with respect to the defect size and location. For signals coming from the backward direction, it is observed that the phases would practically be the inverse of each other for each transducer.

Based on these observations, by detecting the linearity between the phases of the sensors, the axisymmetric waves can be detected. Since not all of the phases would become the same in the case of defect signals, a measure of similarity between the phases must be defined, which can then be the threshold for detection.

4.3.1 General Routine

The first step in the general propagation routine of guided wave devices is to cancel the signal received from the backward direction. For doing so, the signals received from Ring 2 are initially subtracted from Ring 1 and Ring 3, and then the results are phase-delayed with respect to the tool set's ring distancing and the excitation wave mode dispersion curve (T(0,1) in this case). Applying the phase delay algorithm (explained in Section 2.4) results in having two rings of signals where each has the same number of transducers as the original ring. These results are stored in the Signals matrix:

$$\text{Signals}[\text{i, n}] = \begin{cases} \text{PhaseDelayed}(\text{Ring1-Ring2}), \text{for i} \leq \text{NS}/2 \\ \text{PhaseDelayed}(\text{Ring3-Ring2}), \text{for i} > \text{NS}/2 \end{cases} \quad (4.1)$$

where n represents the sample number, i is the sensor number, and NS represents the total number of achieved signals which is twice the number of transducers in a single ring. This process results in T(0,1) components to be overlapped. For the signals received from the

forward test direction, this overlap will be positive, and for the backward direction, the amplitudes are inverted, which allows the unidirectional inspection. The temporal domain signal, which is generally used for inspection, is achieved by taking the mean of the Signals:

$$\text{temporal}[n] = \frac{1}{NS}\sum_{i=1}^{NS} \text{Signals}[i, n] \tag{4.2}$$

4.3.2 Initialization

All of the transducers have the same phase when the sum of all of the signals from the same-phase transducers is equal to the sum of all of the signals. Therefore, the measure of similarity of the phases is defined by taking the difference between the sum of all of the signals and the sum of in-phase signals received from each transducer. The sign of the temporal domain demonstrates which sign is the greater power of iteration. Based on this sign, a mask is created for each transducer as follows:

$$\text{mask}[i, n] = \begin{cases} 1, & \text{sign}(\text{Signals}[i, n]) = \text{sign}(\text{temporal}[n]) \\ 0, & \text{else} \end{cases} \tag{4.3}$$

Using this mask, in-phase signals with the temporal domain of each sample can be identified, and their sum can be calculated as:

$$\text{inPhase}[n] = \left|\sum_{i=1}^{NS} \text{mask}[i,n]*\text{Signals}[i,n]\right| \tag{4.4}$$

Afterward, the similarity can be defined using:

$$\text{comparisonValue}[n] = \text{inPhase}[n] - \left|\sum_{i=1}^{NS} \text{Signals}[i,n]\right| \tag{4.5}$$

4.3.3 Threshold Selection

In cases where a significant proportion of iterations energy is from the T(0,1) wave mode, the comparisonValue will be zero. However, as shown previously, defect signals will contain a mixture of flexural and torsional wave modes, leading this value to be non-zero. Hence, there is a need for defining a threshold for detecting the defects. In this section, three methods are presented defining this threshold.

4.3.3.1 Method One

In this method, a static constant is defined by the inspector. If the comparisonValue is less than this defined threshold, the sample would be marked as one, which means that a feature is detected; otherwise, it would be marked as zero:

$$\text{Result}[n] = \begin{cases} 1, & \text{comparisonValue}[n] \le \text{Threshold}_{\text{One}} \\ 0, & \text{else} \end{cases} \tag{4.6}$$

For small time-domain signals, this formula would not be accurate, since inherently, their sum would be bigger than the threshold; thus, a compensation factor, 0.001, is added to prevent outliers from being detected in the white noise region. This is an acceptable level since the defect signals smaller than 0.001 would not be detected by the analog to digital converters of the device due to their limited discretization range. If the amplitude of the signal in the temporal domain is greater than this compensation factor, the algorithm would work as normal, else it would be zero:

$$\text{Result'}[n] = \begin{cases} \text{Result}[n], & |\text{temporal}[n]| > \text{compensation} \\ 0, & \text{else} \end{cases} \tag{4.7}$$

The disadvantages of this method are that firstly, user input is required, and secondly, the threshold value is fixed for all of the features, disregarding the existing characteristics in each sample.

4.3.3.2 Method Two

To use signal characteristics more effectively, the amplitude of the inPhase signals can be used to define the threshold, since a greater inPhase signal can be the result of greater linearity of the phases. By taking a percentage of the inPhase signals, a higher threshold can be assigned to such cases. In this method, a fixed percentage value needs to be set by the inspector, and the threshold for each iteration would be adaptively changed:

$$\text{Threshold}_{\text{Two,V1}}[n] = \text{inPhase}[n]*\text{percentage} \tag{4.8}$$

Another improvement to this algorithm would be to consider the effect of comparisonValue as well. A higher comparisonValue means that there is a higher chance that the signal is not linearly received by all of the transducers. This effect is significant in the case of signals received from the backward direction. In each iteration, the comparisonValue can be subtracted from the inPhase, which would decrease the resultant threshold value for backward propagating or non-axisymmetric waves:

$$\text{Threshold}_{\text{Two,V2}}[n] = (\text{inPhase}[n]-\text{comparisonValue}[n])*\text{percentage} \tag{4.9}$$

4.3.3.3 Method Three

To reduce human error, the requested input from the user must be eliminated. The phases are the main factor in detecting the results; the percentage can be defined based on the ratio of the in-phase sensors over the total number of sensors:

$$\text{percentage}[n] = \frac{1}{NS}\sum_{i=1}^{NS} \text{mask}[i, n] \tag{4.10}$$

In no iteration is the value of mask zero; it always has a positive offset, which means that the percentage cannot be replaced directly into Equation (4.8). Nonetheless, this offset can be removed by subtracting the mean of the calculated percentage for all the samples from each sample:

$$\text{Average} = \frac{1}{N}\sum_{n=1}^{N} \text{percentage}[n] \tag{4.11}$$

where N is the total number of samples in the test. The final considered percentage for each sample would be:

$$\text{percentage}_{\beta}[n] = \text{percentage}[n] - \text{Average} \tag{4.12}$$

Doing so provides more accurate thresholding with regard to the phases of the signals in each sample; the higher number of the same phase signals means a higher percentage value for the sample, which leads to a higher chance of detection. The formula for the first version (V1) and the second version (V2) of this method can be achieved by substituting the new percentage achieved from Equation (4.12) in Equation (4.8) or Equation (4.9):

$$\text{Threshold}_{\text{Three,V1}}[n] = \text{inPhase}[n]*(\text{percentage}[n] - \text{Average}) \tag{4.13}$$

$$\text{Threshold}_{\text{Three,V2}}[n] = (\text{inPhase}[n]-\text{comparisonValue}[n])*(\text{percentage}[n] - \text{Average}) \tag{4.14}$$

4.3.4 Program Flowchart

The program flowchart is shown in Figure 4.3. As can be seen, the three stages of general routine, initialization, and result generation are the same in all of the methods. However, the threshold value that is used in the result stage is selected based on methods one, two, or three, which are explained in the thresholding section.

4.3.5 Limits Definitions

Three main detection limits exist in these algorithms. (1) The first if the minimum, which is the minimum value required for each method to detect at least one cycle of the defect signal. (2) Second is the maximum, which is the maximum allowable value for the methods to detect the defect without any outliers. By moving toward the maximum value, the detection length increases; however, the accuracy reduces as the chance of detecting outliers increases. Thus, for comparing the methods together, an average value is defined using the minimum and maximum. This value is the best possible compromise between the achieved defect length and the possibility of detecting false alarms. For method three, the average value is calculated using Equation (4.11), and minimum and maximum values are achieved by manually replacing

the average in Equation (4.14). For both of the other methods, the average value is calculated manually from the achieved minimum and maximum values in the tests. Also, the Safe zone margins are defined as the difference between the minimum and maximum, which illustrates the values where manual inputs will produce a result without any false alarms.

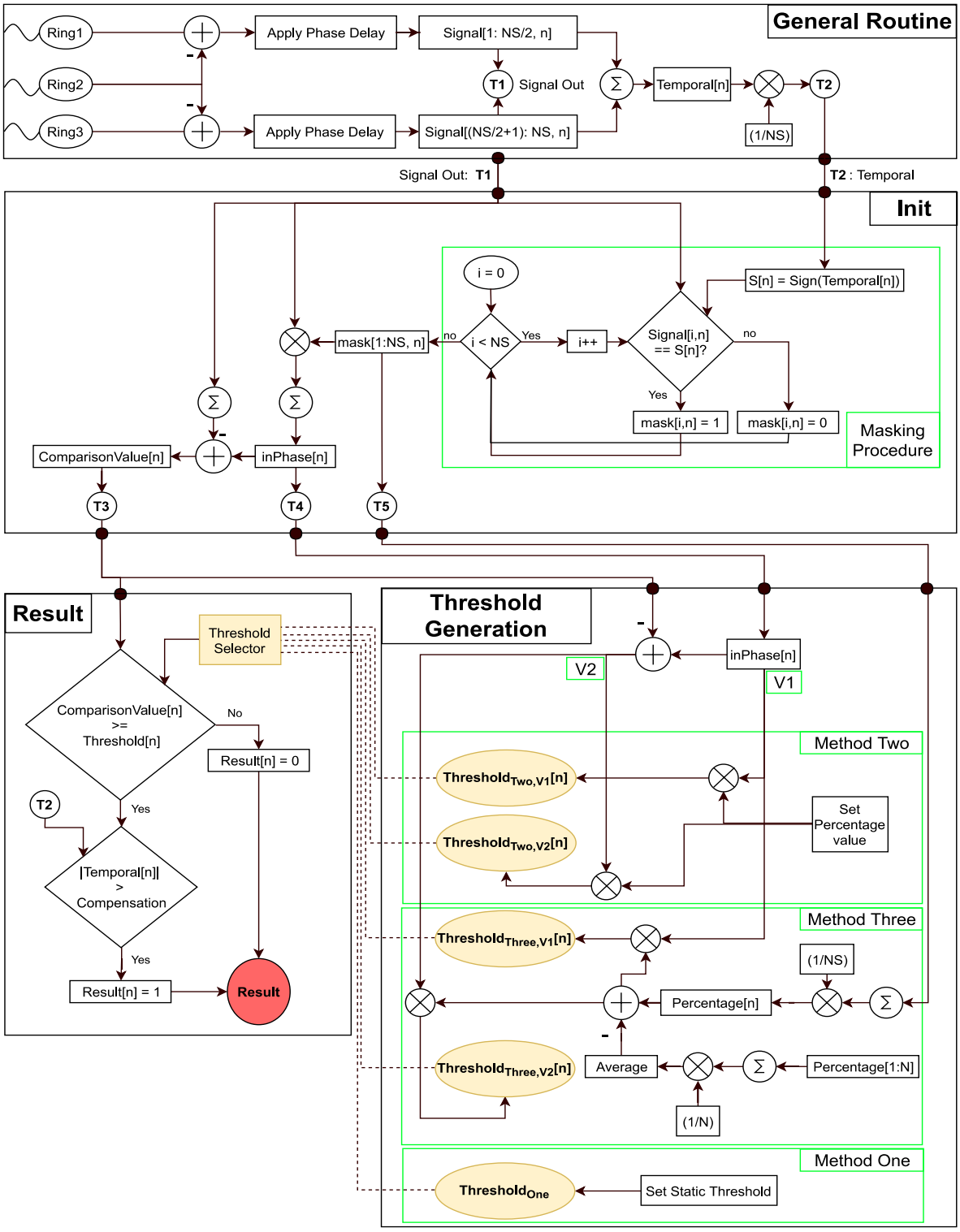

Figure 4.3: System Flowchart

4.4 Example Test Case

The initial verification of this algorithm was done using a FEM signal where a 3% CSA defect is located 3 meters away from test origin. The excitation sequence for generating the results is a 10 cycle hann-windowed sine wave with a frequency of 30 kHz. In order to increase the difficulty of detection and check the workability of the algorithm with a smaller number of source points, only eight source points in each ring are active in the reception side (Figure 4.4a). The resultant time-domain signal is shown in Figure 4.4b.

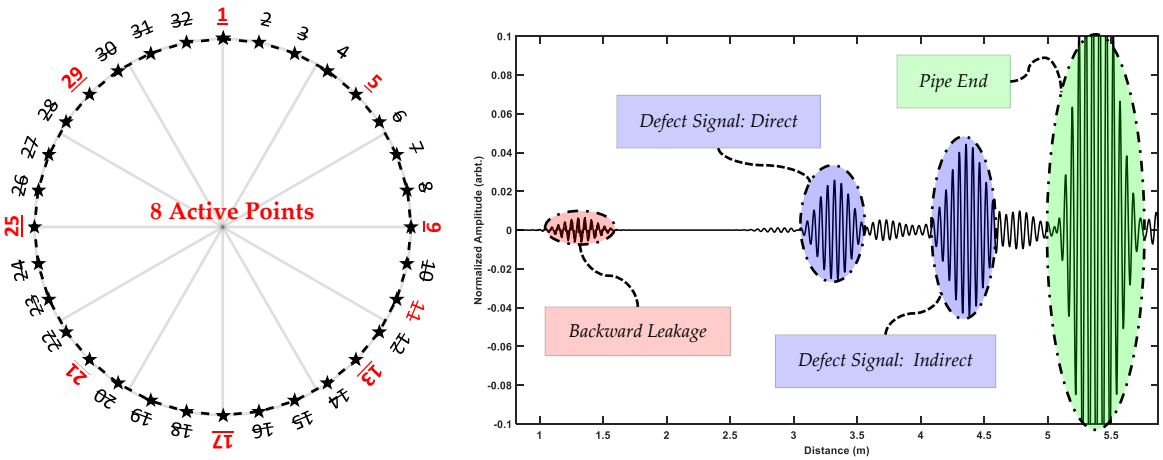

(a) Selected Points (each ring) (b) Signal in time-domain

Figure 4.4: Example signal from FEM. (a) shows the selected point (marked by red) in each ring and (b) shows the time-domain signal.

Figure 4.5 shows the assigned values to the first (black line) and the second version (red line) of thresholding, which is the inPhase and subtraction of the comparisonValue from the inPhase, respectively. As can be seen both in the backward leakage signal and the noise region, the decrease in the assigned threshold is more than the defect and pipe end signals.

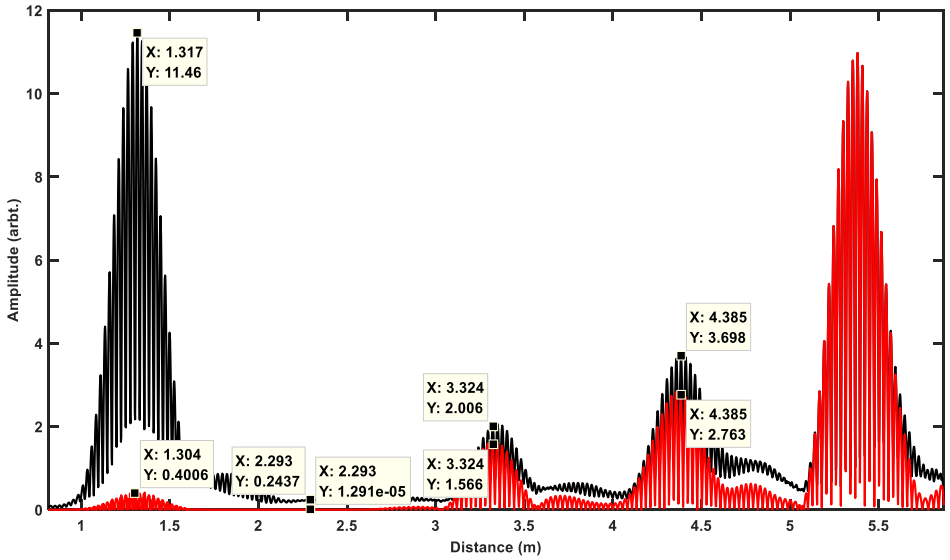

Figure 4.5: Comparison of the first and second thresholding versions. The black and red lines are the values used in each iteration for assigning the thresholds in the first and second versions respectively.

In method two, a static percentage of either of the mentioned values is considered the threshold for each iteration; however, in method three, this percentage is assigned using the ratios of inPhase signals subtracted from its mean, as shown in Figure 4.6.

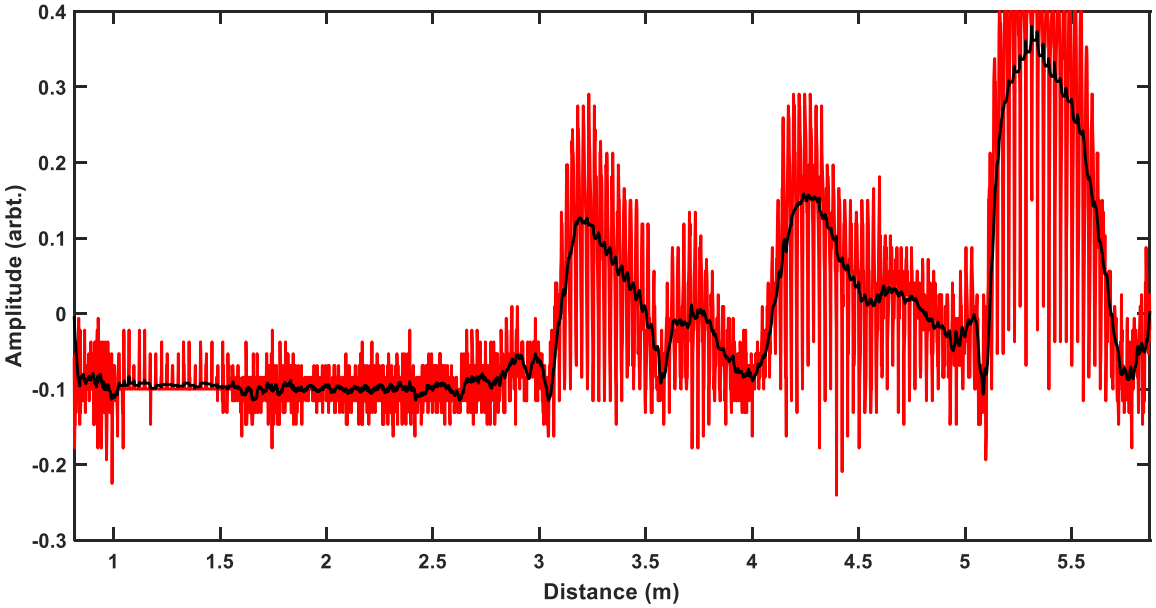

Figure 4.6: Calculated the percentage of sensors with the same phase, where the offset (mean values) are removed (red line); the black signal is showing the filtered version for better illustration.

The calculated threshold for each iteration using the average value of method three is shown in Figure 4.7. In the same figure, if the method one was used, the threshold value would be a constant line for all of the iterations.

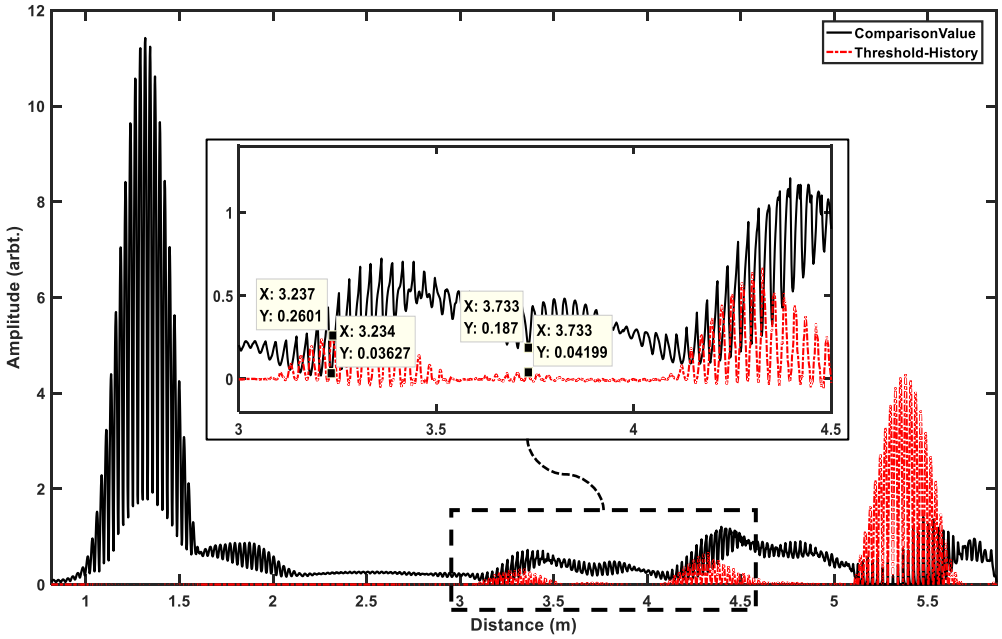

Figure 4.7: Calculated threshold using Method Three-V2 (red) against the comparisonValue (black). In the case of Method One, the threshold becomes a constant line at the value set by the user.

The processed signal calculated from method three is illustrated in Figure 4.8, where it shows the locations at which the comparisonValue is higher than the threshold history. As expected, the pipe end is completely detected, since it is a complete axisymmetric feature, but only the centre part of the defect could be detected.

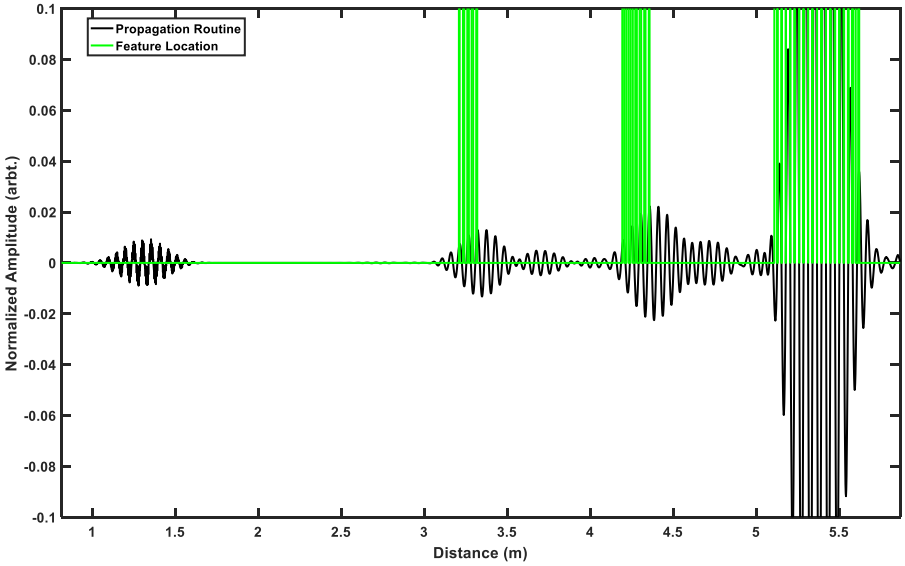

Figure 4.8: The results generated by Method Three-V2 (green signal) against the temporal signal (black).

The figures shown below in Sections 4.5 and 4.6 consist of three lines. Blue represent the minimum allowable threshold amplitude required in order to detect the defect (with or without outliers). Red is the maximum allowable threshold amplitude where the defect could be detected with existence of only one outlier. Hence, the green zones are the regions in between blue and red lines where the defect can be detected without any outliers. On the other hand, cases where red and blue lines are overlaid means that the defect could only be detected in the presence of outlier. The black line is the average value of the threshold amplitude in each scenario.

4.5 First Set of Experimental Tests

The detection of Defect 1 is the focus in the first set of tests. In these test cases, Defect 2 does not exist, and therefore, the region between 4–4.5 is considered noise. Furthermore, the coherent flexural noises existing in two regions varies with the frequency. As an example, in 34 kHz for Defect 1 region and 37 kHz for Defect 2 region results in the weakest flexurals in their respective regions. Furthermore, in most frequencies, Defect 2 is almost always more affected by the flexural waves. In this section, only of the defects with sizes of 2% and 3% CSA is shown since defects with higher sizes followed the same trends.

4.5.1 Method one

Figure 4.9 shows the detection zones of method one with regards to the threshold values. In this figure, the green zone illustrates the region where the defect is detected without the presence of any outliers. As can be seen, this algorithm is capable of detecting both 2% and 3% CSA defects using certain frequencies. Considering the 2% CSA defect, the minimum values required for detection are almost linearly increasing with regards to the frequency.

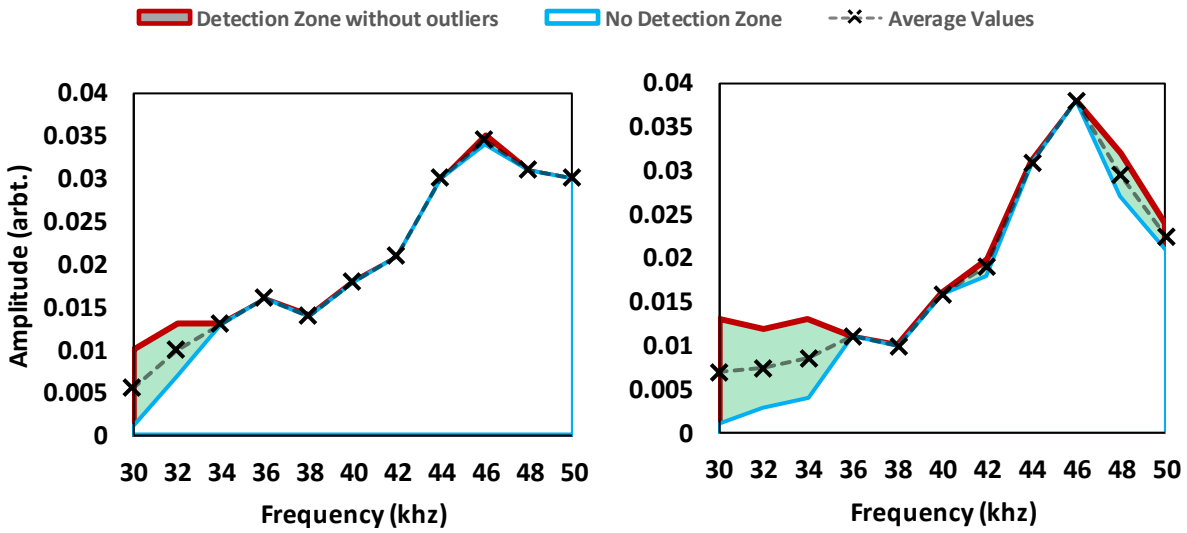

(**a**) 2% CSA (**b**) 3% CSA

Figure 4.9: Detection zones of method one generated from the first set of tests. The minimum, maximum and average showed by the blue, red and black dotted lines respectively. The green region shows the safe zone for detecting the defect without any outlier(s).

The detection using this method is mostly dependant on the local amplitude of the defect wave; stronger defects require lower threshold values in order to be detected and vice-versa. Therefore, as illustrated, lower frequencies of 30 and 32 kHz tend to work better with this method. Furthermore, from the results of the 3% CSA defect, it can be seen that a greater safe zone can be achieved when the defect size is increased. This is due to the fact that the minimum value of detection is decreased since a stronger defect wave is generated from a defect with higher CSA size. In conclusion, it can be challenging to choose a threshold for smaller defects since they can be enormously affected by the regional flexural waves and the excitation frequency.

4.5.2 Method Two

Figure 4.10 shows the detection zones of method two with regards to the threshold values. In this figure, the green zone illustrates the region where the defect is detected without the presence of any outliers. This method can successfully detect the 3% CSA defect without any outliers using both versions; however, in the case of 2% CSA defect, the detection zones

between 30 – 36 kHz and 40 to 48 kHz, using both versions of the algorithm. This means that detection using method two is affected by both noise and defect characteristics, rather than only on the defect. This is due to the fact that the assigned threshold values of this method, to both noise regions and defect regions, are dependent on each iteration's characteristics. Therefore, if the noise region consists of a strong torsional or low-order flexural wave, it will be assigned a higher threshold value. As an example, the strongest SNR of 2% CSA is achieved at 40 kHz. However, at this frequency, it is not possible to detect that defect without calling any outliers since the regional noise regions at that frequency are also stronger. Same as the previous method, as the defect size increases, the minimum limits for detection decreases, which leads to a wider available range for excitation frequency, a wider safe zone margin, and a longer detection length in all frequencies. The trend is also observable when comparing version two with version one where all the mentioned properties increase in version two.

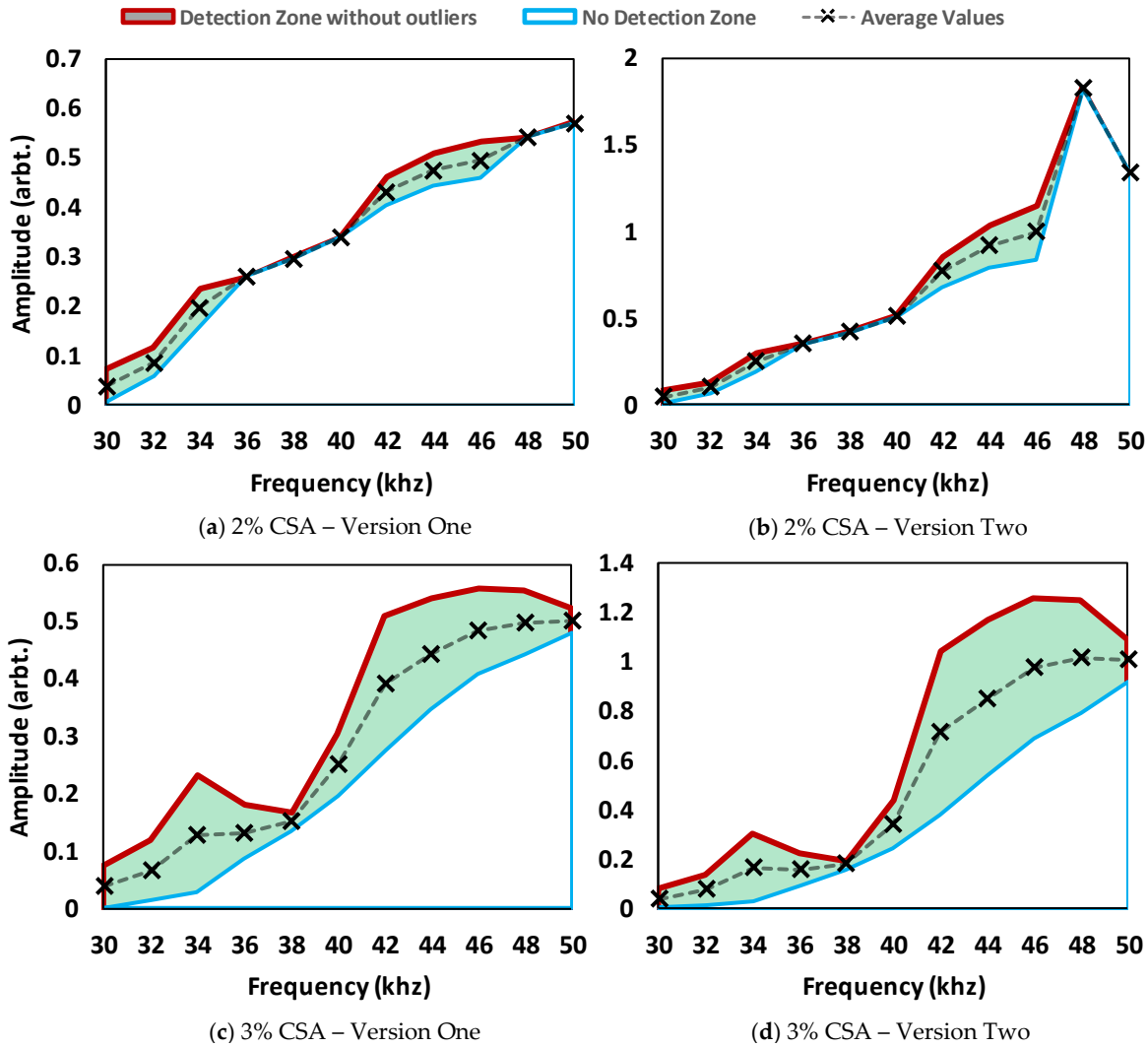

Figure 4.10: Detection zones of method two generated from the first set of tests. The minimum, maximum and average showed by the blue, red and black dotted lines respectively. The green region shows the safe zone for detecting the defect without any outlier(s).

With regards to the threshold limits and dependency on the frequency, it can be seen that the minimum value for threshold (blue) which is required for detecting the defect without any outliers is almost linearly increasing with regards to the frequency for both defect sizes. This means that in the lower frequency regions, a lower value for thresholds is required which is as low as 0.006 for 2% CSA and 0.001 for 3% CSA at 30 kHz frequency. Nonetheless, this frequency is not the best to be used with this method since the detection length and safe zone margin of them is much less than the others. Observing the figure, it can be said that in the lower frequency region (between 30 to 40 kHz), the optimum frequency for detection is 34 kHz since it brought the widest safety margin and the longest defect length (at the average point). In the higher frequency region (40 to 50 kHz), the optimum frequency is 44 kHz. In comparison to method one, this method has a greater range of operating frequencies and provides a larger safety margin for threshold selection.

4.5.3 Method Three

Figure 4.11 shows the detection zones of method three with regards to the threshold values. In this figure, the green zone illustrates the region where the defect is detected without the presence of any outliers. Also, the average values are calculated automatically from the mean of the percentage of active sensors in each iteration. Same as method two, this method is capable of detecting the 3% CSA defect using all frequencies. However, only frequencies of 34 and 36 kHz will result in automatic detection of the defect. As can be seen in Figure 4.11, the threshold limits are inverted in this figure where the blue line is at the top the side (closer to one) and the red line is at the bottom side (closer to zero) of the safe zone margin. The reason is these limits are substituted instead of the average value in equations (4.13) and (4.14); therefore, unlike other methods, stronger defect signals can be detected even if this subtraction value is close to one (rather than zero). For detecting 2% CSA defect, two between zones of 32 – 34 kHz, and 40 – 48 kHz can detect the defect without any outliers. Nonetheless, the optimum frequencies in these two zones can be considered as 34 kHz and 44 kHz. Furthermore, frequencies of 30 and 32 kHz also are capable of detecting 2% CSA defect with a minimum number of outliers (one).

Comparing versions one and two of this method, higher frequencies (between 40 to 50 kHz) are more affected than the ones between 30 – 40 kHz. Furthermore, using version two with higher frequencies shifts the minimum threshold value significantly in some cases it would be below zero. This means that in order for the defect to be detected, the percentage of sensors with the same phase (illustrated in Figure 4.6) needs to be amplified. Nonetheless, it produces a wider safe zone margin to select the threshold value and also a longer detection length. However, it will not be possible to detect the defect using higher frequencies automatically.

To conclude, this method can automatically detect defects with sizes as small as 2% CSA, which are buried in the noise level using a 34-kHz excitation frequency.

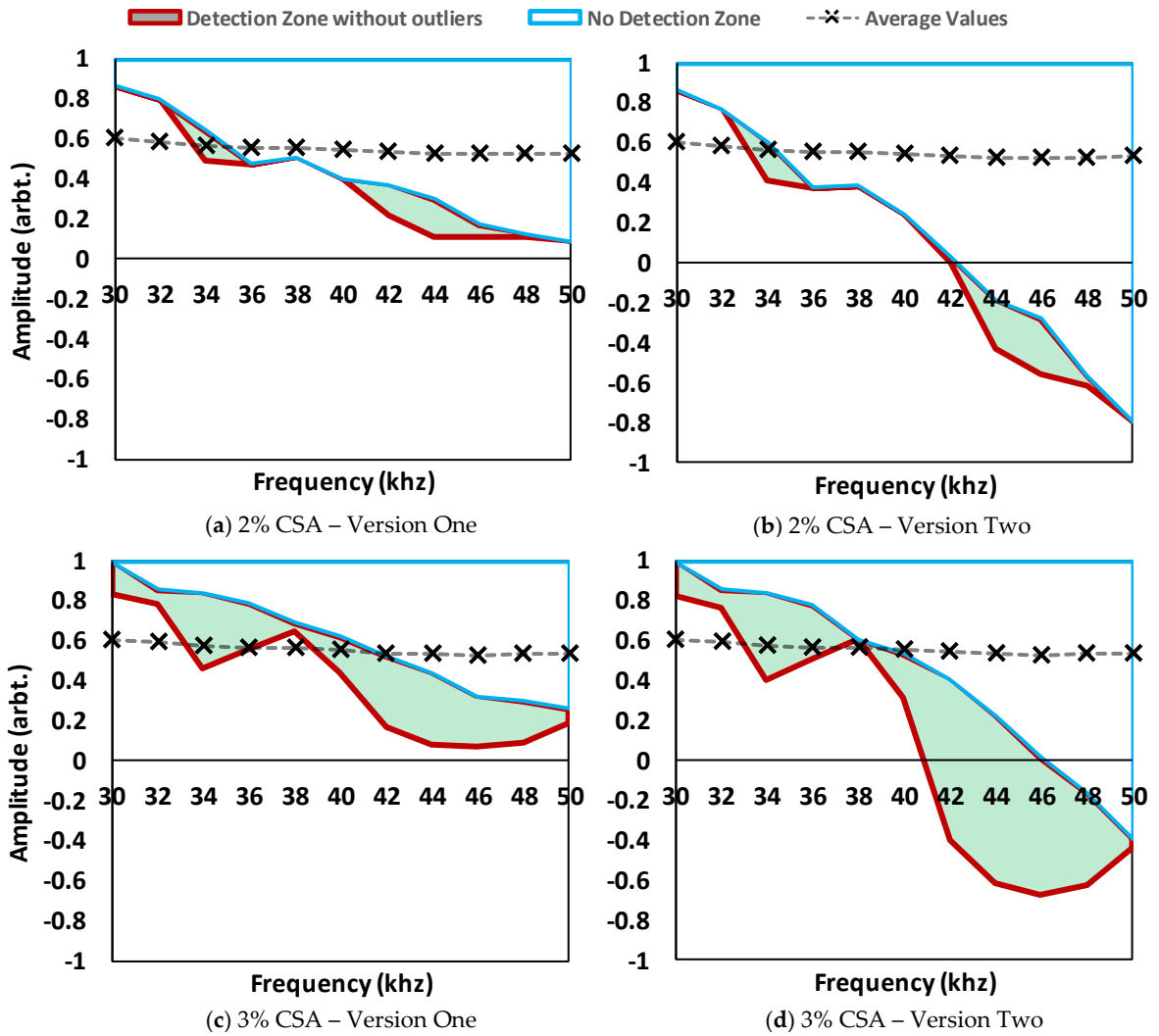

(**a**) 2% CSA – Version One

(**b**) 2% CSA – Version Two

(**c**) 3% CSA – Version One

(**d**) 3% CSA – Version Two

Figure 4.11: Detection zones of method three generated from the first set of tests. The minimum, maximum and average showed by the blue, red and black dotted lines respectively. The green region shows the safe zone for detecting the defect without any outlier(s).

4.6 Second Set of Experimental Tests

In the second set of trials, the focus is on detecting Defect 2. The defect signal is expected to be received between 4–4.5 m. Since the baseline of the defect signal is highly contaminated by the coherent flexural noise, higher detection limits are required for detecting the defects, even when the CSA size of the defect is increased. These tests aim to observe the effect of spatial noise on the algorithm and demonstrate its capability in detecting defects in such scenarios. It is expected that the algorithms perform better using frequencies with limited spatial noise in the defect region. In this section, only the results of the defects with

sizes of 3% and 4% CSA is shown since the larger defect sizes followed the same trends; detection of 2% CSA defect in this location was challenging using most of the frequencies.

4.6.1 Method one

Figure 4.12 shows the detection zones of method one with regards to the threshold values. In this figure, the green zone illustrates the region where the defect is detected without the presence of any outliers. As can be seen, the only excitation frequency that enabled defect detection without any outliers is 36 kHz. The maximum allowable threshold to detect the 3% defect without any outlier using this frequency is 0.01 and the minimum value is 0.009; therefore, smaller defects cannot be detected without any outliers using this method. This is unlike the first set of tests, where it was easier to detect the defect using lower frequencies since the second defect is located in a region with higher energies of flexural noises.

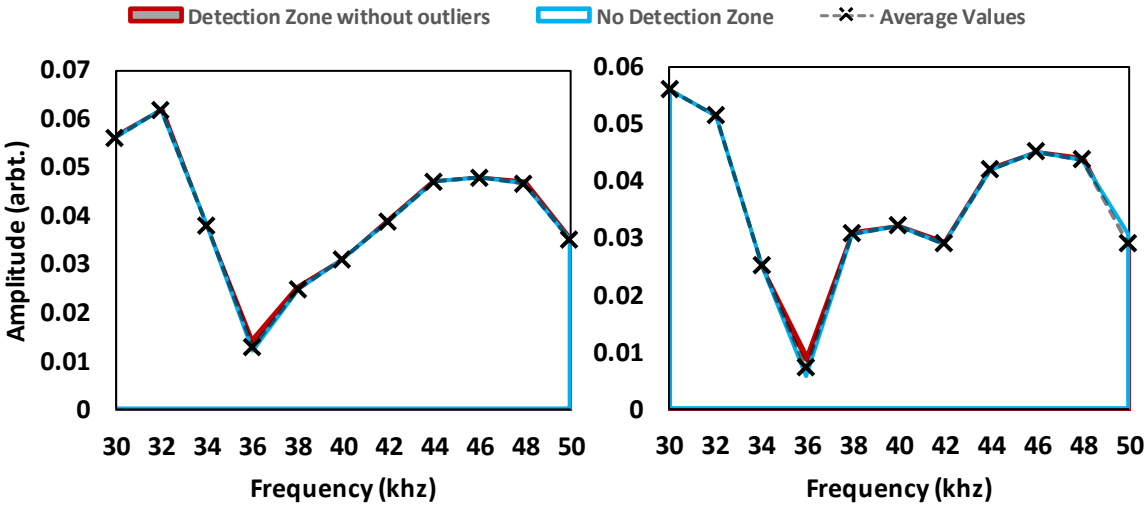

(a) 3% CSA (a) 4% CSA

Figure 4.12: Detection zones of method one generated from the second set of tests. The minimum, maximum and average showed by the blue, red and black dotted lines respectively. The green region shows the safe zone for detecting the defect without any outlier(s).

Comparing the results of method one from both tests, it can be seen that due to the location of the second defect, it is clear that the minimum values required for detecting the second defects are higher than the general noise level of the tests as reported previously. As an example, the maximum allowable threshold value to detect the first defect without any outlier using 34 kHz is 0.013 while the minimum for detecting the second defect of 3% CSA is 0.038. It can be concluded that method one is highly affected by the existing energy of flexurals in the same iteration.

4.6.2 Method Two

Figure 4.13 shows the detection zones of method one with regard to the threshold values. In this figure, the green zone illustrates the region where the defect is detected without the presence of any outliers. This result clearly demonstrates the advantage of using the iteration's characteristics in determining the threshold. Unlike method one, which was using most frequencies results in the detection of outliers, method two is capable of detecting the second defect without any outliers using the majority of frequencies.

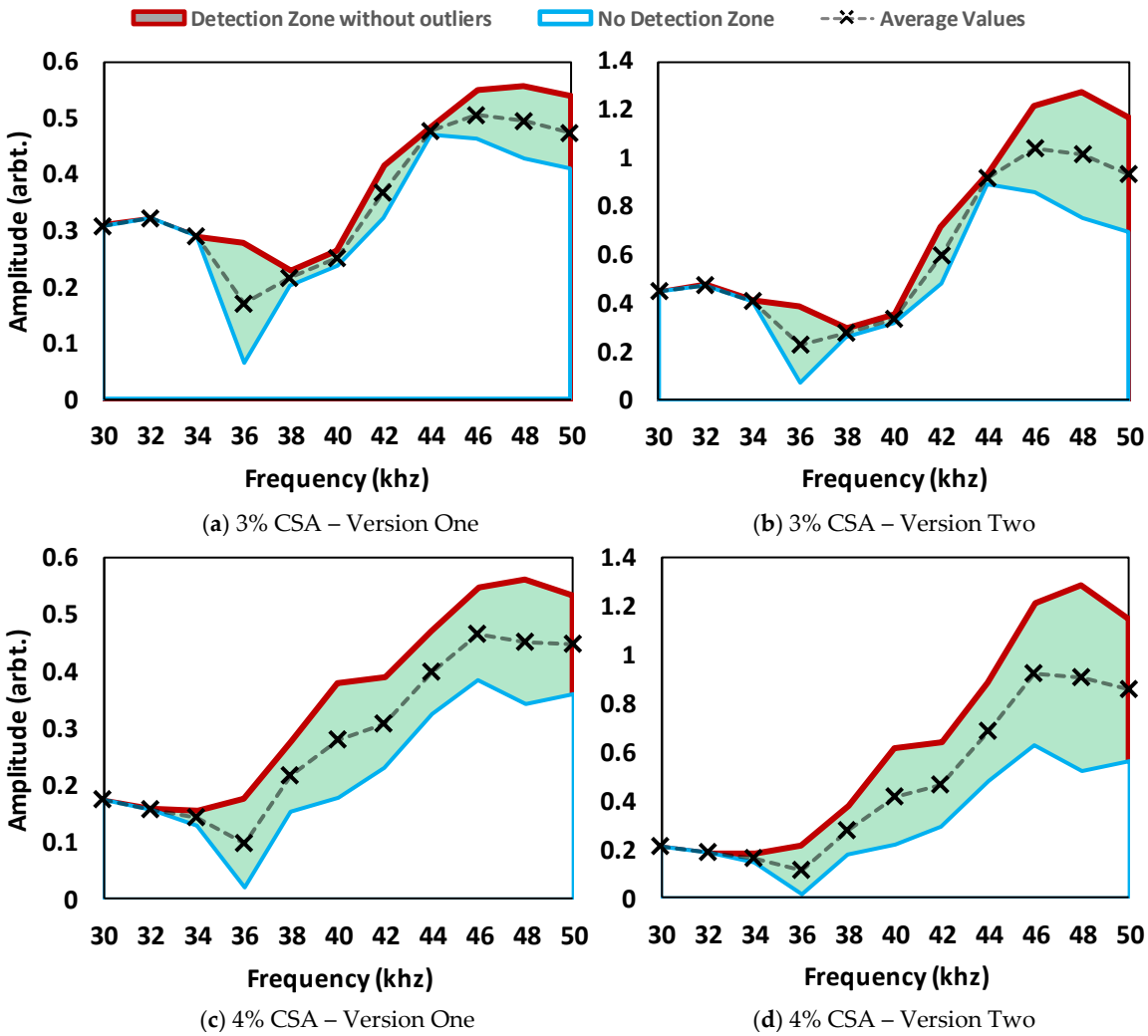

Figure 4.13: Detection zones of method two generated from the second set of tests. The minimum, maximum and average showed by the blue, red and black dotted lines respectively. The green region shows the safe zone for detecting the defect without any outlier(s).

Comparing these results with the ones achieved from the first set of tests of the same method, it can be seen that the same trends are observable. However, the optimum detection regions are now changed. Unlike defect one, two regions between 34-38 and 44-50 kHz tend to work best where the optimum frequencies are 36 and 48 kHz. This validates the previously mentioned argument where lower excitation frequencies (30 and 32 kHz) are not

recommended to be used with method two as it provides limited safe zone margin in comparison to the results achieved from other frequencies. Furthermore, using version two provides the same previously mentioned benefits in the results.

It can be concluded that this method, is less sensitive to the existing spatial noise in the iteration. This is because the characteristics of each iteration are considered for assigning their respective thresholds. As the defect size gets bigger, lower threshold values are needed for defects to be detected without any outliers; this provides a wider safe zone margin and a longer detection length.

4.6.3 Method Three

Figure 4.14 shows the detection zones of method three with regards to the threshold values. In this figure, the green zone illustrates the region where the defect is detected without the presence of any outliers. Also, the average values are calculated automatically from the mean of the percentage of active sensors in each iteration.

The 3% CSA defect can automatically be detected using 36 kHz while the 4% CSA defect using 36, 38, and 40 kHz. This is due to the fact that when the defect size grows, the minimum threshold required for the defect to be detected decreases (moves toward one in this case). In compare to Defect 1, the optimum frequency region is close to 36 kHz. Therefore, the results of both Defect 1 and 2 achieved from the lower frequency band (30 to 40 kHz) show follows a similar trend. Nonetheless, for the second defect, the optimum frequency is 36 kHz since it provides a wider higher safe zone margin, a longer detection length, and the ability to detecting defects with lower CSA sizes automatically. This shift in the optimum frequency happens since this method is also affected by the spatial noises in the defect region; and since there are fewer noises observed when using 36 kHz (in compare to 34 kHz), the results of both methods two and three are better using that frequency. By using 34 kHz, the 4% CSA is detectable without any outliers using version two of this method. This clearly illustrates the advantage of using version two instead of version one.

Same as method two, the advantage of considering the iterations characteristic in determining the threshold is clearly observable in the results. Furthermore, comparing the two versions of the algorithm, it can be that the second version is providing better detection zones.

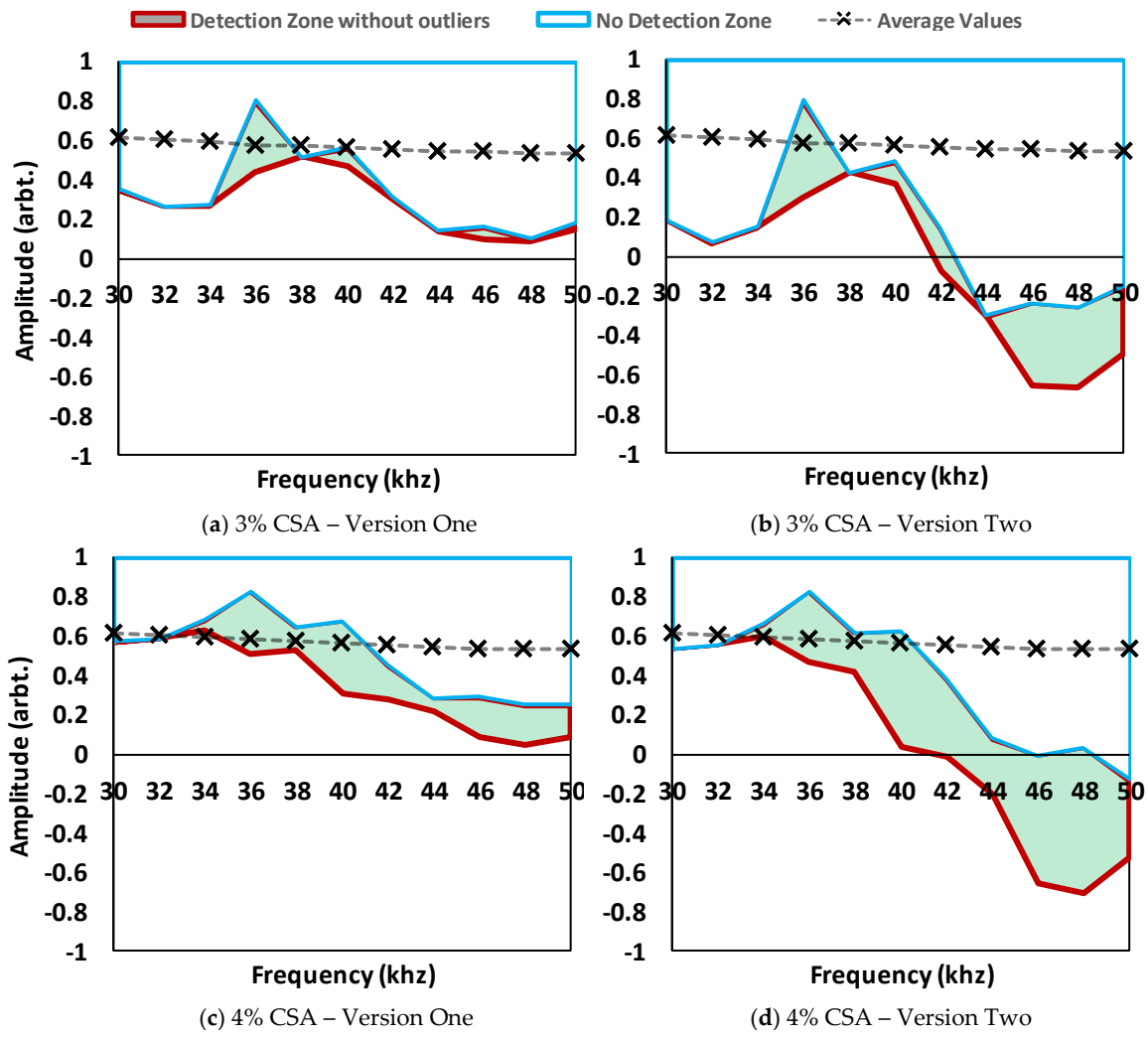

Figure 4.14: Detection zones of method three generated from the second set of tests. The minimum, maximum and average showed by the blue, red and black dotted lines respectively. The green region shows the safe zone for detecting the defect without any outlier(s).

4.7 Discussion

The amount of increase in the minimum and maximum values achieved using the second version of the thresholding instead of the first one is shown in Figure 4.15. In this figure, the blue line (blue zone) illustrates the increase in maximum values and the red-dotted line (red zone) illustrates the increase in the minimum values. The difference between these two amounts is demonstrated using the green bars in between the two lines. As can be seen, except in 50 and 38 kHz in method three for defect one, in all other methods and frequencies, the amount of increase in maximum allowable threshold value to detect the defect without any outliers is higher than the one for minimum threshold values required for detecting the defect. In some cases, such as 46 kHz across all tests, the increase in maximum value is almost as time as the minimum value. Therefore, this result demonstrates that version two of the algorithm can provide a better safe zone margin by increasing the maximum allowable threshold more than the minimum values.

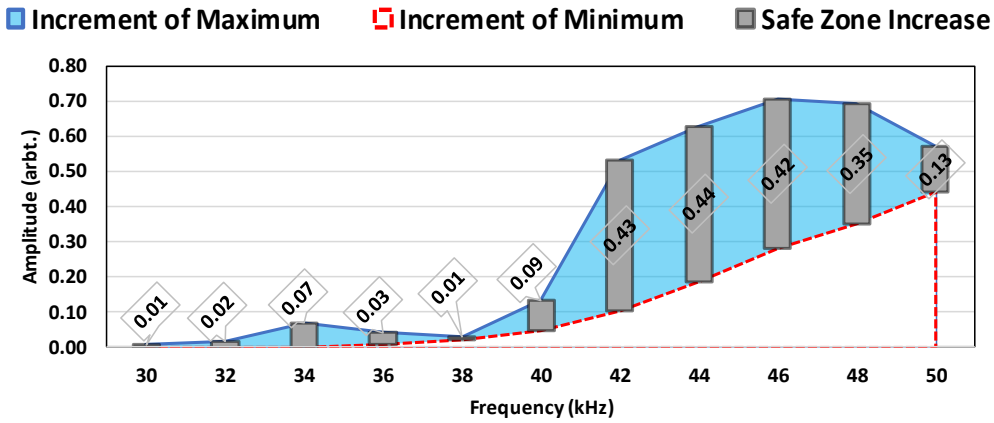

(**a**) Defect 1 – Method Two

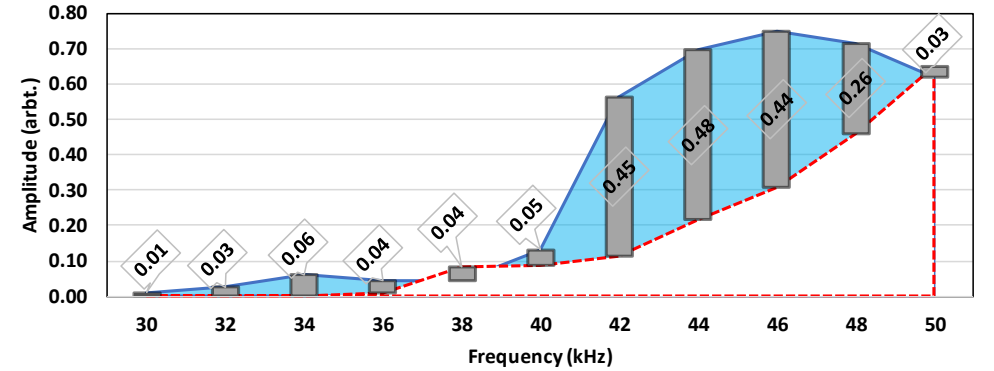

(**b**) Defect 1 – Method Three

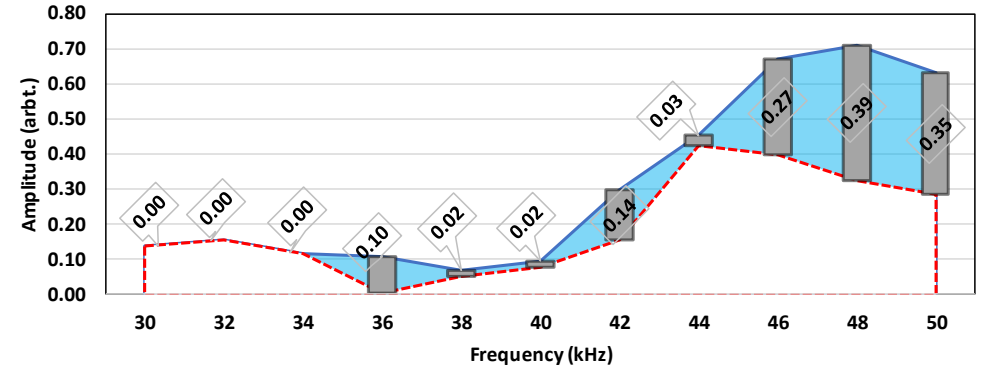

(**c**) Defect 2 – Method Two

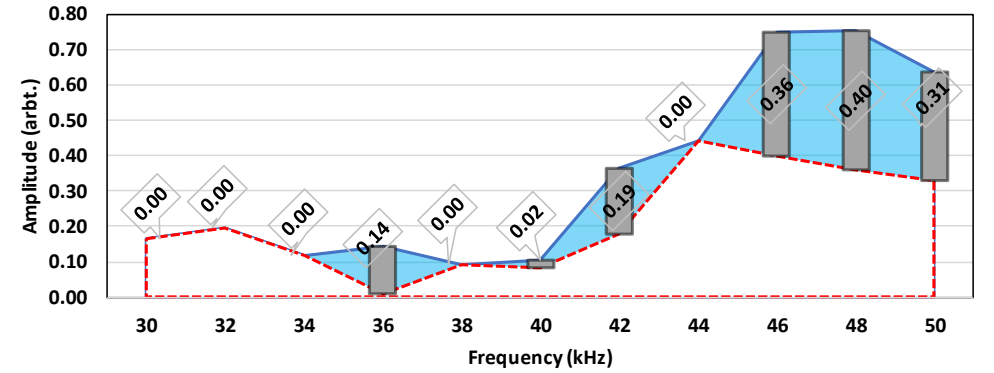

(**d**) Defect 2 – Method Three

Figure 4.15: The increments of minimum (red-dotted line) and maximum (blue line) achieved using the second versions the green bars are showing the amount of increment with regards to each frequency. (a) and (b) shows the results of methods two and three for Defect 1 and (c) and (d) shows results of methods two and three for Defect 2 respectively. Both defect sizes are fixed at 3% CSA.

The safe zone margins for detecting without any outliers using each method for Defect 1 and 2 are shown in Figure 4.16a and b, respectively. The defect size for both defect locations is fixed at 3% CSA. As illustrated previously, the second version of the algorithm always provides a wider safe zone margin. this reduces the risk of outliers getting detected by providing a wider threshold selection area. With regards to Defect 1 results (a), comparing the results of method three and two from the same versions, it can be seen that in almost all frequencies method three is providing a wider safe zone margin. However, for Defect 2 (b), this trend is only observable in a lower frequency region (less than 40 kHz). Furthermore, as it was illustrated in Figure 4.11 and Figure 4.14, the optimum frequency of method three where it is capable of detecting the defects automatically is between 34 to 36 kHz. Therefore, method two can perform better with higher frequencies while method three is better with lower frequencies. In both defect locations, method one tends to provide the worst safe zone margin where it is almost always less than the tenth of the other methods; especially for higher frequencies (above 36 kHz). The reason is that in method one, a static threshold is defined for every iteration while the other methods define the threshold based on the unique characteristics of each iteration. This demonstrates the advantage of using the iterations characteristics in determining the threshold.

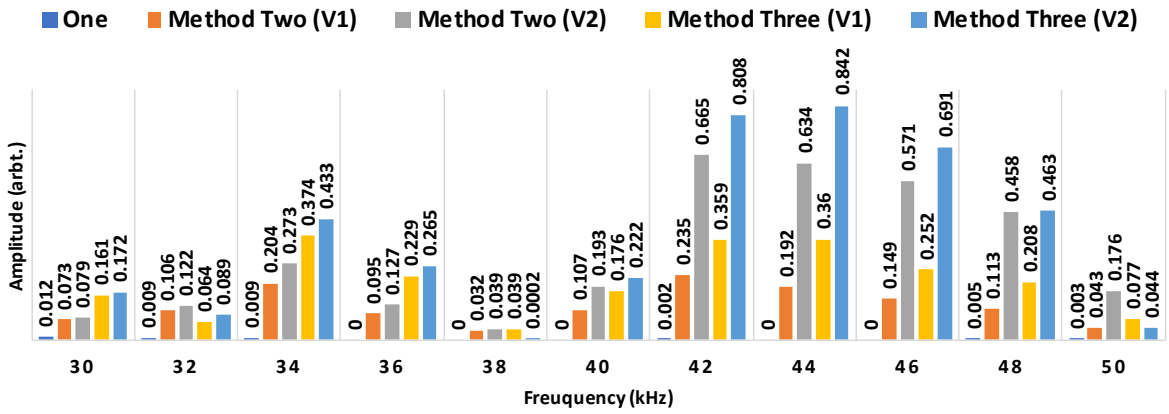

(**a**) Defect 1

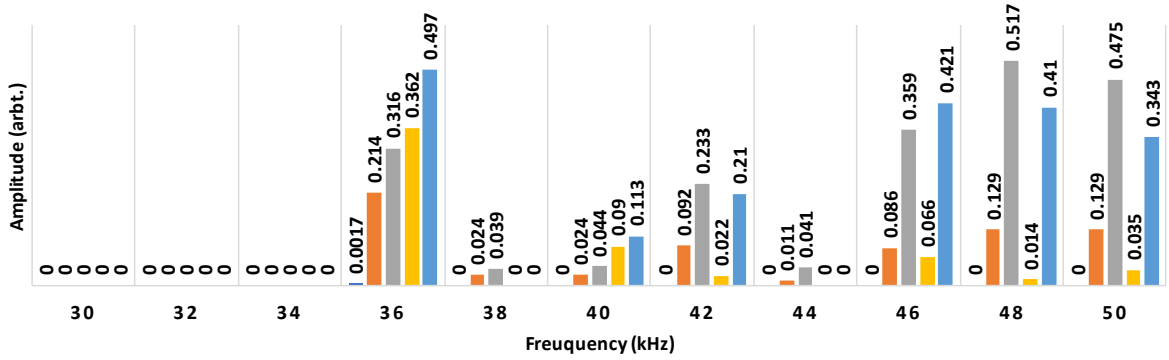

(**b**) Defect 2

Figure 4.16: Comparison of the Safe zone margins using each method for Defect 1 and 2 where both defects have the same size as 3% CSA.

Figure 4.17 illustrates the maximum length of detection achieved using the average threshold values of each different algorithm on both Defects 1 and 2 (where the sizes are fixed at 3% CSA). As can be seen, the maximum detection length of method one is almost always less than the other two methods using almost all frequencies. Hence, a better threshold selection procedure (e.g., method two and three) not only allows a wider safe zone margin but also provides a longer detection length.

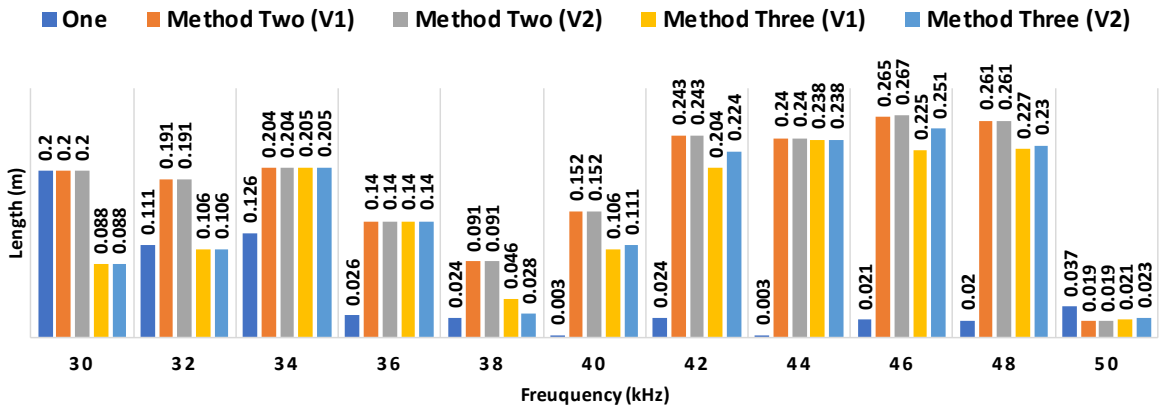

(**a**) Defect 1

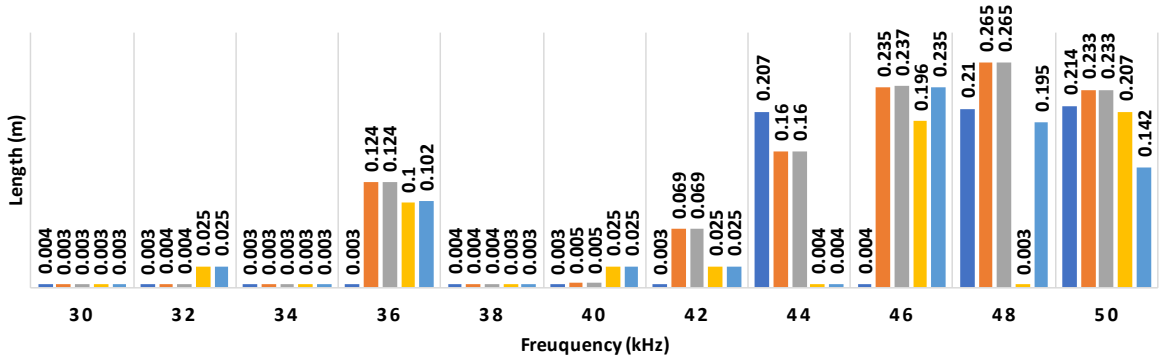

(**b**) Defect 2

Figure 4.17: Comparison of maximum detection lengths using each method for Defect 1 and 2 where both defects have the same size of 3% CSA.

Comparing versions of the same methods together, it can be seen that although a higher safe zone margin is being provided using version two, the maximum detection length increases or remains approximately the same. The only exception is in the case of Defect 2 at 50 kHz was using the second version a reduction of 0.065 m in the maximum detection length is observed. Nonetheless, the safe zone margin is increased from 0.035 in version one to 0.343 in version two; which is almost a tent fold enhancement in the region where the defect will be detected without the presence of any outliers. Hence, as the safe zone margin is increased significantly, even in this case, it is still beneficial to use the second version at the cost of a small reduction in the detection length. Doing so reduces the chance of outliers being detected using this algorithm.

With regards to these achieved results, the following hypothesis can be drawn:

- Method Comparison: Method one tended to produce the worst results, as it solely depended on a static value set by the user without considering the characteristics of the signals received in each iteration. Methods two and three can achieve a similar result in most cases; however, in method three, the threshold value can be set automatically, which provides a great benefit in one-off inspection scenarios.
- Version Comparison: Version 2 always produced a wider safe zone margin while achieving approximately the same detection length.
- Excitation Frequency: lower frequencies (below 40 kHz) tend to work better with method three where its optimum frequency is located in the region of 34 – 36 kHz. However, method two works better in the higher frequency region where it provides the best safe zone margin and the detection length. Nonetheless, determining the thresholds in the higher frequency region, especially in using version two of the methods, is difficult since the minimum threshold required is higher than the ones required for lower frequencies. Therefore, currently, it is suggested to use method three, in their optimum frequency region to provide a more accurate result.
- Defect Location: From the results of Defect 1 and 2, it can be seen all methods are more affected by the existing spatial noises caused by the flexural waves in the same iteration rather than the temporal noise of the neighborhood. In Defect 1 results, all frequencies required a smaller minimum threshold value for the defect to be detected; on the other hand, since Defect 2 was located in an area with stronger flexural noises, higher thresholds were required for detecting that defect. Furthermore, when stronger flexural waves existed, method two and three provided a better safe zone margin and detection length in comparison to method one. This was due to their superior threshold selection procedure where the threshold of each iteration was determined by considering the characteristics of the waves within the same iteration.
- Safe Margin Zones: method three provides a higher safe zone margin using lower frequencies while method two provides a better safe zone margin using higher frequencies. The detection length of each method is also correlated with their safe zone margin.
- With regard to these results, method three (version two) is the best method since the threshold can be determined automatically, and it achieves the highest safe zone margin. The tests prove that this method can detect defects using both 34 kHz and 36 kHz, depending on the existing coherent noise in the defect location. Furthermore, the algorithm is sensitive to the existing coherent noises in the baseline signal rather than the temporal noise in the tests.

4.8 Chapter Summary

In this chapter, a novel statistical algorithm was proposed that uses the full capability of the tool-set array of conventional guided waves inspection devices to identify defect signals that have been contaminated by coherent noise. Laboratory trials confirmed the effectiveness of this algorithm in detecting defects with low SNRs and its dependence on the frequency.

Three different methods and two different Thresholds (See Section 4.3.3) were created for generating the results, in which the thresholding scheme of each was different. In method one, the threshold is a static value set by the inspector. In method two, the assigned threshold to each iteration is a percentage taken from the summation of the amplitude of all of the transducer's signals with the same as the time-domain signal generated by the normal propagation routine. In method three, the percentage value is determined by determining the number of transducers with the same phase over the total number of transducers, subtracted by an offset. Two thresholding versions of each of the method two and method three are also developed, wherein the second version, the summation of signals with the same sign as the temporal signal was subtracted from the comparisonValue, before determining the final assigned threshold of each iteration. In the experimental trials, it could be seen that method three tends to work best using frequencies between 30 to 40 kHz and method two works best using frequencies between 40 to 50 kHz. Furthermore, the optimum reported frequencies for method three is in the region of 34 – 36 kHz. In all tests, method one performed worse than the other two methods. This demonstrates the advantage of using the characteristics of each iteration in order to determine their corresponding threshold value.

These newly developed algorithms can be used to help the inspectors as an additional tool, allowing them an easier interpretation of the results. This is the main reason why all of the different developed methods and thresholding versions are mentioned. It also enables the possibility of developing narrowband transducers, as opposed to the currently used wideband transducers, which have a more focused transfer function and stronger excitation power.

Furthermore, in this chapter, a new pathway for solving the problem of defect identification in the UGW inspection of pipelines is defined. That is to use the information of both space and time to automatically detect defect signals rather than trying to minimize the coherent noise by spatial averaging techniques and interpreting the results based on their properties in a time-domain. This can be considered as one of the main aims of this chapter where the feasibility and effectiveness of such approaches are demonstrated.

Chapter Five

Adaptive Filtering for Enhancement of Signal to Noise Ratio

5.1 Overview

In UGW inspection of pipelines, most of the available SNR enhancement techniques developed in literature use the post-processed signal achieved from the device's propagation routine (See Section 2.4). Nonetheless, inherently the device produces a multidimensional signal. In this chapter, instead of removing the noise from the single time-domain signal achieved from the propagation routine, a novel algorithm is developed to utilize adaptive filtering in guided wave inspection of pipelines; where the input signals to the algorithm are from sensors located on different axial positions of the pipe. The main aims of this algorithm are to achieve SNR enhancement in the results and to demonstrate that guided wave test tools can be utilized differently in order to develop a more efficient post-processed routine for the generation of the test result. This ultimately leads to an easier interpretation of the test result by the inspectors.

The initial development was done using the simulated data generated from the FEM test case. The performance assessment was done using experimental data gathered from laboratory trials on real pipe data using defects in two different locations. Various defect sizes and excitation frequencies were investigated. The results demonstrated the capability of this algorithm in the enhancement of defects SNR using all excitation frequencies. However, the optimum testing frequency is reported as 38 kHz. Furthermore, the filter parameters can be chosen using the simulated data which results in a positive gain of the SNR. The reported results demonstrate the capability of this algorithm in the enhancement of SNR and the feasibility of it in replacing the general propagation routine of the device.

The research conducted in this chapter has been presented in National Structural Integrity Research Centre (NSIRC) Conference, Cambridge, United Kingdom on July 2018 [94] and 57th Annual British Conference on Non-Destructive Testing, Nottingham, United Kingdom on September 2018 [36]. This chapter also resulted in a journal publication in MDPI Applied Sciences [50].

This chapter starts by describing the methodology used for enhancement of SNR using adaptive filtering (in Section 5.2), followed by an example test case to illustrate each stage of the developed algorithm (Section 5.3). The results of experimental trials are reported in Section 5.4. With regard to the achieved results, Section 5.5 reports on the merits and limitations of the developed algorithm. The summary of this chapter is stated in Section 5.6.

5.2 Methodology

In this chapter, adaptive filtering has been used instead of the general propagation routine of the device in order to improve the SNR of the tests. In order to describe the used methodology for noise reduction using adaptive filtering, the differences of the wave modes in terms of their dispersion and spatial arrival must be explained.

Figure 5.1 shows the spatial arrival of the signals from different segments of the pipe. These signals are created using the developed FEM[7], where a three-ring excitation system is used. Each ring contains 32 source points with variable transfer functions. In each polar plot, blue and red lines show the received amplitude from the transducers of two separate rings while the black dotted line serves as the reference. Any point outside the black dotted circle illustrates a positive displacement and the points inside show a negative displacement of their corresponding source point. The following hypothesis can be concluded by comparing the illustrated polar plots:

- The energy of waves received from axisymmetric features (e.g., pipe end) is overwhelmed by the T(0,1) with little variance caused by the existing coherent noise of flexural waves.
- Defect signals have a mixture of both flexural and torsional wave modes; nonetheless, if the cross-sectional area (CSA) of the defect is wide, the T(0,1) will have a greater effect than the flexurals. This is the main reason why adding all the transducers tends to increase the overall energy of T(0,1) while reducing the effect of flexurals.
- Noise regions comprise of mostly flexural waves with almost no axisymmetric wave being detected.

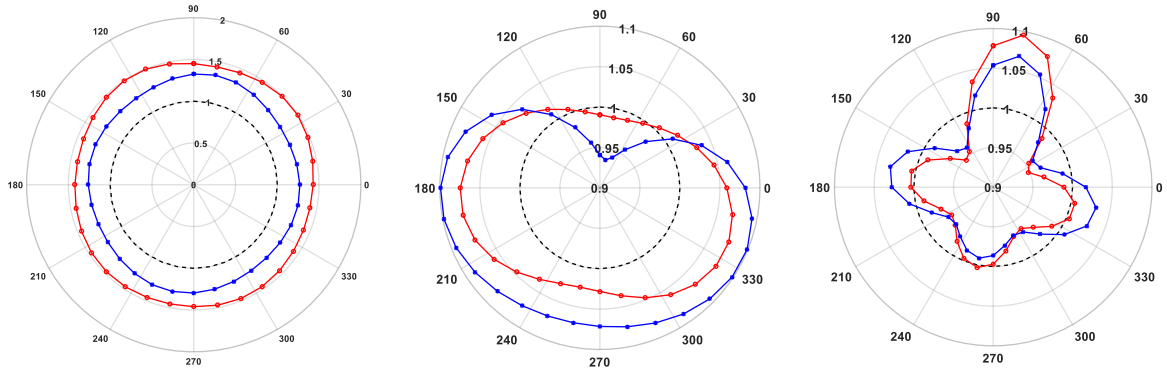

(**a**) Pipe End (**b**) Defect (**c**) Flexurals caused by defect

Figure 5.1: Example of received FEM signals in each individual from different sections of a pipe.

[7] For more information about the design of the model refer to Section 3.3 and for the complete results of the polar plots see Figure 4.1 in Section 4.

To allow inspection of pipelines using guided waves, a single wave mode must be excited in only one direction to allow detection of the anomaly's location. Excitation and detection of flexural waves are difficult and require complex processing algorithms due to their circumferential variation. Therefore, the practice in the general inspection is to excite a unidirectional axisymmetric wave[8]. The most common method of achieving a unidirectional axisymmetric transmission is to use multiple arrays of transducers.

By considering the dispersion curves of the generated wave mode and the placement spacing between the rings, waves can be manipulated in such a way to enforce the forward going propagation and suppress the backward leakage. Hence, the forward propagations of each ring are overlapped while the signals received from backward propagation direction are inversely overlapped. Mathematically, this process is done by manipulating the phase of the signals; in this case, a delay is added to the signals received from the rings in order to synthetically overlay the non-dispersive components within each signal.

The phase-delaying algorithm is applied in both the excitation and reception side in the system to reduce the effect of bidirectional propagation. Afterward, a simple summation is used to achieve the final time-domain signal; this will lead to the generation of a residual noise which might be mistaken as a defect in the inspection. The flowchart for this general routine, which is the common practice of industry, is shown in Figure 5.2. The aim of this chapter is to remove this residual noise generated and improve the defects SNR by enhancing this general routine using adaptive filtering.

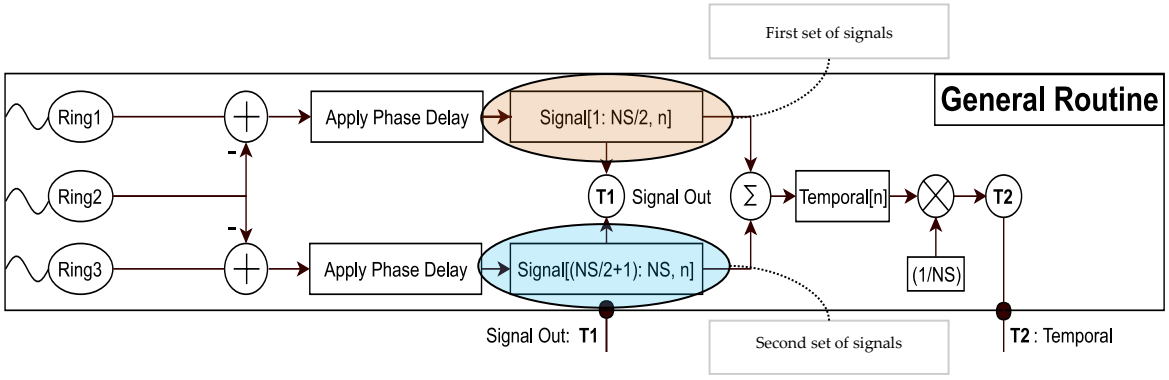

Figure 5.2: Flowchart of the general propagation routine currently used in UGW testing devices. The inputs to adaptive filters are marked by the red and blue circles.

5.2.1 Adaptive Filtering

The main challenge in the inspection of guided waves is to decrease the energy of coherent noise in the test since non-coherent noise is generally removed by bandpass filtering and averaging. Dispersion characteristics of guided wave modes vary with regards to the

[8] For more information, See Section 3.

structural features, frequency, and wave mode. However, the non-dispersive torsional mode is typically constant with an approximate speed of 3260 m/s. By shifting the rings to overlay the T(0,1) signals together, the wave modes which travel at different speeds will be less correlated with those that travel at a constant speed. Furthermore, as shown in Figure 5.1, the flexural waves are highly variable in the space while the torsional mode has a higher correlation. In this case, the existing torsional mode is highly correlated while the noise and flexural modes will be less correlated in time. Therefore, instead of the summation of the signals, adaptive filters can be utilized to enhance the signal resolution. The output signal of a finite impulse response (FIR) filter in time-domain can be achieved by the convolution operation using [73], [95]–[97]:

$$y(n) = \sum_{k=0}^{p} w_k(n)x(n-k) \tag{5.1}$$

where p is the filter length, n is the iteration number, $w_k(n)$ is the filter coefficients with the index of k, and x(n) is the input signal. In the following equations, both **x(n)** and **w(n)** are vectors of size p (represented by bold characters). The resultant error signal would be:

$$e(n) = d(n) - y(n) \tag{5.2}$$

where d(n) represents the required reference (desired) signal; hence, in order to use this algorithm, at least two signals are required. In adaptive filtering, the goal is to minimize the error signal by setting the filter weight. Therefore, in each iteration the filter weights should be updated:

$$w(n+1) = w(n) + \triangle w(n) \tag{5.3}$$

where $\triangle\mathbf{w(n)}$ is the correction step applied to previous filter coefficients to update them for the next iteration; the key component of the adaptive filter is to define $\triangle\mathbf{w(n)}$ in a way that it decreases the mean square error over time. One of the robust methods is the normalized least mean square [71], [96], which tries to minimize the least mean square error by setting the coefficients according to the variable step size. The formula is as follows:

$$\mathbf{w(n+1)} = \mathbf{w(n)} + \beta \frac{\mathbf{x(n)}}{\epsilon + |\mathbf{x(n)}|^2} e(n) \tag{5.4}$$

where β is a normalized step size with $0 < \beta < 2$, ϵ is a small positive number to bypass the problem when $|\mathbf{x(n)}|^2$ becomes too small. The noise in guided waves is highly variable due to the existence of time-varying multiple modes. To make sure the filter is not over-fitted to the characteristics of previous iterations, a leakage factor, α, is added to reduce the effect of previous iterations [97]:

$$\mathbf{w(n+1)} = \alpha\mathbf{w(n)} + \beta \frac{\mathbf{x(n)}}{\epsilon + |\mathbf{x(n)}|^2} e(n) \tag{5.5}$$

The flow chart of this algorithm is shown in Figure 5.3. In this setup, instead of adding the signals received from the rings of transducers, they are selected as the desired response d(n)

and the input signal x(n). Every other signal is updated based on the characteristics of each iteration and y(n) is the output of the filter. The selected reference and input signals are the two sets generated in the general propagation routine, as marked in Figure 5.2. Applying this phase delay and summation of arrays within each ring, two sets of signals are created where both have the following components:

- S(t) - Signals of interest/anomalies: Highly correlated and in phase
- N(t) - Flexural and other noise: That is not correlated to S(t). Furthermore, noise sources of two signals are correlated to each other.

This satisfies the need for a reference signal in using adaptive filtering. To cancel the backward leakage, this algorithm is done with the switching of the input and reference signals, where the final result is the summation of the two generated outputs of the adaptive filters.

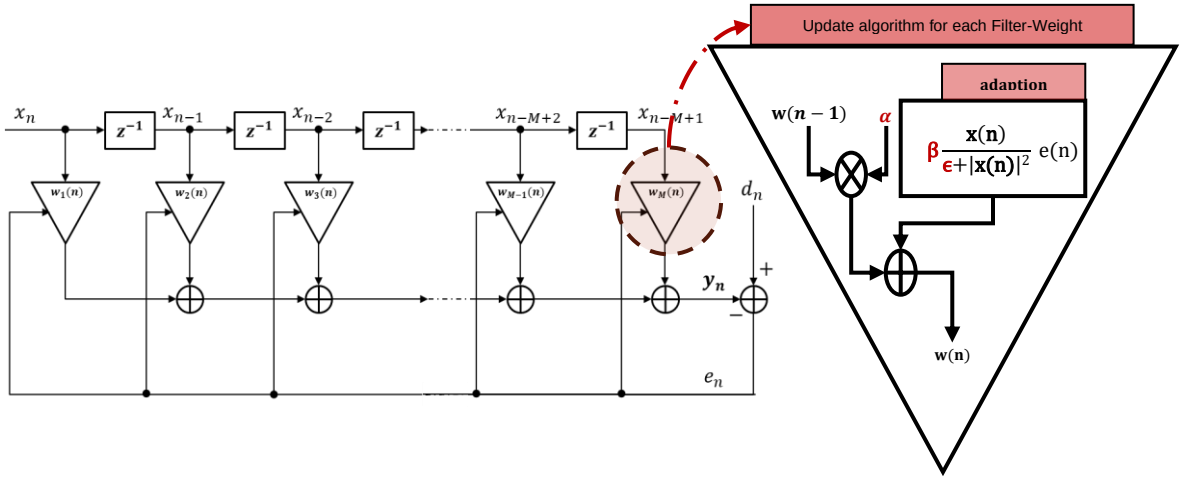

Figure 5.3: Adaptive linear prediction algorithm for noise cancellation where the marked red parameters are fixed by the user.

5.3 Example Test Case

The initial verification of this algorithm was done using a FEM signal where a 3% CSA defect is located 3 meters away from test origin. As explained previously in Section-2, for canceling the effect of flexural waves, at a number of linearly placed excitation points are required. Therefore, in order to check the capability of this algorithm and increase the difficulty of the detection, the signal of only four source points have been selected in the reception side for further processing. These active source points are shown in Figure 5.4a while the resultant time-domain signal is shown in Figure 5.4b.

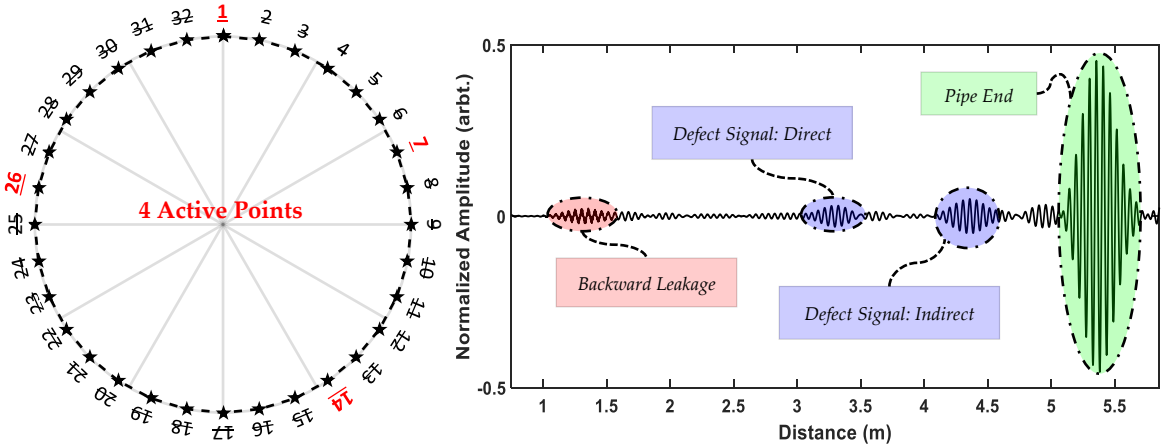

(a) Selected Points (each ring) (b) Signal in time-domain

Figure 5.4: Example signal from FEM. (a) shows the selected points (marked by red) in each ring and (b) shows the time-domain signal.

The used excitation sequence for generating this data set is a 10-cycle Hann window sine wave with a frequency of 30 kHz where variable transfer functions are used for each of the source points. Figure 5.5 shows the two sets of signals achieved after applying the phase delays of the general propagation routine (blue and red). Four regions are of main interest in this figure, which are (a) backward leakage, (b) flexural noise, (c) direct and (d) indirect defect signals. Since both direct and indirect (defect) signals are received from the forward testing direction, they have similar characteristics, and both should be enhanced by this algorithm.

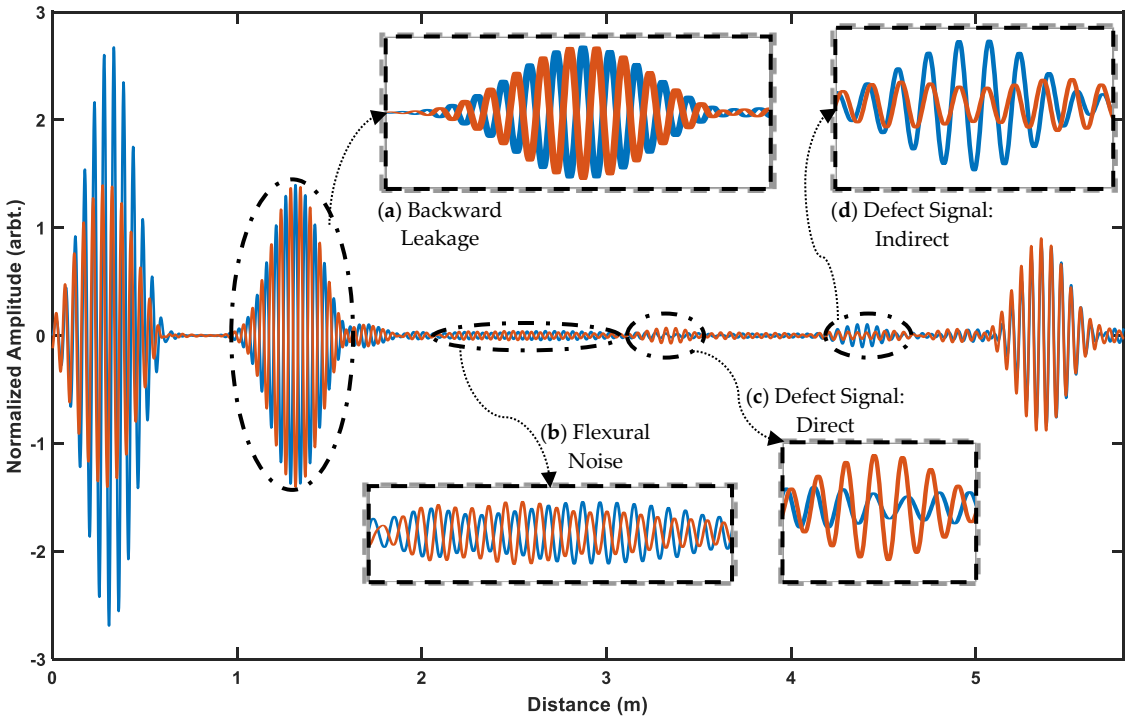

Figure 5.5: Signals generated using FEM (30 kHz) where backward leakage, the flexural noise, and both defect regions are marked. Blue and red lines show the first and second sets of the signals as marked in Figure 5.2.

As can be seen in Figure 5.5, the noise region (b) is significantly less correlated than the defect signals (c and d). Furthermore, although the amplitudes of two sets of signals received in the defect regions are not the same, their phases and polarity are in perfect correlation. Therefore, although in the signal achieved from the general propagation routine their characteristic might be similar, but using the separate rings, the characteristics of defect and flexural signals are distinguishable.

5.3.1 Cancellation of Backward Leakage

Figure 5.5a shows the two sets of signals received from the backward testing direction. As can be seen, these signals are inversely overlapped with little differences in amplitude. This is due to the general propagation routine where the received signals from rings are delayed and inverted depending on the ring spacing.

After applying the filtering, the phase of the outcome does not change, therefore by switching the input and desired signals of the adaptive filter, two sets of results will be generated in which the signals from the forward direction are overlapped and the ones from the backward direction are inversely overlapped. This is illustrated in Figure 5.6, where blue and red signals show the two sets of results achieved from adaptive filtering by switching the inputs. This operation not only enhances the defect signals received from the forward direction (Figure 5.6c) but it also decreases both the backward leakage (Figure 5.6a) and flexural noise regions (Figure 5.6b) significantly.

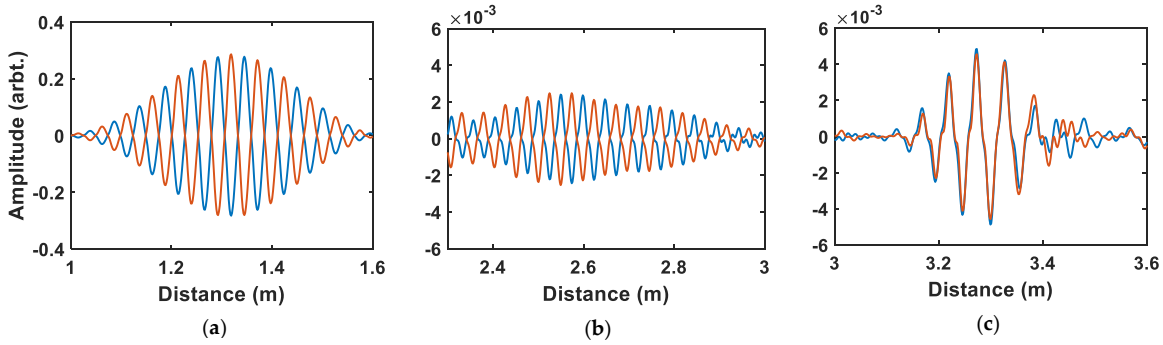

Figure 5.6: Two sets of results (red and blue lines) achieved from switching the input and desired signals of the adaptive filter where (a) shows the signals received from the backward direction, (b) shows the flexural noise, and (c) shows the direct defect signal.

5.3.2 Selection of Filter Weights

The filter order was selected based on the FEM data. A brute force search was applied to maximize the SNR of a direct defect signal. Therefore, the best case for each weight is considered. The generated results are shown in Table 5.1. The SNR of the unfiltered signal is 5.3 dB; Therefore, it is difficult to detect this defect as it is almost buried in the noise level. As can be seen, by increasing the filter order, the SNR is reduced. When the size of the filter

order grows above 8, the SNRs of filtered and unfiltered signals are approximately the same. This is because by growing the number of samples, the differences between a torsional and flexural wave become limited as they are in the same frequency band. However, in smaller steps, the changes in flexural waves are more time varying. Therefore, from these results, eight can be considered as the safest number for filter order where no change will be applied to the signal and two can be considered as the best filter order for maximizing the SNR.

The selection of the filter order is a compromise between the safest option where it results in no change and the best option which maximizes the enhancement of SNR. With regards to the results achieved from FEM (shown in Table 5.2). Filter orders of two and eight provide the maximum and minimum enhancements, respectively. Therefore, using a filter order of five can be considered as a good compromise, as only a drop of only 1 dB is observed from the maximum achieved SNR, which is 8.31 dB. Doing so provides greater safety as more past samples are used in deciding the current filter orders and only a 10% drop of SNR is observed from the maximum achievable SNR of 8.31 dB (using filter order of 2).

Table 5.1: Maximum SNR achieved for each filter on the FEM test signal with a 30 kHz signal.

Filter Order (#)	**2**	**3**	**4**	**5**	**6**	**7**	**8**	**9**	**10**
Maximum SNR (dB)	8.31	8.27	7.76	7.32	6.78	6.07	5.33	5.07	5.02

5.3.3 Adaption of Filter Weights

The best filter order can be dependent on other factors, such as frequency and the existing flexurals of the iteration. The main aim of this chapter is to test the workability of the adaption algorithm to the guided wave scenario; hence, the filter order is fixed to five.

Since the number of available samples is limited, observation of the filter's frequency response is not possible; nonetheless, the orders can be viewed in the time domain. In Figure 5.7b–f, the changes of the first filter value are shown while Figure 5.7a shows their corresponding results in the time-domain. The red signals illustrate the results of the leaky NLMS while the black dotted lines represent the normal NLMS algorithms. Normal NLMS depends more on past values and is not fast enough to adapt to the current iteration; however, leaky NLMS makes this adaption faster by reducing the filter weights' dependence on their past values. After each adaption to a big sequence such as backward leakage or defect, the magnitude of the filter weight tends to move toward zero; in other words, the weights forget the characteristics of past iterations significantly faster, which allows them a quicker adaption to the characteristic of the current iteration. Furthermore, as illustrated by blue dotted regions, in the region of defects, a high peak is generated in the magnitude of each filter order set by the leaky NLMS method. Although other techniques and updated algorithms exist, this fast

adaption algorithm, where the filter can forget the characteristics of the previous wave, is the main reason why leaky NLMS is more effective in the guided wave inspection of pipelines.

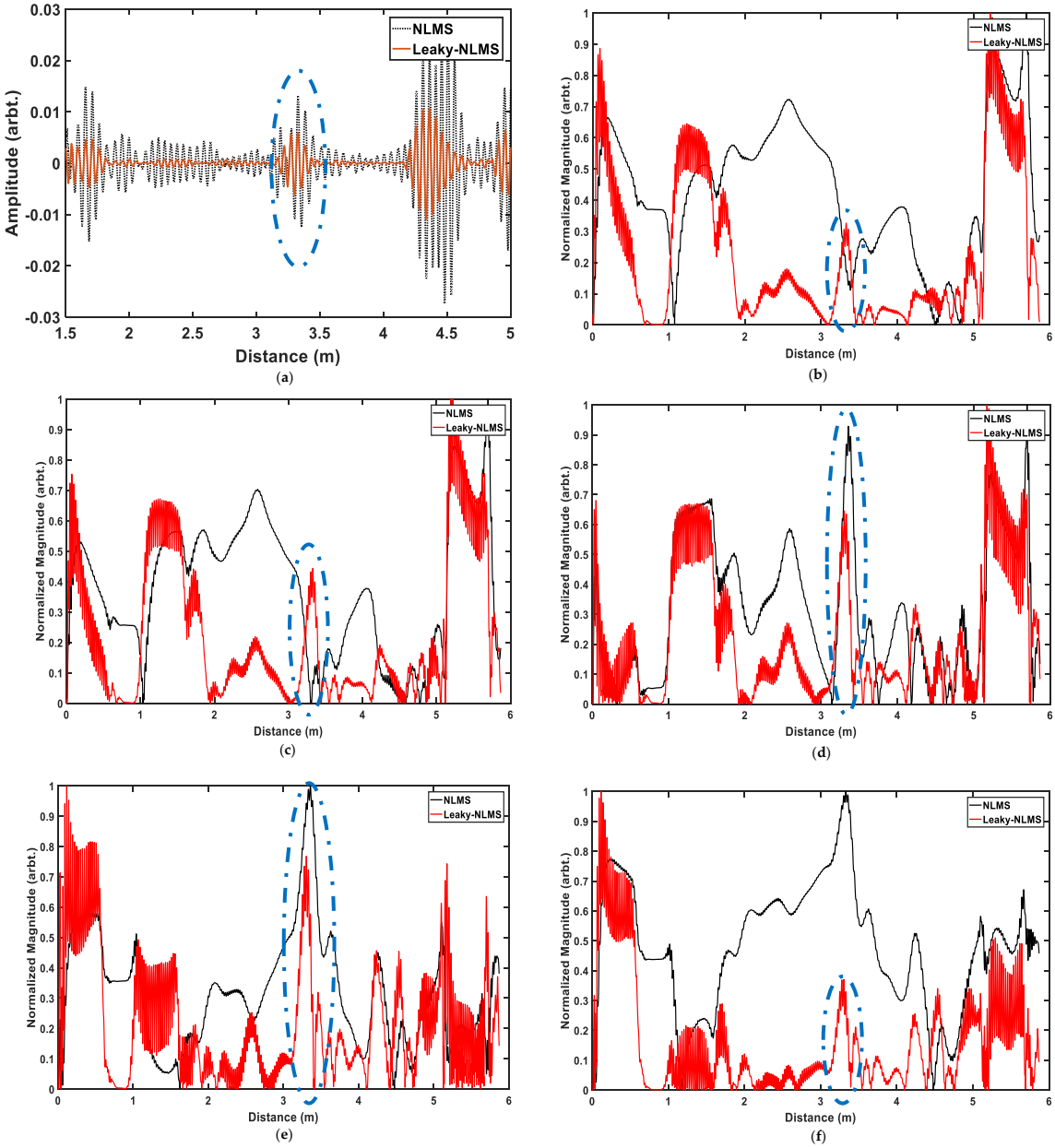

Figure 5.7: Comparison of the results achieved from NLMS (black) vs leaky NLMS (Orange) where (a) shows the time-domain results and (b-f) show the normalized magnitudes of filter orders 1 to 5, respectively.

5.4 Results

The performance of the algorithm was assessed in experimental trials by detecting defects of CSA sizes between (and including) 3% and 8%. The algorithm had a neglectable increment of SNR in 2% CSA defect; hence, the results of 2% CSA defect is not reported. It is expected that the algorithm would be more effective at lower frequencies since they are more dispersive; furthermore, the excitation power of lower frequencies is higher than those of higher frequencies, both due to the duration of the signals as well as the systems

transfer function. Therefore, frequencies between 30 to 50 kHz with a step of 2 kHz were tested. The SNR achieved from the general propagation routine is demonstrated in Section 3.2.2. The peak SNR is always achieved using 40 kHz and 38 kHz in the case of Defect 1 and Defect 2, respectively. Furthermore, the SNRs achieved from each frequency are reduced almost linearly when the defect size is decreased; thus, the noise energy is almost constant while the defect energy is decreasing.

5.4.1 Parameter Selection

The results were generated from two sets of parameters:

- **Model Parameters:** The optimum parameters are achieved by using a brute force search algorithm to find the parameters which give the maximum SNR in the FEM test. The main goal of this test was to assess the response of the algorithm by fixing the parameters to an optimum solution created by the FEM.
- **Experimental Parameters:** The brute force search algorithm was performed on the Defect 1 (with the size of 4% CSA) sample to find parameters that result in most enhancements of SNR for each frequency. The goal was to find the best testing frequency where the least variations in the enhancements are observed and assess whether fixed parameters can enhance the SNR of defects with lower CSA size (3% test case).

Table 5.2 shows the used parameters used in each test with regard to the frequency.

Table 5.2. Used parameters in the Tests

Frequency (kHz)	Step Size	Leakage	Compensation
30 (Model)	0.01	0.96	0.01
30	0.01	0.61	0.21
32	0.01	0.46	0.21
34	0.01	0.46	0.26
36	0.01	0.56	0.06
38	0.16	0.81	0.01
40	0.86	0.76	0.01
42	1.41	0.91	0.01
44	1.21	0.96	0.01
46	1.46	0.96	0.01
48	1.46	0.96	0.01
50	1.46	0.96	0.01

The results achieved for both defect locations using both model and experimental parameters are demonstrated in Sections 5.4.2 and 5.4.3. In each of these sections, the first figure illustrates the results of Defect 1 and the second figure illustrates the results of Defect 2. The results achieved from using frequencies of 34 and 38 kHz have been marked by black dotted square and black oval, respectively.

5.4.2 Model Parameters

The results achieved using model parameters for Defect 1 are illustrated in Figure 5.8 where (a) shows the SNR of the defect and (b) shows the amount of enhancement. The following hypothesis can be extracted from these tests:

- In defects above 5% CSA, the algorithm enhances the results using all frequencies. For defects with CSA size of lower than 4%, the algorithm can enhance the SNR using 30, 32, 34, and 38 kHz.
- Except for the case of 3% CSA test, both maximum SNR and maximum enhancements are achieved using 34 and 38 kHz in the tests. In the 3% CSA test, maximum enhancement is for 30 kHz; nonetheless, the SNRs of 34 and 38 kHz are greater.
- Comparing results achieved from different defect sizes while keeping the frequency constant, the variance of the enhancements achieved using 30 kHz is less in comparison to all other cases.
- Comparing results achieved from using different frequencies on the same defect sizes, higher frequencies (above 40 kHz) will results in a lower enhancement in comparison to the lower frequencies.

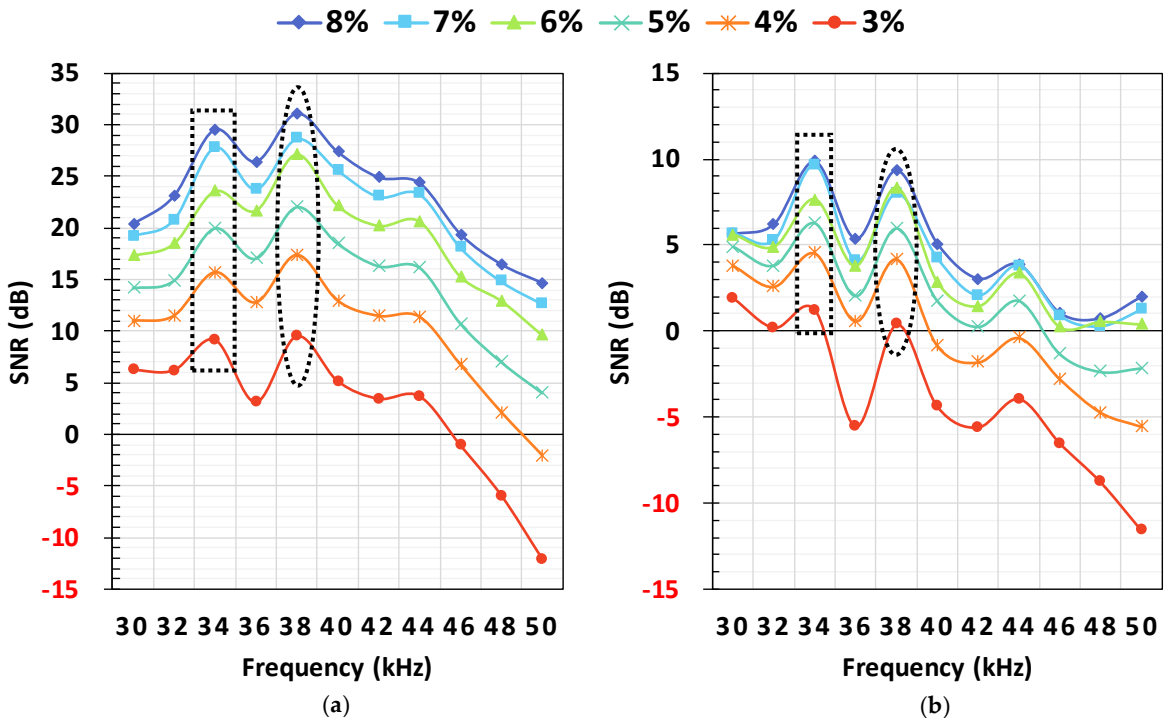

Figure 5.8. Results achieved using fixed model parameters for Defect 1 location using various excitation frequencies where (a) shows the achieved SNR and (b) shows the amount of improvement in comparison to the general propagation routine.

The results achieved using model parameters for Defect 2 are illustrated in Figure 5.9 where (a) shows the SNR of the defect and (b) shows the amount of enhancement. The following hypothesis can be extracted from these tests:

- The algorithm can enhance the results for all defect size using lower frequencies (lower than 40 kHz). This is due to the fact that Defect 2 is located on a location with a higher level of flexurals.
- Both maximum SNR and maximum enhancements are achieved using 34 and 38 kHz in the tests. In the 3% CSA test, the enhancement is for 32 kHz is more in comparison to the one achieved from 38 kHz by a neglectable amount. However, in overall 38 kHz tends to generate higher SNR and enhancements for both Defect 1 and Defect 2.
- Comparing results achieved from different defect sizes while keeping the frequency constant, the variance of the enhancements achieved using 34 kHz is less in comparison to all other frequencies.
- Comparing results achieved from using different frequencies on the same defect sizes, higher frequencies (above 40 kHz) will results in a lower enhancement in comparison to the lower frequencies. The only exception is 36 kHz where it can result in less enhancement in comparison to the higher frequencies for higher defect sizes (above 5% CSA); nonetheless, using 36 kHz generates a higher actual SNR.

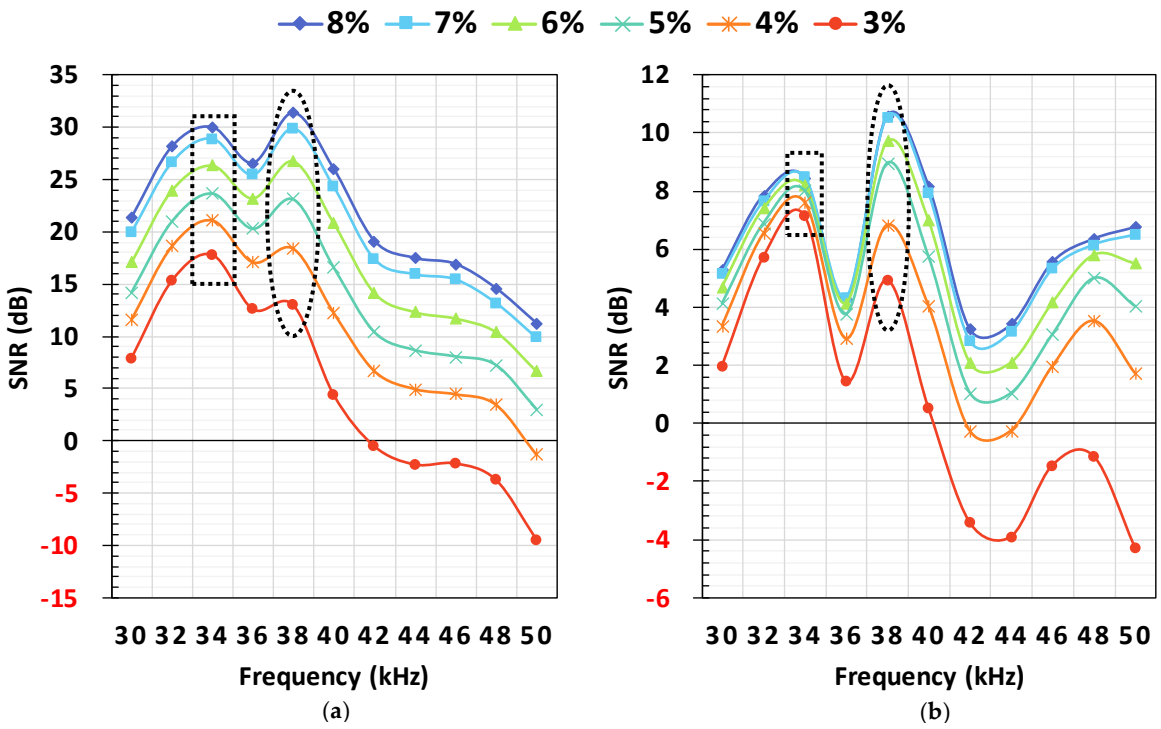

Figure 5.9. Results achieved using fixed model parameters for Defect 2 location using various excitation frequencies where (a) shows the achieved SNR and (b) shows the amount of improvement in comparison to the general propagation routine.

5.4.3 Experimental Parameters

The results achieved using experimental parameters for Defect 1 are illustrated in Figure 5.10 where (a) shows the SNR of the defect and (b) shows the amount of enhancement. The following hypothesis can be extracted from these tests:

- For defects with higher CSA size (above 5%), lower frequencies tend to achieve higher SNR after adaptive filtering where the defect signal was enhanced by at least a factor of 2. The greatest enhancement is achieved from 34 kHz and the maximum SNR is achieved using 36 kHz for these signals.
- Although higher frequencies will result in lower SNR, their enhancements are approximately the same for different sizes of the defect. Nonetheless, their final SNR is almost always lower than all other frequencies, especially in the cases of frequencies above 46 kHz.
- For 3% and 4% CSA defects, the greatest enhancement and gain are achieved using the 38 kHz frequency. Furthermore, as can be seen in Figure 5.10b, the enhancement achieved using this frequency is less affected by the CSA loss of the defect in comparing the ones achieved from using frequencies less than 40 kHz.
- Compare to using model parameters, using experimental parameters resulted in a higher enhancement in most of the frequencies.

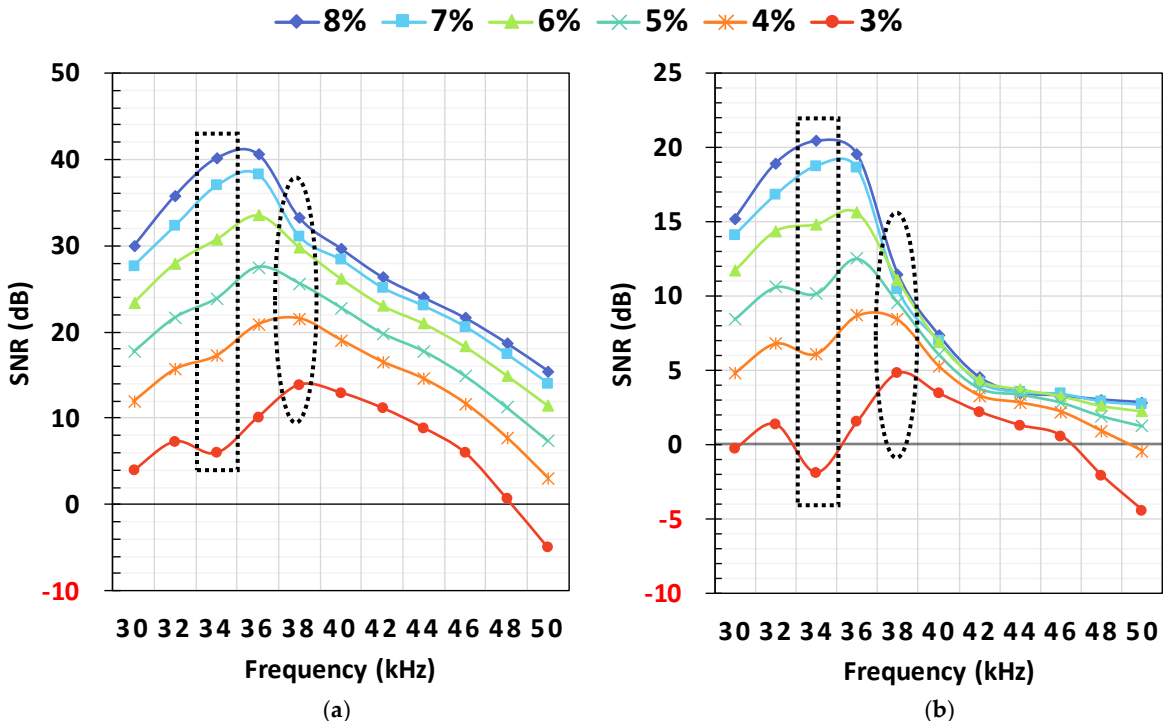

Figure 5.10. Results achieved using experimental parameters for Defect 1 location using various excitation frequencies where (a) shows the achieved SNR and (b) shows the amount of improvement compared to the general propagation routine.

The results achieved using experimental parameters for Defect 2 are illustrated in Figure 5.11 where (a) shows the SNR of the defect and (b) shows the amount of enhancement. The following hypothesis can be extracted from these tests:

- For all defect sizes, using lower frequencies result in higher SNR after adaptive filtering where the defect signal was strength was enhanced by at least a factor of 2. The greatest enhancement and gain are achieved using 34 kHz.
- The enhancements achieved using higher frequencies (above 40 kHz) are almost always close to zero. Hence; using this technique with higher frequencies, wouldn't affect the results significantly.
- Compare to using model parameters, using experimental parameters resulted in a higher enhancement in most of the frequencies. Furthermore, the results tend to be more linearly varying with frequencies with a peak of 34 kHz.
- Even though the experimental parameters were created using another defect location, but they are capable of enhancing the results more than the model parameters in lower frequencies (below 40 kHz). However, as can be seen in Figure 5.9, using model parameters in higher frequencies can result in a higher increase of SNR. This suggests that the selection of optimum parameters can be dependent on the defect location, excitation frequency and the amount of existing coherent noise within the defect region.

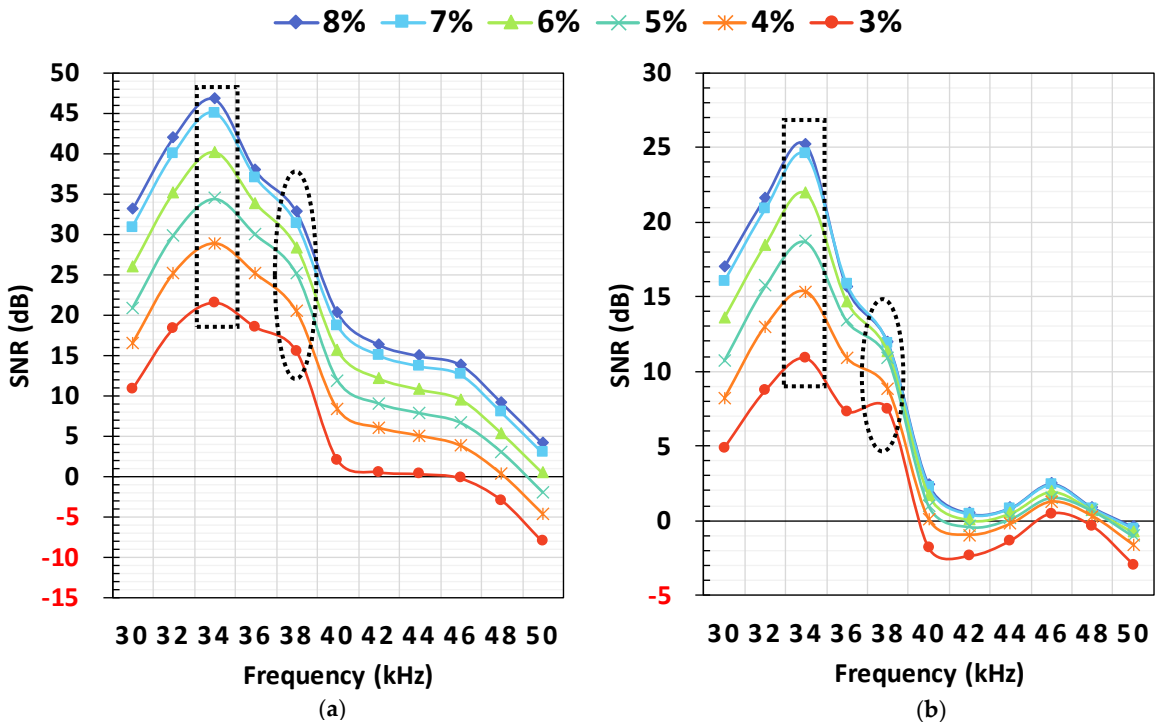

Figure 5.11. Results achieved using experimental parameters for Defect 2 location using various excitation frequencies where (a) shows the achieved SNR and (b) shows the amount of improvement compared to the general propagation routine.

5.5 Discussion

Figure 5.12 shows the difference of enhancements between the results of model parameters and experimental parameters for both (a) Defect 1 and (b) Defect 2. These results show that although temporal SNR of the signals is important, the spatial characteristic of the noise also plays an important role in the amount of enhancement. As an example, while 40 kHz has the highest SNR from the general routine, it does not perform as well as 38 kHz for the algorithm. In most cases of lower CSA defects, the SNR improvements are achieved not by enhancing the axisymmetric signal strength, but by removing the flexural noise. For Defect 1, except for excitation frequencies of 30, 34, and 40 kHz in the 3% CSA defect, all other cases were enhanced when the experimental parameters were used. Nonetheless, for Defect 2, the majority of the higher frequencies (40 kHz) could achieve a better SNR using model parameters. This suggests that the selection of optimum parameters can be dependent on the defect location. On the other hand, in almost all tests, higher frequencies (above 40 kHz) resulted in less enhancement in comparison to lower frequencies regardless of the filter parameters. This suggests that this algorithm tends to perform better at lower frequencies; which is expected since flexurals with lower frequencies are highly dispersive, which adds to the spatial noise of the tests. Furthermore, some frequencies such as 38 and 34 kHz, are more stable with regards to the enhancement achieved using both parameters.

Since signals with SNRs higher than 30 dB are more easily detected, it is better to use a frequency that provides a stable enhancement for both low and higher CSA sizes rather than setting parameters that can greatly increase the higher CSA defects while decreasing the SNR of smaller defects. An excitation frequency of 38 kHz provides approximately the same enhancement using both model parameters and experimental parameters, which shows that this frequency is less affected by the parameters in comparison to the others. Furthermore, for Defect 1, it can also be seen from the results of model parameters that 38 kHz always achieves the maximum gain even though the parameters are optimized for 30 kHz excitation frequency in the model. In the case of Defect 2, the maximum SNR can be gained using 34 kHz; however, the difference between the SNR achieved using 34 and 38 kHz for Defect 2 is neglectable (less than 5 dB) for defects with smaller CSA sizes.

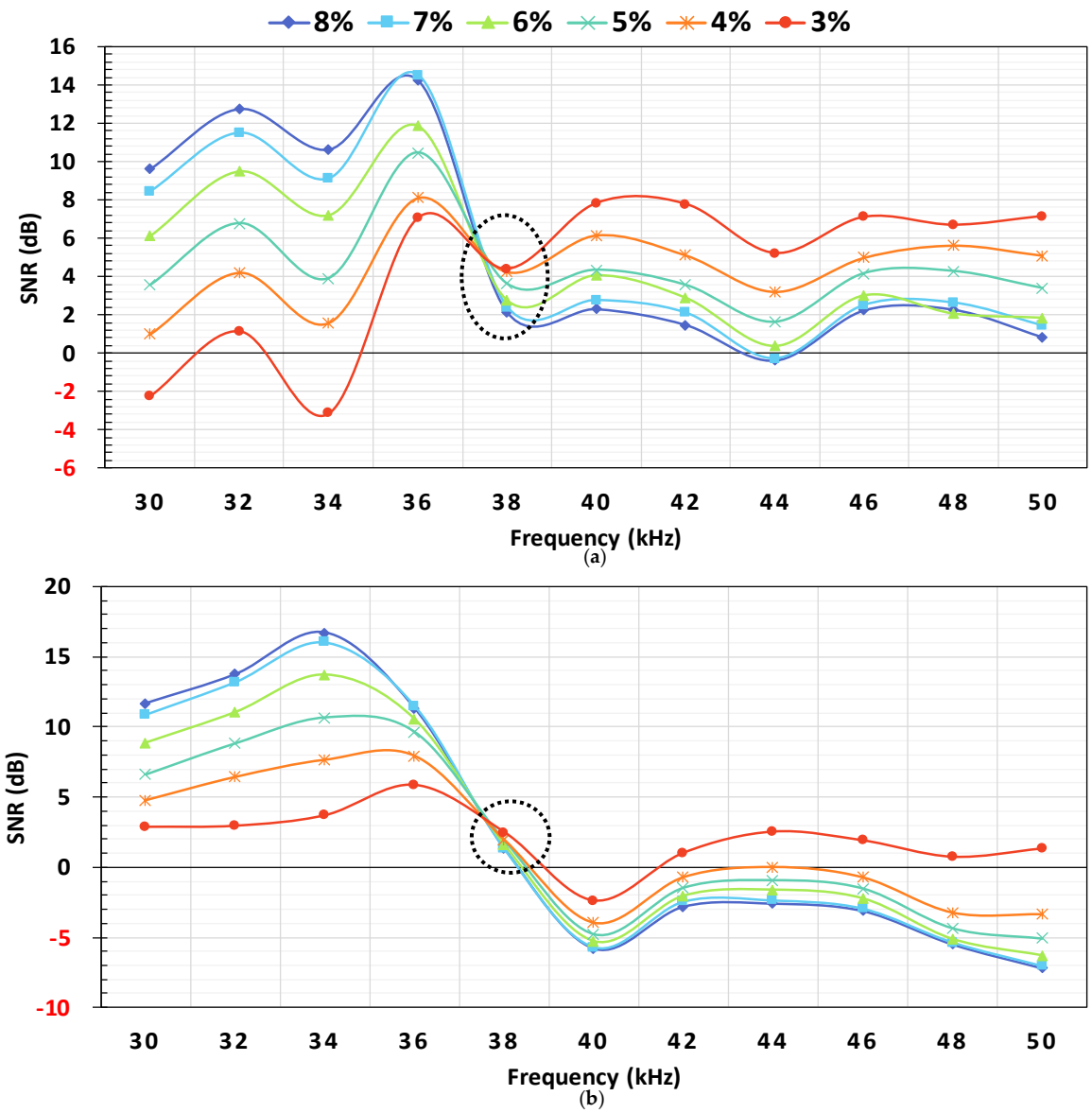

Figure 5.12. Comparison of the improvement achieved by using experimental parameters as opposed to model parameters where (a) shows the results of Defect 1 and (b) shows the results of Defect 2.

It should be born in mind that, even though in some frequencies the mathematically calculated SNR might be less than the one achieved from the general propagation routine, the high order flexurals are always canceled, which leads to an easier interpretation of results by the inspectors. Figure 5.13 shows the results of the 30 kHz excitation sequence for defects with different CSAs. As can be seen, highly variable noises in the region between 2.5 and 3 m are canceled but those caused by low order flexurals at 2 to 2.5 m are enhanced. While in defects with higher CSA sizes most improvement is achieved due to the amplification of the defect signal, in lower CSA defects (especially in the case of 3% CSA), the noise cancellation is the main reason for enhancement. The enhancement of these low order flexurals is the main reason why the algorithm fails to improve the SNR in some of the testing frequencies.

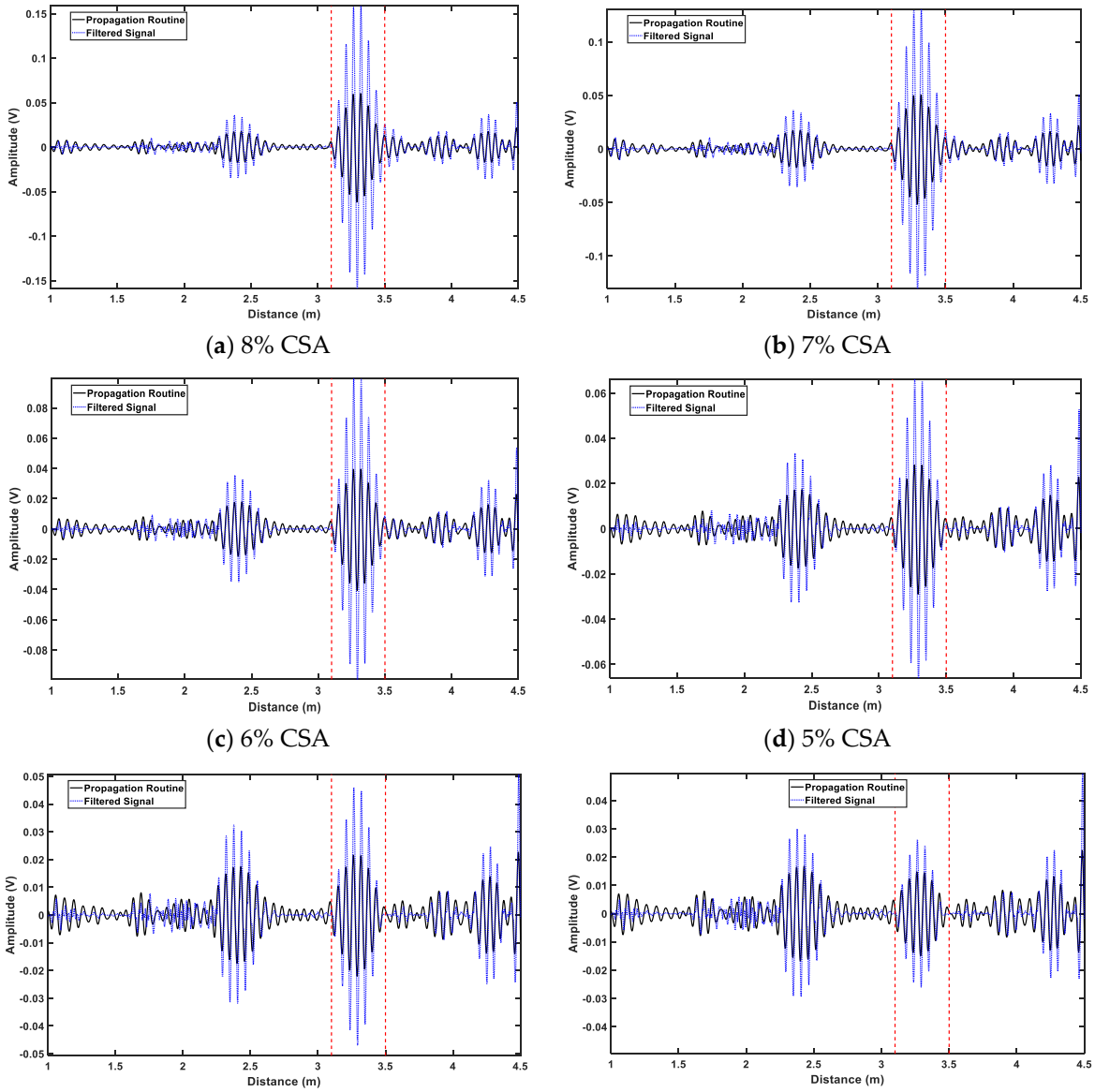

(**a**) 8% CSA (**b**) 7% CSA

(**c**) 6% CSA (**d**) 5% CSA

(**e**) 4% CSA (**f**) 3% CSA

Figure 5.13. Example of filtered signals using 30 kHz excitation and model parameters where defect size is varying.

Low order flexurals are less dispersive on frequencies above 30 kHz with their speed moving toward that of T(0,1), 3260 m/s[9]. Since the phase delays are applied with respect to T(0,1) wave speed, if the flexural waves have the same speed they will be overlapped in the input and desired responses. This is the main reason why such signals might not be canceled and, in fact, in some scenarios, they might even be amplified.

Figure 5.14 shows a comparison between the general propagation routine and the filtered signal. Considering the 34 kHz filtered signal shown in Figure 5.14b, the noise envelope is clearly dispersed (2–2.5 m). Figure 5.15 also shows the results achieved from 38 kHz

[9] See Figure 2.2 in Section 2 for an example of dispersion curve

excitation frequency. In these figures, the input and reference signals for the noise and defect regions are shown as blue and red. The following conclusions can be extracted by observing the difference between a defect and noise signals:

1. If any low order flexurals or noise are overlapping in the input and reference signals, they will not be removed and might be amplified.
2. The amplification of the signals is also dependent on the amplitude of the input signals to the algorithm, e.g., the defect signal in case Figure 5.14 does not have the same enhancement of that in case Figure 5.15 since the blue signal in case Figure 5.15 is much stronger.
3. Although some flexural signals will remain in the resultant signal, there is an option of further post-processing to enhance the SNR. Such is the case of the noise region located at 2–2.5 m in case Figure 5.14, where it is clearly dispersed at the end of its window, and the region of 1.5–2 m in Figure 5.15, which results from backward leakage. Therefore, by considering other characteristics in the signal, the results can be post-processed to distinguish different modes and further increase the SNR of the test.

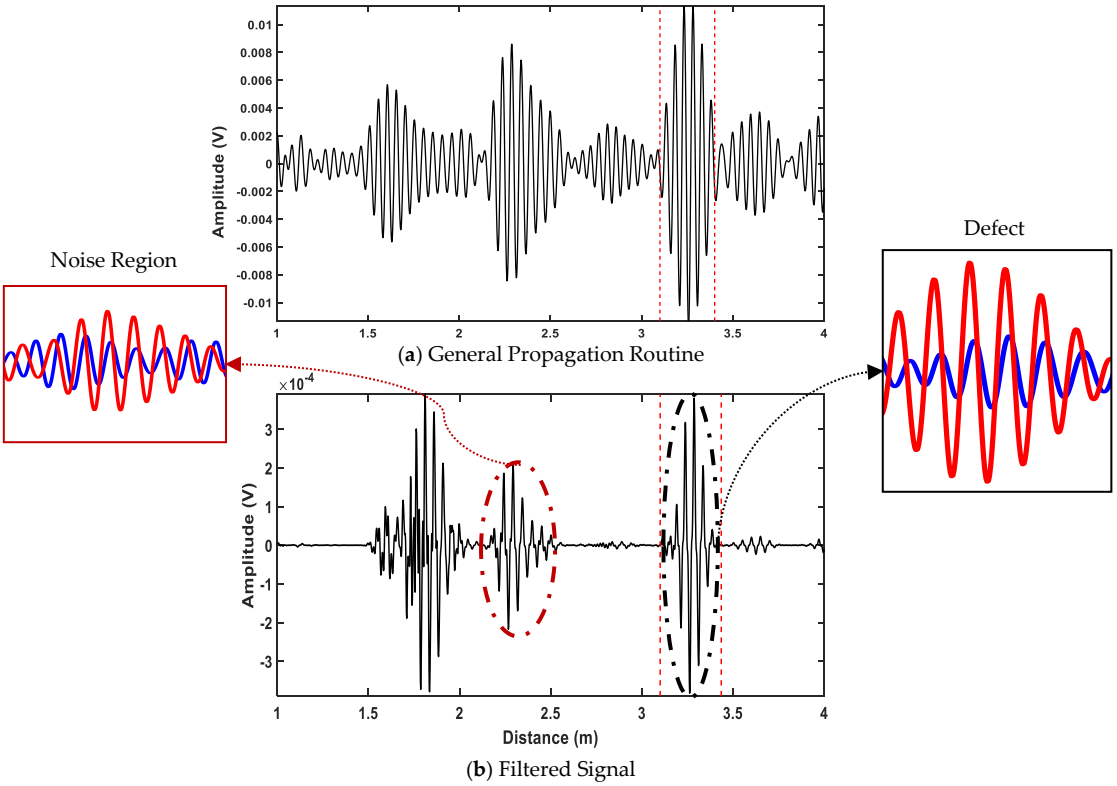

Figure 5.14. The result of (a) general propagation routine vs (b) filtered signal with their corresponding inputs (blue and red lines) of noise (left side) and defect (right side) with the excitation frequency of 34 kHz gathered from an experimental pipe with defect size of 3% CSA (Defect 1).

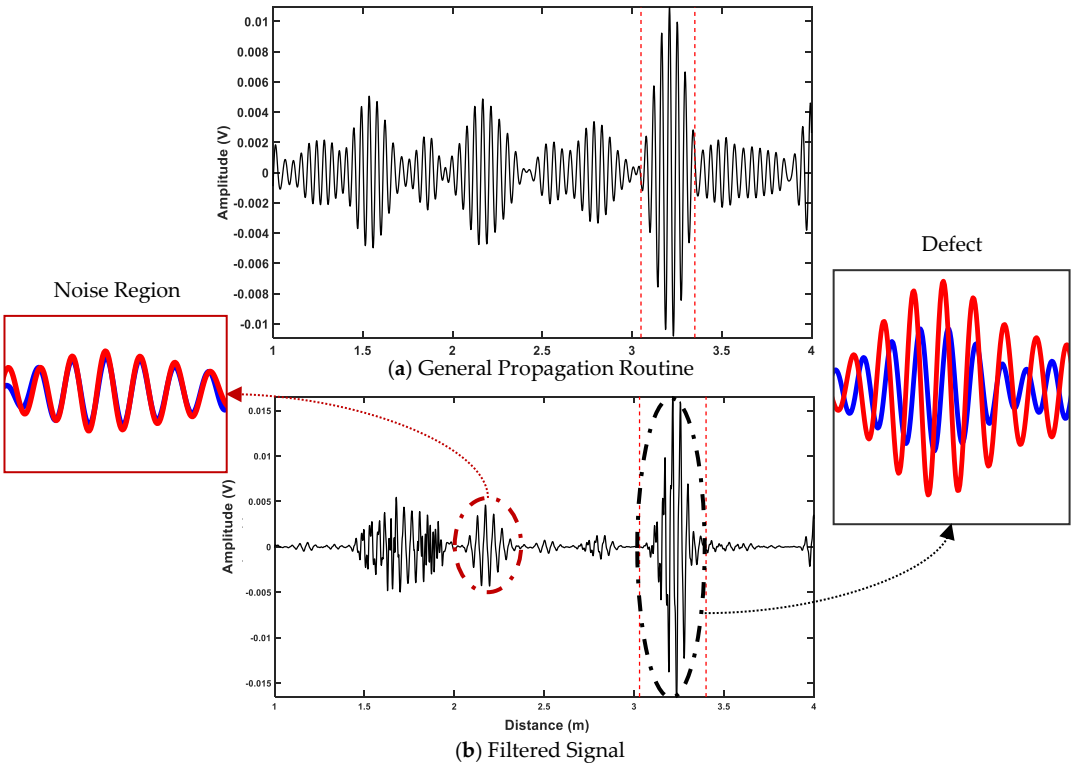

Figure 5.15. The result of (a) general propagation routine vs (b) filtered signal with their corresponding inputs (blue and red lines) of noise (left side) and defect (right side) with the excitation frequency of 38 kHz gathered from an experimental pipe with defect size of 3% CSA (Defect 1).

5.6 Chapter Summary

In this chapter, an adaptive filtering approach is utilized to enhance the SNR of the torsional waves generated from defects in guided wave inspection of pipelines. For doing so, as opposed to using a general propagation routine of guided-wave testing devices, the two sets of signals received from the test tool were used as inputs to the adaptive filter, which resulted in a single output in the time domain. Inherently, in these two sets of signals, the torsional waves are overlapping while the flexurals are varying; this was the basis on which the adaptive filter was able to enhance the SNR of torsional waves. Since flexural waves are variable both in space and time, the used updated algorithm for filter weights was leaky NLMS, which allowed faster adaption to the highly variable flexural noise and enabled a faster reset of the filter weights.

The algorithm was initially developed and validated using the simulated signal generated from the FEM test case. Afterward, laboratory trail validation took place with two sets of filter parameters: model parameters, where the parameters were set to find the highest SNR for the FEM test case with an excitation frequency of 30 kHz; and experimental parameters, where the optimum parameters for each frequency were generated with regards to the real pipe data with 4% CSA defect. In most test cases, all the frequencies resulted in the enhancement of the SNR. Nonetheless, the optimum testing frequency was found to be 38

kHz since it achieved both the maximum and greatest enhancement of SNR in the majority of the results. Also, this excitation frequency was less affected by the change of parameter as limited enhancement was observed between the results achieved by using model parameters and experimental parameters.

Comparing the results from model parameters and experimental parameters, it is evident that setting the parameters with regards to each individual frequency enhances the achieved SNR. Nonetheless, optimum selection of parameters is a trade-off between the maximum achieved gain and the stable enhancement of the SNR of smaller defects. This was assessed using experimental parameters; when the optimum parameters for 4% CSA defect were used for the case of 3% defect, not all frequencies could improve the SNR. The model parameters test proved that the parameters can be chosen using a FEM model, but it will not result in the maximum gain.

The amount of SNR achieved in each test case depends not only on the enhancements of the torsional wave but also the cancellation of the flexural waves. It must be borne in mind that since the physical arrangement of the rings is fixed, in some cases, especially for lower-order flexural waves that have closer wave speeds to torsional waves, the noise will not be canceled. However, the higher-order flexural noise will be canceled in all the tests and the achieved results can be further processed for torsional wave mode detection.

The developed algorithm in this chapter resulted in the enhancement of SNR compared to the devices' general propagation routine. On the other hand, this chapter demonstrated that by considering the spatial placement of the sensors, new propagation routines can be designed which considers both the spatial and temporal characteristics of these signals. This will lead to the development of a more efficient propagation routine that can improve the SNR of the defects and allows easier interpretation of test results by inspectors.

Chapter Six

Defect Detection using Spectral Matching of Torsional wave

6.1 Overview

In this chapter, a new algorithm is proposed for the detection of defects using the power spectrum of the received time-domain signals. This algorithm exploits the differences in the power spectrum of torsional and flexural waves, in order to detect the torsional wave, leading to the defect location. The method is based on a sliding moving window, wherein each iteration the signals are normalised, and their power spectra are calculated. Each power spectrum is compared with the previously known spectrum of excitation sequence. Five binary conditions are defined; all of these need to be met in order for a window to be marked as defect signal. This method is validated using a simulated test case generated by a Finite Element Model (FEM) as well as real test data gathered from laboratory trials. In laboratory trials, the performance of algorithm was assessed using two defects located in different locations with sizes of 2-8% CSA. The used excitation frequencies in each test case varied between 30-50 kHz with steps of 2 kHz. The results demonstrate the capability of this algorithm in detecting torsional waves with low SNR without requiring any change in the excitation sequence. The results of this algorithm can support the inspectors' decision in detection of defects in the tests; hence, it provides more certainty in the interpretation of the results and reduces the number of outliers called due to the coherent noise created by the flexural waves.

The research conducted in this paper resulted in a journal publication in MDPI Applied Sciences [98].

This chapter starts by describing the methodology used for developing the algorithm in Section 6.2. Afterward, each stage of the algorithm is explained thoroughly using an example test case in Section 6.3. The results of laboratory trials are reported in Section 6.4, followed by the discussion which illustrates both the advantages and limitations of this algorithm (Section 6.5). The final Section (6.6) summarises the achievements and concludes this chapter.

6.2 Methodology

The common concept in all the aforementioned signal processing methods in the literature[10] is the usage of dispersion and multimodality of guided waves in order to increase the SNR. The signals are then inspected in the time domain to report on the location of anomalies. It has already been demonstrated in the literature that the spectral domain can be processed to remove the noise. Observing the problem from another perspective, instead of noise removal, the spectral domain can also be used to detect the signal of interests (defect) automatically. In ultrasonic testing, the excitation sequence is known, and the inspectors generally look for signals with the same characteristics in the time domain to find their signals of interest, such as a defect in materials. In UGW, one of the common excitation sequences is a 10-cycle Hann windowed signal with a different frequency, depending on the testing conditions. However, these signals are typically contaminated by coherent noise which has similar temporal characteristics to those of defect signals. The excitation sequence is axisymmetric and not dispersive; hence, no significant changes in the frequency response of the received signal should be inspected. Therefore, the hypothesis used in this chapter for developing the algorithm is that by using a sliding window and comparing the power spectrum of each iteration with the one achieved from the excitation sequence, the defect location can be detected.

The flexurals, which are the main source of coherent noise in the tests, are dispersive and non-axisymmetric. In the power spectrum of an inspected pure torsional wave, the same characteristics of the spectrum of the excitation sequence must be observed; this is not the case for flexural waves due to their temporal and spatial variances. It should also be mentioned that asymmetric features (which is the case for most defects) generally reflect both torsional and flexural waves; where their corresponding reflection coefficients depend on the geometry of the feature. However, in the developed algorithm, the focus is on the detection of the torsional waves since the torsional wave is always reflected, and it is received symmetrically around the pipe circumference regardless of the features' geometry or the wave propagation distance. Furthermore, in some cases, the flexural waves are considered as the coherent noise received due to mode conversion from the known features, leading to the detection of false alarms in the tests.

6.2.1 Algorithm Outline

The developed algorithm is a condition-based comparison of the power spectrum achieved from a moving window of the received signal and the spectrum of the normal

[10] Refer to Section 2 for more information.

excitation sequence. Keeping in mind that, since both flexural and torsional waves have the same main bandwidth (BW), correlating them would not be sufficient for distinguishing between them. Nonetheless, using this proposed method the torsional wave is identifiable. Another advantage of this method is the reliance on the excitation sequence, which is known and set manually by the inspectors.

This algorithm consists of three main aspects: (1) initialisation, which initialises the excitation sequence and extracts the required features for comparison; (2) main loop, that uses the advancing window and carries out the pre- and postprocessing of the conditions; and (3) conditions, which constitute the main processing, where the spectrum of each iteration is compared with the one achieved from excitation sequence.

Since the signals are processed digitally, and due to the limited resolution in this domain, in the following section all formulae and definitions are presented based on the sample number for the time domain and bin number for the power spectrum. In doing so, better performance, in terms of speed is achieved as no unnecessary interpolation, is needed. The sampling frequency (Fs) used in the tests is 1 MHz which is a fairly common sampling frequency of guided wave inspection devices.

For ease of understanding of the developed algorithm, in the following sections, any reference to a variable or function within the text is written in between the quotation marks, E.g., “Fs” is sampling frequency.

6.2.2 Initialization

Initially, the excitation sequence is created where the inspector inputs the centre frequency and the number of cycles. Then, the “windowSize” is calculated based on the number of samples required for the excitation sequence. This sequence is already normalised by its maximum value. The normalisation bounds the signal amplitudes between 1 and −1 by dividing each sample by the maximum amplitude within the signal. Since 10 cycles are typically used for inspection, the duration of the excitation sequence is small; therefore, this signal is zero-padded by a factor of 4 to achieve better resolution in the spectral density. Zero padding is the operation of adding extra zeroes to the end of the sequence in order to increase the resolution of the power spectrum [99]. The power spectrum is then evaluated by applying the fast Fourier transform [99], where the magnitudes of the spectrum are saved in “signalRef” and the corresponding frequency for each bin is saved in “frqList”.

The first extracted feature from the spectrum is the maximum magnitude and its corresponding bin number which are stored in “maxRef” and “idFC”, respectively. This should be the bin representing the centre frequency of excitation as set before by the inspector. Afterward, the

lowest and highest frequencies of the 10 dB BW of this spectrum are calculated. The bin numbers of the lowest and highest frequencies within this BW are saved in “teFLID” and “teFHID”. If the previously calculated “idFC” is not in the centre of this spectrum, these numbers are expanded away from the centre frequency so both the lower half and the upper half of the spectrum have the same amount of bin numbers. Then, the greater magnitude achieved from these (border) bins is stored in “teMax”. The flowchart of this function is shown in Figure 6.1 and a summary of the extracted variables is shown in Table 6.1. All values except “windowSize” are needed for the conditions function.

Table 6.1. Description of variables extracted from the initialization.

Name	Description	Conditions
windowSize	Length of the moving window	-
signalRef	The power spectrum of the normalised excitation sequence	C2, C3, C4
frqList	List of the corresponding frequency for each bin number	C0
maxRef	Maximum magnitude achieved from signalRef	C4
idFC	Bin number of maxRef	C0
teFLID	Bin number of the lowest frequency within 10 dB BW	C0, C1, C3
teFHID	Bin number of the highest frequency within 10 dB BW	C0, C1, C3
teMax	The greater magnitude between teFLID and teFHID from signalRef	C3

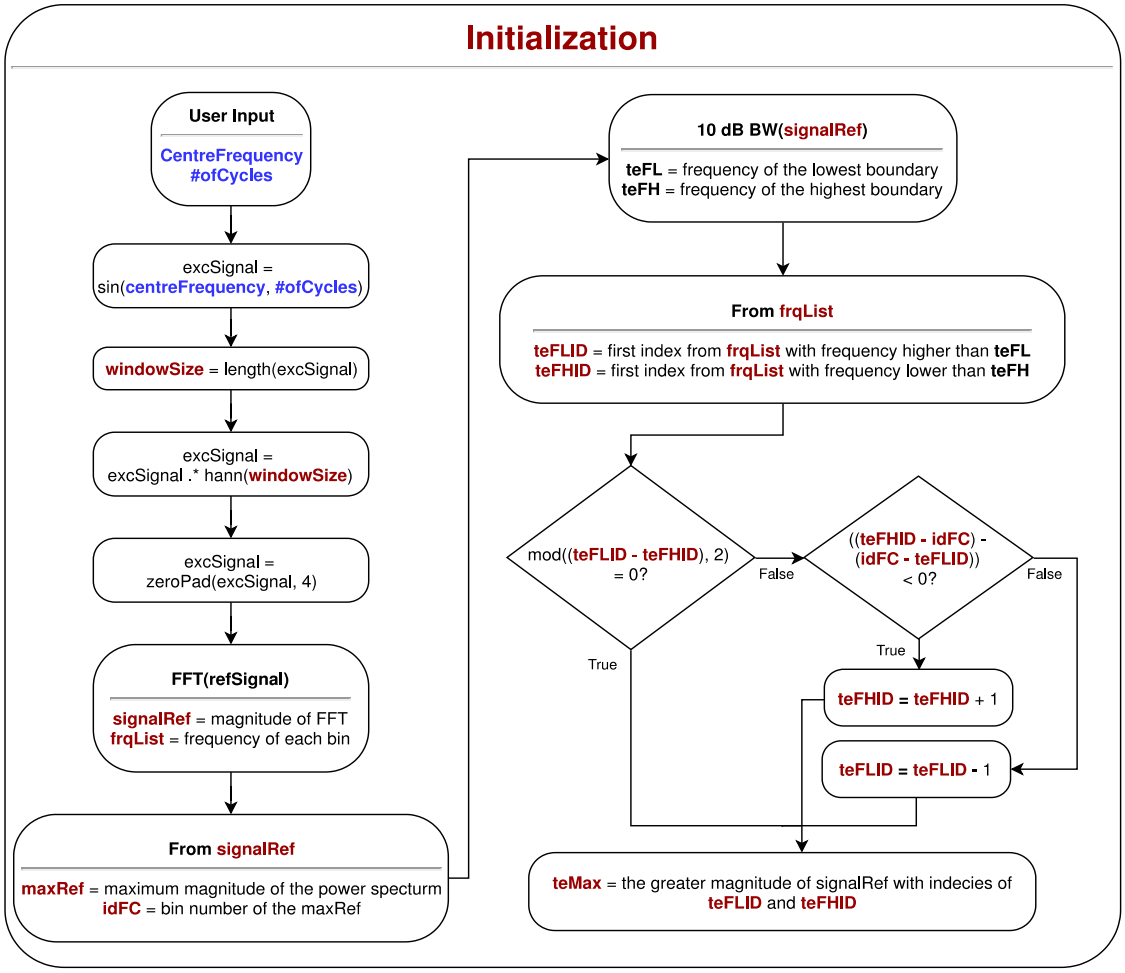

Figure 6.1: Flowchart of initialization.

6.2.3 Conditions

In this function, all previously extracted characteristics are used in order to compare the spectrum of the moving window with the excitation sequence. The focus of this algorithm is on the similarity of the spectrum rather than the energy of the signals; thus, all windowed signals are normalised before calculating the spectrum. Five conditions (features) exist in total. Since defect signals are affected by the flexural noises, it is expected that the received signals from smaller defects would not result in a perfectly matching spectrum. Hence, in each condition, safety variables are defined in order not to over-fit the conditions to the reference. These variables are set by the inspectors to provide a safety tolerance for detecting weak signals. It should be borne in mind that these tolerances have typically small values and can be fixed. Furthermore, they are set only once at the start of the algorithm and do not change iteratively.

6.2.3.1 Condition Zero (C0)

The centre frequency of the windowed spectrum must be near the centre frequency of the excitation sequence, defined by “idFC”. In the case of small defect signals, where less

energy is reflected, they are more affected by the coherent noise which will cause a slight shift in the centre frequency. Therefore, a slight shift in the frequency is acceptable, which is defined by variable “maxFCallow”. If such a shift is detected, the corresponding bin numbers of “idFC”, “teFLID” and “teFHID”, which are required for the other conditions, will be shifted towards the new centre frequency of the spectrum. If this shift of centre frequency is more than the maximum allowable shift, it means that the current iteration is significantly different from the excitation sequence and all other conditions will automatically fail. The maximum allowable shift, “maxFCAllow” is set to 3 kHz, which is a small margin in comparison to the total BW of the signal.

6.2.3.2 Condition One (C1)

In the Hann windowed sine waves, the lower half of the BW tends to increase in magnitude when moving towards the centre frequency, then it starts to decrease. In this condition, it is checked that there is no discontinuity in this trend; in other words that no local maxima exist. In doing so, the 10 dB BW is of the main focus as the outside edges are typically affected by the flexural noises due to their lesser magnitudes. The reason for this is that in guided wave inspection, Hann-windowed, narrowband excitation sequences are used. Therefore, the main energy spread is within the main BW of the signal while a limited amount will be assigned to the borders of the BW. The flexurals are dispersive, depending on their dispersion curves, their spectra tend to shift towards other frequencies, but the nondispersive torsional wave will not observe this change. Therefore, the energy of flexural waves will be stronger outside the main BW. Choosing 10 dB BW is a good compromise since more than 90% of the bins are covered using this value and only a few bins on the sides are neglected. Using the bin number of the lowest and highest frequencies in the 10 dB BW, “teFLID” and “teFHID”, it is checked whether the magnitude of each respective bin is increasing when moving toward the centre frequency. Nonetheless, a variable can also be defined as “diffVal” to allow small differences to be neglected. Currently, no tolerance is needed, and it is kept as zero.

6.2.3.3 Condition Two (C2)

In the excitation sequence, the strongest magnitudes are detected in the region of the centre frequency. Since they have the strongest magnitude, they will be less affected by the noise in the region. In this condition, it is confirmed that the neighborhood of the centre frequency has relatively the same magnitude. The number of neighborhoods on each side of the centre frequency is defined by “cBins“, and the maximum allowable difference is defined based on a percentage of current iteration maximum magnitude defined by “maxPerc”. In this

paper, the number of the neighborhood is set as 2 and the maximum allowable difference is set as 20% of the maximum magnitude of each iteration.

6.2.3.4 Condition Three (C3)

The window size is set as the length of the excitation sequence. Due to the limited duration of the signal, in the iteration's power spectrum, there should not be any magnitudes greater than the 10 dB BW boundary, "teMax", of the excitation sequence other than the frequencies within these boundaries. Nonetheless, in the immediate bins next to the boundaries, "teFLID" and "teFHID", the magnitudes are more affected by the coherent noise and can be greater than the "teMax". Therefore, "sBins" is defined as the allowable number of immediate bins, which will be neglected during this comparison. This value is set to 1.

6.2.3.5 Condition Four (C4)

Each iteration window is normalised before its power spectrum is calculated. As the window size is limited to the excitation sequence, in the power spectrum of the iteration, a loss of magnitude can be expected due to the coherent noise in the signals. However, the maximum magnitude of the iteration cannot be greater than the one achieved from the excitation sequence, "maxRef". Since normalisation is taking place, a small safety margin is defined as "sMargin", to compensate for the small variances between the magnitudes defined. This value is set to 1, which is much less than the maximum magnitudes achieved from excitation sequences.

6.2.3.6 Final Results

Iterations are marked as the signal of interest (one) if all the aforementioned conditions are met and will be marked as noise (zero) if any of them are failed. Afterward, in order to measure the similarity between the sequences, the maximum correlation between the 10 dB BW of the power spectrum of the excitation sequence and current iteration is calculated.

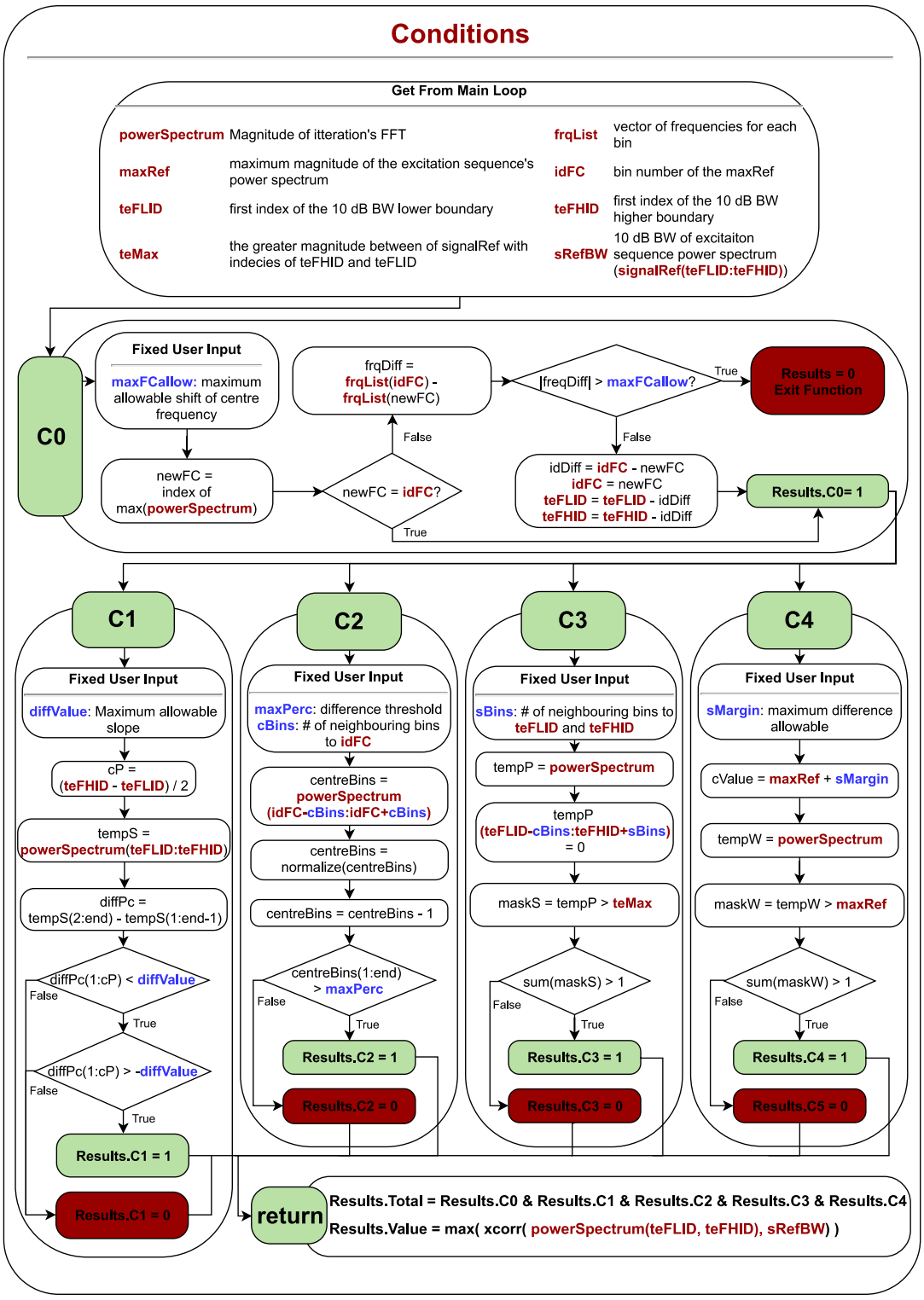

Figure 6.2: Flowchart of conditions.

The cross-correlation of two sequences x[n] and y[n] is defined as [99]:

$$r_{xy}[l] = \sum_{1}^{N} y[n+l]x[n] \tag{6.1}$$

where l is the (time) shift (or) lag, n is the sample number of each sequence and N is the number of samples in the sequences. The correlation operation measures the degree to which

two sequences are similar. As can be seen in the formula, the output is given in a vector of time shifts. Therefore, by considering the maximum amplitude of r_{xy} , the maximum similarity between two sequences is measured. Nonetheless, since in C0, the peaks are shifted, no time-shifting is required to achieve the maximum value and the results will become the summation of multiplication of each corresponding bin. Both the cross-correlation value and the binary condition results ("Total") will be returned to the main loop where the final "detection" results will be generated. The flowchart of this function is shown in Figure 6.2.

6.2.3.7 Main Loop

The initialization is done before the main loop in order to extract the required features. Afterward, the start of the iteration is delayed by the length of the window size. In practice, it means that the system can be linear and time-invariant, which can be implemented in real-time as it only requires past samples of the signals. In each iteration, a temporary signal, "WindowedSignal", is created which holds the past samples of the signals with the same length as the excitation sequence. Since the power spectra are needed to be compared, the signals are first normalised and zero-padded by a factor of 4. The power spectrum of this windowed signal is calculated and passed to the conditions function. After processing, the "Results" object is returned where it contains the detection variable "Total" and the correlation value of the spectrums as "Value". If the signal of interest is detected, e.g., "Total" and is equal to one, then the current iteration represents a similar power spectrum to the one of excitation sequence.

One approach would be to mark the current iteration number as one, which would mean that the current iteration is representing the signal of interest; however, this is not the best representation as the current iteration might not be the best representative of the windowed signal characteristics. In this paper, the index of the maximum amplitude in each windowed signal is detected. This index appears to be a better representation since the region with more energy has a stronger influence on the power spectrum. Since the excitation sequence is Hann windowed, the centre of the signal will hold the highest amount of the signals' energy. In this location, the concentration of signal energy is higher, therefore stronger flexural features are required to disturb reduce/change the characteristics of this region. Therefore, the centre instead of adding the correlation value to the sides of the window (current iteration number), the value is cumulatively added to the location of the highest amplitude within the window, which represents the centre of the Hann windowed sequence in a torsional wave. This value is stored in the "detection" vector. Therefore, the correlation value is added to the location where the signal represents the strongest amplitude in the "detection" vector. The reason why they are added rather than replaced is that since it is an iterative process, different windows

can have the same index as the maximum; by doing a cumulative sum for each index, the certainty in defect detection is increased and the amplitudes assigned for the outliers and noises are decreased. The main loop finishes when the end of the signal is reached, at which point the “detection” vector is normalised and is plotted against the original signal to show the defect locations and their normalised correlation values. The flow chart of this function is shown in Figure 6.3.

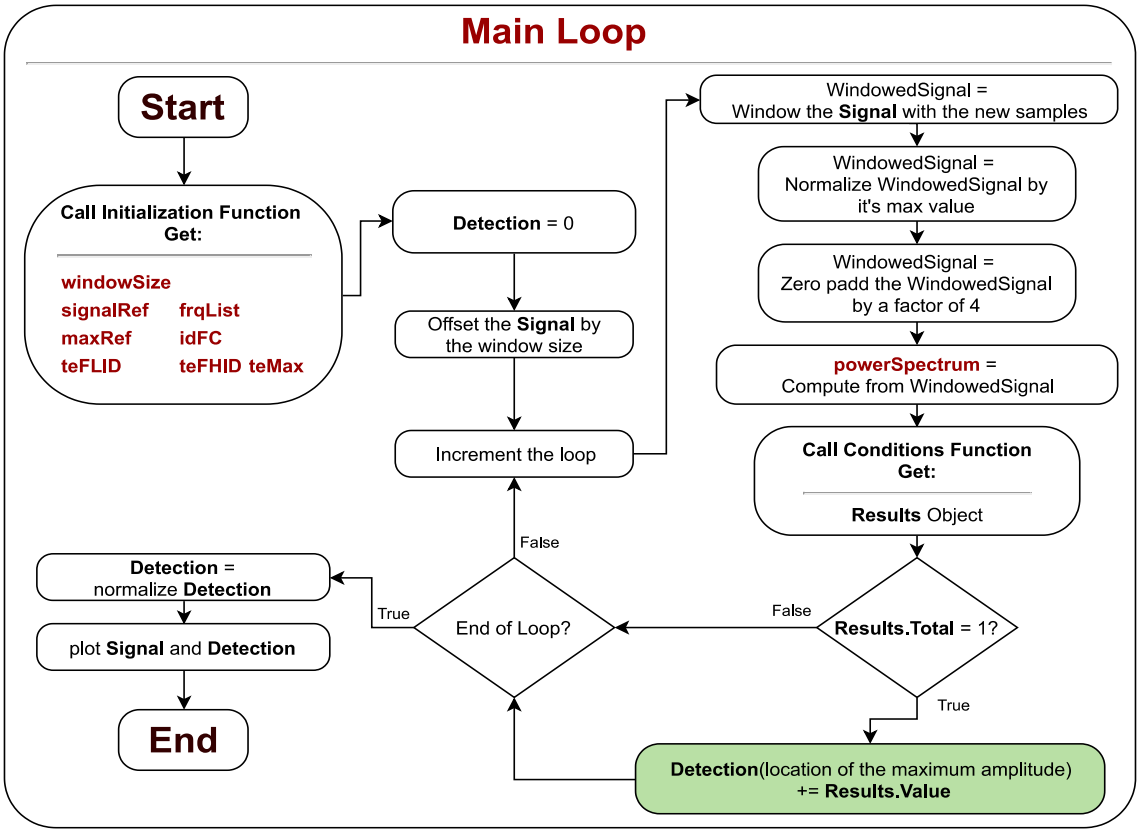

Figure 6.3: Flowchart of the main loop.

6.3 Example Test Case

The initial verification of this algorithm was done using a FEM signal where a 3% CSA defect is located 3 meters away from test origin. As explained previously in Section 2, using linearly spaced source points around the signal would limit the amount of flexurals received after applying the propagation routine. The aim of this algorithm is to detect the defect signal when it is contaminated in flexural noise; therefore, the time domain signal is generated by using only 4 reception points around the circumference of the pipe. These active source points are shown in Figure 6.4a and the resultant time domain signal is showed in Figure 6.4b. The used excitation sequence for generating this data set is a 10-cycle Hann window sine wave with a frequency of 30 kHz where variable transfer functions are used for each of the source points.

In this section, each different condition of the algorithm is thoroughly explained using the simulated signal. The main aim is to detect the Direct defect signal located at 3 – 3.5 meters. Unlike other algorithms, it will be illustrated that the indirect signal is not going to be detected. Since the indirect signal is caused due to the leakage in backward direction, the frequency spectrum of it is no longer matching the main excitation sequence; therefore, it is expected that such signals will not be detected using this algorithm.

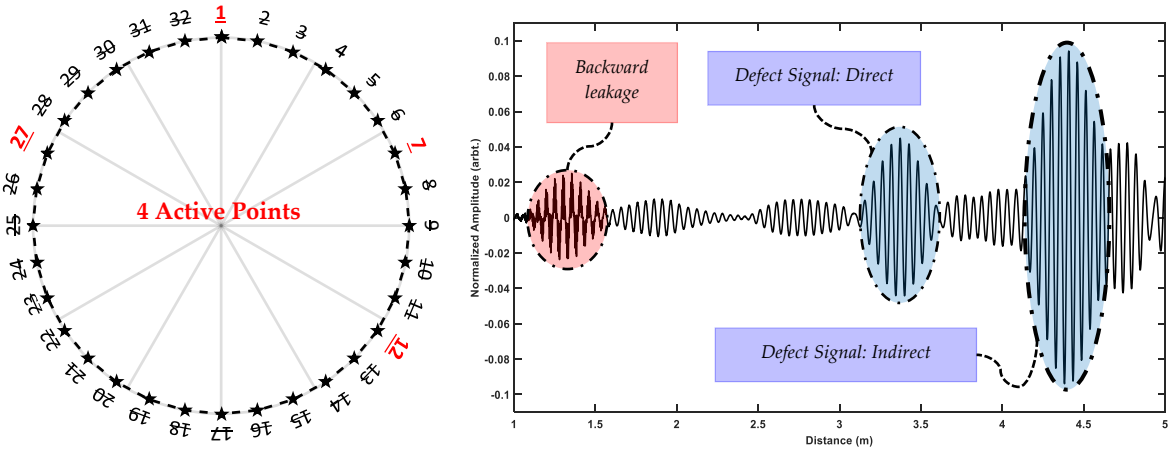

(**a**) Selected Points (each ring) (**b**) Signal in time domain

Figure 6.4. Example signal from FEM. (a) shows the selected point (marked by red) in each ring and (b) shows the time domain signal.

6.3.1 Condition Zero (C0)

The starting condition is that the maximum magnitude of each iteration's power spectrum must belong to the approximate region of the centre frequency. This approximation is set by the inspector ("maxFCAllow"). It is a necessary factor for the detection of smaller defects since the spectrum will be more affected by the flexural waves, which leads to a shift in centre frequency. An example of an outlier based on this condition is shown in Figure 6.5, where the blue box shows an example allowable region for frequency shift, and the grey circle shows the bin with the maximum magnitude in this iteration. Since it is outside the allowable region, the outcome of this condition will be zero, which will automatically force all other conditions to zero. The used value for the maximum allowable shift is 3 kHz which is a small margin in comparison to the overall BW of the excitation sequence. In the case of FEM signal, since the flexural wave does not affect the defect significantly, similar results can be achieved even when this value is set to zero.

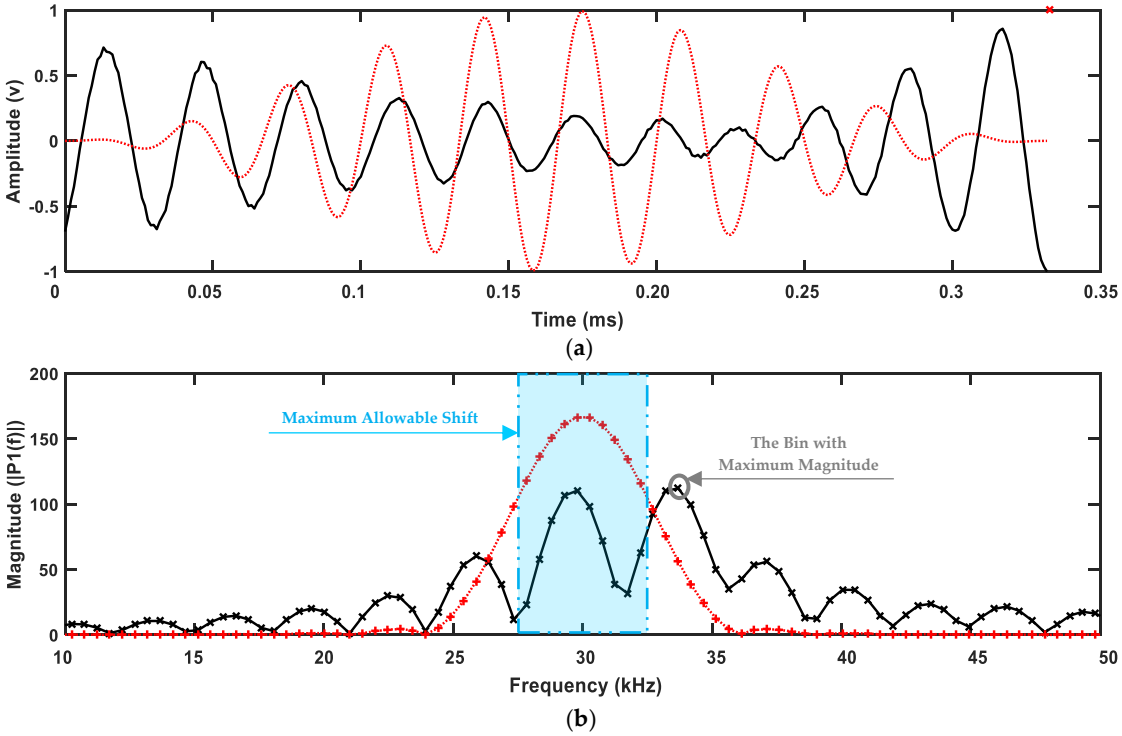

Figure 6.5. An example of an outlier case detected using Condition Zero (C0) where (a) shows the time domain of the iteration window and (b) is its respective power spectrum. The red lines (dotted, +) show the references achieved from excitation sequence and the black lines (x, solid) show the results from each iteration.

6.3.2 Condition One (C1)

In simple terms, the magnitudes of each bin in the 10 dB BW of the iterations' spectra must increase when moving toward the centre frequency. Due to dispersive nature and multimodality of guided waves, this condition is not true for many iterations as a combination of waves will be received with different centre frequencies. Nonetheless, this condition must be true in the case of the torsional wave as it will have the same characteristic of the excitation waveform. Figure 6.6 shows an example of an outlier detected based on this condition. As can be seen, in the region between 26.5 to 27.5 kHz, the magnitude of three frequencies is actually decreasing, and a local minima is created. This suggests that the iteration is actually two separate wave modes with two different centre frequencies.

In this condition, in order to avoid marginal errors due to the limited number of samples in the window, a safety variable ("diffValue"), so the condition holds true if a slight decrease in the magnitude of each consecutive bin is detected. In these tests, this value is kept at zero which means strictly positive increase of the magnitudes must be observed when moving toward centre frequency. The reason is, in case of guided wave testing, if the flexural waves are strong enough that the frequency characteristics of the excitation waveform are changed, the

signal must not be marked as a defect; since, in effect, the iteration is representing a strong existence of a flexural wave.

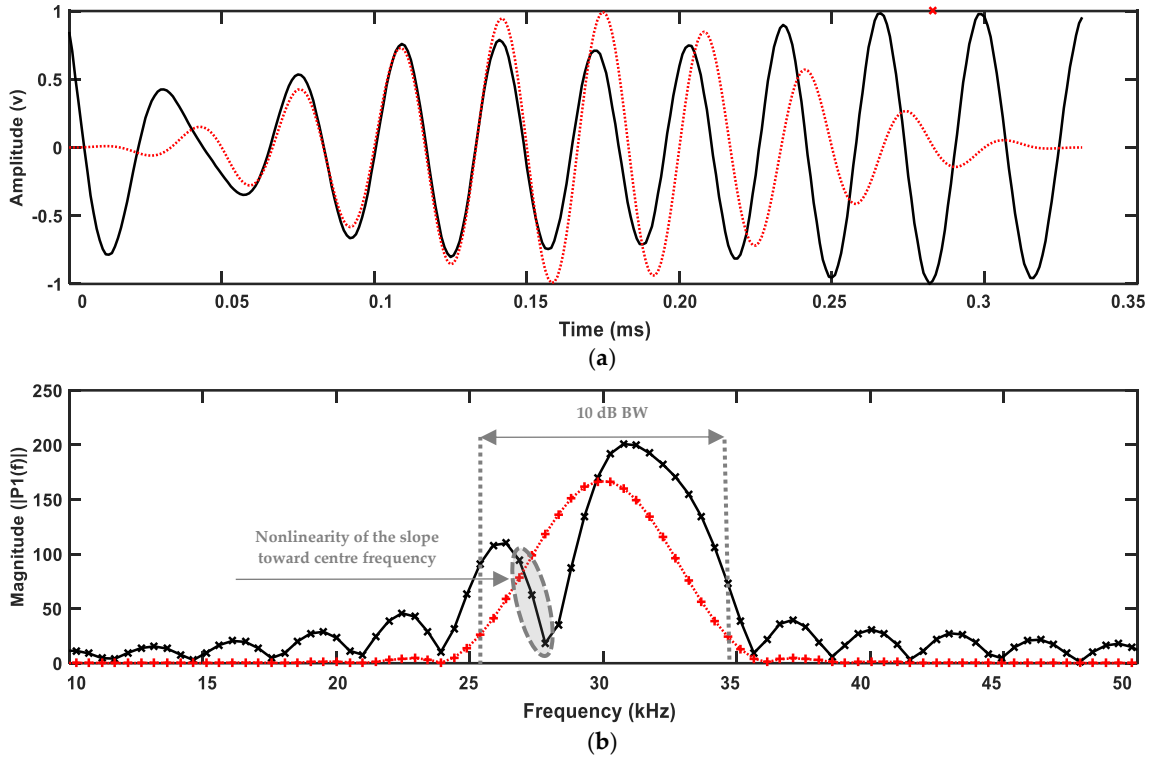

Figure 6.6. Example of an outlier case detected using Condition One (C1) where (a) shows the time domain of the iteration window and (b) is its respective power spectrum. The red lines show (dotted, +) the references achieved from the excitation sequence and the black lines (solid, x) show the results from each iteration.

6.3.3 Condition Two (C2)

The strongest magnitudes are in the neighborhood area of the centre frequency; hence, they are less affected by the flexural waves. This condition verifies that the magnitudes from centre frequencies are not below a certain limit. Figure 6.7 shows an example of an outlier detected from this condition. Two limits must be set for this condition: (1) the number of neighboring in “cBins” and (2) the percentage of allowable drop with regards to the maximum magnitude detected in the iteration (“maxPerc”). In these tests, “cBins” is set as two (of each side of centre frequency), which means a total of four bins is checked and thus limits this validation to the main central bins of the spectrum. In the reference signal, it can be seen that at the border of this region, an approximate 10% drop is observed. Since in practical testing, the magnitudes will be more affected by the flexural waves and testing condition, the allowable drop is set to 20% of the maximum magnitude of each iteration.

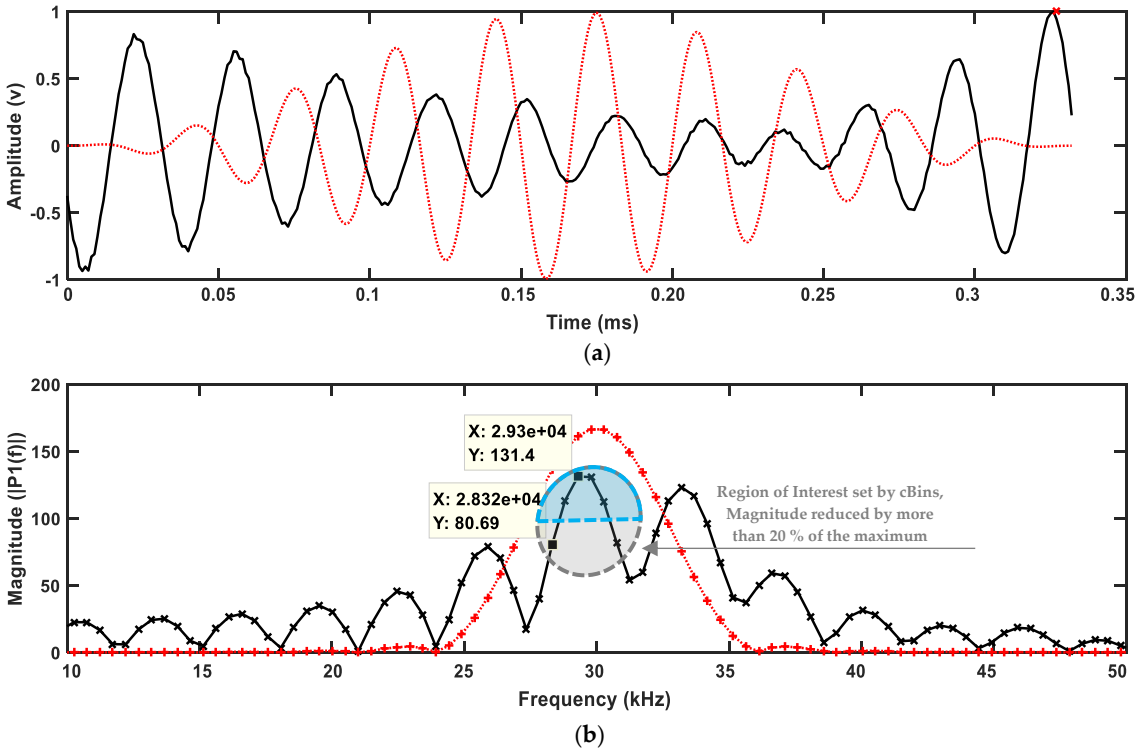

Figure 6.7. Example of an outlier case detected using Condition Two (C2) where (a) shows the time domain of the iteration window and (b) is its respective power spectrum. The red lines (dotted, +) show the references achieved from the excitation sequence and the black lines (solid, x) show the results from each iteration.

6.3.4 Condition Three (C3)

In the third condition, the magnitudes of frequencies outside the 10 dB BW of the excitation sequence are checked. Since the window size is limited to the length of the excitation sequence, no other strong peaks in other frequencies should be detected. This can be verified by confirming that no other magnitudes are above the lowest magnitude within 10 dB BW. Figure 6.8 shows an example of an outlier detected using this condition. The blue boxes illustrate the expected regions while the grey boxes illustrate the bins with higher magnitudes than the thresholds. It should be noted that this threshold is defined using the reference signal rather than the current iterations' sequence and is fixed in all iterations. Since the boundaries are affected more by flexural waves, a safe margin can be provided by expanding the bins away from the centre frequency ("sBins"). In these tests, this value is defined as one, which means only one bin is neglected from each side of the spectrum and all other bins must have magnitudes less than the minimum magnitude detected in the 10 dB BW.

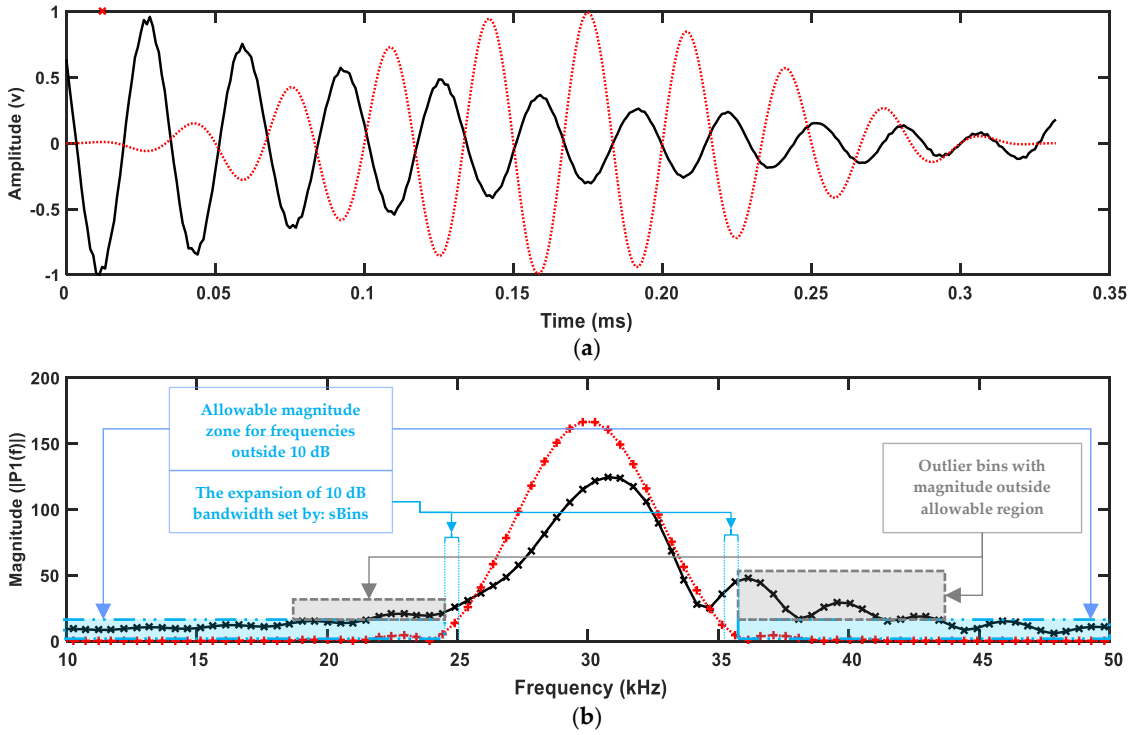

Figure 6.8. Example of an outlier case detected using Condition Three (C3) where (a) shows the time domain of the iteration window and (b) is its respective power spectrum. The red lines (dotted, +) show the references achieved from the excitation sequence and the black lines (solid, x) show the results from each iteration.

6.3.5 Condition Four (C4)

In this condition, it is verified that the magnitude achieved in the power spectrum of iteration is not more than the reference. The reference signal is in the perfect form of the excitation when it is normalised and not affected by any noise, while any windowed iterations are subject to noise; hence, the maximum magnitude of the iteration cannot be more than the reference. Nonetheless, due to the finite resolution of the windows, a safety value is defined as “sMargin” to allow small differences between the two to be neglected.

Keeping in mind that in the case of simulated signal, since source points were not placed linearly and variable transfer functions were used, the characteristics of the generated signals can be different. This is clearly illustrated in Figure 6.9, where the received has more than 10 cycles; hence, the maximum magnitude in the power spectrum of the iteration would be increased. The shown windowed signal is approximately located around the 4-meter region (second torsional wave), where the results of impact from backward leakage and the front defect are received from the forward direction. As can be seen, the condition will not hold in this case; however, when setting the threshold as 10% of the maximum magnitude (15) the result of the first detection is increased, and this wave will also be detected. Changing this value to 15% increases the detection amplitude of the second signal and the pipe end even more, but the first defect signal remains constant. At 20%, the maximum values are achieved

(while the overall detection result of the defect becomes less due to the increment of the associated value to the pipe end), and anything above does not change the generated results. Nonetheless, for the purpose of experimental tests, this value is only set as one which is less even than 1% of the maximum magnitude of the reference. This ensures that only calculation errors due to the limitation of the window size are neglected.

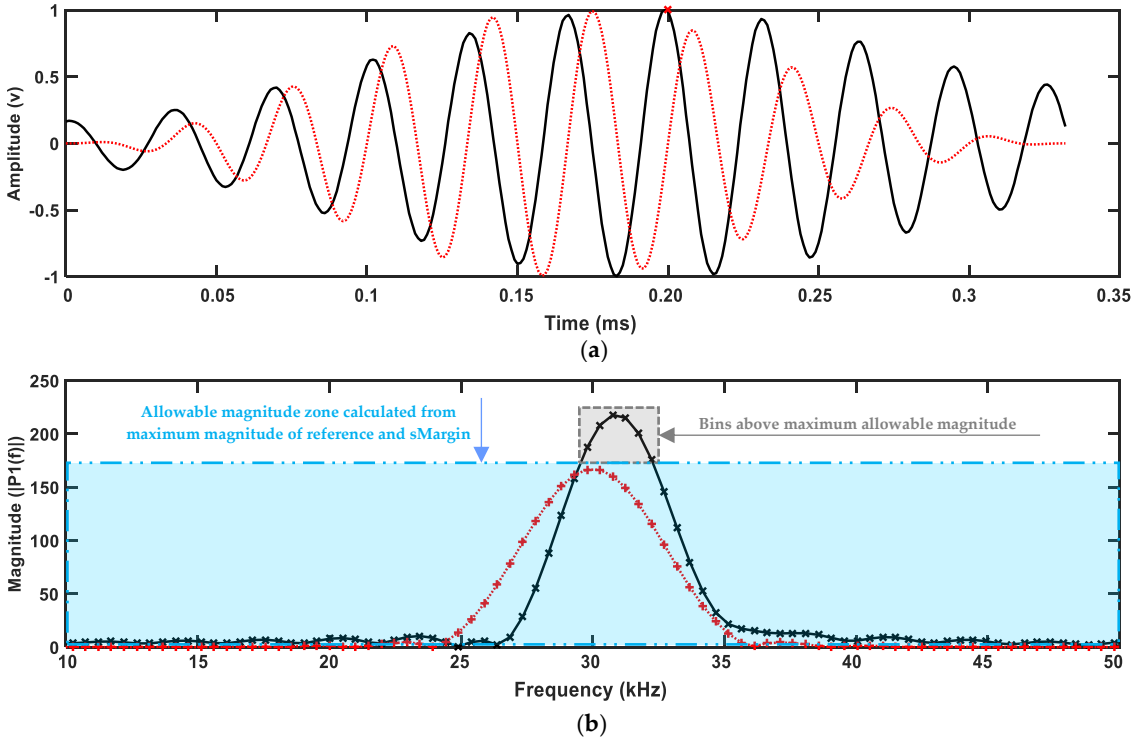

Figure 6.9. Example of an outlier case detected using Condition Four (C4) where (a) shows the time domain of the iteration window and (b) is its respective power spectrum. The red lines (dotted, +) show the references achieved from the excitation sequence and the black lines (solid, x) show the results from each iteration.

6.3.6 Results Total

The maximum value of correlation results of the reference and the iteration's power spectrum are added to the location of maximum voltage in each window. Furthermore, as the correlation result is typically a large number, the final result is normalised by the maximum value, which is typically the pipe end. This is illustrated in Figure 6.10 where it can be seen that the value of 0.1 is associated exactly to the centre of the defect signal. As illustrated, knowing only the excitation waveform, the approximate location of the defect is clearly detectable using this method.

The binary detection results of each condition for each iteration, as well as the total results, is demonstrated in Figure 6.12. In this figure, it is clearly demonstrated outliers exist in the results of each individual condition, but by combining all of them, only the iterations associated with the defect and pipe end are being detected. Furthermore, high correlation results are achieved

from all iterations, irrespective of it being noise or defect; which is the main reason why doing a cross-correlation is not enough for detecting the defect location in the case of guided wave testing. However, even with the existence of the coloured noise, by checking the mentioned condition, the detection becomes possible.

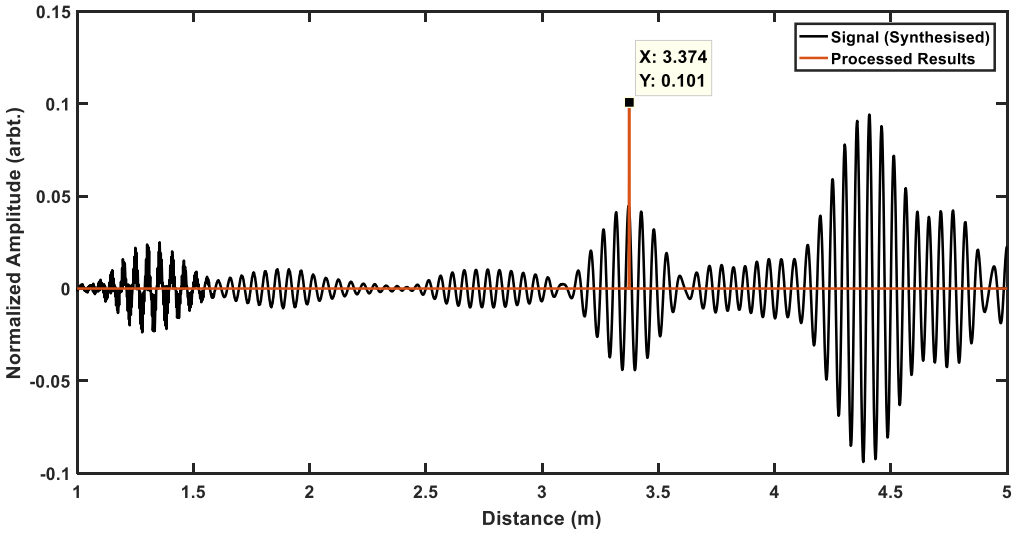

Figure 6.10. The final result (red line) overlaid on the time domain signal (black line) from the FEM case. The defect size is 3% CSA and the excitation frequency is 30 kHz.

In the same format, Figure 6.11 and Figure 6.13 shows the results achieved from the 3% CSA defect from the experimental results. The same aforementioned conclusions can be drawn with regard to Figure 6.13. However, it can be seen that in the experimental results since the transfer functions are more linear, the outcome of condition 4 (C4) is true in most iterations. The results are shown in Figure 6.11, where the defect location is clearly marked using this algorithm. Overall, conditions one and three are the most effective ones which filter out most of the outliers from the tests.

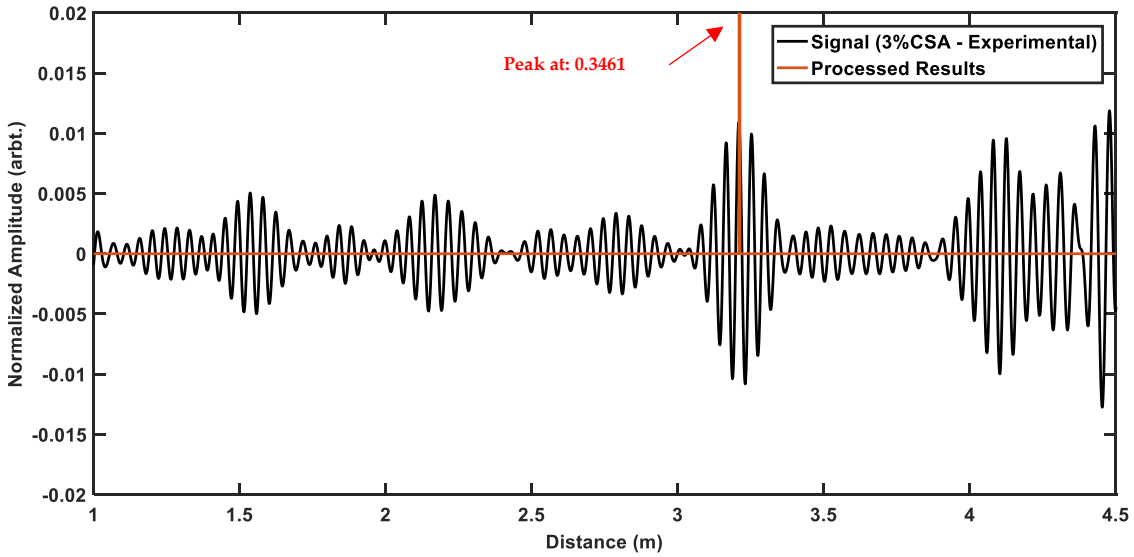

Figure 6.11. The final result (red line) overlaid on the time domain signal (black line) from the experimental test case with the excitation frequency of 38 kHz and defect size of 3% CSA.

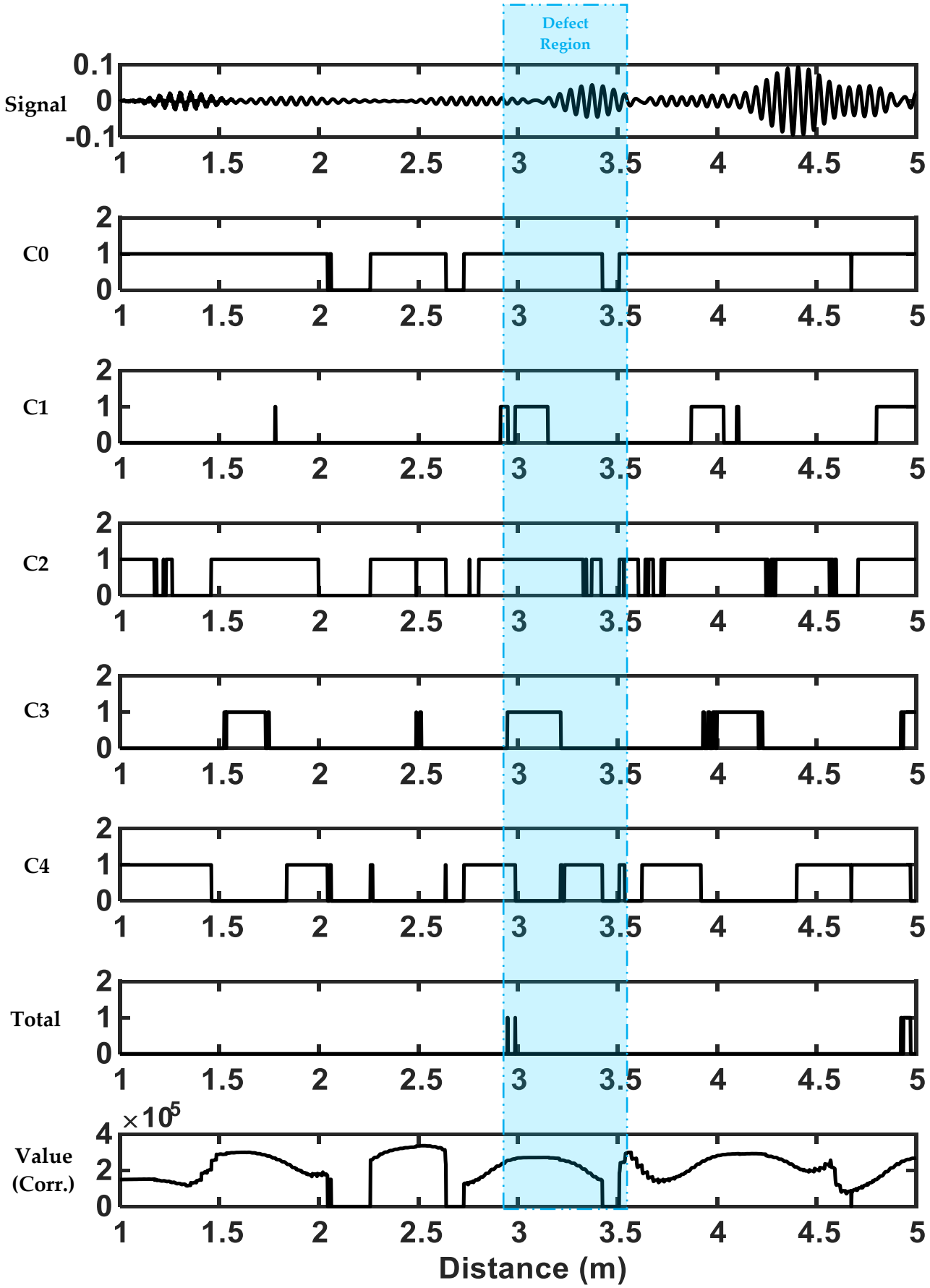

Figure 6.12. The generated results from the FEM test case.

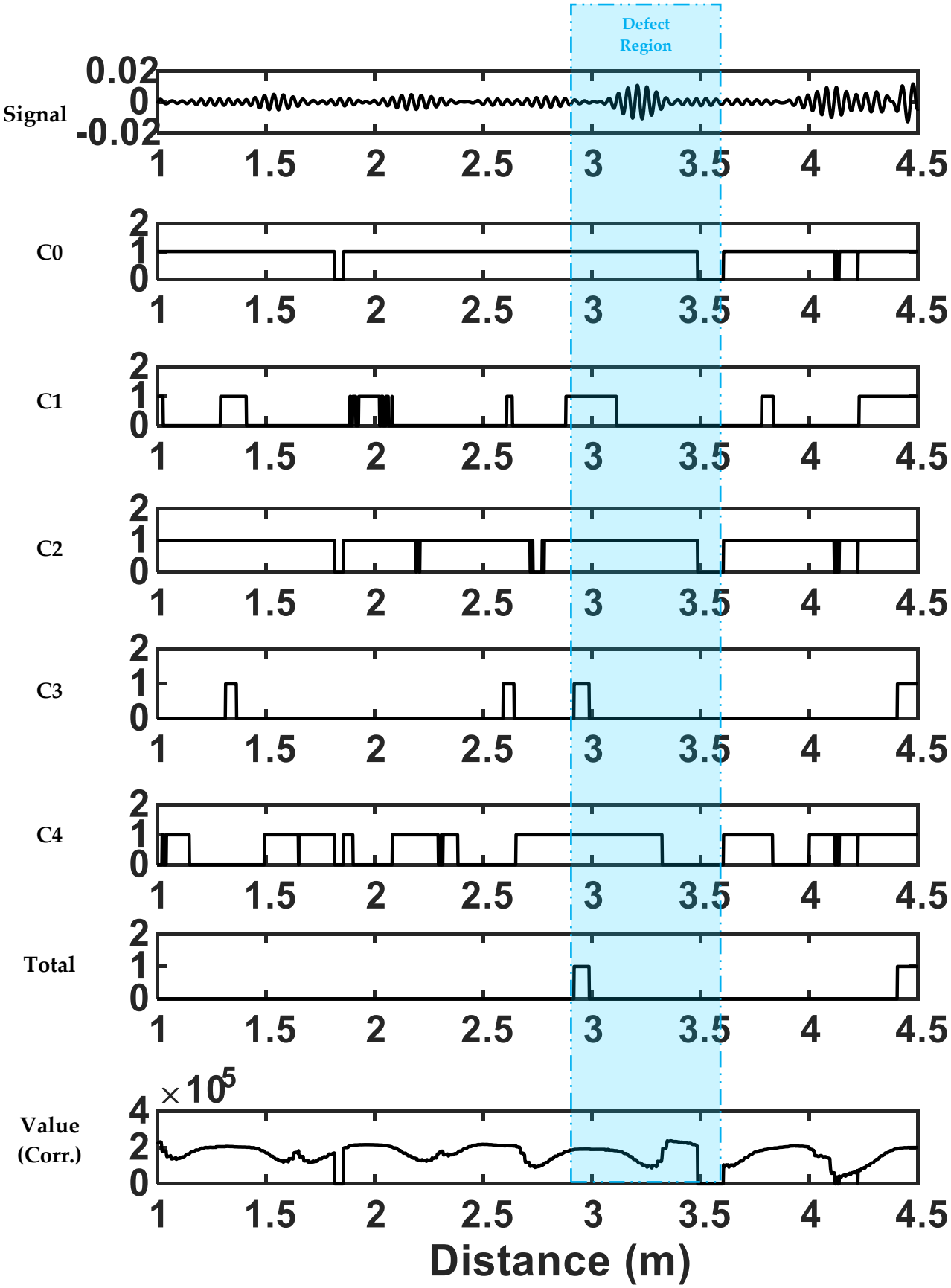

Figure 6.13. The generated results from the experimental pipe with a defect of 3% CSA and testing frequency of 38 kHz.

These five conditions have not been optimised. Nevertheless, they were all designed based on the physical phenomena of guided wave propagation within pipes. As can be seen in both the results of FEM and experimental tests, using only in C3 and C4 could the defects be detected. However, having more relevant conditions, especially for practical inspection of pipes, may increase the certainty of the generated results. Nonetheless, the conditions are not necessarily required to be in the same Fourier Domain as stated in this algorithm, and the technique can be combined with other approaches, such as Wiener filtering, in order to improve its performance.

6.4 Results

The algorithm was assessed using data gathered from real pipes with two defects located in different locations with varying sizes of 2-8% CSA. In order to assess the dependency of the algorithm to the excitation frequency, each defect size was tested with multiple frequencies. Starting frequency and ending frequency of the tests are 30 and 50 kHz respectively, and a total of 10 frequencies with linear incremental steps of 2 kHz were used.

As it was mentioned previously in Section 2.2.2, dispersion affects the power spectrum of the received signal and most of the created flexurals from conversion of torsional wave is highly dispersive in the lower frequency region; hence, it is expected that this algorithm works better with lower frequencies as the power spectrum of flexural noise significantly differs from the excitation sequence due to the dispersion. Nonetheless, the final choice of excitation frequency is a trade-off between the capability of the system to excite the required waveform and having highly dispersive flexural waves. Furthermore, it should be noted that the reflected wave amplitude at different frequencies is generally dependent on the flaw geometry. This could affect the detection capability at different frequencies.

Figure 6.14 shows the processed results from Defect 1 where (a) shows the detection amplitude of the defect and (b) shows the amplitude of the outlier in the test. Outliers in these tests are considered as any detection corresponding to the regions where the signal from neither defect nor pipe features is expected to be received. In this figure, each bar represents the results of a defect with a different CSA size and is categorised based on the tested frequencies. Using 48 and 50 kHz resulted in the detection of no feature or outlier; hence the results of these two frequencies are not reported.

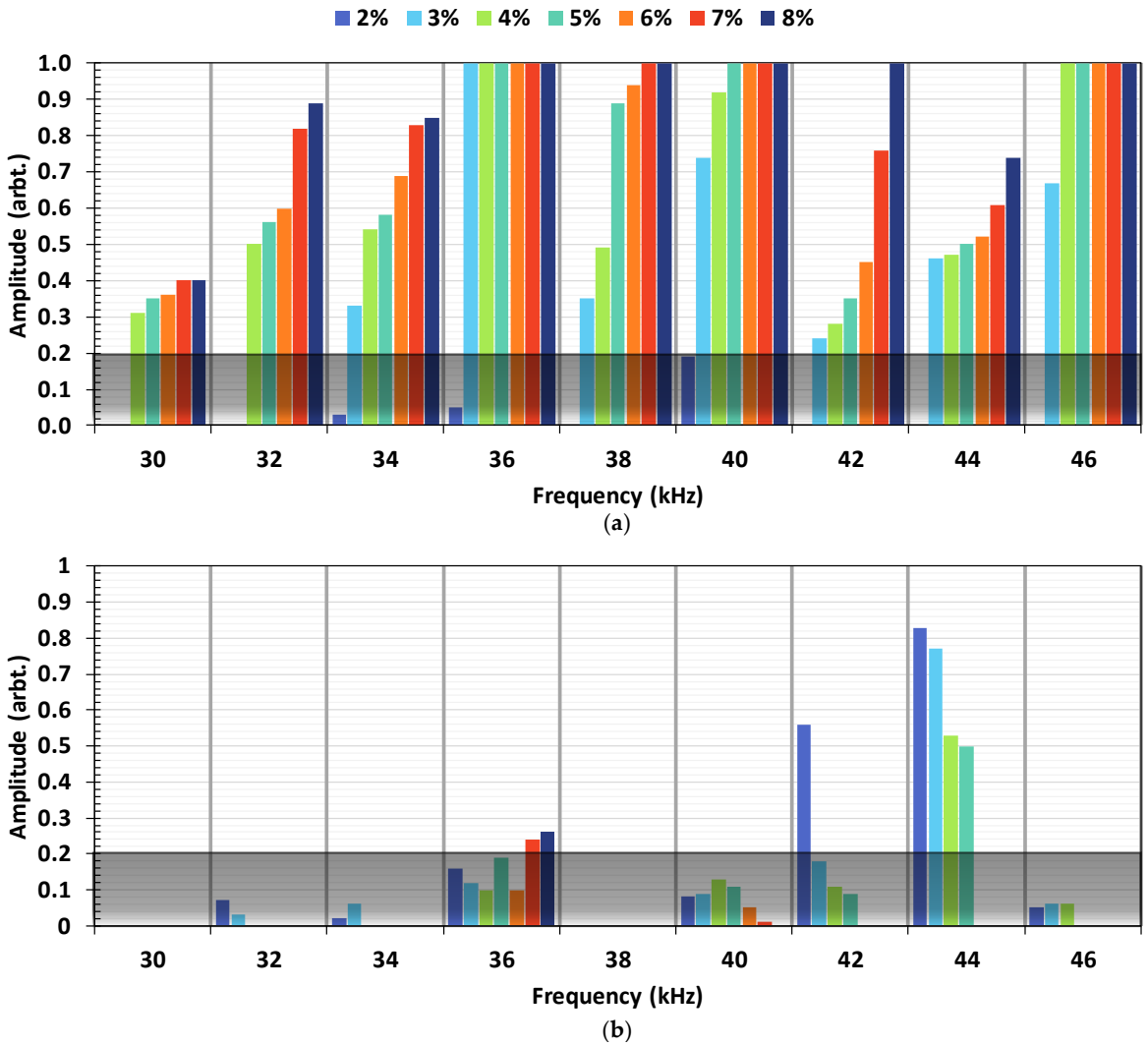

Figure 6.14. Results of Defect 1 achieved using the algorithm where (a) shows the detection amplitude of defect signal and (b) shows the detection amplitude of the outlier. Each bar represents the results achieved from a defect with different CSA size. The grey area represents the threshold region for calling outliers.

As can be seen in Figure 6.14, the algorithm works best in the frequency range of 34-40 kHz. Using these frequencies results in detection of defects with CSA sizes of greater than 3% without any outlier or outliers with significantly lower detection amplitude in comparison to the defect signals. Using lower frequencies (30-32 kHz), although the amplitude of outliers is smaller than most test cases, defects smaller than 4% CSA cannot be detected. On the other hand, frequencies above 42 kHz resulted in detection of outliers with higher amplitudes and in the case of 48-50 kHz, no detection could be acquired. The main reason is the transfer function of the system, where it is not capable of generating the expected power spectrum for the excitation waveform. As an example, consider the received signal from 50 kHz test case on 4% CSA pipe, is shown in Figure 6.15. The pipe end signal is a pure reflection of the excitation sequence where limited changes should be observed due to the coherent noise. The retrieved signal from the pipe end observes a 5 kHz shift in centre frequency.

Furthermore, the generated sequence can also have a greater number of cycles which will result in higher maximum energy in an iteration's power spectrum in comparison to the reference. Therefore, because of these significant changes which are caused by generation of the sequences, it is not recommended to use higher than 42 kHz excitation frequencies with this algorithm. The only frequencies capable of detecting 2% CSA defect are 34, 36 and 40 kHz.

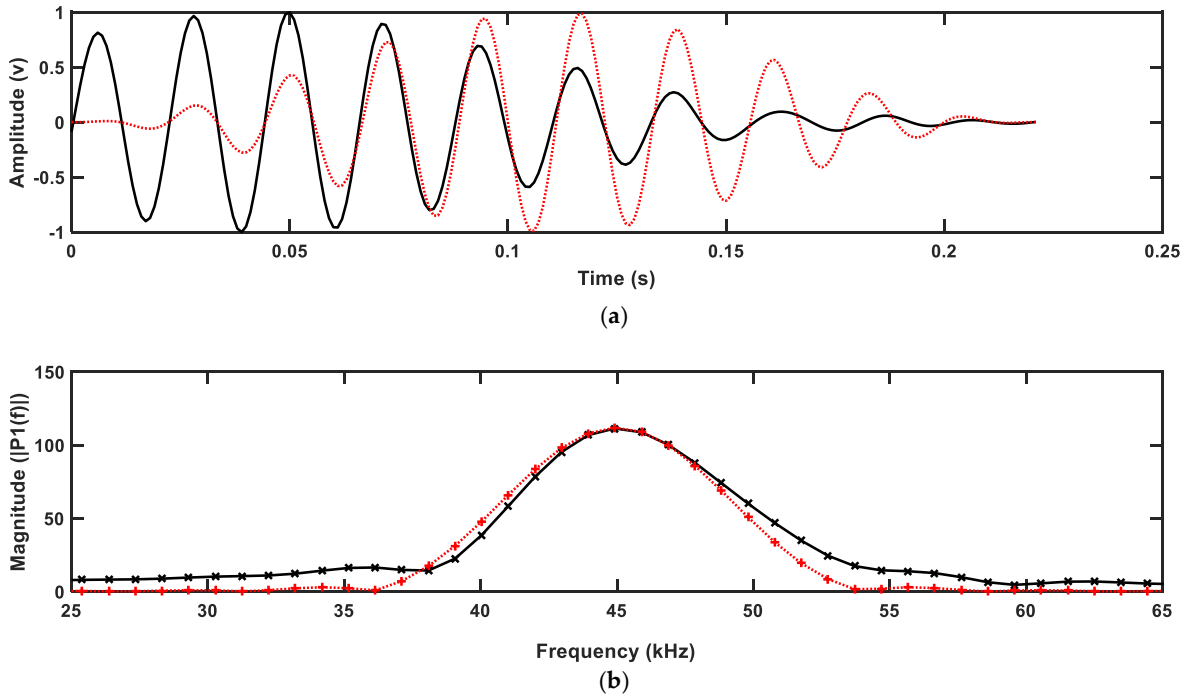

Figure 6.15. (a) The signal received from the pipe end using 50 kHz and (b) it's corresponding power spectrum. The red lines (dotted, +) show the references achieved from excitation sequence and the black lines (solid, x) show the results from each iteration.

Figure 6.16 shows the results achieved from Defect 2 where (a) shows the detection amplitude of the defect and (b) shows the amplitude of the outlier in the test. Each bar represents the results of a defect with a different CSA size and is categorised based on the tested frequencies. The achieved results from Defect 2 follow approximately the same trend as the one achieved from Defect 1; Lower frequencies cannot detect defects with smaller than 7% CSA sizes and 34-40 kHz can detect most of the defect sizes. However, unlike Defect 1, the performance of higher frequencies is significantly better as they result in higher detection amplitude for the defects and no outliers. Furthermore, the lowest defect size detectable is 2% CSA which could be detected only using 46 kHz. In most test cases, the detection amplitudes are significantly reduced. This is due to the placement of Defect 2 in a region where a significant amount of flexural wave exists.

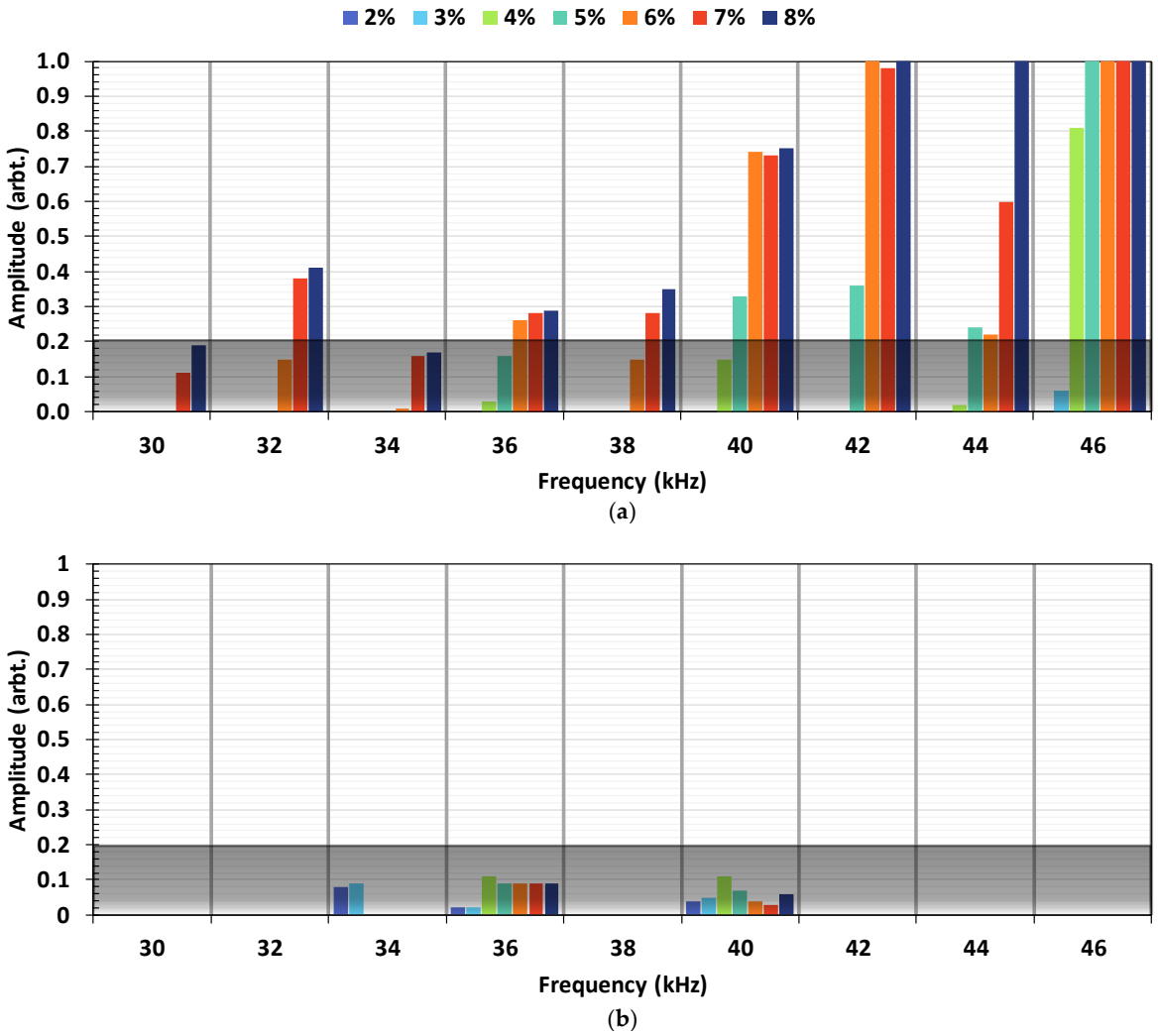

Figure 6.16. Results of Defect 2 achieved using the algorithm where (a) shows the detection amplitude of defect signal and (b) shows the detection amplitude of the outlier. Each bar represents the results achieved from a defect with different CSA size. The grey area represents the threshold region for calling outliers.

6.5 Discussion

The algorithm was tested in two defect locations: Defect 1 and 2 where the first location (Defect 1) was less affected by the flexural waves. As was mentioned in the previous section, the detection amplitudes are significantly reduced in Defect 2 location. These differences of amplitude between Defect 1 and 2 are shown in Figure 6.17, where (a) shows the amplitude of the defects and (b) shows the outlier's amplitudes. As can be seen, in most frequencies, it was easier to detect Defect 1 as it resulted in higher amplitude for all defect sizes. Nonetheless, the amplitude of outliers did not vary significantly for all frequencies except from 42 and 44 kHz. This is because flexural waves of higher frequencies are less dispersive, and their characteristics are closer to the torsional wave. Therefore, in some cases, isolated low order flexural waves with low amplitudes can be mistaken as torsional waves (Figure 6.19). Furthermore, the minimum detection size for Defect 2 location is increased to 5%. These

results suggest that this algorithm performs best for detecting isolated defects where they are not significantly affected by flexural waves located in the defect region.

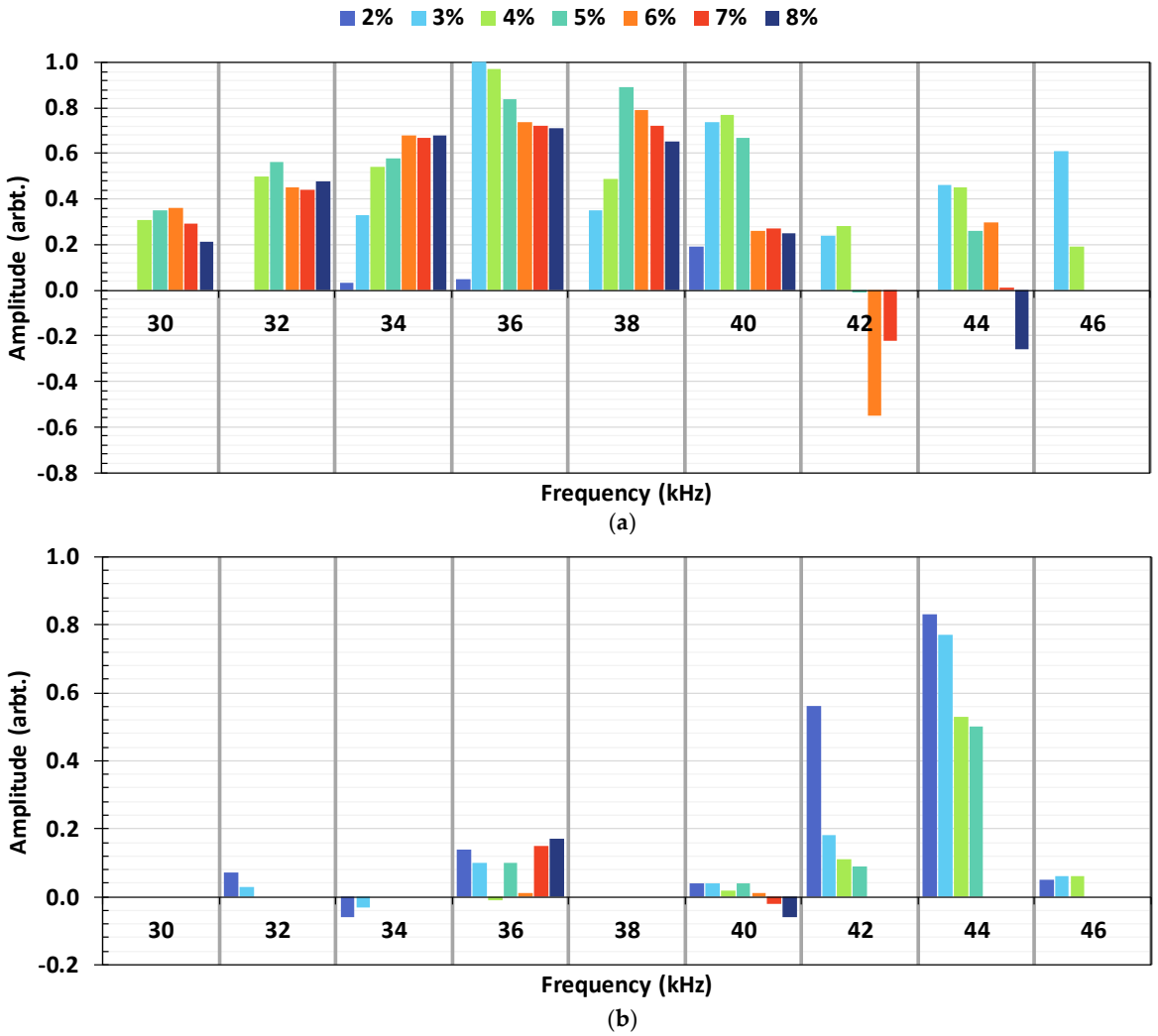

Figure 6.17. Difference between the results of Defect 1 and 2 where (a) and (b) shows the detection amplitude of defects and outliers, respectively.

Figure 6.18 demonstrates the defect to outlier detection ratios achieved for (a) Defect 1 and (b) Defect 2. In this figure, the maximum ratio is capped at 10 which means that the defects are evidently distinguishable in their respective cases; also, zero amplitudes illustrate that the defects were not detectable in such cases. For most defect sizes and frequencies, the achieved ratios are higher than a factor of 2. In the case of Defect 1, the smallest defect size of 2%, this ratio was achieved only using 40 kHz. For the other two cases of 34 and 36 kHz where this defect could be detected, ratios of 1.5 and 0.36 were achieved. Nonetheless, as expected for Defect 2, this ratio could be achieved only for defect sizes greater than 5%. In both cases, defect sizes of above 6% could significantly higher ratios and thus were much easier to detect.

This suggests that by setting an amplitude threshold, larger CSA size defects can be detected without any outliers. This threshold is shown in Figure 6.14 and Figure 6.16 using the greyed area which filters the amplitudes less than 0.2. It should also be borne in mind that doing so, would remove the detection of 2% CSA defect, especially in the case of 40 kHz since even though the values are smaller than this threshold, the amplitude of defect detection (0.19) is approximately twice than those of outlier (0.08). However, all other detections below the set threshold (such as 2% CSA defect using 40 kHz), can be used by the inspectors as supporting evidence where it supports in determining the signals type with the help of other traditional defect detection methods such as inspecting the time domain or using multiple frequencies. It was illustrated previously in Figure 6.17 that, when using some frequencies such as 42 and 44 kHz, the outliers' amplitude decreases as defect size increases. While the existence of the outlier in the higher frequencies was explained, the cause of this decrease was not mentioned.

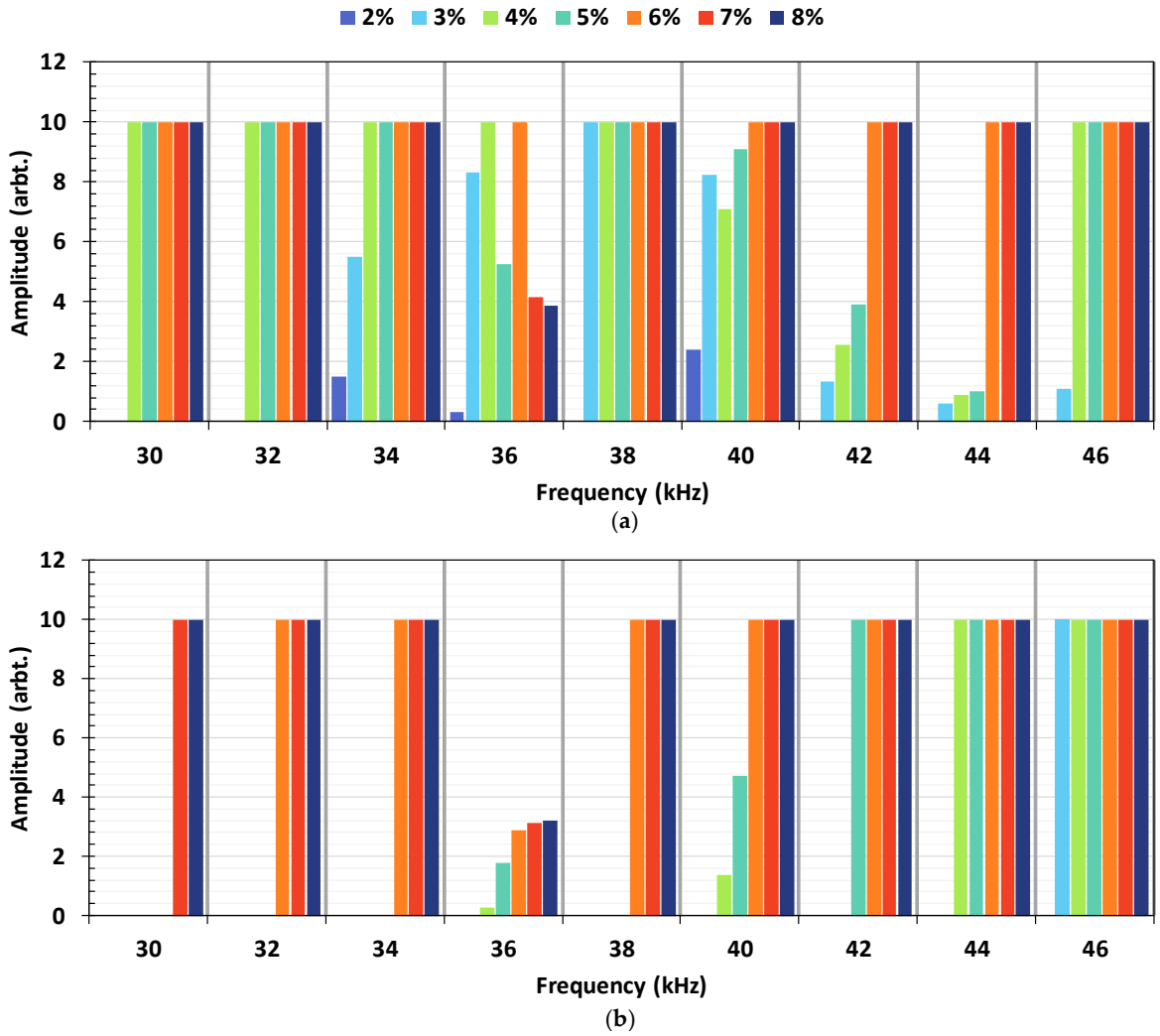

Figure 6.18. The ratio of detection amplitude of defect to an outlier in each test case. The amplitudes are capped at 10 for cases where outliers are not detected or have a small amplitude in compare to the defect. Any amplitude of zero represents detection of no defect. (a) and (b) are the results of Defects 1 and 2, respectively.

Figure 6.19a shows the time domain signals achieved for Defect 1 using 44 kHz for various defect sizes. Three main regions are the main focus of this figure: (c) which illustrates the defect and (b,d) which illustrate the noise regions. Evidently, when the defect size is increasing, the amplitude and energy of defect signal (c) increase. Since the only change in the physical characteristics of the pipe is the increment of defect size, the major change is expected in the defects' signal. However, other regions' signal can be changed too due to two main factors: the variability of system's transfer function and the amount of flexural wave mode conversions due to the increase in defect size.

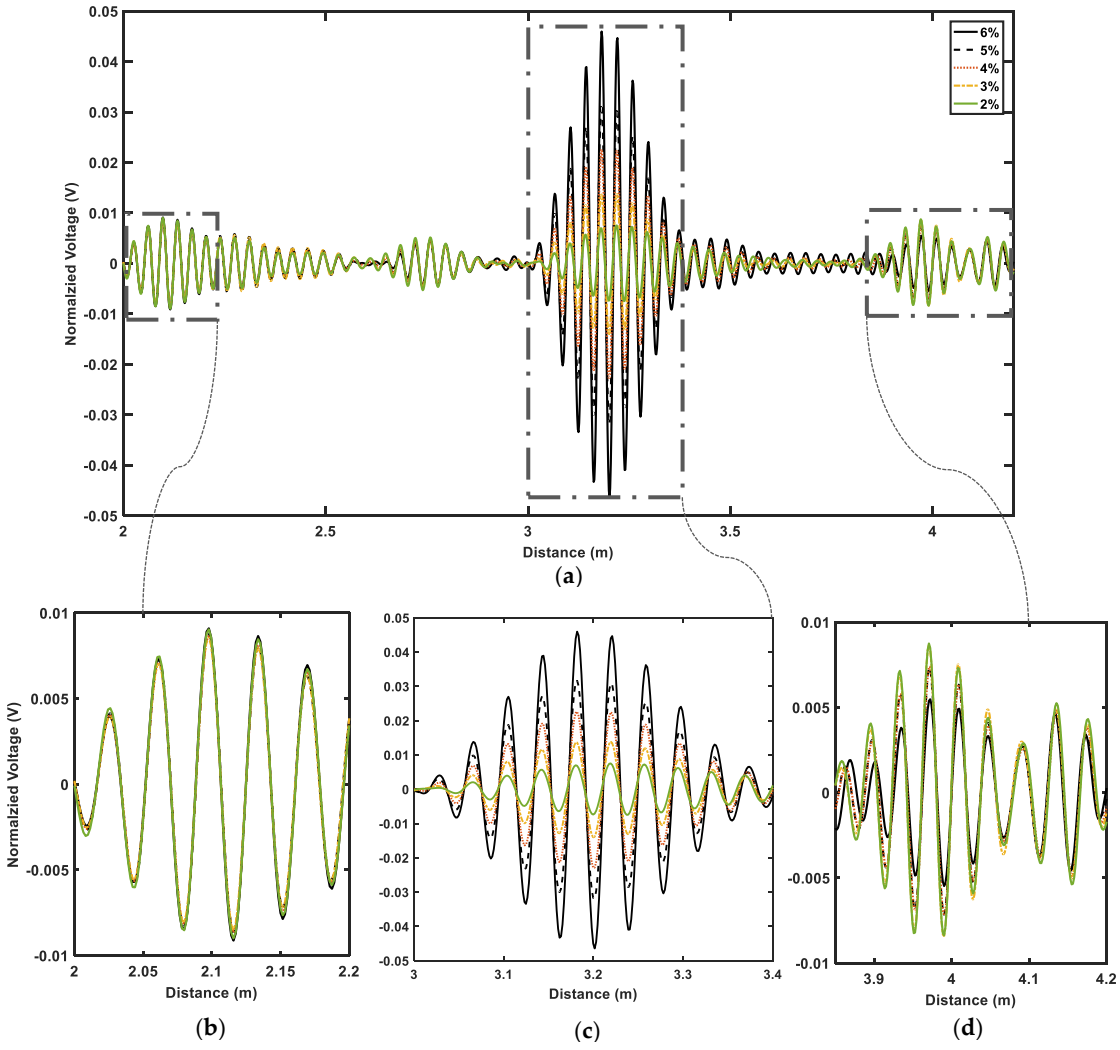

Figure 6.19. Experimental results of Defect 1 using excitation frequency of 44 kHz (a). Three regions are marked and zoomed in on the figure: (b) the noise region no change in amplitude, (c) the defect region with a significant change in amplitude, and (d) the outlier region with change in amplitude.

The introduced defects in the tests are non-axisymmetric and the excitation waveform is not purely torsional, the resultant scattering waves will include flexural waves. As the defect size increases, the amount of this wave mode conversion which is also frequency-dependent can vary. Hence, the signals in other regions can also be affected by increasing only the defect size and differences in the outliers' amplitude can be expected. Observing the same figure,

this is demonstrated using two noise regions located in (b) 2 – 2.2 and (d) 3.8 – 4.2. The first noise region (b) is far behind the defect location (c) and thus it is not affected by the wave mode conversions of the defect. The second noise region (d) is located after the defect location. As can be seen, when the defect size is increased, the amplitude and energy of this region is changed and is decreasing (in this case). This results in change of the spectrum in the affected iterations; hence, it affects the achieved amplitude generated from the outliers in such regions. Since the located outlier in region (d) is small in amplitude, when the defect size increases, it is easily affected by the resultant wave mode conversion, until the case of 6% CSA where the outlier is no longer detectable.

Most of the flexural waves have a slower speed than the torsional wave, in this case, the changes observed after the defect signal are significantly more than the ones from before the defect. As can be seen from Figure 6.17 most of the significant variations are when higher frequencies are used. This is due to the fact that the dispersion characteristics of flexural waves with higher frequencies are getting more similar to the torsional wave; especially in the case of low order flexural waves. Furthermore, tests using 48 kHz and 50 kHz did not result in any detection. Therefore, this algorithm works better with using frequencies lower than 40 kHz.

Figure 6.20 shows the generated results from Defect 1 with a size of 3% CSA using two excitation frequencies of (a) 36 and (b) 34 kHz. In this figure, the red lines demonstrate the processed result and black lines are the time-domain signals which are used as inputs to the algorithm. Also, the blue and grey regions demonstrate the defect and coherent-noise regions, respectively. As it was reported previously, using 36 kHz in this case results in detection of only the defect. Using 34 kHz, it results in detection of the defect along with an outlier. Nonetheless, the amplitude of outlier is at 0.05 while the defect is at 0.33; hence, the ratio of the defect to outlier is 5.5. In both cases, the defect signal is almost buried in the coherent-noise level and is not easily distinguishable in the time-domain. However, using this algorithm in the first case (a) results only in detection of defect, and in the second case (b) results in the detection of defect with a minor outlier with lower amplitude. Hence, using this algorithm can support the decision of the inspectors in calling defects that are close to the coherent noise-level and hold similar characteristics to the flexural waves in the time-domain. Doing so results in providing inspections with higher accuracy.

It should be noted that the experiments were performed with a shorter pipe length. Nevertheless, the detectability of the defects is mostly dependent on the characteristics of the received signal. The algorithm can easily detect a perfect axisymmetric feature such as a weld in long-range. Nonetheless, for defects that are generally smaller in size and asymmetric, the

hypothesis is that the feature can be detected if the characteristic of the torsional wave is not lost in the received signal. It should also be noted, that as the inspection pipe length increases the energy of the flexural waves reduce due to their dispersion in time and the effect of attenuation on them. Therefore, false alarms using this method would be expected to be less in long-range inspections.

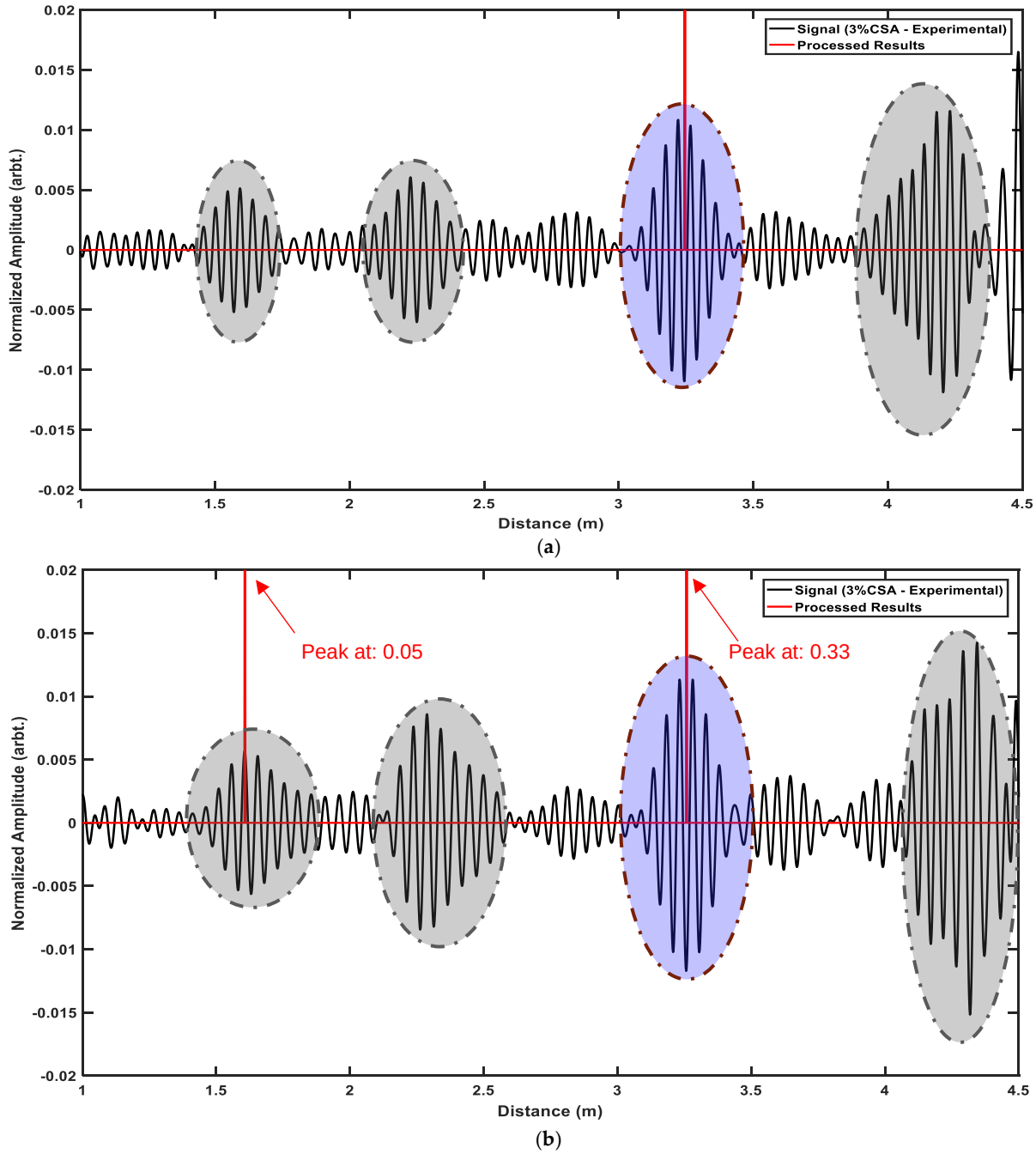

Figure 6.20. Experimental results of Defect 1 with CSA size of 3%. (a) shows the results using 36 kHz and (b) shows the results using 34 kHz. Blue and grey regions illustrate the defect and noise signals, respectively.

6.6 Chapter Summary

In this chapter, a novel method is proposed to detect the location of defects using the known excitation power spectra of the torsional waves in guided wave inspection of pipelines. For doing so, as opposed to traditional inspection using a time-domain signal, the spectral domain of the signal is compared with the characteristics of the known excitation sequence. The method works by applying a moving window to the received signal from the inspection, wherein each iteration the signal is normalised, and its corresponding power spectrum is generated. Since both defect signal and noise are within the same frequency band, by only measuring the correlation between reference and iterations power spectrum, the defect signal will not be distinguishable. Therefore, before measuring the correlation, a total of five conditions were checked to verify that a similar power spectrum to the reference was achieved:

- The centre frequency shift must be small (See Sections 6.2.3.1, 6.3.1).
- Considering the 10 dB bandwidth of the iteration's power spectrum, the magnitude of each respective frequency bin must be increased when moving toward the centre frequency (See Sections 6.2.3.2, 6.3.2).
- The achieved magnitude from the neighboring bins to the centre frequency must be closely related (See Sections 6.2.3.3, 6.3.3).
- Frequencies outside the 10 dB bandwidth must have less magnitude than the minimum one achieved from within the 10 dB bandwidth (See Sections 6.2.3.4, 6.3.4).
- The maximum magnitude achieved must be less than the one from the reference. (See Sections 6.2.3.5, 6.3.5).

For each condition, a safety margin is set by the user to neglect minor differences due to the digitisation of the signals and the limitation of the available sample in each window. Nonetheless, before applying the algorithm on guided-wave data from pipes, these limits can be fixed as they are set to provide tolerance. On the other hand, this method can also be tested using traditional ultrasonic testing, where there might be a need for tweaking these parameters.

The algorithm was initially developed and validated on simulated data from FEM. Afterward, the performance of the algorithm was assessed in the laboratory trials using real pipes with defects. In these trials, multiple excitation frequencies starting from 30 – 50 kHz (with linear steps of 2 kHz) was used in order to assess the performance of algorithm by varying the frequency. Furthermore, for evaluating the performance of algorithm with regards to different defects, two defect locations with sizes varying from 2 – 8 % CSA was used (with linear steps

of 1% CSA). It was demonstrated that the choice of excitation frequency is a trade-off between the ability of the system to generate the given excitation sequence and having highly dispersive flexural waves (which are considered as the main source of the noise in these tests). Frequencies in range of 34 to 40 kHz resulted in detecting the majority of defects, including the case of the 2% CSA defect (located in Defect 1 location). Also, the dispersion speed of flexural waves with higher frequencies are closer to torsional waves and the possibility of having an isolated outlier using these frequencies are higher. Furthermore, due to the systems' transfer function, defects could not be detected using frequencies higher than 46 kHz. Frequencies lower than 34 kHz was only capable of detecting defects with higher CSA losses. Hence, frequencies in the range of 34 to 40 kHz are optimal. Two defect locations were tested where the first location (Defect 1) is less affected by the flexural waves than the second defect location (Defect 2). It was observed that this algorithm works best when the defect signal is isolated and is less affected by the flexural waves. Furthermore, it was demonstrated that using this method can support the inspectors in determining the signal types in the results, especially in cases where defects and outliers have approximately the same amplitude in the time domain (see Figure 6.20 in Section 6.5). This method only requires a time-domain signal and knowledge of the characteristics of the excitation sequence; hence, it can easily be combined with other methods to further enhance the reliability of defect detection in guided wave testing of pipelines.

In this chapter, it was illustrated that instead of detecting the defect in the time-domain signal, the windowed frequency spectrum of the signals can be used in order to enable detection of defects based on the power spectra of the excitation sequence. The developed algorithm can be used as a tool, along with conventional detection methods, to provide more certainty in the interpretation of the results and reduce the number of outliers called due to the coherent noise. It is expected that experience of this algorithm will help develop automated inspection of pipelines.

Chapter Seven

Conclusions and Recommendations for Further Works

The aim of the work presented in this thesis was to enable easier and more accurate inspection by developing novel signal processing techniques in ultrasonic guided wave testing of pipelines (Chapter 1). In order to do so, two main parts of literature were required to be investigated:

1. **A background review of the UGW inspection of pipelines (Chapter 2):** The physics, features, and challenges of guided waves were investigated. Parts of this included an investigation of the state-of-the-art signal processing techniques applied to guided waves in order to find their respective challenges and their proposed solutions.
2. **The capability of the current inspection devices (Chapter 3):** The main focus was to develop signal processing techniques without applying any modifications to the hardware of the inspection device. Therefore, by investigating the device, working knowledge of how the data is generated was achieved and possible gaps of improvement in different stages of this process were found.

From the reviewed literature review, it was learned that great potential exists for development of signal processing techniques for this UGW inspection of pipelines. In this thesis, three main pathways were selected for development of signal processing techniques. The first one was to enable identification of the defects' location using data gathered from the sensor array of the inspection device (Chapter 4) The second was to enhance the SNR of the defects by altering the signal recombination processes of the inspection device (Chapter 5). The third pathway was to use the power spectrum of the excitation sequence and the results provided by the inspection device, in order to detect the defect location (Chapter 6).

Each of the aforementioned pathways leads to development of a new signal processing algorithm. The algorithms were initially developed using a simulated signal generated using a FEM test case (Chapter 3). This was done in order to save the cost in terms of both time and expenditure for validating the techniques before applying them to laboratory trials. As opposed

to other FEM test cases developed in the literature, this model inherently used variable transfer functions in order to generate coherent noise. This made processing and development of techniques more challenging. Afterward, the performance of each algorithm was assessed in the experimental trials using real pipe data. The focus on these trials was on three main factors: first and foremost, to test the feasibility of achieving the results and verifying the concept behind their respective pathway. Secondly, the dependence of the algorithm on the excitation frequency. Lastly, to find out the results with regards to different defect locations and coherent noises.

The tests validated the stated hypothesis in each pathway and proved the feasibility of achieving them using the current testing device. Moreover, it also demonstrated that using these approaches, it is possible to further develop the current signal generation routine of the device in order to increase the accuracy of inspection and support the decision-making process of the inspectors. Hence, all of the developed methods can be readily implemented in the inspection device and help the inspectors in results interpretation. Since this research was tested with Teletest device, the closest industrial application would be to implement the developed algorithms in the device to enable advanced post-processing of signals. Currently, these algorithms can be used to help the inspectors as an additional tool, allowing them an easier interpretation of the results. The conclusion with respect to each of these individual algorithms is stated below in this section.

7.1 Defect Detection Using Spatial Differences between UGW modes

In Chapter 4, a statistical algorithm was introduced which uses the full capability of the sensor array of conventional guided waves inspection devices to identify defects in the test specimens. In contrast to other defect detection techniques in the literature that use a single time-domain signal generated by the inspection device after processing, this algorithm uses the signals from each individual transducer in the array for each data sample in time and determines the defect location. In doing so, both spatial and temporal characteristics of the signals are used which leads to a more accurate method of distinguishing noise from the signal of interest. Since flexural waves are generally considered as the coherent noise, the main focus of this algorithm is to detect the axisymmetric (torsional) which leads to the defect location.

Currently, guided wave inspection devices are capable of having multidimensional excitation and reception. Therefore, no hardware modification is required for using this method. The only requirement is that a threshold is set by an inspector. Perfect axisymmetric features such as weld or pipe-end can be detected without any threshold. However, since the defects are

generally non-axisymmetric, the resultant received signal would be a mixture of flexural and torsional waves. This threshold, in simple terms, defines the allowable level of flexural waves for each sample of time.

Three different methods and two different thresholding versions of this algorithm are developed using the simulated signal generated by a FEM model. Afterward, the performance of each was assessed in laboratory trials. It was demonstrated that subsequent development of the methods resulted in more accurate detection of defects, where defects with lower CSA sizes could be detected with wider excitation frequency range. This is due to the fact that in the initial method, a static threshold was used while in the later methods the thresholds were defined using the statistical characteristics of each time sample. Doing so improved the results significantly where defect sizes as low as 2% CSA could be detected using this algorithm.

The achieved results confirmed the capability of this algorithm in detecting defects contaminated by coherent noise. Furthermore, it demonstrated the advantage of using the information of both space and time in the signals achieved from each transducer in order to detect defect signals rather than trying to minimize the coherent noise by spatial averaging techniques and interpreting the results based on their properties in the time domain.

7.2 Adaptive Filtering for Enhancement of Signal to Noise Ratio

In Chapter 5, an adaptive filtering algorithm is utilized to enhance the SNR of the torsional waves generated from defects in guided wave inspection of pipelines. As opposed to using the post-processed signal of the device, in this approach, two sets of signals received from the test toll were used as inputs to the adaptive filtering algorithm. Inherently, in these two sets of signals, the torsional waves are overlapping while the flexurals are varying; this was the basis on which the adaptive filter was able to enhance the SNR of torsional waves. Since flexural waves are variable both in space and time, the algorithm used for updating the filter weights was leaky NLMS, which allowed faster adaption to the highly variable flexural noise and enabled a faster reset of the filter weights.

The algorithm was initially developed and validated using the simulated signal generated from the FEM test case and is quantitively assessed in the laboratory trials. Adaptive filters require a set of parameters for operation. In order to investigate the feasibility of using this method, two sets of parameters were considered. In the first case the parameters are set with regards to the FEM and in the second case using the experimental data gathered from 4% CSA defect.

The results demonstrated that using this algorithm with the correct parameter scan resulted in enhancement of SNR of defects as small as 3% CSA could be improved. Furthermore, a

significant reduction in flexural waves, especially in the case of higher-order flexural waves, could be achieved. This leads to easier detection of defects in the inspection. However, the optimum selection of parameters is a trade-off between the maximum achieved gain and the stable enhancement of the SNR of smaller defects. Currently, the adaptive filter parameters can be using a simulated FEM signal; but it will not result in achievement of the maximum possible gain.

In conclusion, the results in this chapter confirm that by using an adaptive filter, the defects' SNR is increased in comparison to the device's propagation routine. This was possible without any changes required in the hardware. Furthermore, it was illustrated that by developing algorithms considerate of the spatial placement of the sensors, it is possible to further enhance the overall SNR of the achieved signal by either amplifying the defect signals or reducing the noise signal's energy. This will lead to the development of a more efficient propagation routine that considers both spatial and temporal characteristics of the signals in order to enhance the overall quality of the achieved results and allows easier interpretation of test results by inspectors.

7.3 Defect Detection using Spectral Matching of Torsional wave

In Chapter 6 a novel algorithm is proposed to detect the location of defects in the pipes using the known excitation power spectra of the torsional waves. The objective is to detect the defect based on comparing the power spectra of the (reference) excitation sequence and the received spectra from each time-sample.

The method works by applying a moving window to the received signal from the inspection, where for each time sample the signal is normalised and its corresponding power spectra are generated. Afterward, a binary comparison is done between the power spectra of the reference and the generated spectrums. These conditions compare the centre frequency, the magnitudes, the overall noise outside the main bandwidth, and the maximum magnitude achieved from the generated spectrum with the reference spectrum. In order for a signal to be marked as a defect, all five conditions must be satisfied. For each condition, a safety margin is set by the user to neglect minor differences due to the digitisation of the signals and the limitation of the available sample in each window. Nonetheless, before applying the algorithm on guided-wave data from pipes, these limits can be fixed as they are set just to provide tolerance.

This algorithm was developed using a simulated signal generated from the FEM test case. Afterward, the performance of the algorithm was assessed in experimental trials using

excitation frequencies in range of 30 – 50 kHz and defect sizes in range of 2-8% CSA. In these trials, it was demonstrated that the choice of excitation frequency is a trade-off between the ability of the system to generate the required excitation sequence and having highly dispersive flexural waves. Excitation frequencies in range of 34 to 40 kHz are the most suitable frequencies to be used as an excitation sequence while using frequencies higher than 46 kHz does not result in detection of the defect and frequencies lower than 34 kHz are only capable in detecting larger defects (with higher CSA losses). Moreover, two different locations were assessed where one location was more contaminated by the flexural wave. The tests showed that this algorithm works best when the defect signal is isolated and is less affected by the flexural waves. Nonetheless, it was demonstrated that using this method can support the inspectors in determining the signal types in the results, especially in cases where defects and outliers have approximately the same amplitude in the time domain.

In conclusion, it was illustrated that instead of detecting the defect in the time-domain signal, the windowed frequency spectrum of the signals can be used in order to enable detection of defects based on the power spectra of the excitation sequence. The developed algorithm can be used as a tool, along with the conventional detection methods, to provide more certainty in the interpretation of the results and reduce the number of outliers called due to the coherent noise. It is expected that experience of this algorithm will help develop automated inspection of pipelines.

7.4 Recommendations for Further Works

One of the limitations for the development of signal processing algorithms in UGW inspection of pipelines was the availability of experimental test data. Such database can allow creation of a benchmark for comparison of different signal processing techniques. Also, can ease the validation processes of newly developed algorithms. Therefore, creation of such database is highly recommended. Furthermore, this database can be used in order to assess the workability of the developed algorithms in this thesis.

7.4.1 Defect Detection Using Spatial Differences between UGW modes

In summary, there are two main parts of this algorithm:

1. The measurement which defines the amount of existing axisymmetric wave.
2. The threshold which defines the allowable amount of non-axisymmetric.

These two parts can be further investigated and improved. The main focus should be on developing these parts so more representative characteristic of the defect signal is considered in calculating their values. As an example, by assigning the threshold value with regards to

the amount of flexural wave, a more accurate threshold value which changes iteratively according to the characteristics of each time sample can be gained (Methods Two and Three, See Section 4.3.3). As illustrated, doing so significantly improves the results. Also, this algorithm can be combined with other methods where the current threshold values can be amplified or reduced based on the results of other detection methods (such as the algorithm developed in Chapter 6). Further research needs to be conducted in an attempt to enable the automated selection of thresholds for a wider range of excitation frequencies.

7.4.2 Adaptive Filtering for Enhancement of Signal to Noise Ratio

Further research is required in order to develop a robust method for the detection of the most optimum parameters for each frequency. Instead of determining the parameters using a FEM test case which is a slow process, it can be possible that extract the parameters using formulas with regards to the pipes' characteristics. On the other hand, the algorithm can be applied to various pipes where the optimum parameters are set at the time of inspection. This results in creation of a database where the optimum parameters are set with regards to the received signals characteristics (rather than the pipe's characteristics). Using this database, it is possible to create a feature map where, based on the features of the received signal in the inspection, the parameters of the signal with closest features are chosen and are used for adaptive filtering.

Furthermore, the main concept is to use the signals of the rings which inherently have correlated torsional waves and less correlated flexural waves, in order to enhance the SNR of the torsional wave. Therefore, other algorithms can be explored to replace the adaptive filtering algorithm of this approach. Currently, it was found out that the leakage factor is a significant parameter in filtering the noise. This is because the flexural waves are highly variable in time and space, and therefore the filter weights must be able to forget the previous characteristics of previous time samples quickly in order to adapt faster to the current time sample. Also, this method can be further developed in order to apply the filtering on each individual sensor rather than the signals received from the rings; the main difficulty in doing so is that the torsional wave received from individual transducers' signal are generally buried in coherent-noise, especially for small defects (lower than 4% CSA).

7.4.3 Defect Detection using Spectral Matching of Torsional wave

This algorithm only requires a time-domain signal (achieved from the propagation routine) and knowledge of the characteristics of the excitation sequence; hence, it can be combined with other methods to further enhance the reliability of defect. As an example, instead of using the results generated from the current propagation routine of the device, the

output of the newly developed routine in Chapter 5 which is generated using adaptive filtering can be used. Doing so, initially amplifies the SNR and reduces the high-variable flexural noise the signal and then allows detection of defects using this method. On the other hand, the algorithm can be modified in order to compare more representative conditions of the excitation sequence's power spectra. These can increase the accuracy of the results achieved by reducing the number of reported outliers. It was illustrated that using the frequency domain, it is possible to detect the defect signal; therefore, it might be possible to use Frequency Domain Adaptive Filtering in order to enhance the SNR of the defect rather than detecting the defect location. This method can also be tested in traditional ultrasonic testing, where there might be a need for tweaking the safety-parameters.

Bibliography

[1] P. Hopkins, “1.06 - The Structural Integrity of Oil and Gas Transmisison Pipelines,” *Compr. Struct. Integr.*, vol. 1, pp. 87–123, 2003.

[2] S. Fateri, “Advanced Signal Processing Techniques for Multimodal Ultrasonic Guided Wave Response,” Brunel University, 2015.

[3] AMSE, “AMSE B36.10M-2015: Welded and Seamless Wrought Steel Pipe Welded and Seamless Wrought Steel,” *Am. Scoiety Mech. Eng.*, 2015.

[4] P. Hopkins, “Learning From Pipeline Failures,” in *WTIA / APIA Welded Pipeline Symposium*, 2008, pp. 0–15.

[5] A. Ghavamian, F. Mustapha, and B. T. H. T. Baharudin, “Detection , Localisation and Assessment of Defects in Pipes Using Guided Wave Techniques : A Review,” *MDPI Sensors*, vol. 18, pp. 1–48, 2018.

[6] C. Lam, “Statistical Analyses of Historical Pipeline Incident Data with Application to the Risk Assessment of Onshore Natural Gas Transmission Pipelines,” The university of Western Ontario, 2015.

[7] Pipeline Data and Statistics, “Pipeline Incident 20 Year Trends,” Washington, 2019.

[8] U.S. Department of Justice, “U.S. V. BP Products N. AM.,” *United States Department of Justice*, 2015. [Online]. Available: https://www.justice.gov/enrd/us-v-bp-products-n-am. [Accessed: 01-Sep-2019].

[9] G. White, “US sues BP over Prudhoe Bay oil Spill,” *telegraph*, 2009. [Online]. Available: https://www.telegraph.co.uk/finance/newsbysector/energy/oilandgas/5091013/US-sues-BP-over-Prudhoe-Bay-oil-spill.html. [Accessed: 01-Sep-2019].

[10] R. A. Smith, “Non-Destructive Testing (ND) – Guidance Document : An Introduction to NDT Common Methods,” *BINDT*, no. 2, 2015.

[11] IAEA, “Non-destructive testing for plant life assessment,” Vienna, Austria, 2005.

[12] TWI Training and Examination, “TWI Training School,” 2019. [Online]. Available: www.twitraining.com. [Accessed: 01-Aug-2019].

[13] IAEA, “Training Guidelines in Non-Destructive Testing Techniques,” Vienna, 1987.

[14] H. R. Vanaei, A. Eslami, and A. Egbewande, “A review on pipeline corrosion , in-line inspection (ILI), and corrosion growth rate models,” *Int. J. Press. Vessel. Pip.*, vol. 149, pp. 43–54, 2017.

[15] S. Ge, M. Asce, S. Sinha, and M. Asce, “Failure Analysis , Condition Assessment Technologies , and Performance Prediction of Prestressed-Concrete Cylinder Pipe : State-of-the-Art Literature Review,” *J. Perform. Constr. Facil. © ASCE*, vol. 28, no. June, pp. 618–628, 2014.

[16] P. Belanger and P. Cawley, “Feasibility of low frequency straight-ray guided wave tomography,” *NDT&E Int.*, vol. 42, pp. 113–119, 2009.

[17] M. J. S. Lowe and P. Cawley, “Long Range Guided Wave Inspection Usage – Current Commercial Capabilities and Research Directions.”

[18] A. Demma, “Guided Waves: Opportunities and Limitations,” in *Cofrend 2011, National NDT Seminar & Exhibition*, 2011, pp. 1–6.

[19] Teletestndt, “Long Range Guided Wave Testing with Teletest Focus+,” 2018. [Online]. Available: https://www.teletestndt.com/. [Accessed: 14-Jan-2019].

[20] J. L. Rose, “A Baseline and Vision of Ultrasonic Guided Wave Inspection Potential,” *J. Press. Vessel Technol.*, vol. 124, no. 3, p. 273, 2002.

[21] J. L. Rose, “Successes and Challenges in Ultrasonic Guided Waves for NDT and SHM,” in *Indian National Seminar & Exhibition on Non-Destructive Evaluation*, 2009.

[22] B. A. Engineer, “The Mechanical and Resonant Behaviour of a Dry Coupled Thickness-Shear PZT Transducer used for Guided Wave Testing in Pipe Line,” Brunel University, 2013.

[23] K. Thornicroft, “Ultrasonic Guided Wave Testing of Pipelines using a Broadband Excitation,” Brunel University London, 2015.

[24] X. Niu, W. Duan, H. Chen, and H. R. Marques, “Excitation and propagation of torsional T (0 , 1) mode for guided wave testing of pipeline integrity Excitation and propagation of torsional T (0 , 1) mode for guided wave testing of pipeline integrity,” *Measurement*,

vol. 131, no. August, pp. 341–348, 2018.

[25] F. Bertoncini, G. De Lorenzo, G. Giunta, M. Raugi, and F. Turcu, “Effect of Attenuation on Inspection Range and Sensitivity in Long- Range Guided Wave NDT of Coated and Buried Pipes,” *NDT.net*, 2010. [Online]. Available: www.ndt.net/?id=9985. [Accessed: 05-Dec-2016].

[26] W. M. (Wiesław M. . Ostachowicz, *Guided waves in structures for SHM : the time-domain spectral element method*. Wiley, 2012.

[27] R. Mallet, “Signal processing for Non-destructive testing,” Brunel Unviersity, 2007.

[28] A. H. Meitzler, “Mode Coupling Occurring in the Propagation of Elastic Pulses in Wires,” *J. Acoust. Soc. Am.*, vol. 33, no. 4, pp. 435–445, 1961.

[29] P. Catton, “Long Range Ultrasonic Guided Waves for Pipelines Inspection,” Brunel University, 2009.

[30] Nurmalia, “Mode conversion of torsional guided waves for pipe inspection : an electromagnetic acoustic transducer technique,” Osaka University, 2013.

[31] P. D. Wilcox, “A rapid signal processing technique to remove the effect of dispersion from guided wave signals,” *IEEE Trans. Ultrason. Ferroelectr. Freq. Control*, vol. 50, no. 4, pp. 419–427, 2003.

[32] J. L. Rose, *Ultrasonic Guided Waves in Solid Media*. New york: Cambridge University Press, 2014.

[33] R. Guan, Y. Lu, W. Duan, and X. Wang, “Guided waves for damage identification in pipeline structures : A review,” *Struct. Control Heal. Monit.*, no. February, pp. 1–17, 2017.

[34] R. Sanderson, “A closed form solution method for rapid calculation of guided wave dispersion curves for pipes,” *Wave Motion*, vol. 53, pp. 40–50, 2015.

[35] P. Wilcox, M. Lowe, and P. Cawley, “The effect of dispersion on long-range inspection using ultrasonic guided waves,” *NDT E Int.*, vol. 34, no. 1, pp. 1–9, 2001.

[36] H. Nakhli Mahal, P. Mudge, and A. K. Nandi, “Noise removal using adaptive filtering for ultrasonic guided wave testing of pipelines,” in *57th Annual British Conference on Non-Destructive Testing*, 2018, pp. 1–9.

[37] B. Vogelaar and M. Golombok, “Dispersion and attenuation by transmission , reflection

, and mode conversion in welded pipes," *Appl. Acoust.*, vol. 110, pp. 1–8, 2016.

[38] L. Zeng, J. Lin, L. Huang, and M. Zhao, "Amplitude Dispersion Compensation for Damage Detection Using Ultrasonic Guided Waves," *Sensors*, vol. 16, no. 10, p. 1623, 2016.

[39] M. J. S. Lowe, D. N. Alleyne, and P. Cawley, "The Mode Conversion of a Guided Wave by a Part- Circumferential Notch in a Pipe," *J. Appl. Mech.*, vol. 65, no. 649, 1998.

[40] W. Duan, R. Kirby, and P. Mudge, "On the scattering of elastic waves from a non-axisymmetric defect in a coated pipe," *Ultrasonics*, vol. 65, no. 17, pp. 228–241, 2016.

[41] V. Chayer, "Eddyfi Technologies Acquires the Teletest Product Portfolio," 2018. [Online]. Available: https://www.eddyfi.com/news/eddyfi-technologies-acquires-the-teletest-product-portfolio/. [Accessed: 01-Sep-2019].

[42] Teletestndt, "Guided Wave Pipe Corrosion Inspection System," 2019. [Online]. Available: https://www.teletestndt.com/focus-guided-wave-inspection/. [Accessed: 01-Sep-2019].

[43] M. Zennaro, A. Haig, G. Park, D. J. O. Boy, and S. J. Walsh, "AN INVESTIGATION OF ULTRASONIC TRANSDUCER LOADING ON A," pp. 1–6, 2018.

[44] P. Cawley and M. J. S. Lowe, "Practical long range guided wave inspection-applications to pipes and rail," *Mater. Eval.*, pp. 66–74, 2003.

[45] A. Chaston, "Development of a transducer to be used in Long Range Ultrasonic Testing by."

[46] H. Miao, Q. Huan, Q. Wang, and F. Li, "Excitation and reception of single torsional wave T(0,1) mode in pipes using face-shear d24 piezoelectric ring array," *Smart Mater. Struct.*, vol. 26, pp. 1–9, 2017.

[47] M. J. S. Lowe, D. N. Alleyne, and P. Cawley, "Defect detection in pipes using guided waves," *Ultrasonics*, vol. 36, no. 1–5, pp. 147–154, 1998.

[48] D. N. Alleyne, B. Pavlakovic, M. J. S. Lowe, and P. Cawley, "Rapid, Long Range Inspection of Chemical Plant Pipework Using Guided Waves," *Key Eng. Mater.*, vol. 270–273, pp. 434–441, 2004.

[49] ASTM Standard E2775 - 16, *Standard practice for guided wave testing of above ground steel pipeword using piezoelectric effect transducer*. West Conshohocken, 2017.

[50] H. Nakhli Mahal, K. Yang, and A. K. Nandi, “Improved Defect Detection Using Adaptive Leaky NLMS Filter in Guided-Wave Testing of Pipelines,” *Appl. Sci.*, vol. 9, no. 2, pp. 1–23, 2019.

[51] C. Holmes, A. Velichko, and P. D. Wilcox, “Post-processing of the full matrix of ultrasonic transmit-receive array data for guided wave pipe inspection,” *NDT&E Int. 38*, vol. 38, pp. 701–711, 2005.

[52] L. Zeng, J. Lin, Y. Lei, and H. Xie, “Waveform design for high-resolution damage detection using lamb waves.,” *IEEE Trans. Ultrason. Ferroelectr. Freq. Control*, vol. 60, no. 5, pp. 1025–9, 2013.

[53] M. Garcia-Rodriguez, “Lamb Wave generation with an air-coupled piezoelectric array using square chirp excitation,” in *International Congress on acoustics*, 2007, no. 19, pp. 2–7.

[54] M. Garcia-Rodriguez, Y. Yaez, M. J. Garcia-Hernandez, J. Salazar, A. Turo, and J. A. Chavez, “Application of Golay codes to improve the dynamic range in ultrasonic Lamb waves air-coupled systems,” *NDT E Int.*, vol. 43, no. 8, pp. 677–686, 2010.

[55] M. K. Yücel *et al.*, “Pulse-compression based iterative time-of-flight extraction of dispersed Ultrasonic Guided Waves,” *Proceeding - 2015 IEEE Int. Conf. Ind. Informatics, INDIN 2015*, pp. 809–815, 2015.

[56] M. K. Yücel *et al.*, “Coded Waveform Excitation for High-Resolution Ultrasonic Guided Wave Response,” *IEEE Trans. Ind. Informatics*, vol. 12, no. 1, pp. 257–266, 2016.

[57] S. Malo, S. Fateri, M. Livadas, C. Mares, and T. Gan, “Wave Mode Discrimination of Coded Ultrasonic Guided Waves using Two-Dimensional Compressed Pulse Analysis,” *IEEE Trans. Ultrason. Ferroelectr. Freq. Control*, no. May, pp. 1–10, 2017.

[58] S. K. Pedram, S. Fateri, L. Gan, A. Haig, and K. Thornicroft, “Split-spectrum processing technique for SNR enhancement of ultrasonic guided wave,” *Ultrasonics*, vol. 83, pp. 48–59, 2018.

[59] S. K. Pedram, A. Haig, P. S. Lowe, K. Thornicroft, L. Gan, and P. Mudge, “Split-spectrum signal processing for reduction of the effect of dispersive wave modes in long-range ultrasonic testing,” *Phys. Procedia*, vol. 70, pp. 388–392, 2015.

[60] S. K. Pedram, P. Mudge, and T.-H. Gan, “Enhancement of ultrasonic guided wave signals using a split-spectrum processing method,” *Appl. Sci.*, vol. 8, no. 10, p. 1815,

2018.

[61] W. Duan, J. Kanfoud, M. Deere, P. Mudge, and T.-H. Gan, “Spectral subtraction and enhancement for torsional waves propagating in coated pipes,” *NDT E Int.*, vol. 100, no. July, pp. 55–63, 2018.

[62] M. G. Bellanger, *Adaptive Digital Filters, Revised and Expanded*, Second. New York: Marcel Dekker, Inc, 2001.

[63] B. Widrow *et al.*, “Adaptive Noise Cancelling: Principles and Applications,” *Proc. IEEE*, vol. 63, no. 12, pp. 1692–1716, 1975.

[64] P. Rajesh, K. Umamaheswari, and V. N. Kumar, “A Novel Approach of Fetal ECG Extraction Using Adaptive Filtering,” vol. 3, no. 2, pp. 55–70, 2014.

[65] W. Hernandez, “Improving the response of a wheel speed sensor using an adaptive line enhancer,” *Measurement*, vol. 33, pp. 229–240, 2003.

[66] R. M. Ramli, A. O. A. Noor, and S. A. Samad, “A Review of Adaptive Line Enhancers for Noise Cancellation,” *Aust. J. Basic Appl. Sci.*, vol. 6, no. 6, pp. 337–352, 2012.

[67] K. Murano, S. Unagami, and F. Amano, “Echo Cancellation and Applications,” *IEEE Commun. Mag.*, vol. 28, no. 1, pp. 49–55, 1990.

[68] D. Messerrschmi, “Echo Cancellation in Speech and Data Transmission,” *IEEE J. Sel. Areas Commun.*, vol. SAC-2, no. 2, pp. 283–297, 1984.

[69] W. Bürger, “Space-Time Adaptive Processing : Fundamentals,” *Adv. Radar Signal Data Process.*, vol. 6, no. 14, pp. 6-1-6–14, 2006.

[70] C. Schwark and D. Cristallini, “Advanced multipath clutter cancellation in OFDM-based passive radar systems,” *2016 IEEE Radar Conf. RadarConf 2016*, 2016.

[71] Y. Zhu and J. P. Weight, “Ultrasonic nondestructive evaluation of highly scattering materials using adaptive filtering and detection,” *Ultrason. Ferroelectr. Freq. Control. IEEE Trans.*, vol. 41, no. 1, pp. 26–33, 1994.

[72] D. Monroe, I. S. Ahn, and Y. Lu, “Adaptive filtering and target detection for ultrasonic backscattered signal,” *2010 IEEE Int. Conf. Electro/Information Technol. EIT2010*, 2010.

[73] M. H. Hayes, *Statistical Digital Signal Processing and Modeling*. New york: John Wiley & Sons, Inc., 1997.

[74] S. Haykin, *Adaptive Filter Theory*, 5th editio. Harlow: Pearson, 2014.

[75] J. Cioffi and M., “Limited-Precision Effects in Adaptive Filtering [invited paper, special issue on adaptive filtering],” *IEEE Trans. Circuits Syst.*, vol. 34, no. 7, pp. 821–833, 1987.

[76] T. Y. A.-N. Ali H. Sayed, “MEAN-SQUARE ANALYSIS OF NORMALIZED LEAKY ADAPTIVE FILTERS,” *Acoust. Speech, an Proc. IEEE Int. Conf. Acoust. Speech, Signal Process. - ICASSP*, vol. 6, pp. 3873–3876, 2001.

[77] D. Bismor and M. Pawelczyk, “Stability Conditions for the Leaky LMS Algorithm Based on Control Theory Analysis,” *Arch. Acoust.*, vol. 41, no. 4, pp. 731–739, 2016.

[78] H. Nakhli Mahal, P. Mudge, and A. K. Nandi, “Comparison of coded excitations in the presence of variable transducer transfer functions in ultrasonic guided wave testing of pipelines,” in *9th European Workshop on Structural Health Monitoring*, 2018.

[79] J. L. Rose, J. Mu, and Y. Cho, “Recent Advances on Guided Waves in Pipe Inspection,” *17th World Conf. Non-destructive Test.*, pp. 25–28, 2008.

[80] W. Luo, J. L. Rose, J. K. Van Velsor, and J. Mu, “Phased-array focusing with longitudinal guided waves in a viscoelastic coated hollow cylinder,” *AIP Conf. Proc.*, vol. 820 I, no. 2007, pp. 869–876, 2006.

[81] E. Leinov, M. J. S. Lowe, and P. Cawley, “Ultrasonic isolation of buried pipes,” *J. Sound Vib.*, vol. 363, pp. 225–239, 2016.

[82] A. Demma, D. Alleyne, and B. Pavlakovic, “Testing of Buried Pipelines Using Guided Waves,” in *3rd MENDT - Middle East Nondestructive Testing Conference & Exhibition*, pp. 2–8.

[83] P. D. Wilcox, michael J. S. Lowe, and P. Cawley, “Mode and Transducer Selection for Long Range Lamb Wave Inspection,” vol. 12, no. August 2001, pp. 553–565, 2001.

[84] H. Kwun, S. Y. Kim, M. S. Choi, and S. M. Walker, “Torsional guided-wave attenuation in coal-tar-enamel-coated, buried piping,” *NDT E Int.*, vol. 37, no. 8, pp. 663–665, 2004.

[85] Ssanalysis, “Abaqus/Explicit.” [Online]. Available: http://www.ssanalysis.co.uk/. [Accessed: 14-Jan-2019].

[86] D. N. Alleyne, M. J. S. Lowe, and P. Cawley, “The Reflection of Guided Waves From Circumferential Notches in Pipes,” *J. Appl. Mech.*, vol. 65, no. 635–641, 1998.

[87] P. S. Lowe, R. M. Sanderson, N. V Boulgouris, and A. G. Haig, “Inspection of Cylindrical Structures Using the First Longitudinal Guided Wave Mode in Isolation for Higher Flaw Sensitivity,” *IEEE Sens. J.*, vol. 16, no. 3, pp. 706–714, 2016.

[88] W. Duan, X. Niu, T. Gan, J. Kanfound, and H.-P. Chen, “A Numerical Study on the Excitation of Guided Waves,” *Metals (Basel).*, vol. 7, no. 12, pp. 1–21, 2017.

[89] S. Fateri, P. S. Lowe, B. Engineer, and N. V. Boulgouris, “Investigation of ultrasonic guided waves interacting with piezoelectric transducers,” *IEEE Sens. J.*, vol. 15, no. 8, pp. 4319–4328, 2015.

[90] D. N. Alleyne and P. Cawley, “The excitation of Lamb waves in pipes using dry-coupled piezoelectric transducers,” *J. Nondestruct. Eval.*, vol. 15, no. 1, pp. 11–20, 1996.

[91] Mathworks, “Matlab.” [Online]. Available: https://uk.mathworks.com/products/matlab.html. [Accessed: 18-Apr-2018].

[92] H. Nakhli Mahal, A. K. Nandi, and K. Yang, “Detection of Defects in Guided-Wave inspection of pipelines,” in *NSIRC 2019*, 2019.

[93] H. Nakhli Mahal, K. Yang, and A. Nandi, “Detection of Defects Using Spatial Variances of Guided-Wave Modes in Testing of Pipes,” *Appl. Sci.*, vol. 8, no. 12, p. 2378, 2018.

[94] H. Nakhli Mahal, A. K. Nandi, and P. Mudge, “Enhancement of Signal to Noise Ratio in Ultrasonic Guided Wave Inspection of Pipelines,” in *NSRIC 2018*, 2018.

[95] S. C. Douglas, “Performance Comparison of Two Implementations of the Leaky LMS Adaptive Filter,” *IEEE Trans. Signal Process.*, vol. 45, pp. 2125–2129, 1997.

[96] D. A. Cartes, L. R. Ray, and R. D. Collier, “Experimental evaluation of leaky least-mean-square algorithms for active noise reduction in communication headsets,” *J. Acoust. Soc. Am.*, vol. 111, no. 4, pp. 1758–1771, 2002.

[97] W. T. Sen M. Kuo, Bob H. Lee, *Real-Time Digital Signal Processing : Implementations and Applications*. Chichester: John Wiley & Sons, Incorporated, 2006.

[98] H. Nakhli Mahal, K. Yang, and A. K. Nandi, “Defect Detection using Power Spectrum of Torsional Waves in Guided-Wave Inspection of Pipelines,” *Appl. Sci.*, vol. 9, no. 7, 2019.

[99] J. G. Proakis and D. G. Manolakis, *Digital Signal Processing*, Fourth Edi. New Jersey: Pearson, 2007.